AN AUTOMATED MONITORING SYSTEM FOR THE PRODUCTION AND MEASUREMENT OF METAL FATIGUE

by

DAVID MARK UPTON

Submitted to the University of Cape Town
in fulfilment of the requirements for the degree of
Master of Science in engineering

April 1988

SYNOPSIS

New equipment for producing and following the fatigue process, in metals, has been developed. The specimens, which must be in the shape of tuning forks, are resonated at high amplitudes. This is achieved by attaching small, powerful, samarium-cobalt magnets to the ends of the tynes, enabling them to be driven efficiently by a "U"-core electromagnet. A small, piezoceramic strain gauge provides a method of picking up the vibrations. To maintain resonance, the signal is used in a positive feedback loop, which incorporates an analogue multiplier to provide AGC. This also keeps the amplitude constant at any desired level, throughout the duration of an experiment.

A computer interfaced measuring and control system, allows readings of frequency, loss and temperature to be made at fixed number-of-cycle intervals during a test run. The data is stored on magnetic disk or tape for later analysis. The loss is found by measuring the Q of the system, using the free-decay of amplitude decrement technique. The decrement is not sampled until the amplitude has fallen to low values, where the envelope is truly exponential. This eliminates the non-linear effects of air-damping and anelasticity. It was found necessary to measure the specimen temperature to a considerable accuracy, as both frequency and loss are very thermally dependant, and material changes are obscured unless temperature is allowed for.

Typically in a fatigue run, well over 200 sets of readings are made. In the analysis, the raw data can be processed in any required way. In particular, the temperature coefficients are found, so that the values of frequency and loss can be referred to an arbitrary fixed temperature. This gives good sensitivity and enables meaningful observations to be made of the changes of stiffness and internal friction, which occur over the fatigue life of the specimen.

The values, uncorrected for temperature, remain steady for about 65% of the fatigue lifetime of a typical experiment. The use of a temperature correction gives excellent sensitivity, allowing the onset of crack initiation to be observed at about 50% of the life-time.

The loss and frequency cycles of the fatigue region seemed very similar, one appearing as the mirror image of the other. Plotting one against each other gave a straight line. This would indicate, rather surprisingly, that the same fatigue law governs both parameters. All specimens showed this phenomena but it was felt that further investigation was outside the scope of instrument development.

DECLARATION

I wish to declare that this thesis, unless indicated to the contrary in the text, is my own work.

Signed by candidate

Signature removed

D. M. UPTON

24th April 1988

ACKNOWLEDGEMENTS

The author wishes to thank everyone who has been of assistance with the completion of this project.

First and foremost to my supervisor Professor J F W Bell DSc who gave me much encouragement and enthusiasm and who was always available for assistance. Thanks Prof.

The other students of the lab Dr Tony Surtees and Bertrand Meyer who also gave valuable assistance.

The CSIR Foundation for Research and Development for their financial support.

Kevin Marcus for the use of his CAD system

My colleague Clinton Clark for assistance in matters "material" and for taking the electron microscope photographs.

Finally, thanks to my Father for taking the general photographs.

TABLE OF CONTENTS

page

SYNOPSIS I
DECLARATION II
ACKNOWLEDGEMENTS III
TABLE OF CONTENTS IV
LIST OF ILLUSTRATIONS XI
LIST OF TABLES XIV
GLOSSARY OF TERMS XV

CHAPTER 1. INTRODUCTION

1.0 Background 1-1
1.1 Objectives of the project 1-3
1.2 Contents of report 1-4
1.3 Limitations 1-5

CHAPTER 2. THE STRUCTURE OF REAL ENGINEERING MATERIALS AND ITS EFFECT ON THE FATIGUE OF METALS.

2.0 Introduction 2-1
2.1 Crystal defects 2-1
2.1.1 Point defects 2-1
2.2.2 Dislocations 2-1
2.2 Polycrystalline materials 2-4
2.2.1 Strain or work hardening 2-4
2.2.2 Annealing of metals 2-5
2.3 Mechanical behaviour 2-5
2.3.1 Elastic deformation 2-5
2.3.2 Anelastic deformation 2-6
2.4 Internal friction and energy losses 2-7
2.4.1 Anelastic energy losses and damping 2-7
2.4.2 Dislocation damping in metals 2-8
2.4.3 The Frank-Read mechanism of dislocation damping 2-11

2.4.4 The application of the vibrating string model and the Frank-Read mechanism to the fatigue process 2-13

CHAPTER 3. AN OVERVIEW OF METAL FATIGUE

3.0 Introduction 3-1
3.1 Crack initiation and propagation 3-1
3.1.1 Stage 1: micro-crack formation 3-2
3.1.2 Stage 2: macro-cracks 3-3
3.1.3 Stress concentrations 3-3
3.1.4 Crack propagation mechanism 3-4
3.2 Final fracture 3-5
3.3 Changes in mechanical properties during fatigue 3-5
3.3.1 Hardness 3-5
3.3.2 Strain ageing or coaxing 3-6
3.4 Factors affecting the fatigue strength 3-6
3.4.1 Tensile strength 3-6
3.5 Factors affecting fatigue life 3-7
3.5.1 Applied static stress 3-7
3.5.2 Applied stress profile 3-7
3.5.3 Mechanical factors 3-9
3.5.4 Metallurgical factors 3-10
3.5.5 Temperature effects 3-11
3.5.6 Test frequency 3-11
3.6 The appearance of fatigue 3-11
3.6.1 Microscopic appearance 3-12
3.7 Fatigue testing 3-12

CHAPTER 4. THE MODELLING OF DAMPED RESONANT SYSTEMS

4.0 Introduction 4-1
4.1 The damping of resonant systems 4-2
4.2 A mathematical study of viscous damping 4-3
4.2.1 The logarithmic decrement of oscillations 4-5

4.2.2 Terms related to the damping of oscillations ...4-6
4.3 Hysteretic damping 4-10
4.4 Variation of damping with frequency 4-12

CHAPTER 5. EXPERIMENTAL TECHNIQUES USED TO STUDY MATERIAL PROPERTIES BY RESONANCE METHODS

5.0 Introduction 5-1
5.1 Experimental techniques for damping measurements 5-2
5.2 The use of resonance techniques for fatigue testing 5-7
5.2.1 The use of flexural resonance 5-8
5.2.2 The effect of air damping on flexural resonators 5-9
5.3 Literature review of some previous research work 5-12
5.3.1 Damping measurements using longitudinal resonance 5-12
5.3.2 Damping measurements using torsional resonance .5-13
5.3.3 Damping measurements using flexural resonance ..5-13
5.3.4 Fatigue experiments using longitudinal resonance 5-14
5.3.5 Fatigue experiments using torsional resonance ..5-15
5.3.6 Rotating beam tests 5-16
5.3.7 Fatigue experiments using flexural resonance ...5-16

CHAPTER 6. THE TUNING FORK AND DRIVE MECHANISM

6.0 Introduction 6-1
6.1 The electromagnetic drive 6-3
6.2 Clamping of the tuning forks 6-7
6.3 The final assembly 6-8
6.4 Choice of material for the tuning forks 6-8
6.5 Geometry of the tuning forks 6-9
6.6 The resonant frequency of a tuning fork 6-9

CHAPTER 7. THE ANALOGUE ELECTRONIC DRIVE SYSTEM

7.0 Introduction 7-1
7.1 The analogue electronic system 7-2
7.2 Description of AGC oscillator system 7-2
7.2.1 PZT pre-amplifier 7-4
7.2.2 AGC circuitry 7-5
7.2.3 Pre-amplifier/Power amplifier combination 7-5
7.2.4 Power supplies for the pre-amplifier and power amplifier 7-7
7.2.5 Over temperature protection circuit 7-7
7.3 The setting up of a tuning fork prior to an experiment ...7-8
7.3.1 Gluing the PZT disk and magnets 7-8
7.3.2 Adjusting for oscillation 7-11
7.3.3 Adjustment of flexure amplitude 7-12

CHAPTER 8. THE COMPUTER CONTROLLED MEASUREMENT SYSTEM

8.0 Introduction 8-1
8.1 A brief description of the GPIO interface 8-1
8.1.1 The codes used for the various registers 8-2
8.2 Interfacing of the ICM 7226 universal counter 8-3
8.3 The interface circuitry 8-5
8.4 Description of the various measurements performed 8-11
8.4.1 Measurement of Q 8-11
8.4.2 Fixed number of cycle interrupts 8-16
8.4.3 Measurement of temperature 8-17
8.5 The start-up oscillator 8-20
8.6 Testing the spread in frequency and Q measurements 8-21
8.7 The HP-85 computer program 8-24

CHAPTER 9. THE IMPLEMENTATION OF THE 7226 INTERFACE ON THE IBM-PC

9.0 Introduction 9-1

9.1 The interface circuitry 9-3
9.1.1 The Q measurement module 9-9
9.2 The computer program 9-9

CHAPTER 10. THE RESULTS OF THE EXPERIMENTAL WORK

10.0 Introduction 10-1
10.1 The various experiments performed 10-1
10.1.1 Fatigue tests 10-1
10.1.2 Temperature dependence tests 10-2
10.1.3 Relationship between temperature coefficients of frequency, length and elastic modulus 10-2
10.2 A typical fatigue experiment 10-5
10.2.1 Temperature dependence 10-5
10.2.2 First fatigue run 10-6
10.2.3 Second fatigue run 10-7
10.3 The amplitude dependence of damping 10-9
10.3.1 Effect of extra air-loading 10-10
10.3.2 The efficiency of the drive system 10-11
10.3.3 The amplitude dependence of frequency 10-14
10.4 Microscopic investigations of fatigue surfaces 10-15
10.4.1 Scanning electron microscope photographs 10-16

CHAPTER 11. CONCLUSIONS

Conclusions 11-1

APPENDICES

Appendix A Diagrams of the analogue electronic drive system
Appendix B Diagrams of the HP-85 computer interface
Appendix C Diagrams of the IBM-pc computer interface
Appendix D Graphs of results from the experimental work
Appendix E Listing of the HP-85 computer program

Appendix F Data sheet of the ICM 7226 BIPL universal counter
Appendix G Scanning electron microscope and general photographs

LIST OF REFERENCES R-1

BIBLIOGRAPHY B-1

LIST OF ILLUSTRATIONS

page

Figure:

2.1 Dislocations in a crystal 2-3
2.2 Stress-strain relationship of elastic solid 2-5
2.3 Stress-strain relationship of anelastic solid. 2-6
2.4 Vibrating string model of dislocation damping 2-9
2.5 Stress-strain paths for the model 2-11
2.6 The Frank-Read dislocation source 2-13
2.7 The production of jogs 2-15

Figure:

3.1 Intrusions and extrusions formed by irreversible slip 3-3
3.2 The growth of fatigue cracks 3-4
3.3 Stress profiles for fatigue testing 3-8

Figure:

4.1 Viscously damped mass-spring system 4-3
4.2 Exponential decay of a damped oscillating system 4-5
4.3 The variation in natural frequency with damping 4-9
4.4 The variation in damping with frequency 4-13

Figure:

5.1 Non-linear decay 5-3
5.2 Resonance curve for lightly damped systems 5-4

Figure:

6.1 Tuning forks 6-2
6.2. Shape of a vibrating bar clamped at one end 6-2
6.3 Magnetic drive of tuning forks 6-3
6.4 The tuning fork used in this work 6-12

Figure:
7.1 The overall system 7-1

Figure:
9.1 Overall system using the IBM-pc 9-2

Diagram:
A.1 Block digram of the AGC system .....APPENDIX A
A.2 Full circuit diagram of AGC system
A.3 The pzt pre.amplifier
A.4 The pre-amplifier and power amplifier
A.5 The power supply
A.6 The over-temperature protection unit

Diagram:
B.1 The overall system .....APPENDIX B
B.2 The GPIO timing diagram
B.3 Pin configuration of the ICM 7226 BIPL
B.4 Block diagram of the 7226 interface
B.5 Basic connection diagram of the 7226
B.6 The BCD latches
B.7 The HP85/GPIO interface circuitry
B.8 The Q-meter
B.9 The start-up oscillator
B.10 Temperature measurement circuit 1.
B.11 Temperature measurement circuit 2

Diagram:
C.1 Overall diagram using the IBM-PC .....APPENDIX C
C.2 Timing diagrams of the IBM-PC
C.3 PC36 circuit diagram

C.4 Basic connection diagram of the 7226
C.5 Block diagram of the interface
C.6A Address decoding and data buffering
C.6B Address decoding and data buffering
C.7 Capture data sub-module
C.8 The Q meter

Graph:

D.1 Histogram showing the spread in Q readings .....APPENDIX D
D.2 Histogram showing the spread in f readings
D.3 Heating curve for frequency
D.4 Cooling curve for frequency
D.5 Heating curve for Q
D.6 Cooling curve for Q
D.7 Overall changes in frequency for fatigued fork
D.8 Frequency to 4 M-cycles corrected for temperature.
D.9 Temperature changes to 4 M-cycles
D.10 Frequency to 4 M-cycles uncorrected for temperature
D.11 Overall changes in Q for fatigued fork
D.12 Overall changes in loss for fatigued fork
D.13 Q to 4 M-cycles uncorrected for temperature
D.14 Q to 4 M-cycles corrected for temperature
D.15 Loss to 4 M-cycles uncorrected for temperature
D.16 Loss to 4 M-cycles corrected for temperature
D.17 Loss versus frequency for points beyond final knee
D.18 Amplitude dependence of Q
D.19 Amplitude dependence of Q for extra air-loading
D.20 Amplitude dependence of loss
D.21 Amplitude dependence of loss for extra air-loading
D.22 Calibration of temperature measurement circuit
D.23 Input power versus vibration amplitude
D.24 Plot of quadratic fitted to Plost versus Pinput.
D.25 Efficiency versus amplitude
D.26 Pzt pre-amplifier voltage versus vibration amplitude
D.27 The variation of frequency with amplitude

LIST OF TABLES

page

10.1 Temperature coefficients 10-6

10.2 Equivalent mass values 10-13

10.3 Efficiency test values 10-18

GLOSSARY OF TERMS

1. Mathematical symbols:

αf -- Temperature coefficient of resonant frequency

αl -- Temperature coefficient of linear expansion

α_E -- Temperature coefficient of Youngs modulus

A -- Amplitude of decaying oscillations

A_0 -- Initial amplitude

A_N -- Amplitude after N oscillations of decay

C -- Longitudinal velocity of sound

E -- Energy of oscillating tuning fork or the Youngs modulus of the material.

ϕ -- phase angle

f -- Fundamental frequency of an undamped system or the frequency of a tuning fork.

f_1 -- Frequency of tuning fork with added mass m

f_d -- Fundamental frequency of a damped system

F_d -- Damping force of the dash pot of a viscously damped mass-spring system

F_m -- Force due to the mass of a mass-spring system

F_s -- spring force of a mass-spring system

I_{rms} -- The rms current of the electromagnet coil

k -- Stiffness of the spring in a lumped mass-spring system

L -- Length of the tynes of a tuning fork

m -- Small added mass to tuning fork

M -- Equivalent mass of tuning fork modelled as a lumped mass-spring system

Ωa -- Specific damping capacity of the air

P_{input} -- Input power to tuning fork drive system

P_{lost} -- Power loss due to internal friction

Q -- The Q factor of a tuning fork

R -- damping constant of dash pot

s -- Laplace transform operator

θ -- Temperature

t -- Time

Vpzt -- The voltage output of the pzt pre-amplifier
Vrms -- The rms voltage of the electromagnet coil
w -- The thickness of the tynes of a tuning fork.
w_0 -- Fundamental undamped angular frequency
w_d -- Fundamental damped angular frequency
w_n -- Natural angular frequency
x -- Distance moved from equilibrium for a mass-spring system

2. Miscellaneous:

AGC -- Automatic gain control
amp -- Amplifier
BASIC -- A computer programming language
damping -- Characteristic of a lossy resonant system
DFM -- Digital frequency meter
f-f -- Flip flop
HP -- Hewlett Packard
IBM pc -- The personal computer from the IBM company.
internal friction -- A term describing the source of internal loss of a material
loss -- Degree of energy loss within a material (loss=1/Q)
MS-DOS -- Micro-soft Disc Operating System.
PC35 -- A version of prototyping board for use with the IBM pc.
pk-pk -- Peak to peak
ppk -- Parts per thousand
ppm -- Parts per million
pre-amp -- Pre-amplifier
pzt -- Lead zirconate titanate piezoelectric transducer
Q -- An electrical term which describes the quality of a resonant system. One with a high Q has little loss or damping (loss=1/Q).

SDC -- Specific Damping Capacity. The ratio of energy lost per cycle to the total energy of the system

SEM -- Scanning electron microscope

strobe light -- An instrument consisting of a xenon flash tube which can be operated at a variable rate.

travelling microscope -- a microscope attached to a vernier gauge enabling accurate measurements of small distances.

TRUE BASIC -- a recently developed programming language far superior to the old BASIC language.

tyne -- A single vibrating beam of a tuning fork

---X---

CHAPTER 1

INTRODUCTION

1.0. Background

The study of materials and their behaviour under various externally applied influences is generally confined to the field of mechanical and materials engineering. This is of course rightly so, but is a situation that brings with it several disadvantages. The researchers in these disciplines usually have no formal training in electronic measurement techniques and especially automated measuring systems. They therefore may not be aware of the full potential of employing them in their work.

The use of resonance techniques for studying materials is part of the overall field of physical acoustics. The techniques have been applied extensively in determining the properties of solids and of liquids and gases. The elastic properties and internal friction can be investigated including the testing of models and hypotheses concerning solid-state phenomena such as dislocation movement. The use of high amplitude vibrations can be used to study the elastic and internal friction properties of metals undergoing fatigue.

The fatigue properties of materials are traditionally tested using machines which simply apply a cyclic stressing load to the sample. The power can be applied using hydraulics. Other machines use a resonance method where the sample provides the stiffness component of a lumped element system. The inherent force amplification effect at resonance eliminates the need for the powerful actuating force of a hydraulic system and the higher testing frequency speeds up fatigue experiments. However, the actual resonance parameters are not part of the testing procedure, and therefore these machines are equivalent to those of the hydraulic type. The information this type

of testing provides is limited to the number of cycles to fracture and the stress or strain level, producing the traditional stress-cycle (S-N) diagram.

A wealth of information can be obtained by using instrumentation during a resonance fatigue test. The characteristics of the resonance are a direct reflection of the material properties, i.e the stiffness of the material is dependant upon the Young's modulus and which determines the frequency. The internal friction provides a path of energy loss from the system and characterises the bandwidth of the resonance curve.

This work is concerned with the design and construction of a computer based apparatus that can be used to study the properties of materials undergoing flexural resonance at vibration amplitudes up to and including fatigue. The samples are in the form of tuning forks which are kept at their fundamental frequency during a test. A tuning fork provides an ideal dynamically balanced resonator which is easily supported and from which the extraneous energy losses can be made very small. This gives a good sensitivity for the measurement of amplitude decrement (Q), from which a direct value of loss can be obtained.

Electronic feedback circuitry is used to maintain the resonance point and a small piezoelectric disk fixed to the fork at the base of the tynes provides a measure of the strain, which enables the amplitude to be accurately and constantly controlled. A measurement system takes readings of frequency, internal friction and temperature. These readings are taken at fixed number-of-cycle intervals for fatigue tests. The measurement electronics is interfaced to a computer which provides overall control and data storage facilities. The temperature sensor is positioned near to the base of the tynes, close to the stress antinode, where the internal friction increases with fatigue, and hence a source of temperature rise in the specimen.

It is important to note that the bandwidth of a resonance curve

depends entirely on the amount of energy loss from the system. The bandwidth is defined as the difference in frequency values corresponding to a drop of $1/\sqrt{2}$ either side of the centre resonant frequency. In electrical terms, this is described by the Q factor, which denotes the "quality" of the resonance. One with a high Q has low loss and consequently a sharp resonance curve. The energy loss in a material occurs due to a phase delay between the applied stress and the resulting strain. This time delay effect is called anelasticity and gives rise to a hysteresis loop for the stress versus strain diagram, the area of which corresponds to the energy loss per cycle. The loading and unloading cycles do not exactly coincide and the overall effect is called hysteretic damping. The term damping arises from the fact that if the energy supply is removed, then the oscillations will decay away, or in other words, are damped. The loss of such a system is denoted by the specific damping capacity (SDC) and is equal in value to 2π x sin(phase angle). The Q of the same system is simply the inverse of the loss. If the decay of energy is linear, then the envelope of the amplitude decrement is exponential. This fact is used in this work for the measurement of loss. Due to the electrical background of the author, the term Q is preferred, but can be interchanged with the terms loss or damping if the inverse relationship is borne in mind..

1.1. Objectives of the project

There were two main objectives in undertaking this thesis project. They are:

1.

a. To design and construct a computer based apparatus for performing fatigue experiments on samples of any material (other than steel) in the form of tuning forks. The tuning forks are to be driven electromagnetically using powerful samarium cobalt magnets fixed to the ends of the tynes. Included is all the electronics neccessary to complete the drive system so that resonance is maintained at a constant

but adjustable amplitude.

b. A computer based system is to be used to provide overall control of an experiment. A measurement system is to be interfaced so that a series of measurements will be performed on the tuning forks during an experiment, under program control, so that averages and formulae may be applied to the readings. The computer also provides mass storage facilities for the data on magnetic disk or tape for later analysis. The measurements are: frequency, temperature and decrement Q.

2. To use the above apparatus for performing several different experiments:

    1. Temperature dependence of frequency and Q
    2. Fatigue experiments

    From the results of the above, to see the suitability of the apparatus as a possible research tool.

1.2. Contents of report

The report can be broken down into three main sections:

1. Background information about material defects and their effect on the damping and fatigue of metals. The fatigue process in greater detail and a mathematical treatment of resonant systems that have damping. This is contained in chapters 2 to 4.

2. The description of the electronics required to complete the system. This is further broken down into:
    a. The analogue electronics for the drive of the tuning forks and the maintenance of the resonant frequency and amplitude.
    b. The digital electronics for the measurement system and its interface to the HP85 and IBM pc computers.

This is contained in chapters 5 to 9.

3. The use of the apparatus for performing various experiments:

    1. Temperature dependence of frequency and Q (loss)
    2. A typical fatigue experiment
    3. Amplitude dependence tests:
        a. The variation in efficiency of the apparatus
        b. The effect of air-damping
        c. The amplitude dependence of frequency

    The measurement of temperature allows the temperature coefficients of frequency and loss to be measured so that the data may be referred to an arbitrary fixed temperature. This is of fundamental importance in obtaining a high degree of sensitivity for monitoring changes in the material properties. If the frequency data for a fatigue experiment before the main knee of the curve is corrected for temperature, then the changes in frequency due only to material changes can be observed and the point of micro-crack initiation can be seen on re-plotting. The results of these experiments is given in chapter 10.

1.3. Limitations

This project was limited to the building and testing of the apparatus with no serious experimentation performed. This was due mainly to the lack of good samples which are essential for performing meaningful fatigue experiments. Samples made of mild steel only were tested. It was hoped that aluminium specimens could also be tested but this was inhibited by cost.

CHAPTER 2

THE STRUCTURE OF REAL ENGINEERING MATERIALS AND ITS EFFECT ON THE FATIGUE OF METALS

2.0. Introduction

The crystals or grains of real engineering materials contain defects which upset the regular repeated pattern of the crystal structure or lattice. These imperfections are of great importance to the nature of materials, and in particular give metals their ductility, and allow them to be deformed plastically (permanently strained). If metal grains did not contain defects they would be brittle in nature, and hence it is a fortunate natural phenomena[1,2,3].

2.1. Crystal defects

2.1.1. Point defects

This type of defect manifests itself in two ways. Firstly, if an atom is missing from the structure altogether, then the defect is called a vacancy. Secondly an impurity atom or, alternatively, a displaced indigenous atom could be residing in the interstitial spaces. The last type being called interstitial defects.

2.1.2. Dislocations

This is the most important defect in metals and plays a major role in the fatigue process. The theoretical strength of crystals is several orders of magnitude greater than that of real crystals. The discrepancy is due to dislocations in the crystal lattice allowing deformation to occur at much lower stresses.

Dislocations are formed, in a crystal being subjected to a shearing force, when the upper part of the crystal is displaced from the lower part resulting in permanent strain called plastic deformation. The atoms retain the same geometric coordination but are displaced by an integral number of inter-atomic spaces. The remaining discontinuity is known as a dislocation.

A dislocation occurs to there being an extra half plane of atoms inserted into the lattice structure. This is best explained by means of Figure 2.1. If the crystal is now subject to a shearing force τ, a series of local bond breaking and re-making occurs, and the extra half plane ripples through the lattice until the crystal boundary is met. The crystal is left deformed with the lower half of the crystal slipped by a distance b under the top half. The unit of slip b is known as the Burger's vector. This deformation requires much less energy than if the whole top half of the crystal had been macroscopically sheared, where all the bonds would have to be broken simultaneously. The process is analogous to moving a carpet across a room by working a ruck from one end to the other: the force required is less than if the whole carpet had to be moved at once.

In order for a dislocation to move through a crystal, the intrinsic friction to the movement must be overcome. Additionally, interstitial atoms and other dislocations in the path cause obstructions, and the applied stress to the crystal has to push the dislocations past these obstacles. This is analogous to blowing up a balloon inside a bird cage: a large pressure is required to bulge the balloon between the bars, but once the bulge is large enough, further expansion is easier.

In most crystals a large number of dislocations are present, known as the dislocation network, and this has an enormous effect on the properties of the material.

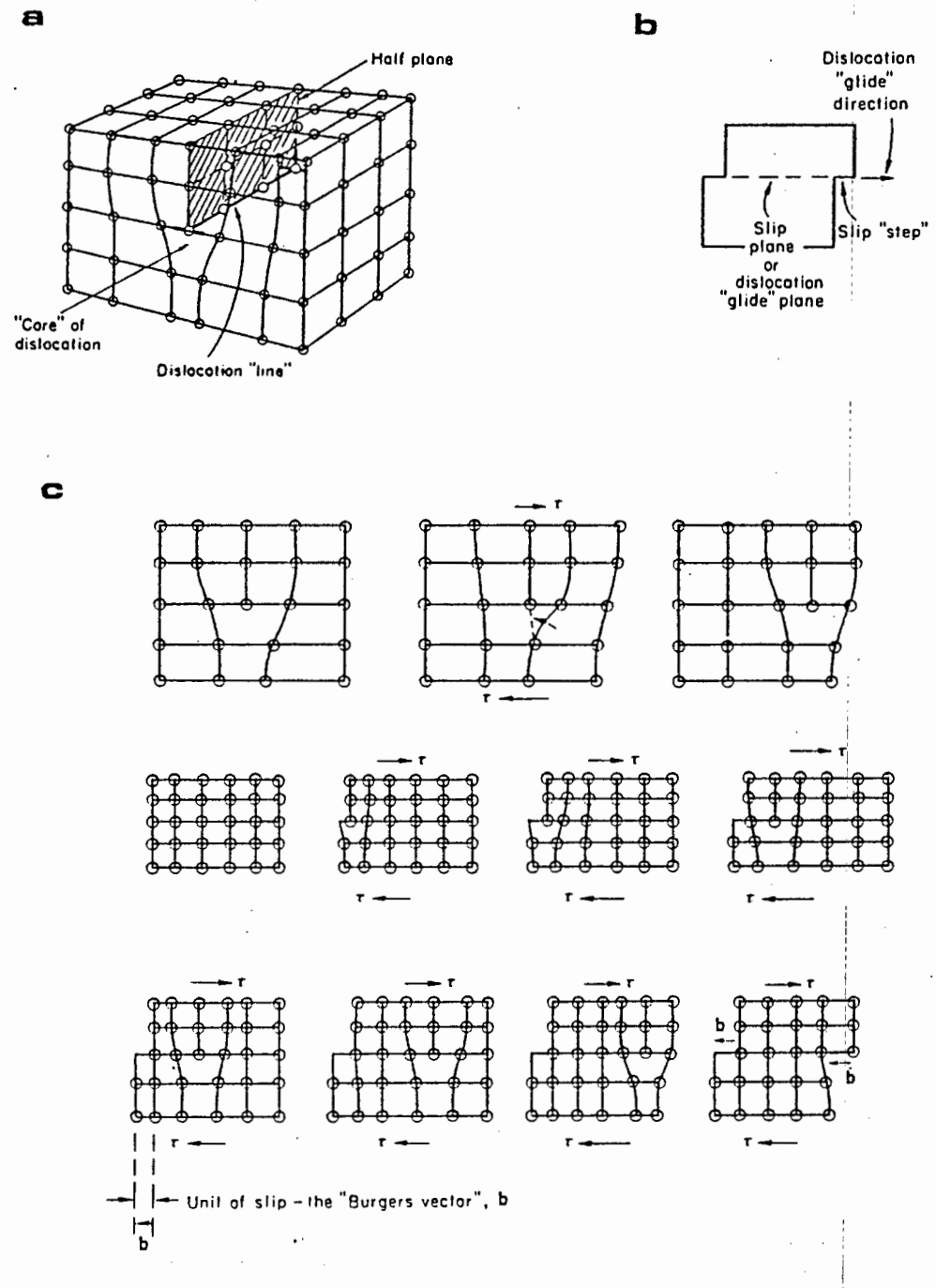

Fig.2.1. Dislocations in a crystal. (a) Shows the positions of the atoms near the dislocation. (b) Shows how the atomic bonds break and remake allowing the dislocation to move. (c) Shows the migration of a dislocation from the left hand side of a crystal to the right. The lower and upper halves slip by a distance b.

2.2. Polycrystalline materials

Most materials contain a large number of crystals and are therefore called polycrystalline materials. This is especially true of metals where the crystals are referred to as grains. Areas of mismatch occur where adjacent crystals meet at the grain boundaries and most properties are discontinuous across them. Usually all the grains in a metal have the same structure, known as the microstructure, and is characterised by grain: size, shape and orientation. In a metal there is an almost random arrangement of grain orientation, hence on a microscopic scale they are anisotropic but overall they are virtually isotropic. Further alignment is usually caused by rolling, etc.

The large number of grains that make up a polycrystalline material give rise to a correspondingly large number of defects. The interaction of these defects (dislocations and point defects), have a great influence on the behaviour of these materials, especially during cyclic stressing.

2.2.1. Strain or work hardening

If a stress is applied to a metal, the first plastic deformation occurs relatively easily by the movement of dislocations. However, this first dislocation movement interferes with the formation and movements of subsequent dislocations. Crystals have several planes, and the dislocations from one plane can form obstacles to other dislocations on other planes, which have to cut through them. The points of intersection are called anchor or pinning points and restrict dislocation movement. Hence the stress necessary to cause plastic deformation increases and the metal is said to have become work hardened or cold-worked. Copper is especially prone to work hardening.

2.2.2. Annealing of metals

The effects of strain hardening can be removed by heating the metal at a certain temperature for some time. The temperature is known as the re-crystallisation temperature where new crystals or grains are formed, with a fresh network of dislocations and point defects. The annealing time is important and the temperature required for re-crystallisation is lower for a longer annealing time.

2.3. Mechanical behaviour

2.3.1. Elastic deformation

Elastic deformation is strain occurring in crystals which is completely reversible, as opposed to plastic deformation which is not.

In the elastic region of deformation of metals, there is a linear relationship between stress and strain, known as Hooke's Law. The Young's modulus or elastic modulus, describes the ratio between stress and strain and is a measure of the stiffness of a material (Figure 2.2).

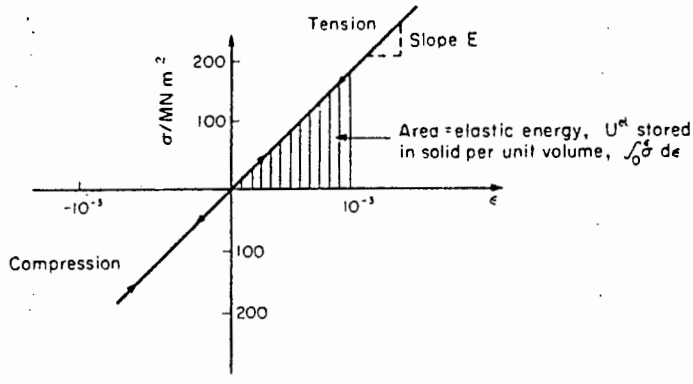

Fig.2.2. The stress-strain relationship for a linear elastic solid.

Generally crystals or grains of a metal are anisotropic: having different elastic constants for different orientations. However, the grains are virtually randomly orientated in a polycrystalline metal and hence a mean value results for the overall material. A consequence of this is that if a material is subjected to an external stress, the grains will be equally strained, but will be stressed differently.

2.3.2. Anelastic deformation

Deformation which is time dependant is called anelasticity. It occurs in most metals because some atoms or molecules can relocate themselves within the total structure, on the appplication of a stressing force. The stress loading curve does not exactly follow the unloading curve with the result that energy is dissipated within the material. Most solids are anelastic to a certain extent. Metals have a definite stress limit below which they deform elastically and above, anelastically (Figure 2.3).

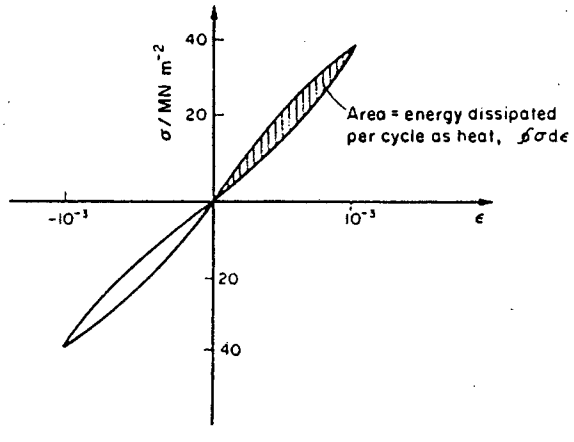

Fig.2.3. The stress-strain relationship of a solid undergoing anelastic deformation.

As an example of what can happen, consider an interstitial atom residing alongside a unit cell of the crystal lattice. If this interstitial atom is large enough, it will cause distortion to the surrounding structure in order for it to fit. If a stress is now applied, the elastic strain will distort the unit cell and the interstitial atom may be able to move to a larger site, causing a lowering of the strain energy. Hence, this can be described as a stress induced ordering process. If the stress is removed the interstitial atom will be forced to move back to its original position.

2.4. Internal friction and energy losses

2.4.1. Anelastic energy losses and Damping

Elastic deformation requires energy to occur since a force is being applied over a finite distance. The energy is the area under the stress-strain curve describing the deformation (Figure 2.2):

$$\text{energy } U = 1/2 \text{ stress x strain} \quad \ldots\ldots\ldots \qquad (2.1)$$

If time is not involved in the deformation process, then all the energy will be recovered once the stress is removed.

If the deformation occurs anelastically, then an energy loss will occur because the strain will lag the applied stress, causing a phase lag between stress and strain. This creates a hysteresis loop, the area of which represents the energy loss (Figure 2.3).

$$\text{energy loss } \square U = \int \sigma \; d\epsilon \quad \ldots\ldots\ldots\ldots\ldots\ldots \qquad (2.2)$$

If we consider a cyclic sinusoidal stress being applied to a material then:

$$\text{Stress, } \sigma = \sigma_m \sin wt \quad \ldots\ldots\ldots\ldots\ldots\ldots\ldots \quad (2.3)$$

$$\text{Strain, } \epsilon = \epsilon_m \sin(wt-\phi) \quad \ldots\ldots\ldots\ldots\ldots\ldots\ldots \quad (2.4)$$

In the case of elastic deformation, the strain will be in phase with the stress and $\phi = 0$.

In the anelastic case ϕ is not equal to 0 and the energy lost per cycle can be calculated as follows:

$$\square U = \int_0^{2\pi} \sigma \, d\epsilon = \int_0^{2\pi} \sigma_m \, \epsilon_m \sin wt \, d(\sin(wt-\phi))$$

$$= \pi \sigma_m \epsilon_m \sin\phi \quad \ldots\ldots\ldots\ldots\ldots\ldots\ldots \quad (2.5)$$

The maximum elastic strain energy is $\frac{1}{2}\sigma m \epsilon m$ and therefore each cycle dissipates:

$$SDC = \frac{\square U}{U} = 2\pi \sin\phi \quad \ldots\ldots\ldots\ldots\ldots\ldots \quad (2.6)$$

Since $Q = 2\pi/SDC$ then:

$$Q = \frac{1}{\sin\phi} \quad \ldots\ldots\ldots\ldots\ldots\ldots\ldots \quad (2.7)$$

The larger the lag the greater will be the energy loss which manifests itself as a hysteresis loop of larger area.

2.4.2. Dislocation damping in metals

Damping describes a materials ability to dissipate energy when subject to cyclic stresses. It therefore also describes the internal energy loss within the material.

There is a definite increase in damping in metals between the elastic and anelastic stress regions. There has been a tremendous amount of research to discover the causes of anelasticity in metals undergoing cyclic stressing, and it has been found that the major cause is the movement of dislocations.

One of the most famous models for dislocation-damping is that by Granato and Lùcke, which is based on the concept by Koehler that a dislocation could behave as a vibrating string. It is therefore known as The Vibrating String model which operates as follows:

In pure single crystals before deformation has taken place, there is a network of dislocations which intersect at various places, forming strong anchor-points which do not yield. Furthermore, if there is a high enough concentration of impurity atoms forming interstitial defects, then the dislocation line between the anchor points will be pinned down by them (Figure 2.4).

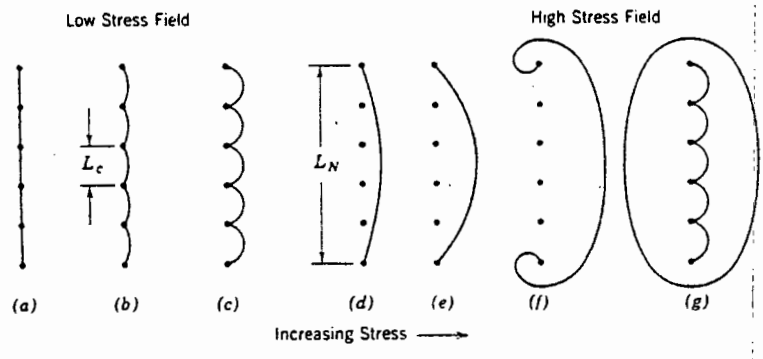

Fig.2.4. Vibrating string model of dislocation damping.

Therefore, from the above scenario, there are two lengths involved:

1. L_N = network length between anchor-points
2. L_C = length between the impurity atoms

If an external stress is applied to the metal, there will be elastic strain plus extra strain due to dislocation movement called dislocation-strain.

If the applied stress is cyclic, then during a quarter cycle when the stress is increasing from zero to a maximum value, the following steps occur according to this model:

1. At zero stress the whole network length L_N is pinned down by interstitial impurity atoms.

2. For a small stress, the lengths L_C bow outwards and continue to do so until the stress reaches the break-away value. The effective modulus of the material is determined by L_C in this region.

3. At the break-away stress there is a large increase in dislocation-strain for no increase in stress. Hence, the strain leads the stress.

4. Further increase in applied stress cause the activation of the Frank-Read mechanism, which causes further dislocations to be generated. It is assumed that the anchor-points are so strong that no break-away of network lengths occurs. The effective modulus is determined by L_N in this region.

5. At this stage, further stress aids the Frank-Read mechanism, creating closed dislocation loops which expand and the material becomes irreversibly or plastically deformed.

If the stress begins to reduce after (3) during the next quarter cycle, the long loops L_N collapse elastically along a path determined by L_N, creating a hysteresis loop. Once they have completely collapsed, they become pinned again by the impurity atoms. No permanent change has occurred in the metal and the same path is followed in the next half cycle (Figure 2.5).

The losses are made up of essentially two parts:

1. The inherent friction opposing the motion forced by the external stress.

2. The elastic collapse of the long loops.

The second factor gives rise to a lag between stress and strain, creating a hysteresis loop for the motion.

Steps (4) and (5) occur at higher maximum stresses, and cause fatiguing of the material. At lower stresses, where no fatiguing occurs, the model describes the method by which damping losses occur.

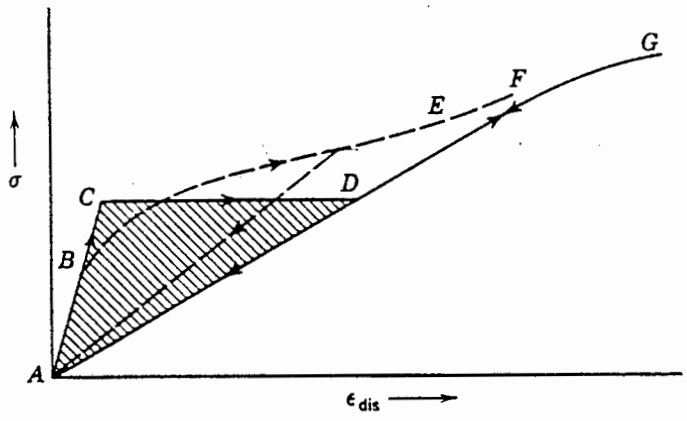

Fig.2.5. Stress-strain paths for the model. The elastic strain has been subtracted leaving only the dislocation strain. The path ABCDEF is followed for increasing stress while path FA is followed for decreasing stress. The dashed curve represents the more realistic model that results from not all the loops having the same lengths, but a distribution of lengths Lc.

2.4.3. The Frank-Read Mechanism of dislocation Generation

This mechanism describes a process by which further dislocations can be generated from a single dislocation (Figure 2.6).

(a) Consider a dislocation line CD between two anchor-points formed by the intersection of previous dislocations.

(b) If shear stress τ_b is applied to the material then the dislocation will bow outwards.

(c) The stress reaches a maximum value when the radius of curvature reaches half the anchor-point spacing, and the dislocation is hemispherical in shape.

(d) Further movement of the dislocation causes an increase in the radius but also a reduction in the shear stress required, causing the dislocation to become unstable. This is analogous to blowing soap bubbles from a loop of wire dipped in a soap solution.

(e) The dislocation continues to pivot around the anchor points C and D.

(f) Eventually the arms join at a point behind the dislocation line and a new dislocation is formed. Continued application of the shear stress causes the second dislocation to duplicate the above process, and hence repeating generations of dislocations move through the crystal.

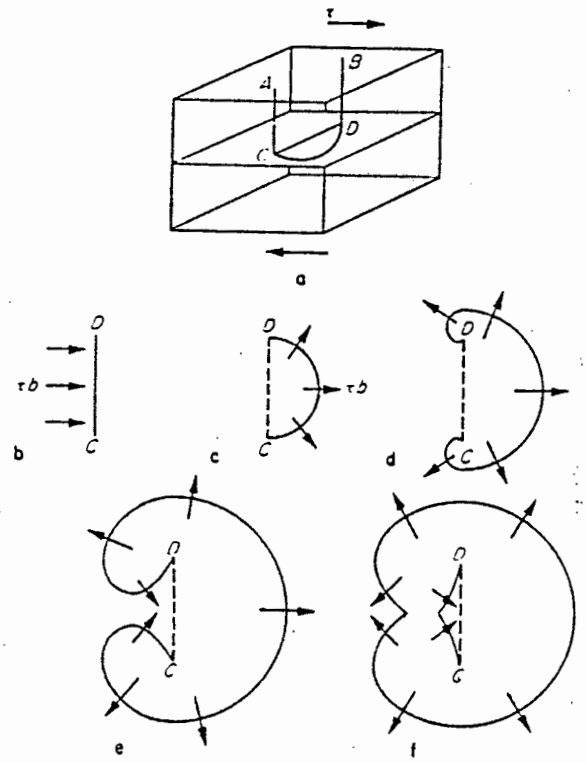

Fig.2.6. The Frank-Read dislocation source.

2.4.4. The application of the vibrating string model and the Frank-Read mechanism to the fatigue process

Mason successfully applied the above two concepts to the fatigue of metals. The increase in internal-friction between the elastic region and the anelastic region is due to the production of unstable Frank-Read dislocation loops according to the Granato-Lucke model. The interaction between dislocations and interstitial atoms determine to a large extent the fatigue characteristics of metals.

Since the internal-friction values are repeatable, this implies that when the stress is reduced from the anelastic to the elastic range, the production of dislocation loops is reversible. Generally there will be obstructions at a certain distance from the centre which will not allow the Frank-Read process to generate more than one unstable loop.

When the stress corresponds to the generation of Frank-Read loops of about 50% longer than the previous peak length, the loss increases very rapidly with amplitude. At a stress about twice that necessary to produce unstable dislocation loops of the peak length , the metal fatigues. This is due to the dislocation loops having enough energy to cut through the anchor-point dislocations producing jogs, vacancies and an uncontrolled number of Frank-Read loops. Jogs are produced when two dislocation lines running at right angles to each other intersect, causing a step in one or both dislocation lines (Figure 2.7).

When jogs are produced, a large number of vacancies are also usually produced, requiring a large amount of energy. This increases the energy loss (increase in damping). According to Mott, these vacancies can diffuse together to form cracks. Fatigue cracks usually start at the surface of the metal where the Frank-Read sources will be single ended, and therefore can operate at about half the stress normally required. The production of jogs similarly can occur at lower stresses and hence it will be easier to form vacancies near the surface which can combine to form cracks.

The dislocation-vacancy model shows good agreement with experimental results. One property that is easily explained by this model is that of coaxing and is due to the work hardening of the metal by the production of more dislocation loops forming closer anchor-points in the dislocation network and hence a shorter Frank-Read source. This increases the resistance to fatigue because more anchor-points have to be cut through.

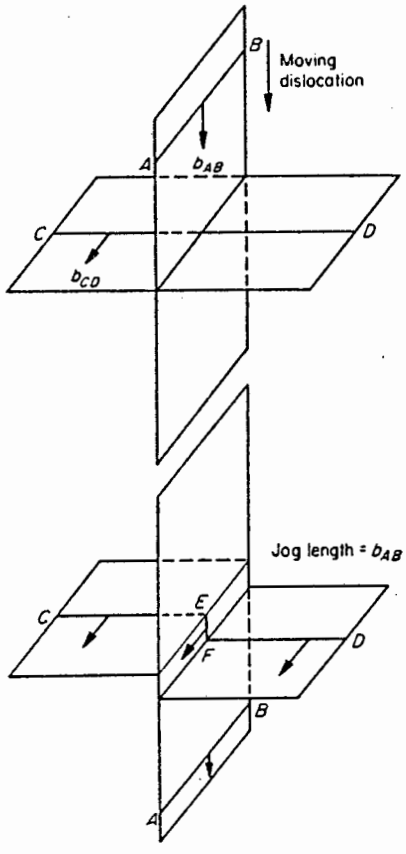

Fig.2.7. Production of jogs. (a) The dislocation AB is moving on its slip plane at right angles to the dislocation CD. (b) When AB intersects with CD, a jog EF is introduced in the dislocation CD and moves freely with it.

--- X ---

CHAPTER 3

AN OVERVIEW OF METAL FATIGUE

3.0. Introduction

Fatigue is the term given to the process by which a specimen undergoing applied stress cycles gradually deteriorates[1,2,9,10,11,12]. The maximum applied stress is usually well below the tensile strength, and the yield strength, of the material. The deterioration is due to the propagation of a fracture or crack through the specimen, until a final rapid fracture occurs which separates the material completely.

There are three main phases in the fatigue process:

1. Crack initiation
2. Crack propagation
3. Final fracturing

These phases depend upon each other and hence cannot be completely separated.

3.1. Crack initiation and propagation

There are two steps in the crack initiation and propagation phases.

Stage 1 is the development and then propagation of a micro-crack, followed by:

Stage two where the micro-crack develops into a macro-crack, which then continues to propagate.

The cracks propagate by plastic deformation in ductile metals due to the movement of dislocations (chapter 2).

3.1.1. Stage 1: micro-crack formation

Cracks usually begin at the surface of a specimen where the grains are not supported on all sides. Dislocation lines are anchored only at the end within the material. The grains having a free surface are more easily plastically deformed than a grain within the body of the material. Evidence to support the surface theory is that if a fatigue test is stopped after a fraction of the life-time and a thin layer of metal is removed, on continuation of the test at the same applied stress, the life-time will be extended. Secondly, any process which hardens the surface can improve the fatigue life-time of the whole specimen.

Fatigue cracks start at some sort of imperfection on the surface of a specimen where the stress concentrations are high enough to cause plastic deformation by dislocation movement.
These imperfections are most often caused by machining marks, a surface finishing process or from surface damage through use.

However, even the most highly polished surfaces can develop irregularities by the process of irreversible slip. The surface grains of the material are not held tightly on all sides, as are the adjoining sub-surface grains, and hence can be displaced due to dislocation movement along slip-planes. The repeated stress cycling can cause slip to take place accompanied by strain hardening (increased pinning of dislocations), which prevents back slip along the same plane. The process continues and new bands form beside the old ones, until a series of intrusions and extrusions are formed, where again the stress concentrations can be high enough to cause plastic deformation (Figure 3.1).

No matter how the surface imperfections are formed, they are the places where a micro-crack can form after a certain number of stress cycles. These micro-cracks slowly grow by localised plastic deformation at the crack tips. They follow the grain orientation of the material for a short distance (intergranular).

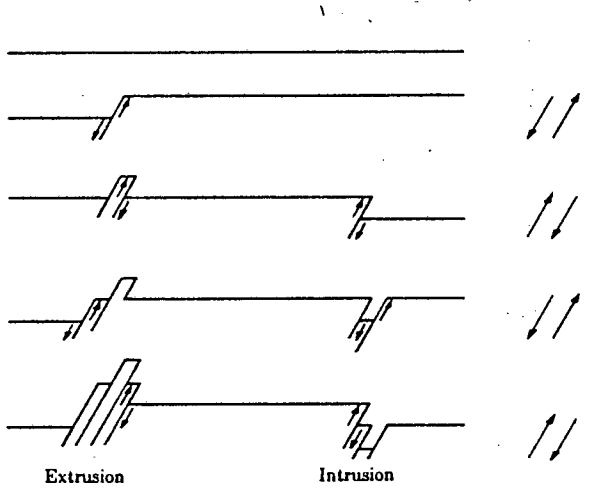

Fig.3.1. Intrusions and extrusions formed by irreversible slip.

3.1.2. Stage 2: macro-cracks

Once the stage-1 micro-cracks have reached a certain length, they change direction and grow normal to the maximum principle stress axis (transgranular), but at a much faster rate. They are now termed macro-cracks and comprise the majority of the crack propagation lifetime.

3.1.3. Stress concentrations

The stress concentrations in the cracks are not normally high enough to produce rapid fracture because in a ductile metal the crack tips are not atomically sharp. The plastic deformation occurring at the tip causes blunting.

Griffith found a relation that describes the concentration of stress at a crack tip:

$$\sigma_c = 2\sigma_n\sqrt{\frac{c}{r}} \qquad \text{.....} \qquad (3.1)$$

Where:

σ_c = concentrated stress
σ_n = nominal stress
c = length of crack
r = radius of crack tip

Since r can be small compared to c, then the concentrated stress can be much larger then the nominal stress.

3.1.4. Crack propagation mechanism

In pure metals the propagation can be described by the following steps (Figure 3.2):

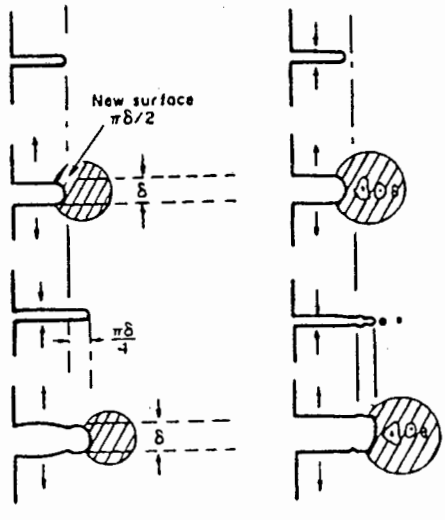

Fig.3.2. The growth of fatigue cracks.

1. The tensile cycle opens the crack producing a stress high enough to give rise to a zone of plastic deformation concentrated along a slip-plane. This zone is stretched open by an amount d creating a new surface at the crack tip.

2. The compressive cycle squeezes the crack shut forcing the new surface forward and extending the crack by approximately the distance d above.

3. The process repeats on successive cycles until the material becomes sufficiently weakened and final catastrophic failure occurs.

3.2. Final fracture

The macro-crack eventually propagates deeply enough so that the material left is subjected to a stress greater than the yield stress of the material (or to a stress greater than for which the specimen was designed). Sudden catastrophic fracture then takes place, completely separating the specimen.

3.3. Changes in mechanical properties during fatigue

3.3.1. Hardness

Generally soft materials (annealed steel) will become work hardened, while hard metals become softened to an extent.
However, no matter what state of hardness a particular material had at the start of the test, there is a tendency for the hardness to reach the same value. The number of cycles to fracture for two specimens of the same material, but at opposite states of hardness, are nearly the same once the stable hardness value is reached.

3.3.2. Strain-ageing or coaxing

The fatigue strength of many metals can be increased by first subjecting the specimen to a large number of cycles (10^7) at a stress below the fatigue limit. The fatigue limit will now be higher than it was before. This process is called coaxing and can give a considerable increase (30%), especially if the process is repeated, increasing the stress just slightly each time. Only those metals that can be strain hardened can have their fatigue limits increased by coaxing. The dislocation network within the material becomes increasingly tangled up, inhibiting dislocation movement.

3.4. Factors affecting the fatigue strength

3.4.1. Tensile strength

Generally the fatigue strength increases as the tensile strength of the metal increases.

Steels having a tensile strength less than 1100 MNm^{-2} have a definite fatigue limit which increases linearly with increasing tensile strength. It does not matter how the tensile strength is increased (alloying, heat-treatments or cold-work) as long as this does not crack the sample.

Steels with a tensile strength greater than 1250 MNm^{-2} lose the linearity with the fatigue limit and further increases show little improvement.

Many attempts have been made to produce a general relation to estimate the fatigue strength from the static properties of metals. None has been found, but a useful figure is the ratio:

fatigue stress/tensile stress ..... (3.2)

Steels having tensile strengths up to 1250MNm-2 have a ratio of approximately 0.5.

In steel there is a lower stress limit, below which fatigue does not occur and specimens have an infinite life.
Non-ferrous metals have no lower limit and will always fatigue (finite life).

3.5. Factors affecting fatigue life:

3.5.1. Applied stress

If a low nominal stress is applied to the specimen then fatigue takes a large number of cycles to occur. This is termed high cycle fatigue. Most of the fatigue lifetime is utilized in the initiation of a crack. There are only local plastic zones at the crack tips.

As the applied stress is increased, the crack initiation phase becomes less predominant.

If the stress is high enough then significant generalised plastic straining can occur which quickly roughens the surface from which cracks can form. The cracks propagate at a much faster rate and the process is termed low-cycle fatigue.

The two categories cannot be clearly defined.

3.5.2. Applied stress profile

The stress can be applied to the specimen following three main profiles (Figure 3.3).

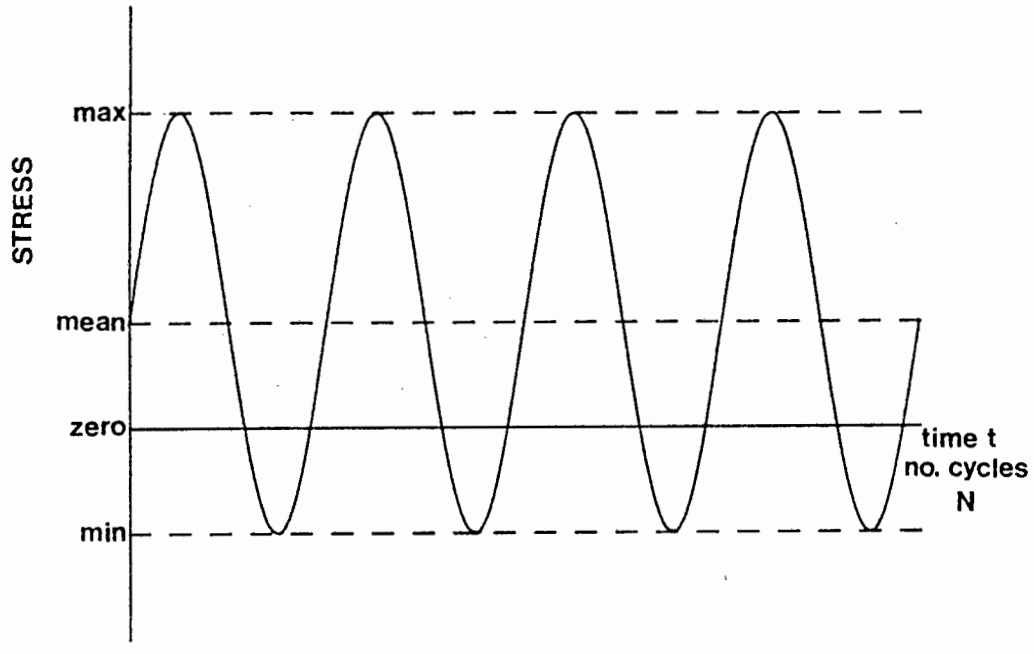

Fig.3-3. Stress profiles for fatigue testing

$$\Box\sigma = \sigma_{max} - \sigma_{min} \quad \ldots\ldots\ldots\ldots\ldots\ldots\ldots\ldots \quad (3.3)$$

$$\sigma_m = \tfrac{1}{2}(\sigma_{max} - \sigma_{min}) \quad \ldots\ldots\ldots\ldots\ldots\ldots\ldots\ldots \quad (3.4)$$

$$\sigma_a = \tfrac{1}{2}(\sigma_{max} - \sigma_{min}) \quad \ldots\ldots\ldots\ldots\ldots\ldots\ldots\ldots \quad (3.5)$$

The ratio of minimum (σ_{min}) to maximum (σ_{max}) stress is called the stress ratio. A value of -1 implies zero mean (σ_m) stress. A value of 0 implies that there is a mean stress half that of the maximum.

1. Complete stress reversal

   The stress is usually applied sinusoidally about a mean of zero. This is the type considered in this work.

2. Cyclic stress about a mean

   Again the stress is applied sinusoidally but about a non-zero mean. This can be compressive or tensile and means the specimen is always subjected to a static stress. A mean

tensile stress is the most common and causes the fatigue limit to decrease linearly with an increasing mean. Provided the specimen does not buckle, then a mean compressive stress causes an increase in the fatigue limit.

3. Complex cyclic stress

Each stress cycle follows a complex pattern. This type of profile has to be applied using electrically operated servo-hydraulic actuators.

3.5.3. Mechanical factors:

1. Size:

As the specimen size increases, the fatigue life generally decreases because the higher the surface area, the greater is the probability of a flaw existing. This can be improved by stress relieving the specimen.

2. Surface effects:

This is probably the most important effect on the specimen life, because micro-cracks are associated with conditions of the surface. Machining leaves small notches, and their depth is dependant on the coarseness of the machining itself. The fatigue life is reduced by increasing surface roughness. Therefore, usually some type of surface finishing process is employed. This typically involves grinding and/or polishing the surface. The fatigue life of a ground and polished specimen can be up to 10 times that of a lathe finish.

3. Surface residual stresses:

Machining and finishing processes can set up residual stresses on the surface of a specimen.

Compressive residual stress decreases the effect of the applied stress, resulting in an increased fatigue life.

Tensile residual stress aids the applied stress and can cause early crack initiation and thus a reduced fatigue life time

Specimens finished by a fine grind have a higher fatigue life for a given applied stress than those finished by fine grinding, followed by electro-polishing. This removes the surface stresses set up by the grinding process.

The depth to which the surface stresses extend is also important because the micro-crack has to penetrate this layer before it can open out and grow as a macro-crack

If the sample is stress relieved this destroys the surface stresses and reduces the benefits of cold-working.

Therefore the two main factors affecting the fatigue life of a given material are:

1. The surface finish (size of imperfections)

2. The type of finishing process (surface stresses)

3.5.4 Metallurgical factors:

1. Grain size:

   This is affected by the micro-structure of the material. Non-ferrous metals and annealed steel have increased fatigue life time as the grain size decreases. A material's resistance to plastic deformation generally increases as the grain size decreases. The sharpness of the knee of a fatigue graph depends on grain size: smaller grains cause sharper knees.

2. Orientation:

   The working of metals causes mechanical fibering by the alignment of grains. The fatigue life is lower when the fatigue occurs transverse to the rolling direction. The transverse life

can be 0.6 to 0.7 that of the longitudinal life. The effect becomes more pronounced with increasing applied stress.

3.5.5. Temperature effects

The higher the temperature above room temperature, the lower is the life time, and vica-versa. However, temperature only starts to become an important consideration above about 200 degC for steels.

3.5.6. Test frequency

Over the frequency range 0 to 200 Hz, the high cycle fatigue limit is not affected by the test frequency. However this is only true provided that there is not considerable temperature rise above normal. (above 50 degC).
At higher frequencies, the fatigue limit increases with increasing frequency.

The cyclic stress required to cause continuing plastic deformation at the crack tip increases with frequency increase because there is less time available in each cycle during which plastic deformation can occur. The effect is more evident in softer materials.

3.6. The appearance of fatigue

Macroscopically, a fatigue fracture surface has a smooth matt appearance usually free from markings to the naked eye. The final fracture position is usually readily visible by its rough, sharp nature.

3.6.1. Microscopic appearance

Fracture surfaces are usually studied under optical or electron microscopes (fractography).
The prominent feature is shell marks or striations which represent the position of the crack tip on successive load cycles.

The regular spacing of the striations suggests a direct relationship with the number of stress cycles. This is not always the case, because a striation is formed in one stress cycle, but each cycle does not necessarily produce a striation. Hence, there are some cycles during which the crack does not propagate.

In this work some scanning electron microscope photographs were taken of a typical fatigue surface. The striations of the crack propagation stage were clearly visible, as was the final fast fracture region (see chapter 11).

3.7. Fatigue testing

The fatigue limit/strength of a material can be defined as that stress that does not cause fatigue after 10 million cycles (10^7 cycles), but a slightly higher applied stress will cause fatigue in less cycles.

There are two main traditional methods of performing a fatigue test.

1. Reversed direct stress
2. Rotating bending

The direct stress method is preferred because:

1. The stress distribution over the specimen is uniform.
2. Static mean stresses can be applied and the specimen cross-section can be any shape.

Direct stress machines have control equipment to ensure that the desired stress cycle is constant over the whole test.

There are two classes of conventional direct-stress machines:

1. Power for the stress is produced by resonance of the system.
2. Power is provided directly by hydraulics.

Examples of resonance machines are:

(a). Schenck pulser
(b). Amsler vibrophore

These machines use an electromagnetic drive method to resonate a lumped element system in the longitudinal mode. The sample provides the stiffness component,and large weights form the mass of the system. However, these machines do not have sensitive instrumentation for taking measurements of the actual resonance parameters, such as frequency and energy loss, and they simply provide stressing energy. Dorn[26] has suggested the adding of instrumentation to such a standard machine in order to measure the parameters of the resonance and thus provide a sensitive means of studying materials undergoing cyclic stressing.

An example of a hydraulic machine is the Losenhausen UHS machine which uses hydraulics to provide the energy. The hydraulic valves of this machine are electrically operated allowing complicated stressing profiles to be produced using an electronically derived input signal.

The rotating bending machine is also very common. One end of the sample is clamped into something like a lathe chuck while the other end is subject to a perpendicular loading force. The sample is then rotated, causing tension of the upper surface and compression of the lower. It is thus a rotating cantilever. This method has many advantages:

1. The speed is varied easily
2. The number of cycles easily measured
3. The specimen does not need any elaborate features.

However, a different value for the fatigue limit is obtained by the two methods. There is also a size effect in rotating bending: the fatigue limit value shows a decrease as the diameter of the specimen increases when compared to direct stress tests.

When a material is to be fatigue tested, two main types of testing can be carried out:

1. The life at a specific stress can be determined. The number of cycles required to produce failure at the value of stress is determined.

2. The fatigue limit can be determined for a particular material, specimen shape or metallurgical format. The stress required to produce fatigue failure in less than 10^7 cycles is determined. A slightly lower stress causing no fatigue after 10^7 cycles.

---X---

CHAPTER 4

THE MODELLING OF DAMPED RESONANT SYSTEMS

4.0. Introduction

If a specimen of some material is utilised as part of a resonant system, the oscillations will be damped according to the amount of energy loss: if the energy source to the resonant system is removed then the oscillations will begin to decay in amplitude. This energy loss arises from the mounting, the drive, acoustic radiation and dissipation within the material itself. The latter is due to the internal friction of the material where the vibrational energy is converted into heat, and is the energy loss of interest in this work. The bulk properties of a material characterise the resonant system, such as the frequency which depends upon the stiffness. Since the bulk properties are affected directly by the internal atomic structure, the study of materials by their use in resonant systems provides an important technique for monitoring the internal changes of a material undergoing cyclic stressing.

The study of damping provides an important technique for the study of dislocation motion and particularly dislocation-interstitial interactions, as previously discussed in chapter 2. In the fatigue mechanism the interaction of dislocations with interstitial atoms and other lattice defects like jogs, tangled dislocations, etc play a large part.

On a macroscale, damping describes the ability of a material to dissipate energy when subject to cyclic stresses. It is important to remember that damping loss and internal friction are essentially the same thing: the internal friction of the material gives rise to damping.

Therefore, since the structure of materials and various deformation mechanisms can be studied efficiently and accurately by the monitoring of damping, considerable research has been done in this field.

Experimentally, the other loss factors are minimised as far as possible, so that the internal friction damping predominates. In this work, extraneous losses have been reduced to about one tenth of the ultimate fatigue loss, resulting in excellent sensitivity.

4.1. The Damping of Resonant Systems

As already stated, damping is the process by which vibrations steadily diminish in amplitude as energy is dissipated from the system by heat, friction or sound or as is most likely, a combination of all three. There are several types of damping models used, allowing the application of mathematics[13,14].

1. Viscous damping

   This type of damping is met with fluids, where the damping force is proportional to the velocity of motion.

2. Coulomb damping

   Damping of this nature occurs when two dry surfaces slide against each other creating kinetic friction. The damping force has a constant value.

3. Hysteretic damping

   This type of damping occurs in solids when they are deformed. It is caused by internal friction created by the deformation process and is the type of damping of interest in this work.

4.2. A Mathematical study of Viscous Damping

The classical study of a damped resonant system is one which has viscous damping. This is because the equations of motion of such a system are linear, and it is usual to try and approximate a damped system to be of the viscous type, so far as the error is not too large. However, if the internal damping of materials is represented by the viscous approximation, a large error results. This is due to the frequency dependance of viscous damping where the energy dissipated/cycle increases with frequency. In the case of material damping of the hysteretic type, the damping is virtually independant of frequency, until fairly high stressing frequencies are met, at which point other factors come into play, and the damping decreases slightly with frequency.

Consider a series mass-spring system, which is damped by a dash-pot.

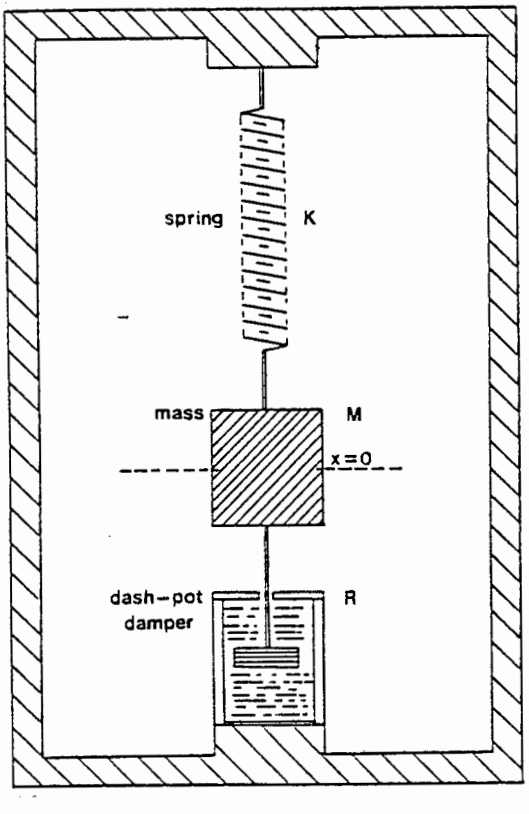

Fig.4.1. Viscously damped mass-spring system.

The damping force of the dash pot is proportional to velocity:

$$F_d = -R \frac{\delta x}{\delta t} \quad \ldots\ldots\ldots\ldots\ldots\ldots\ldots\ldots \quad (4.1)$$

The force of the spring is proportional to distance (Hooke's law for elastic deformation):

$$F_s = -Kx \quad \ldots\ldots\ldots\ldots\ldots\ldots\ldots\ldots \quad (4.2)$$

The force of the mass is proportional to acceleration:

$$F_m = M \frac{\delta^2 x}{\delta t^2} \quad \ldots\ldots\ldots\ldots\ldots\ldots\ldots\ldots \quad (4.3)$$

The forces must balance and thus combining (4.1), (4.2), (4.3):

$$-Kx - R\frac{\delta x}{\delta t} = M\frac{\delta^2 x}{\delta t^2} \quad \ldots\ldots\ldots\ldots\ldots\ldots\ldots \quad (4.4)$$

If a solution of the form Ce^{st} is assumed, this produces a characteristic equation for (4.4):

$$s^2 + s\frac{R}{M} + \frac{K}{M} = 0 \quad \ldots\ldots\ldots\ldots\ldots\ldots\ldots \quad (4.5)$$

The roots of this equation are:

$$s_{1,2} = -\frac{R}{2M} \pm \sqrt{\frac{R^2}{4M^2} - \frac{K}{M}} \quad \ldots\ldots\ldots\ldots\ldots\ldots \quad (4.6)$$

The roots of interest are those which represent a damped oscillatory system:

$$\frac{R^2}{4M^2} < \frac{K}{M} \quad \ldots\ldots\ldots\ldots\ldots\ldots\ldots\ldots \quad (4.7)$$

It can be shown that this condition produces a solution for the equation of motion as:

$$x = X_0 \exp\frac{Rt}{2M} \quad (A\cos w_d t + B\sin w_d t) \quad \ldots\ldots\ldots \quad (4.8)$$

where $$wd = \sqrt{\frac{K}{M} - \frac{R^2}{4M^2}} \quad \ldots\ldots\ldots\ldots\ldots\ldots \quad (4.9)$$

and w_d = damped radian frequency

The undamped natural frequency w_0 for this system is given by:

$$w_0 = \sqrt{\frac{K}{M}} \quad \ldots\ldots\ldots\ldots\ldots\ldots\ldots \quad (4.10)$$

Inserting (4.10) into (4.9) reveals:

$$w_d = w_0\sqrt{1 - \frac{R^2}{4M^2}} \quad \ldots\ldots\ldots\ldots\ldots \quad (4.11)$$

Hence the damping alters the natural frequency of oscillation.

4.2.1. The Logarithmic Decrement of oscillations

If the energy source sustaining the resonance is removed, then the oscillations will begin to decay exponentially by viscous energy loss (Figure 4.2).

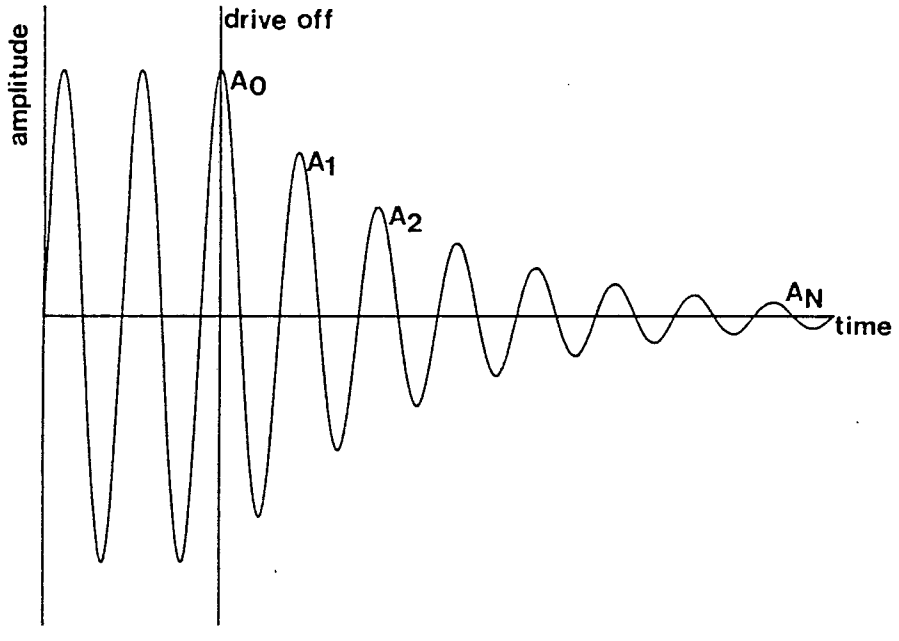

Fig.4.2. Exponential decay of a damped oscillating system.

The successive amplitudes have a simple logarithmic relation to one another.

If the amplitude at time t = 0 is A_0 then

One cycle later the amplitude will be A_1 at $t = \tau_d$
Two cycles later the amplitude will be A_2 at $t = 2\tau_d$
After N cycles the amplitude will be A_N at $t = N\tau_d$

Thus:

$$t = 0 \qquad A_0 = A \qquad \ldots\ldots\ldots\ldots\ldots\ldots \qquad (4.12)$$

$$t = \tau d \qquad A_1 = A_0 \exp\left(-\frac{R\tau d}{2M}\right)$$

$$t = 2\tau d \qquad A_2 = A_0 \exp\left(-\frac{R2\tau d}{2M}\right)$$

$$t = N\tau d \qquad A_N = A_0 \exp\left(-\frac{RN\tau d}{2M}\right) \qquad \ldots\ldots\ldots \qquad (4.13)$$

Equation (4.13) can be re-written in a logarithmic form:

$$\mathrm{Ln}\left(\frac{A_n}{A_0}\right) = \frac{NR}{2M}\,\tau_d \qquad \ldots\ldots\ldots\ldots\ldots\ldots\ldots\ldots \qquad (4.14)$$

4.2.2. Terms related to the damping of oscillations

1. The Specific-Damping-Capacity is defined as the ratio between the energy dissipated per cycle to the total energy in the system:

$$\mathrm{SDC} = \frac{\text{Energy lost/cycle}}{\text{Total energy}} = \left| -\frac{\delta E/\delta N}{E} \right| \qquad \ldots\ldots \qquad (4.15)$$

2. The "quality-factor" or Q factor is an electrical term used to describe the quality of an electrical resonator. One with a high Q has a very sharp resonance curve and therefore a low energy loss. The SDC is inversely related to the Q-factor by a factor of 2π. In this work, it is The Q of the resonant system that is measured, and therefore, it is important to relate it to the mechanical system term.

$$Q = \frac{2\pi}{SDC} = -2\pi \frac{E}{\delta E/\delta N} \quad \ldots\ldots\ldots\ldots\ldots\ldots \quad (4.16)$$

re-arranging:

$$\frac{\delta E}{E} = \frac{-2\pi}{Q} \delta N \quad \ldots\ldots\ldots\ldots\ldots\ldots\ldots\ldots \quad (4.17)$$

Integrating both sides yields the following:

$$E_N = E_0 \exp\left(\frac{-2\pi N}{Q}\right) \quad \ldots\ldots\ldots\ldots\ldots\ldots\ldots \quad (4.18)$$

Since the energy is proportional to the square of the amplitude:

$$A \equiv \sqrt{E}$$

and so:

$$A_N = A_0 \exp\left(-\frac{\pi N}{Q}\right) \quad \ldots\ldots\ldots\ldots\ldots\ldots\ldots \quad (4.19)$$

Again this can be re-written in a logarithmic form:

$$Q = \text{Ln} \frac{\frac{\pi N}{A_0}}{A_N} \quad \ldots\ldots\ldots\ldots\ldots\ldots\ldots\ldots \quad (4.20)$$

Referring back to equation (4.13) and noting that for a decaying waveform of frequency w_d, then the period τ_d is:

$$\tau d = 2\pi/w_d \quad \ldots\ldots\ldots\ldots\ldots\ldots\ldots\ldots \quad (4.21)$$

Thus we can insert (4.21) into (4.13):

$$A_N = A_0 \exp\left(-\frac{\pi NR}{wM}\right) \quad \ldots\ldots\ldots\ldots\ldots\ldots\ldots \quad (4.22)$$

Thus comparing the exponential power expressions for equations (4.19) and (4.22) yields:

$$Q = Mw/R \quad \ldots\ldots\ldots\ldots\ldots\ldots\ldots\ldots \quad (4.23)$$

Inserting (4.23) into (4.11) gives:

$$w_d = w_0\sqrt{1 - \frac{1}{4Q^2}} \quad \ldots\ldots\ldots\ldots\ldots\ldots\ldots \quad (4.24)$$

or

$$f_d = f_0\sqrt{1 - \frac{1}{4Q^2}} \quad \ldots\ldots\ldots\ldots\ldots\ldots\ldots \quad (4.25)$$

The Q and the loss are inversely related.

$$L = 1/Q \quad \ldots\ldots\ldots\ldots\ldots\ldots\ldots\ldots \quad (4.26)$$

Inserting (4.31) into (4.30):

$$f_d = f_0\sqrt{1 - \frac{L^2}{4}} \quad \ldots\ldots\ldots\ldots\ldots\ldots\ldots \quad (4.27)$$

Equation (4.31) can be re-written as:

$$\frac{f_d}{f_0} + \frac{L^2}{4} = 1 \quad \ldots\ldots\ldots\ldots\ldots\ldots\ldots \quad (4.28)$$

This is the equation of a circle and shows how the frequency varies as a ratio of the undamped frequency with the loss (Figure 4.2).

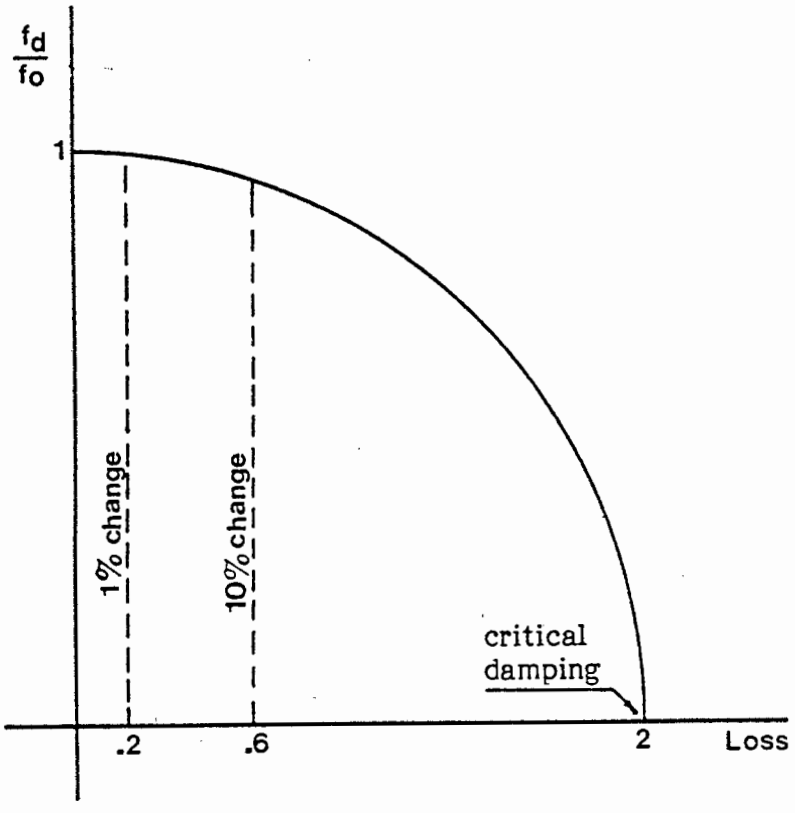

Fig.4.3. The variation in natural frequency with damping.

Hence, it can be seen that if the loss is small, then the almost zero slope region at the top of the circle is the region of operation and the damped and undamped frequencies will nearly be equal (ratio ≈ 1.000). A value of 2 for the loss (a Q of 0.5), corresponds to a critically damped system. A slight increase in loss from this value, implies that the system will not oscillate.

The equation for the decrement of amplitude is used as the basis of Q-measurement for this work, and is discussed in chapter 6. The implementation as an electronic system is described in chapter 10.

It is important to realise that the change in frequency during a fatigue experiment is not due to the change in damping but a metallurgical change which alters the Youngs modulus and hence the stiffness of the material. The change in damping during an experiment causes little change in frequency.

The following demonstrates this for a typical experiment:

f at start = 149.2 Hz
Q at start = 820

f at end = 143.1 Hz
Q at end = 230 Hz

If the starting frequency is corrected for the change in Q alone then the end frequency should be:

f_d at end = 149.1986 Hz

Hence, the $1/Q^2$ term of the equation ensures that the Q has little effect on the frequency until it drops to about 5, where it produces a 1% change in frequency.

4.3. Hysteretic damping

In the case of hysteretic damping of materials, the damping force can be modelled as being proportional to velocity and inversely proportional to frequency. The damping constant in this case is the hysteretic damping constant h:

$$F_d = \frac{h}{w}.\frac{\delta x}{\delta t} \quad \ldots\ldots\ldots\ldots\ldots\ldots\ldots\ldots \quad (4.29)$$

If the steps for the case of viscous damping are repeated then:

The total force:

$$F_T = Kx + \frac{h}{w}\cdot\frac{\delta x}{\delta t} \quad \ldots\ldots\ldots\ldots\ldots\ldots\ldots \quad (4.20)$$

but

$$x = X\sin wt \quad \ldots\ldots\ldots\ldots\ldots\ldots\ldots\ldots \quad (4.31)$$

and

$$\frac{\delta x}{\delta t} = wX\cos wt \quad \ldots\ldots\ldots\ldots\ldots\ldots\ldots\ldots \quad (4.32)$$

Inserting (4.31) and (4.32) into (4.30) gives the total force as:

$$F_T = KA\sin wt + \frac{h}{w} A\cos wt \quad \ldots\ldots\ldots\ldots\ldots \quad (4.33)$$

This represents the equation of an ellipse, or a hysteresis loop:

$$\left(\frac{x}{A}\right)^2 + \left(\frac{F_T - Kx}{hA}\right)^2 = 1 \quad \ldots\ldots\ldots\ldots\ldots\ldots\ldots \quad (4.34)$$

The intercept of the hysteresis loop on the force axis F, depends on the value of the hysteretic damping constant and the maximum displacement A.

$$\text{When } x = 0 \quad f = \pm hA \quad \ldots\ldots\ldots\ldots\ldots\ldots \quad (4.35)$$

If d is the intercept on the displacement axis x then:

$$\text{When } f = 0 \text{ then } x = d = -\frac{h^2A^2}{h^2+K^2} \quad \ldots\ldots\ldots \quad (4.36)$$

$$\text{and } \frac{h}{K} = \frac{d}{X^2-d^2} \approx \frac{d}{X} \quad \ldots\ldots\ldots\ldots\ldots\ldots\ldots \quad (4.37)$$

For light damping the value of d is small compared to A and the approximation above is adequate for evaluating the hysteretic damping constant.

The decay of oscillations for an hysteretically damped system has the same logarithmic relationship as for the viscous damping case: the hysteretic decrement can be found as for the viscous case.

$$A_N = A_0 \exp(-hN/\pi k) \qquad \ldots\ldots\ldots\ldots \qquad (4.38)$$

Comparing equations (4.13) with (4.38) shows that the hysteretic model for damping is independant to frequency.

The hysteretic damping constant h is a measure of the hysteresis loop and is a property of the material.

4.4. Variation of damping with frequency

In practice, materials do exhibit some variation of damping with frequency. Usually this only starts to become prominent for higher frequencies (above 1KHz, say). This frequency dependence is probably due to thermal effects where the high frequency does not allow a sufficient heat flow rate across grain boundaries, causing local hot-spots.

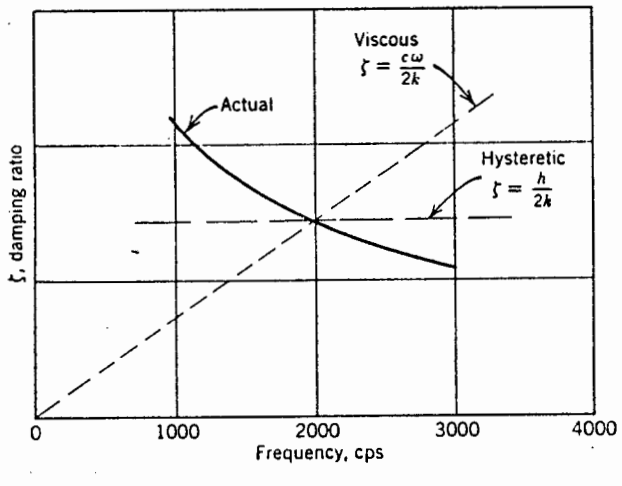

Fig.4.4. The variation in damping with frequency.

CHAPTER 5

EXPERIMENTAL TECHNIQUES USED TO STUDY MATERIAL PROPERTIES BY RESONANCE METHODS.

5.0. Introduction

When a wave travels through a medium, or when resonance occurs, a fraction of the energy is dissipated into heat by internal friction. In wave propagation, this gives rise to attenuation, and in a resonator, to a finite "Q"-factor. There are many mechanisms for this loss, but in this work, it is that due to the defects produced by fatigue, which is to be measured. A convenient way of expressing the loss is by the loss angle (in radians), as used in electrical and mechanical sytems. In wave propagation, it is equal to 0.037 x attenuation (in dB per wavelength), and in resonators it is 1/Q (in radians). In a typical test, the initial loss angle is about 10^{-3} and this rises to 10^{-2} when material fracture occurs.

The earliest measurements of internal friction were made by observing the decay of the torsional resonance of wires loaded by an end weight. This was done by Weber in 1837[7]. The free decay of oscillations was found to be directly related to the internal friction. Torsional methods are still used today as it provides a means of observing slowly occuring processes: eg the diffusion of ions through metals and the motion of grains in polycrystalline metals.

The present technique is to measure the frequency and internal friction (damping), of resonant bars in longitudinal, torsional and flexural modes. The latter being used in this work. One of the first to use this method was Wegel and Walther in 1935[14]. The particular method used depends upon various criteria:

1. The phenomenon to be observed
2. The size of the specimens to be tested
3. The cyclic stress required
4. The availability of apparatus.

5.1. Experimental techniques for damping measurements

There are six main techniques for the measurement of energy loss or damping of a resonant system.

1. The free-decay of oscillations

   The energy source sustaining the resonance is removed and the decay of the oscillations is observed, from which the damping or internal friction can be calculated directly. This is the technique used in this work, but it does have several disadvantages. The damping is amplitude dependant due to air-loading effects and material non-linearities (anelasticity). Therefore, it is impossible to measure the true damping at a specific amplitude with this method. The decay envelope is non-exponential, and hence the damping coninually changes during the decrement, causing an average value to be measured over the sampling period (Figure 5.1).

   The main advantage is that it is an easy type of measurement method for implementation under electronic control, and it is very accurate for cases of low damping. The non-linear effects can be virtually eliminated by sampling the envelope once the amplitude has fallen to low values. Here the decrement has reached the exponential form.

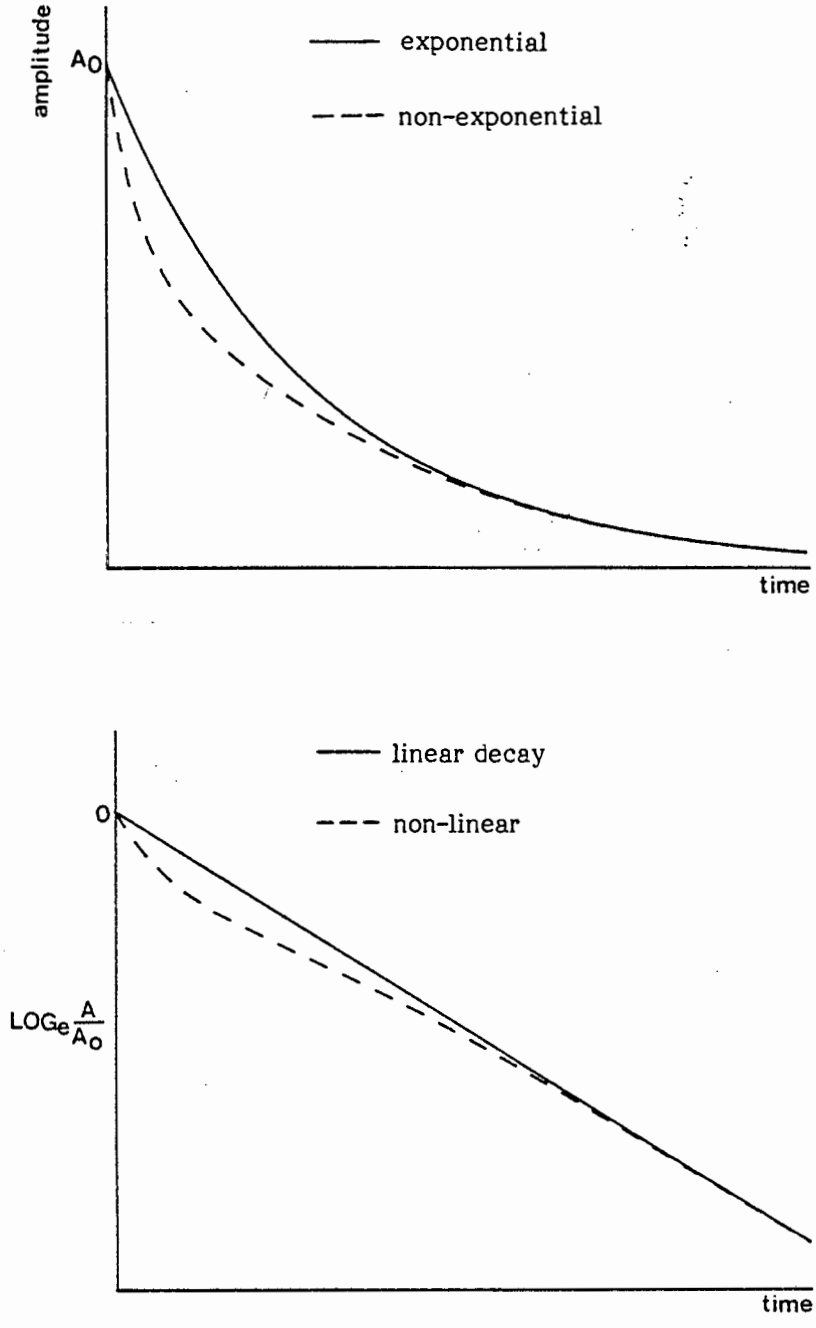

Fig.5.1 Non-linear decay. a. decay envelope. b. variation in decay constant.

2. The Bandwidth of the resonance curve

With this method the frequencies f_1 and f_2, corresponding to a drop in amplitude of $\sqrt{2}$ from the peak amplitude are found, either side of the resonance point (Figure 5.2). These frequencies correspond to the -3dB points in electrical resonating systems, where the power has dropped to half the initial value.

This technique is virtually impossible to implement for this type of work because of the inherent low damping in metals. A resonating system with little damping has an exremely sharp resonance curve, hence the -3dB points have to be determined on an almost infinite slope, where the amplitude is sensitive to frequency changes (Figure 5.2). This creates the problem of amplitude dependence of damping, since in the process of searching for the -3dB points, the accompanying amplitude change will cause their values to change from what they were at the resonant frequency.

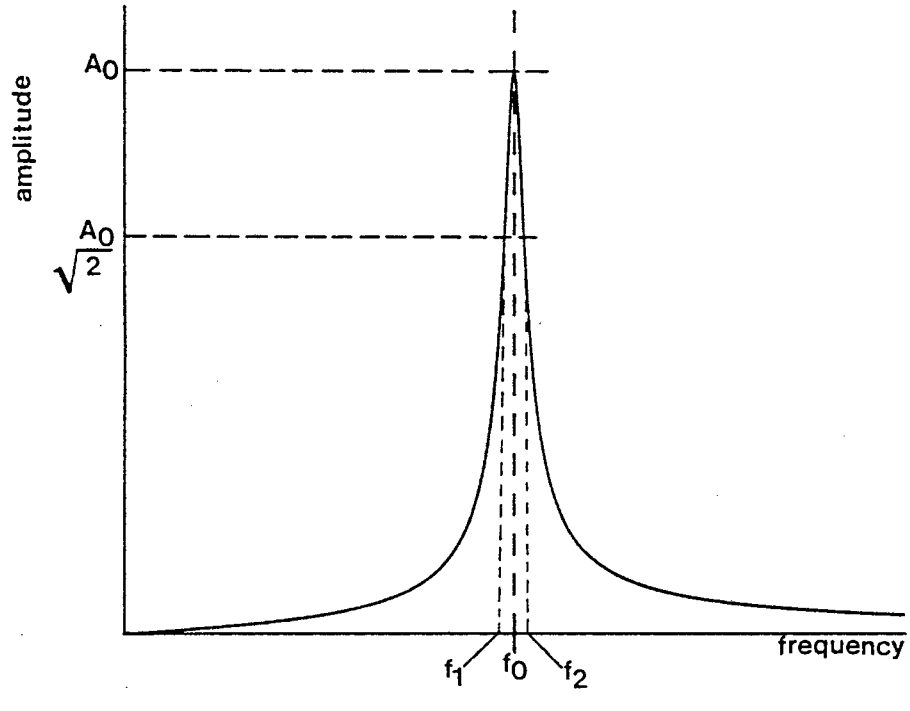

Fig.5.2. Resonance curve for lightly damped systems.

3. The rate of temperature rise

This method requires the temperature to be measured at several spaced sections along the resonating specimen, at which the stress amplitude must also be known. Axial thermal conduction along the specimen produces temperature changes at the measurement points, due to energy dissipation within the material. The damping is calculated by applying the appropriate thermodynamic equations to the data.

The chief advantage of this method is that the results are not affected by windage and support losses. However, the method is rather cumbersome and the accuracy depends upon the extent to which extraneous heat lost due to radiation and convection can be corrected.

4. Energy input to the system

This is a good method because the damping is measured in steady-state vibration so that the damping at a specific amplitude can be measured unambiguously. The damping is calculated from the energy input to the system, and from the amplitude of the oscillations. This technique however includes the energy losses of the other components of the system: eg the losses due to the inefficiency of the resonance actuator.

5. The resonant-dwell technique

The damping is found directly by measuring the phase lag between stress and strain. This method enables steady-state damping to be measured, but it does have several draw-backs: The strain cannot be measured directly by using strain gauges since these usually fail, especially during fatigue tests. The strain is usually calculated from the amplitude and by applying the dynamic equations to the beam.

6. Impedance measurements

The dynamic impedance of the resonating system is measured and the loss component found. This is analogous to an electrical resonator consisting of a series RLC circuit. At resonance the impedance of the inductance and capacitance components (L&C) exactly cancel each other out, leaving the resistance or loss component (R).

This technique allows steady-state measurements to be made, but again the losses due to other components of the system are included in the measurement.

The difficulty with any damping measurement is to try and isolate the resonator from the surroundings as much as possible, to eliminate extraneous energy loss. The main losses are due to the support and the drive mechanism. Since the energy supply for the oscillations must be coupled to a certain degree to the resonator, some energy will always be lost by the coupling between the drive and resonator. Similarly, energy will be lost through the support, depending upon the resonator/support coupling. The tuning fork has the particular advantage that it is dynamically balanced and hence the clamping loss is second order compared to, say, a vibrating reed.

The methods which measure the damping at steady-state amplitudes, are unsuitable for this work because of the considerable air-damping and anelasticity effects found with the tuning forks. The free-decay method is the best, because it allows the damping to be measured at low amplitudes, where these effects are reduced to low values.

5.2. The use of resonance techniques for fatigue testing

There are many advantages in using resonance for performing fatigue tests:

1. There is an inherent force amplification with vibrating systems, which eliminates the need for powerful sources to apply stresses to the test specimens. This is the case with hydraulic fatigue testing machines, as described in chapter 3, which soon become worn and require servicing.

2. Fatigue cracks which are visually obscurred can be detected by changes in the resonant properties of the system, namely resonant frequency and damping.

3. The inherently higher testing frequency using resonance, speeds up otherwise tedious testing by the much slower conventional hydraulic machines.

4. A resonant system is very sensitive to any changes in the parameters (stiffness and internal friction) of its elements, and hence very small changes can be detected.

5. The internal changes to the material can be investigated on an atomic or crystal scale, allowing various mechanisms and models to be studied.

6. The testing frequency can be changed by altering the parameters of the system, such as mass loading or geometry[24].

The latter point could also be considered a disadvantage since the frequency is not entirely a freely adjustable parameter. Another drawback is that the waveform of the stressing cycles is always approximately sinusoidal.

5.2.1. The use of flexural resonance

Flexural resonance is the type considered in this work. It is ideal for specimens that are non-circular in shape and for single-plane cyclic stressing. Flexural testing is usually required separately, since it is difficult to relate tests performed in some other mode of resonance, particularly torsion. Flexure is also the most common mode of structural vibration.

There are four main types of flexural configurations that the specimens can have, all of which have disadvantages.

1. Double cantilever beam:

   An electromagnetic shaker is usually used to provide energy for the system, and it also forms the support. Therefore, it is intimately coupled to the system, acting as a damper, and producing a fairly high energy loss. An additional problem is that of exactly balancing the beams so that a double resonant peak does not occur. This however is easy to cure by using small amounts of putty as balancing weights until the double peaked response disappears.

   The advantage is that this shape of beam provides an unambiguous stress concentration at the base.

2. Tuning fork:

   The tuning fork provides an ideal dynamically balanced system for oscillation, which is easily supported. There is a large amount of coupling between the tynes at the root, reducing the effect of any imbalance. There is no net force exerted on the support or clamp, nor on the drive mechanism. The extraneous losses due to the clamp and the drive can be made very small. The disadvantage is that there is a complicated stress field at the base of the tynes, and the shape of the specimens is very limited. This problem was solved by Dolan[15] where the specimen actually formed the root of a tuning fork like system.

3. Centre driven clamped-clamped beam:

It is very difficult to reduce the external energy losses in this configuration according to Adams and Bacon[16].

4. Centre driven free-free beam:

This configuration is the least susceptible to extraneous damping[16]. However, it is difficult to optimise the supports and is only suitable for small amplitudes of vibration where the supports do not have to be strong. Therefore it is of no use in fatigue studies which require substantial stress amplitudes.

5.2.2. The effect of air damping on flexural resonators

In any type of flexurally oscillating system, the part of the resonator subject to the least stress (antinode), has the greatest freedom of motion and consequently the largest amplitude of vibration. In the case of the double cantilever beam, this occurs at the ends of the beams, and similarly with a tuning fork, at the ends of the tynes. Considerable displacement of air can take place, especially at large vibration amplitudes, resulting in a significant energy dissipation.

The air-damping loss factor is proportional to the (velocity)^2 (Gibson and Plunkett[17]). This makes the damping non-exponential at high amplitudes.

$$\Omega_a = K\frac{p_a}{p_m}\frac{wL}{h} \qquad \text{.....} \qquad (5.1)$$

Where:

Ω_a = air damping
K = coefficient
p_a = air density
p_m = beam density
w = beam deflection
L = beam length
h = beam thickness

According to Adams and Bacon[16], air damping is due to the viscosity and inertia of the air which are functions of the Reynolds number (Re) defined by:

$$Re = \frac{p_a v h}{\mu} \quad \ldots\ldots\ldots\ldots\ldots\ldots\ldots\ldots\ldots\ldots \quad (5.2)$$

Where:
v = beam velocity
μ = air viscosity

According to Hoener 1965[16], the drag coefficient Cd of rectangular plates can be split into either viscous loading or inertial loading depending on the Reynolds number:

For Re < 10 Cd is proportional to 1/Re (viscous)
Re > 100 Cd is ≈ constant (inertial)

$$Cd = \frac{\text{drag force}}{\frac{1}{2}p_a v^2 bL} \quad \ldots\ldots\ldots\ldots\ldots\ldots\ldots\ldots \quad (5.3)$$

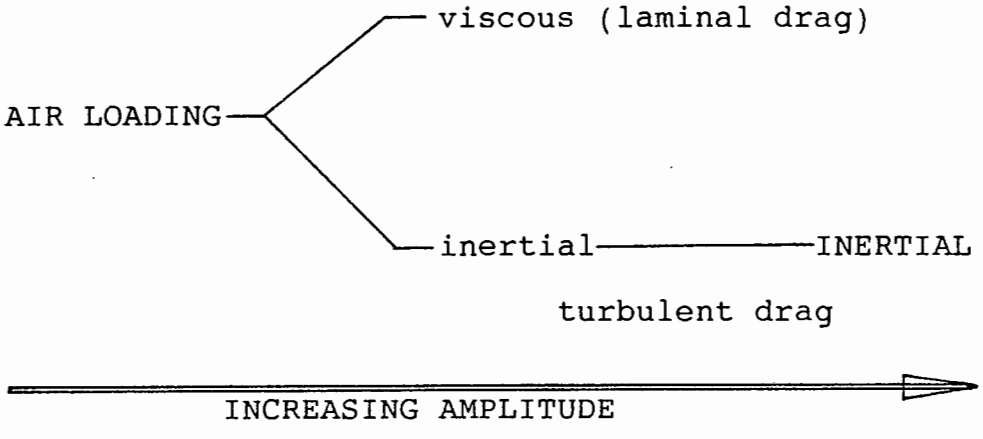

However, it is difficult to calculate the air damping in practice because the velocity of the beam changes along its length from zero at the base to a maximum at the free ends. Furthermore, Hoerners results are for steady flow, whereas in this case, due to the oscillation of the beam, the flow is accelerating and reversing.

An approximate value for the specific damping capacity can be found:

$$SDC \approx \mu f \quad \text{for } Re < 10 \quad \ldots\ldots\ldots\ldots\ldots\ldots \quad (5.4)$$

$$SDC \approx p_a f^2 w \quad \text{for } Re > 100 \quad \ldots\ldots\ldots\ldots\ldots\ldots \quad (5.5)$$

Where f = frequency of vibration.

Air damping depends on the following factors:

1. The mode of vibration (fundamental, 1st overtone, etc)
2. The beam geometry
3. The amplitude of vibration
4. The frequency of oscillation
5. The air temperature which affects the density and viscosity.

It is thus an extremely complex phenomena to try and predict by theory, and it is best investigated by experimentation, by testing first in air and then in vacuo.

In this work, the air was found to have a considerable damping effect. This was investigated by increasing the air loading by inserting flat pieces of plastic in the space between the electromagnet core and the oscillating magnets stuck to the ends of the tynes. The slightest change in thickness produced a fairly large change in Q factor. Hence, during the free-decay of the oscillations, the initial large amplitude has a significant air damping term and the decay is thus non logarithmic. The decay is further complicated by the amplitude dependance of damping in the anelastic region (Figure 5.1).

Therefore, in order to obtain an accurate measure of the internal friction of the sample, the Q measurements were performed by sampling the decay once the amplitude had fallen to a low value. This is where the envelope is approaching linearity, and hence where the effects of air damping and non-linearities due to anelasticity

are reduced to low values. The Q value obtained in this way then gives a reasonably good picture of the internal changes only of the metal.

5.3. Literature review of some previous research work

There are two main classes of experimental that has been done; the measurement of damping at stresses below the fatigue limit, and studies that have included fatigue

5.3.1. Damping measurements using longitudinal resonance.

1. Lee and McConnell 1975 [18]: Five different techniques were used to measure the internal losses of aluminium, steel and brass in the form of thin cylindrical rods undergoing longitudinal resonance. The results of the different techniques were compared to check their validity.

2. Guberman and Beshers 1968 [19]: Cylindrical rods were driven in the longitudinal mode using an electromagnetic drive. The sample was held at a nodal point in the centre and the amplitude dependence of damping in iron was investigated.

3. Adams 1972 [20]: Specimens in the form of round bars were vibrated in the longitudinal free-free mode by the use of a magnetostrictive transducer. The damping was measured using the temperature rise technique. The experimental technique is described in another paper by Adams and Percival 1969[33]. The specific damping capacity of a wide range of engineering materials was determined for stresses up to the fatigue limit.

4. Adams and Fox 1972 [21]: An axially vibrating lumped element type system was used, where the specimen provides the stiffnes element connecting two large masses. The system was driven into resonance by an electromagnetic shaker. The specific damping

capacity was measured from the input electrical power and the displacement amplitude. This technique is most suitable for measurements on high damping capacity materials, e.g. cast iron. An attractive feature is that the region fatigued undergoes uniform stress.

5.3.2. Damping measurements using torsional resonance

1. Butera and Craig 1966 [22]: The internal friction of specimens in the form of wires, forming part of a torsional pendulum, were measured at constant amplitude. Here, of course, the stress is concentrated at the surface. A positive feedback system was used to maintain the amplitude at a constant value. The damping was measured from the input power to the system.

2. Miszenti 1966 [23]: The internal friction of specimens was measured by utilising them as part of a low frequency torsional oscillator. The oscillations were maintained at constant amplitude using a feedback system. The damping was measured from the free-decay decrement.

5.3.3 Damping measurements using flexural resonance

1. Adams and Bacon 1973 [16]: The dynamic properties of specimens in the form of thin flat strips was investigated by vibrating them in flexure. This type of specimen could not be longitudinally vibrated as they are likely to buckle during a compressive cycle. Two types of flexural resonator were considered: a double cantilever beam and a free-free beam excited in the centre. The damping was measured from the energy input to the system.

2. Gibson and Plunkett 1977 [17]: A double cantilever beam specimen driven in the centre by an electromagnetic vibrator was used to investigate the damping of structural materials at various frequencies and amplitudes. In order to reduce the effects of

air damping, the specimens were tested in a plexiglas chamber at low pressure. The damping was measured using the resonant dwell technique (phase relationship between force and displacement).

3. Schabtach C. and Fehr R.O. 1944 [24]: Damping tests were performed on specimens in the shape of tuning forks, very similar to those used in this work. A series of small feet were machined along the length of the tynes in order to narrow the gap between them. No continuous drive was employed to sustain the oscillations and only damping measurements by the free-decay of oscillations were performed. The forks were set into resonance by pulling out a spreader between the feet, and recording the free-decay on paper. An electrical signal corresponding to the oscillations was derived by the use of a strain gauge and the temperature was monitored using a thermocouple. Different frequencies were chosen by cutting down the tynes to the next pair of feet.

5.3.4. Fatigue experiments using longitudinal resonance

1. Barker and Noble 1978 [25]: A system was developed for testing the fatigue life of helical coil springs. The springs were vibrated axially by an electromagnetic shaker. An elaborate microprocessor control system was devised to keep the amplitude constant during a test and to perform automatic measurements of frequency, amplitude and number of cycles ellapsed.

2. Dorn 1982 [26]: A standard resonance fatigue machine of the lumped element type, where the specimen provides the stiffness element for axially vibration, was modified and instrumentation added. The damping and resonant frequency of the system were recorded during fatigue tests. The damping being measured from the input power to the sytem.

3. Schlät 1982 [27]: The specimen forms part of a lumped mass-stiffness, axially vibrating system. A control system is utilised to keep the amplitude constant during a fatigue test. The dynamic compliance (1/stiffness), and the resonant frequency were monitored during fatigue tests.

4. Mason 1956 [8]: An ultrasonic method was used to fatigue small samples of metal to destruction. The power for the resonance was provided by a barium-titanate piezoelectric transducer fixed to an exponentially tapered horn to concentrate the stress waves over a small surface area. The internal friction was determined by measuring the Q of the system with and without the sample attached.

5. Klimasara, Fiore and Kuczynski [32]: The sample was kept at the resonant frequency by means of a phase-locked loop. The damping was found from the bandwidth or by recording the free-decay on a chart recorder. The main benifit of this system was that the sample may be placed in a hostile environment at a far distance from the monitoring and recording components.

5.3.5. Fatigue experiments using torsional resonance

1. Hanstock 1946 [28]: Torsional resonance vibrations were excited by an electromagnetic drive system. A control circuit was employed to keep the amplitude constant during a test. The damping capacity was found from the free-decay of the oscillations. It was found that the formation of a fatigue crack caused a sharp increase in the damping capacity and a fall in resonant frequency.

5.3.6. Rotating beam tests:

1. Lazan and Wu 1951 [29]: The specimens used were in the shape of rods and were clamped at each end to a support. The support at one end is rotated and the support at the other end was fixed to a loading weight. The system operates as a rotating cantilever and the damping capacity was found from the force required to keep the rod rotating at a constant velocity.

5.3.7. Fatique experiments using flexural resonance

This is the method used in this work and therefore more interest was taken in the previous research using similar methods.

1. Marloff 1980 [30]: The fatigue strength of turbine blade components were tested. The specimens were vibrated in flexure by an electromagnetic shaker and at the same time subjected to a static axial force in order to try and model the real life conditions in use. A control system was used to keep the oscillations sustained at constant amplitude during a fatigue test. The damping was measured from the input power to the system and from the amplitude of the oscillations.

2. Whaley, Chen and Smith 1984 [31]: Fatigue tests were performed on specimens in the shape of double cantilever beams and energy was provided by an electromagnetic shaker. Only one beam was instrumented, the other providing a balanced system. In order to eliminate the effects of air damping, the experiments were performed inside an evacuated plexiglas chamber. Damping was calculated from the input force and strain amplitude by employing the dynamic equations of motion to the beams.

3. Dolan 1951 [15]: The test specimen was suspended between two heavy masses which exert bending stresses to the specimen. The system operates as a large tuning fork where the tynes are formed by the heavy masses and the specimen forms the root. The

vibration was excited by an electromagnetic shaker and a control circuit was used to keep the amplitude constant. No measurements of damping or resonant frequency were made, the main advantage of this system being the force amplification at resonance.

Studying the above was useful in providing a good background to the different methods tried and their merits.

---X---

CHAPTER 6

THE TUNING FORK AND DRIVE MECHANISM

6.0. Introduction

The tuning fork was invented in 1704 by John Shore to give musicians a precise reference of pitch, which we now identify as frequency[34]. In the standard configuration, the tynes vibrate in and out with a relatively large amplitude and the spigot at the root vibrates axially at the same frequency, but with a smaller amplitude.

When held against a sounding board, enough energy is transmitted by the spigot to produce a good audible sound. In the late 19th century Lissajou, Koënig and Rayleigh used it as a frequency standard, Rayleigh maintaining the oscillations electrically.

An empirical understanding of the vibrational pattern and frequency was given by Rayleigh. He considered the flexural vibration of a straight uniform bar with two nodes half a wavelength apart and about a quarter of a wavelength from the end, and having an antinode at the centre. If the bar is progressively bent to the shape of a fork, the two nodes move together with the antinode between them. The form of the vibrations is shown in Figure 6.2. The frequency is approximately equal to that of a reed of the same dimensions where the length is equal to that of the tynes but with a small added end correction. The first overtones of both reed and fork are approximately the same: about six times the fundamental, an agreement which underlines the usefulness of Rayleighs model.

In this work, the oscillations are sustained electrically using an electromagnetic drive system. An electronic control circuit keeps the vibration amplitude constant throughout the life of an experiment. The purpose of this chapter is to describe the tuning fork in general and the drive system.

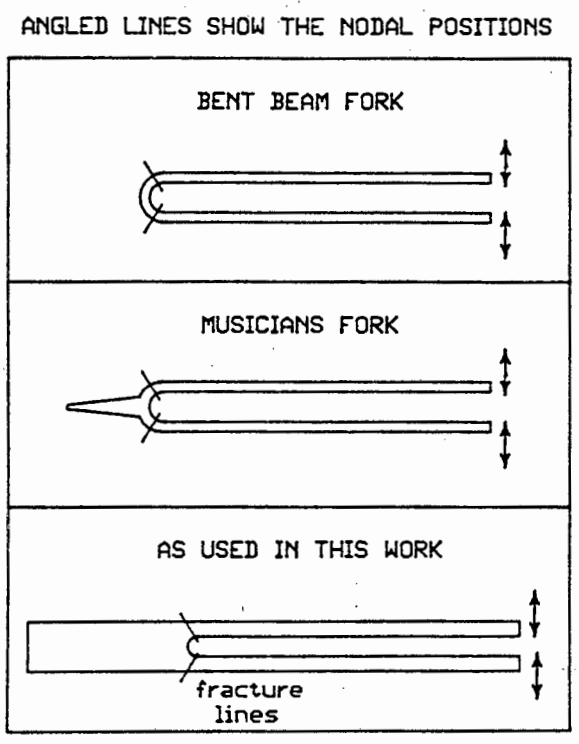

Fig.6.1. Tuning forks

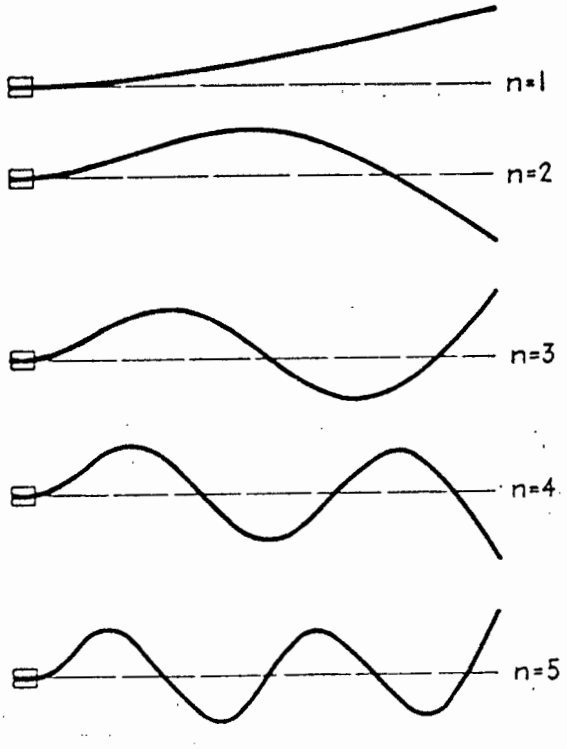

Fig.6.2. Shape of a vibrating bar clamped at one end for the first five overtones.

6.1. The electromagnetic drive

The ends of the tuning fork tynes are positioned between the pole faces of an electromagnet. If a sinusoidal current is fed through the winding of the electromagnet, then an oscillating magnetic field is set up, which attracts and repels the tynes, provided of course that they magnetic. At the resonant frequency, a large amount of energy can be transferred to the motion of the tynes, and they will begin to oscillate.

There are essentially two ways in which this method can be implemented (Figure 6.3):

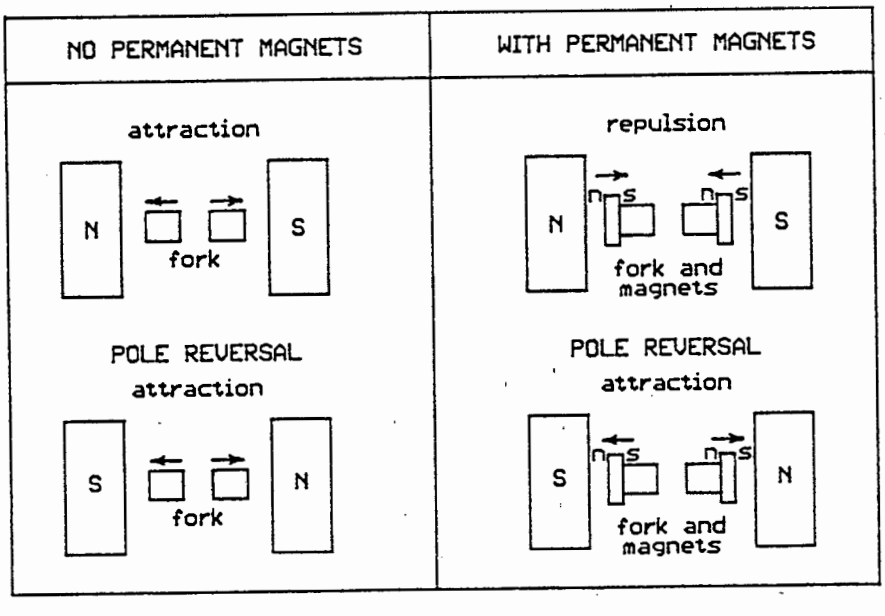

Fig.6.3. Magnetic drive of tuning forks

1. The material of the tynes must be magnetic or at least metallic, in which case they will be attracted at every half cycle of the magnetic field and the electromagnet coil frequency will then operate at half the resonant frequency of the tuning forks. The disadvantage of this method is that only magnetic materials can

be used for the tuning forks and a fairly high current will be required to produce enough magnetic force. Furthermore, the electronics will be more complicated in order to accommodate the halving in frequency of the drive current.

2. The second method uses small powerful magnets which are glued to the ends of the tynes with opposite polarity. The tynes will be attracted in one half cycle and repelled in the next, therefore the drive current frequency will be identical to the resonant frequency simplifying the electronics. Since the magnets are very powerful, they are sensitive to magnetic fields, and a much lower drive current will be required to produce the required force, making this method more efficient. Furthermore, any material may now be used for the tuning forks, because the magnets provide the magnetic interaction. This is the method adopted in this work and the use of the magnets give a high electro-mechanical efficiency that was hitherto unattainable.

The magnets used are of the samarium-cobalt type and are very powerfully magnetised. They are in the shape of thin rectangles, magnetised across the width, an ideal configuration for this work. The electromagnet was constructed out of a finely laminated "U" core of the normal 50Hz power transformer variety. The dimensions of the tuning forks were chosen so that the resonant frequency would not be more than 200Hz, so that this core would work satisfactorily without large eddy current losses. The main problem with an electromagnet of this type is the inductance of the winding which limits the current flowing through it.

The design of the winding is a trade-off between more turns which increases the magnetic flux produced, but which also increases the inductance giving a lower current.

The flux produced by a coil is:

$$\phi = k_1 IN \qquad \ldots\ldots\ldots\ldots\ldots\ldots\ldots\ldots\ldots\ldots \qquad (6.1)$$

where:

k_1 = constant
I = coil current
N = number of turns of coil

The inductance of a coil is given by:

$$L = k_2 N^2 \quad \ldots\ldots\ldots\ldots\ldots\ldots\ldots\ldots\ldots\ldots \quad (6.2)$$

where:

k_2 = constant

The impedance of a coil of inductance L and resistance R is:

$$Z = R + wL \quad \ldots\ldots\ldots\ldots\ldots\ldots\ldots\ldots\ldots\ldots \quad (6.3)$$

which if wL>>R then

$$Z \approx wL \quad \ldots\ldots\ldots\ldots\ldots\ldots\ldots\ldots\ldots\ldots \quad (6.4)$$

where:

w = angular frequency

The current flowing in this coil is then given by:

$$I = \frac{V}{wL} \quad \ldots\ldots\ldots\ldots\ldots\ldots\ldots\ldots\ldots\ldots \quad (6.5)$$

where:

V = voltage applied to the coil

If w and V are constant then

$$I = \frac{k_3}{L} \quad \ldots\ldots\ldots\ldots\ldots\ldots\ldots\ldots\ldots\ldots \quad (6.6)$$

where:

$$k_3 = \frac{V}{w} \quad \ldots\ldots\ldots\ldots\ldots\ldots\ldots\ldots\ldots\ldots \quad (6.7)$$

Substituting (6.2) for L in (6.6):

$$I = \frac{k_3}{k_2 N^2} \quad \ldots\ldots\ldots\ldots\ldots\ldots\ldots\ldots\ldots\ldots \quad (6.8)$$

and substituting (6.8) for I in (6.1) gives:

$$\phi = \frac{k_1 k_3 N}{k_2 N^{\frac{1}{2}}} = \frac{k}{N} \qquad \ldots\ldots\ldots\ldots\ldots\ldots\ldots\ldots \qquad (6.9)$$

Thus, by halving the number of turns the flux is doubled. This implies that if there are zero turns then the flux is infinite. Obviously this is ridiculous and occurs because the resistance of the winding has been neglected in equation (6.4). Thus, the result in (6.9) is only used as an indication as to the effect of adding or subtracting turns from an already existing winding.

An optimum value of 100 turns was found after some experimentation.

The inductance and resistance of the coil were measured using a Fluke multimeter and a Radiometer RLC meter:

$L = 1.2$ mH
$R = 1.4\ \Omega$

The frequency of operation was always nearly 150 Hz due to the dimensions of the forks and thus the impedance of the coil was:

At 150Hz $Z_L = 2\pi fL = 1.13\ \Omega$

Thus the impedance of the coil at 150 Hz is:

$$Z_{coil} = 1.4 + j1.13\ \Omega$$

The phase shift in the coil is:

$$\theta = \tan^{-1}(1.13/1.4) = 38.9°$$

The final arrangement of electromagnet and magnets stuck to the ends of the tuning forks worked exceedingly well, with a good efficiency, i.e small currents were needed to drive the tuning forks in the absence of fatigue. See Photograph G.3.

6.2. Clamping of the tuning forks

The clamping of the tuning forks is a very important aspect of this work since there is a source of energy loss by propagation down the bar.

A tuning fork is a dynamically balanced resonator and therefore the loss is small but significant as the root is an antinode (Figure 6.1). However, the coupling of the tynes at the base causes tension and compression of the material in this region, causing it to oscillate with small amplitude in an axial direction. Waves, called Lamb waves, are launched down the length of the support (extended base section) due to this motion of the base, causing energy to be transferred to the clamp[34,35]. Since these waves travel along the edge of the support, care must be taken to ensure the tuning fork is clamped at the top and bottom only, and that the clamp does not come into contact with the sides.

The clamp was machined out of mild steel and is shown in Photographs G.4 and G.5. Since the tuning forks were also made of mild steel, they have the same properties, enabling easy energy transfer. A strip of aluminium was placed along the top and bottom of the tuning fork during clamping in order to introduce a mismatch between the fork/clamp interface. Aluminium is a good material to use for this purpose due to its low acoustic impedance.

The base extension bar of the tuning forks was made quite long, almost as long as the tynes themselves, in a further effort to reduce energy loss, since the Lamb waves will be attenuated along the length of the extension. The forks were then clamped at the end of this extended base section.

The use of all these precautions resulted in very high Q factors for the tuning forks. However, the low damping values obtained means that the system is extremely sensitive to energy loss, and it was impossible to obtain consistent results if the same fork was clamped and then re-clamped. Therefore, once clamped, a fork was not

removed, or the clamp altered in any way, until an experiment had been completed. This clamping was more than adequate as the loss associated with it was little more than one tenth of the ultimate fatigue loss.

6.3. The final assembly

The electromagnet and tuning fork clamp were mounted onto a heavy channel-section steel structure, forming the base for the experimental rig assembly. Initially this was constructed out of wood, but this was found to have insufficient rigidity and problems with sympathetic oscillation caused energy loss. This was due mainly to sound radiation; the use of the steel base prevented this and formed a firm, vibration free platform. See Photographs G.2, G.4 and G.5.

A wooden housing was made for the rig. This was to provide thermal insulation for performing temperature dependance test (chapter 10), and to prevent air currents blowing across the temperature sensor. The housing was made in two parts. The top section was made to be easily removable, enabling adjustments to be made without tedious dis-assembly problems. The housing can be seen in Photograph G.1.

6.4. Choice of material for the tuning forks

It was decided upon to use ordinary commercial grade mild steel on which to perform fatigue experiments. This was due to the following reasons:

1. It is cheap and easily obtainable
2. It is a widely used engineering material
3. It is available in large quantities from the same batch.

6.5. Geometry of the tuning forks

The tuning forks are based on the classical form, and are machined from mild steel strip 25mm x 9mm ($1"x^3/_8"$). The gap between the tynes is approximately the same as the tyne width, giving a maximum vibration peak-peak amplitude of half the tyne width. This was always more than required to cause metal fatigue. See Figure 6.4 and Photograph G.10.

The tynes were made 190 mm long corresponding to a resonant frequency of about 150 Hz (Figure 6.4).

The inner base region between the tynes was radiused during the production of the tuning fork by milling machine. This was further carefully finished, by filing and then smoothing, with emery cloth. This was done to try and remove any machining nicks or grooves, where fatigue cracks can easily form due to the high stress concentration, and to try and make the surface finish between different forks uniform. Further refinement such as grinding and etching were not considered worth while at this stage of instrument development.

6.6. The resonant frequency of a tuning fork

By considering a tuning fork to consist of two reeds clamped at one end, it can be shown that the allowed frequencies of oscillation are determined by the following equation[36]:

The fundamental frequency f_1 is given by:

$$f_0 = 0.55966 \frac{k}{L^2}\sqrt{\frac{E}{p}} \quad \ldots\ldots\ldots\ldots\ldots\ldots\ldots\ldots \quad (6.10)$$

Where:

L = length of tynes
k = radius of gyration
E = Young's modulus of the material
p = density of the material

The radius of gyration k is given by:

$$k = \frac{w}{\sqrt{12}} \quad \ldots\ldots\ldots\ldots\ldots\ldots\ldots\ldots\ldots\ldots \quad (6.11)$$

Where:

w = thickness of tynes in the bending plane.

For mild steel:

$$E = 19.5 \times 10^{10}$$
$$p = 7700 \text{ kg/m}^3$$

A typical set of dimensions for one of the tuning forks gives:

L = 190 mm
w = 8.5 mm

Using the formula (6.10) with (6.11) to calculate the fundamental resonant frequency gives:

f_0 = 191.4 Hz

This obviously is considerably out from the actual value of 149.2 Hz, and is due to the added mass loading of the magnets, glued to the ends of the tynes. The mass of one magnet is 74g.

Using the formula for the change in frequency due to an added mass (chapter 10):

$$f_1 = f_0 \sqrt{\frac{M}{M+m}} \quad \ldots\ldots\ldots\ldots\ldots\ldots\ldots\ldots\ldots\ldots \quad (6.12)$$

Where M is the equivalent mass of the tuning fork as a lumped element system, and m is the added mass.

This is explained in chapter 10 where the equivalent mass of the tuning fork is found in order to calculate the efficiency.

Re-calculating the frequency with:

M = 99.46g
m = 74g

gives

f_1 = 144. Hz

However, this still produces quite a large error. This can be improved by considering that the centre of mass of the magnet is not right at the end of a tyne and therefore its inertia is reduced. The centre of mass is in fact 25mm from the end.

Applying a simple ratio to the mass at the tyne length and at (tyne length-25mm) gives:

Effective mass at tyne length = 74g x (190-25)/190
m = 64.3g

Re-calculating the frequency gives:

f_1 = 149.2 Hz

This is much closer to the actual value and gives a useful indication of what the working frequency will be. It is by no means an accurate value.

---X---

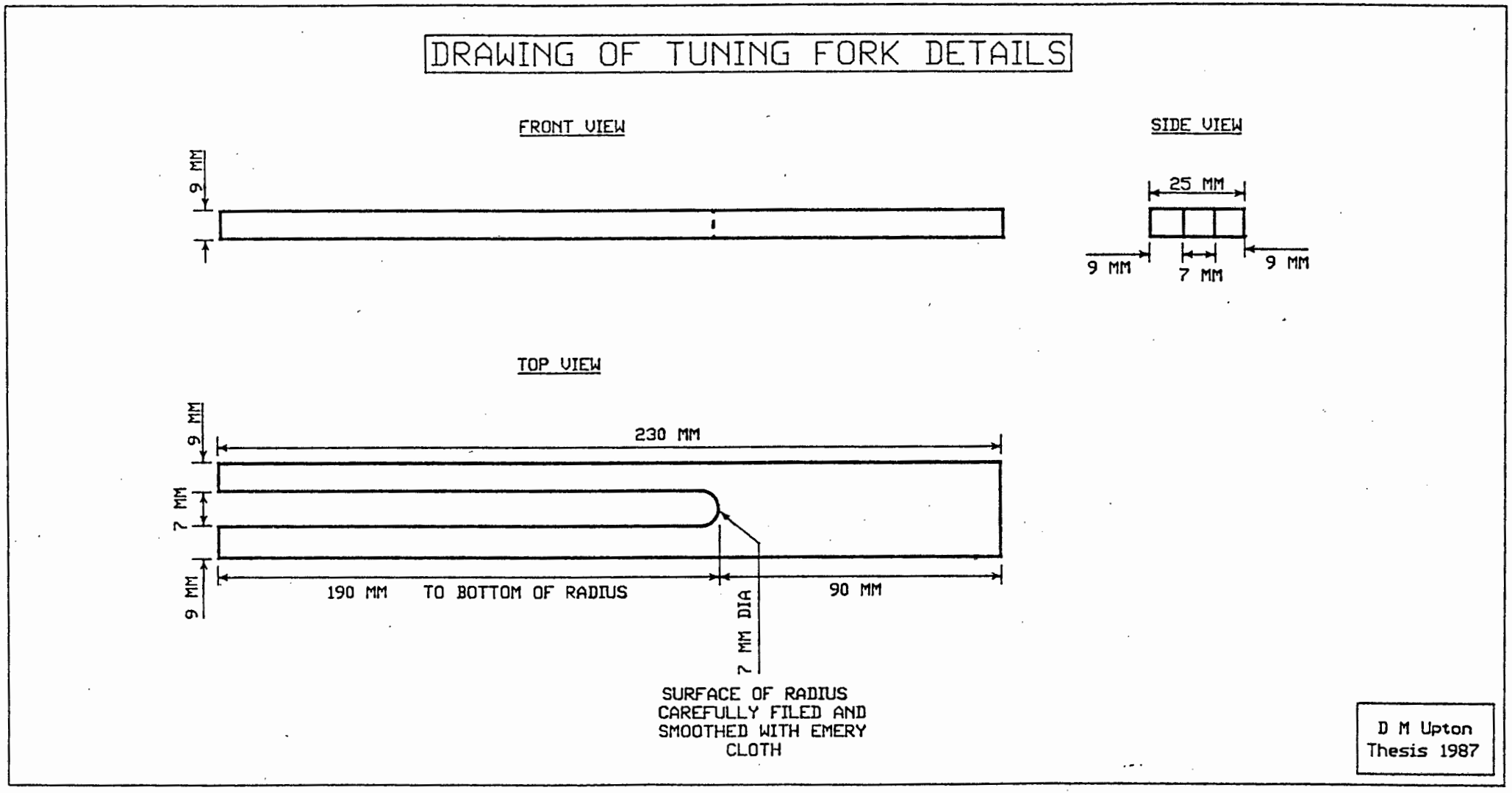
DRAWING OF TUNING FORK DETAILS
FRONT VIEW
9 MM
SIDE VIEW
25 MM
9 MM
7 MM
9 MM
TOP VIEW
9 MM
230 MM
7 MM
9 MM
190 MM
TO BOTTOM OF RADIUS
90 MM
7 MM DIA
SURFACE OF RADIUS
CAREFULLY FILED AND
SMOOTHED WITH EMERY
CLOTH
D M Upton
Thesis 1987

Figure 6.4.

CHAPTER 7

THE ANALOGUE ELECTRONIC DRIVE SYSTEM

7.0. Introduction

The electronic system needed to perform automatic measurements and control of experiments can be broken down into two main areas:

1. An analogue electronic system to keep the fork at resonance and to maintain a constant vibration amplitude throughout an experiment. This requires a double feedback control, one to maintain oscillations, the other to maintain a preset amplitude.

2. An analogue to digital interface system so that measurements can be taken, as required, under computer control and stored on tape or disk for later analysis.

The circuit diagrams can be seen in appendix A. The overall system is shown in Figure 7.1 and Photographs G.1 and G.2.

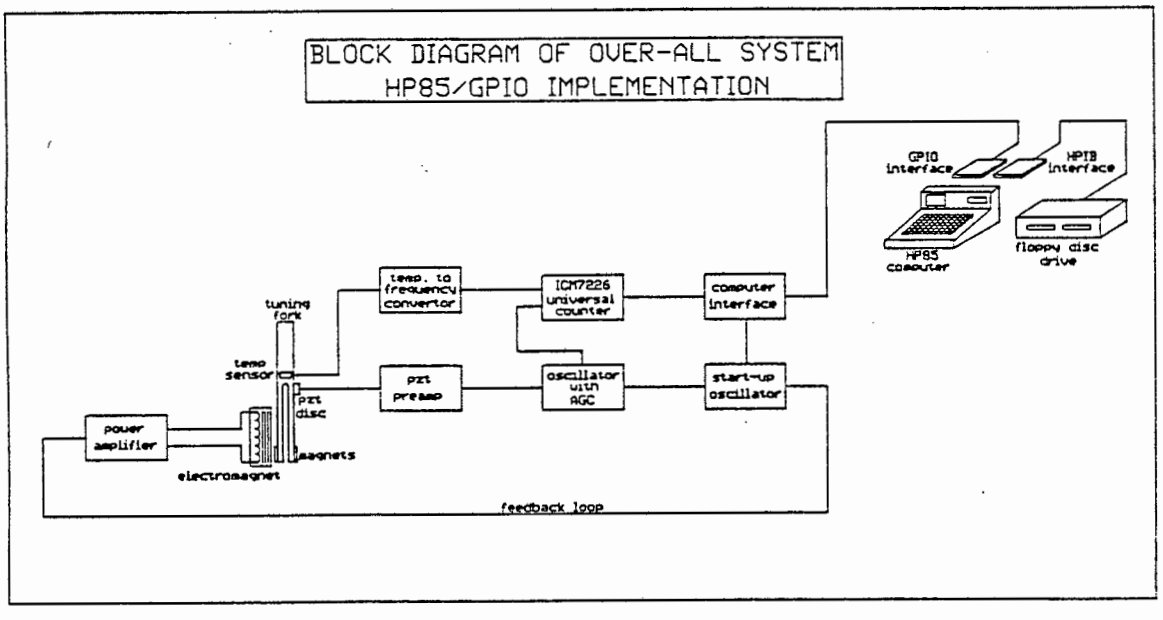

Fig.7.1. The overall system

7.1. The analoque electronic system

The main requirement of this section of the overall electronic system is:

1. The tuning fork must be maintained as close to resonance as possible. This is to gain the maximum force amplification effect for efficiency.

2. The amplitude of the oscillations must be kept constant throughout an experiment so that the material is subjected to a constant stressing amplitude.

A simple, positive feedback oscillator system, incorporating automatic gain control (AGC), was decided as being the best solution because:

1. It is a simple and yet reliable technique.

2. It requires relatively few electronic components for it to be implemented, keeping the amount of electronics susceptible to temperature fluctuations to a minimum.

7.2. Description of AGC oscillator system

Consider block Diagram A.2, and the complete circuit details in Diagram A.3. The operation of the system can best be explained by following the signal path step by step.

1. If the fork is assumed to be in resonance, then there will be an alternating stress set up at the base of the tynes. The small pzt disc glued to the side of the fork at the maximum stress position, will thus have an alternating charge set up between its plates. This charge corresponds directly to the strain. The

equilibrium value such that the desired-amplitude and actual-amplitude are nearly equal.

8. The output from the multiplier is fed to a further amplifier of gain 20, forming the overall loop gain of the system, ensuring that there will always be enough gain in reserve for oscillation to occur.

9. The output from (8) is fed to a switchable inverter circuit so that any unintentional 180° shifts can be eliminated at ease, particularly during the development stage when the circuit is continually being modified.

10. The signal is finally fed to a pre-amp/power amplifier combination which drives the coil of the electromagnet, providing energy for the oscillations.

11. A further addition to the AGC circuitry is a variable gain amplifier which feeds an analogue signal to the computer-interface/measurement unit. The input to this amplifier comes from the output of the pzt pre-amplifier (the input to the AGC unit). Its purpose is to allow the signal level to be adjusted independantly to the correct value for the Q-meter circuitry. It is mounted on the AGC board, and the adjustment pot is mounted on the front panel.

7.2.1. PZT Pre-amplifier

The charge and variable gain amplifiers were constructed out of an LF353 dual op-amp (diagram A.3). The components are built on a small board and housed in grounded aluminium box 80x50x15 mm. This is placed as close to the pzt disc as possible, but is kept outside the rig housing to eliminate temperature effects, especially during experiments at raised temperatures. Signal connections are made with single core screened cable. The above precautions were necessary to eliminate noise pick-up.

charge is converted to a voltage using a charge amplifier. This is followed by a variable gain amplifier allowing signal levels to be adjusted as required (Diagram A.4).

2. The signal is fed to a variable phase shifter circuit which enables the conditions for positive feedback oscillation to be achieved: zero phase shift around the loop and a gain greater than unity.

3. Automatic gain control is achieved by incorporating a secondary loop in the system. A signal proportional to the difference between the actual amplitude and the desired amplitude is developed, and is used to control the gain in the main loop, using an analogue multiplier.

4. The signal from (2) is fed to a full-wave, negative peak, envelope follower, producing a dc voltage very close in value to the negative peak value of the input signal. It is given a time constant of 5 seconds in order to eliminate any noise and instability problems due to the high Q of the tuning forks. This voltage constitutes the "actual-amplitude" signal.

5. The "desired-amplitude" signal is derived from a high stability, low temperature coefficient, positive, variable, dc voltage supply based on the LM 723 voltage regulator.

6. The actual-amplitude and desired-amplitude signals are added together by a summing amplifier, the output of which represents the difference between the two (one is a positive voltage and the other negative). The summing amplifier has a gain of 20 so that the difference signal is amplified, in order to keep the error small. The output signal is called the "difference-signal".

7. The signal from (2) is also fed to one input of an analogue multiplier chip (MC 1495) and the difference-signal to the other. Hence, the main signal from (2) will be scaled up or down depending on the difference-signal which will reach an

7.2.2. AGC Circuitry

All the components are mounted on a single board with separate voltage regulators and housed in an aluminium box. See Photograph G.2.

The front panel controls are as follows from the left:

1. Variable level adjustment pot for the analogue signal fed to the computer interface.
2. Variable phase adjustment pot
3. Desired amplitude adjustment pot
4. Optional inverter switch
5. Output grounded switch, so that the drive to the fork can be switched without changing the settings of the controls.

There is no power on-off switch since a standard laboratory power supply was used, having its own power switch.

7.2.3. Pre-amplifier/Power-amplifier combination

These are housed in separate boxes so that the pre-amp can be positioned close to the AGC unit, and the bulky power amplifier, can be positioned close to the high current power-supply

Diagram A.5 shows the complete circuit of both units, combined into one. The pre-amp consists of the circuitry up to and including the 4:1 ratio transformer. The power amplifier consisting only of the high current Darlington pair output transistors and biasing diode network.

THe final design of these units was only arrived at after much experimentation. The problem encounted was due to large phase shifts introduced by the inductance of the electromagnet, causing instability problems. Hence, it was decided to split the unit into

two sections: the low current pre-amp and the high current power-amp, running off separate supplies. The use of a transformer is a little unorthodox, but since the amplifier only has to operate at low frequencies (< 1kHz) it is no problem and greatly simplifies the design[39]. Since the output from the pre-amp is stepped up in voltage, the pre-amp can be operated from standard supply voltages (+12 0 -12v), enabling standard op-amps to be used instead of a discrete transistor design, as is used in most audio amplifiers.

To begin with, only two feedback loops were used. The first from the primary of the transformer, and the other from the secondary. The second loop operates at low frequencies, whilst the first takes over at higher frequencies in case any phase shifts in the transformer cause instability. No feedback was incorporated from the output stage because it was thought that there would be instability due to the phase shift in the electromagnet load. However this arrangement was unacceptable, because of a high degree of distortion of the sinusoidal waveform. Hence, a third feedback loop was added, as can be seen from the circuit diagram. This again operates at low frequencies, being over-ridden by the first feedback loop at higher frequencies. A reasonably low distortion waveform was then produced by this arrangement. This is important so that higher harmonics are not excited in the tuning fork, and power is not wasted in the electromagnet. The output transistors are biased into conduction by the diode network reducing cross-over distortion even further.

The output Darlington pair configuration transistors are mounted on a large aluminium heatsink and blown with a couple of 110v cooling fans. This enables the relatively few transistors to supply a large amount of power at a reasonable operating temperature. The amplifier can deliver up to about 300 watts which is necessary, because towards the end of a fatigue test when the internal loss of the specimen is high, a large amount of power is used in driving the tuning fork at the same amplitude as at the start.

See photographs G.1 and G.2.

7.2.4. Power supplies for the pre-amp and power-amplifier

The power supply consists of two sections (Diagram A.6):

1. A high voltage, high current, unstabilised but smoothed supply for the power amplifier output stage.
2. A +12, 0, -12v regulated, smoothed supply for the pre-amplifier.

These supplies are derived from a 220 to 45-22-0-22-45v, 5A transformer. The high voltage supply is taken from the 45-0-45v outputs, and the low voltage supply from the 22-0-22v tappings. The high voltage supply was made variable by supplying the primary of the transformer from a variac, so that a maximum of 50v dc could be obtained for the power amplifier, being the maximum voltage the particular transistors used can withstand. Smoothing was provided by a 30 000uF/80v capacitor across each rail.

7.2.5. Over temperature protection circuit

A very important part of the power supply was an over-temperature protection circuit for the transformer (Diagram A.7). At prolonged high current drain, the transformer became under-rated with associated high temperature rise, and since experiments were left running, unattended at night, it was thought a prudent addition.

The circuit operates by latching in the mains supply via a relay on the momentary pressing of a push button. If the temperature rises above approximately 80°C, then the relay coil current is switched off, disconnecting the mains supply, which will not be re-latched once the temperature has dropped.

At a later stage, several 110v cooling fans were used to cool the transformer, and this was found to be sufficient to never cause the over-temperature circuit to operate.
All the power supplies had fuses on input and output.

7.3. The Setting up of a tuning fork prior to an experiment

The setting up procedure consists of three parts:

1. Glueing of the pzt disk and magnets to the tuning fork specimen.
2. Manual adjustments to achieve the correct conditions for oscillation
3. Adjustment of the amplitude of flexure, to the required value.

7.3.1. Glueing the pzt disk and magnets

1. PZT discs

There is considerable technique involved in attaching the pzt disk by the use of glue. The requirements for the attachment are:

1. The glue must withstand high strain amplitudes, as is met during a fatigue test, without a weakening in the intimate contact of the pzt disk and the strained surface.

2. The surface to which the pzt disk is glued, must provide the electrical connection to the glued face of the pzt disk, which also must not fail.

The pzt discs used were of dimension:

diameter = 5mm
thickness = 1mm

The discs are made of ceramic material, and have silver contacts plated onto each side. These form the contacts, between which the charge is developed, according to the amount of strain exerted on the disc. The discs are effectively capacitors, and have a nominal capacitance at room temperature of 300pF. The capacitance and piezoelectric coefficient, are radically affected by temperature changes above 50°C. At temperatures below this, they are fairly exclusive to thermal effects.

The discs are not glued directly to the tuning forks because mild steel does not make a good conductor, and is not easily soldered to. Furthermore, it is not possible to recover the disc after completion of an experiment, if done in this way.

The discs are first glued to a thin piece of brass shim (0.1mm), which is then, in turn, glued to the tuning fork. The shim provides an ideal connection material because it is easily soldered to. The glue used is thermo-setting Araldite, and is ideal for this application. It is in the form of white powder at the start, and must be cured at 180°C for several hours, before bonding takes place. The result is a straw colored, glass hard, ceramic which does not deteriorate during a fatigue test. Initially, two-tube epoxy resins were tried, but the bond failed after a relatively few stress cycles.

The brass shim is first scored in a chequer pattern with a scriber, over an area just bigger than the pzt disc. This causes a network of raised fillets to be made across the surface of the shim, which is then cut to a square of size 12x12mm. It is placed on a hot plate at 180°C, and a small amount of thermo-setting Araldite is poured onto it. This turns to a clearish liquid after a short time and the pzt disc carefully placed on top, and then pushed down. The raised fillets make electrical contact with the silver plated contact of the pzt disc.

The tuning fork is placed edge-up on the hot plate and when the temperature is high enough, some more thermo-setting Araldite is

sprinkled over the area where the pzt disc is to be attached. The brass shim plus pzt disc, from above, is placed on top of the glue, and weights are applied to the top of the disc. This forces the pzt disc onto the shim for electrical contact, and then the shim onto the side of the tuning fork for mechanical contact.

The electrical connection is monitored by measuring the capacitance between the top contact (plus loading weights) and the brass shim, with a Radiometer RLC bridge. If the connection is good, then the capacitance will be about 300 pF, otherwise it will be a very low value of a few pF. The complete set-up is then left for several hours, while the glue is cured. The capacitance is checked every now and again.

This method proved to be very reliable, and no problems of bond failure were experienced. The draw-back is that the curing of the Araldite at raised temperature, causes slight annealing of the tuning fork sample.

2. Magnets

The magnets are glued at the ends of the tynes, to the outer edges, using two-tube epoxy resin. The magnets must be of opposite polarity, otherwise the electromagnetic drive will not work. The glue is allowed at least 12 hours in which to cure. It is important that the magnets are attached in a mechanically firm way, with no yielding, so that they become an intimate part of the tuning fork system. This gives the drive good efficiency and reliability.

A better understanding will be achieved by studying Photographs G.6, G.7 and G.10.

The disc plus brass shim can be recovered intact after an experiment is finished, by heating the tuning fork to about 150°C, at which the Araldite becomes tacky. A thin blade can be run under the shim, removing it from the tuning fork. At the same time, the magnets may

be removed in a similar way, because the epoxy resin glue virtually crumbles away at this temperature. Hence, both the pzt disc and magnets may be re-used for the next sample.

Thus there is a considerable setting up procedure for the samples, and takes a full 24 hours to complete. The result is a sample that is reliable and which forms a unique way of measuring internal changes, with high sensitivity.

7.3.2. Adjusting for oscillation

1. The system is operated in the open-loop condition by disconnecting the AGC unit from the pre-amp. Using a high stability sine-wave generator connected to the input of the pre-amp, the resonance peak is found by adjusting the frequency. This is done by observing the output of the pzt pre-amp on an oscilloscope at a high sensitivity setting. The frequency which gives the maximum output constitutes the resonance point. Care is taken during this procedure to never cause the tuning fork amplitude to be higher than about 2mm peak-peak, ensuring no damage is done before the experiment has started.

2. Once the resonant frequency has been found, the phase shift around the loop must be adjusted to be zero. Using a double beam oscilloscope, the output from the generator, and that from the AGC unit, are observed on separate channels. The phase adjust pot is then used until the two signals are exactly in-phase.

3. The conditions for resonance have now been fulfilled. The sine-wave generator is removed and the AGC unit is connected to the input of the pre-amplifier. The system should then sustain resonance on its own.

7.3.3. Adjustment of flexure amplitude

This is more time consuming because it is an adjustment that needs to be performed very accurately. The stress at the base of the tynes depends upon the vibration amplitude, and due to the length of the tynes, a small change in amplitude results in a much larger change of stress.

Before the start of an experiment, a vertical reference mark must be made through the centre of the end of one tyne. This is done by filing and smoothing the end with emery cloth to form a flat surface. This is then blacked out with two or three coats from a black, felt-tipped pen. Once this has dried, a fine vertical line is scribed through it, using a needle.

Once the tuning fork has been set-up according to 7.3.1 above, a variable strobe light is used to illuminate the ends of the tynes. The flash rate is adjusted until the tynes appear to oscillate very slowly.

The reference mark is observed through a high precision travelling microscope, of resolution 0.02 mm. The measurements of the left and right extreme amplitudes are noted down, and the peak-peak amplitude of the oscillations is then obviously the difference between them. The desired amplitude is achieved by adjusting the control pot of the AGC unit in conjunction with the strobe-light/travelling microscope combination. This is a tedious task but once completed the amplitude is kept to within 0.1 mm over the whole experiment.

For a fork oscillating at amplitudes below the fatigue limit, temperature effects are the main cause for amplitude variations.

---X---

CHAPTER 8

THE COMPUTER CONTROLLED MEASUREMENT SYSTEM

8.0. Introduction

The computer controlled data collection system was implemented with an HP-85 computer in conjunction with an HP-GPIO interface.

The measurement of frequency, decrement and temperature make use of a digital counter which is interfaced to a computer. The latter providing overall control and data storage. The temperature, which is in the form of a voltage, can be converted to a frequency with sufficient precision (0.01°C) for a voltage to frequency IC device to be quite adequate. The digital counter was fabricated from an ICM 7226 universal counter chip from Intersil. This was interfaced to the HP-85 to constitute the computerised measurement system. Refer to Diagram B.1.

8.1. A brief description of the GPIO interface

The GPIO interface offers excellent flexibility for non-standard interfacing purposes[40]. Essentially it consists of four 8 bit ports, two of which (A and B) are low-current bidirectional, and the other two (C and D) are high current, output only ports, of the open collector type. The ports may be combined to form 16 bit ports if required. The type of handshaking used is completely flexible: full-handshake, strobe handshake, and no-handshake. Two handshake lines are provided for each port. In the case of the A and B ports the output handshake lines are denoted by CTL and the input lines by FLG. The C and D ports have their input handshake lines denoted by ST instead of FLG.

The operation characteristics of the GPIO are selected by writing various codes to control registers, via the HP-85 computer, using the CONTROL statement.

For the purposes of this work a simple strobe type handshake is required and the A and B ports were used, where the interface simply outputs a strobe pulse on the CTL line to indicate to the peripheral that the data is ready (Diagram B.2). The handshake method is chosen by writing to register 4 which also provides a means of selecting whether the data is positive or negative true. The width of the strobe pulse is set by register 6. The output drivers of ports A and B are protected against an electrical fault and in order to activate them, an enable bit must be set on register 8.

A further useful feature used here is the ability to inhibit data output operations with the use of one of the handshake lines of the unused ports. Since output operations on port A need to be inhibited, the ST0 line of port C is used. Inhibition occurs if this line is taken high. This feature is enabled by writing to register 9.

The GPIO allows the use of interrupts. These are used in this work to indicate when a sequence of measurements is required. The interrupt line becomes the input handshake line (FLG). Interrupts on port A are required using the FLGA line.

8.1.1 The codes used for the various registers

1. Register 3

   0 is written to set the strobe handshake line of port A (CTLA) as positive true.

2. Register 4

   160 is written to select strobe handshaking and to set the data as being positive true.

3. Register 6

   129 is written to choose a strobe pulse width of 1mS.

4. Register 8

   3 is written to enable the output drivers of ports A and B.

5. Register 9

   1 is written to select the output inhibit feature.

8.2. Interfacing of the ICM 7226 universal counter

Refer to the data sheet of the 7226 in appendix F, and to Diagram B.3, B.4, B.5.

The operation of the 7226 is as follows:

1. Three outputs are provided so that the operation can be monitored to facilitate external interfacing. These are: $\overline{\text{MEASUREMENT-IN-PROGRESS}}$, $\overline{\text{STORE}}$, and RESET OUT.

2. During a measurement, the $\overline{\text{MEASUREMENT-IN-PROGRESS}}$ output remains low, once completed it goes high and about 30-40 mS later the $\overline{\text{STORE}}$ output goes low, storing the value of the main counter into data latches, for use by the display section.

3. A few mS after the $\overline{\text{STORE}}$ pulse goes high, there is a reset pulse, available on the RESET-OUT output, which resets the main counter ready for the next measurement. This begins a short time later, indicated by the $\overline{\text{MEASUREMENT-IN-PROGRESS}}$ output going low again.

4. There are two important inputs provided on the chip, being HOLD and RESET. If the HOLD input is taken high, then the current measurement in progress is aborted and the last measurement is displayed, until the HOLD input is set low again. If the RESET input is held low, the main counter is reset and zeros are output on the display, until it is set high again.

5. The display of the 7226 is multiplexed at a 500Hz rate with a blanking period between digits to prevent display ghosting. The BIPL version of the 7226 was used in this work which operates common cathode type displays. When a particular digit is switched on the digit driver output goes low. The BCD representation of each digit appears on a BCD bus when its corresponding digit driver is operated. Hence, the BCD data of a particular digit cyclically appears on the bus and is available a few uS before its digit driver goes low. In order for the whole display reading to be input to the computer, the individual BCD representations of each digit must therefore be stored in separate 4 bit latches with the digit driver outputs used to provide latching signals. Refer to diagram B.6.

6. When a reading is required by the computer, the 7226 must stop updating the measurement reading in order for a stable value to be available to the interface circuitry, so that it can be captured in latches, as described above. Thus, at the start of a measurement transfer to the computer, the HOLD input must first be taken high. This is not done immediately because the current measurement is allowed to be completed, by waiting for the rising edge of the $\overline{\text{STORE}}$ output, before the HOLD input is taken high. Further operation is thus stopped until the HOLD input is taken low again.

6. The 7226 uses a clever technique of time multiplexing to choose the range and function of its operation. This is achieved by connecting the pre-designated digit driver output to the RANGE or FUNCTION inputs. There are five possible ranges that can be selected, corresponding to the number of counts of the reference counter over which the measurement is taken: 1, 10, 100, 1000 or an external range. The latter is not used in this application. There are six possible functions: frequency, period, time-interval, unit-counter, frequency-ratio and internal oscillator frequency. For the purposes of this work only four are used being: frequency, period, unit counter and internal-oscillator frequency.

8.3. The Interface Circuitry

Refer to diagrams B.4, B.5, B.6. B.7.

The 7226 is constructed using CMOS technology and therefore level shifting and current buffering is required to drive TTL chips. This is done by using available buffering chips. The 74C901 is a non-inverting CMOS to TTL buffer while the 74C902 is an inverting buffer. Both types are used. It was found to be uneccessary to buffer the inputs to the 7226, and these were driven directly by the TTL circuitry.

The control of the 7226 for interfacing purposes requires a large number of single line triggers to initiate each step (Diagram B.7). The sequence is program controlled which allows for easy expansion. A 4 to 16 line multiplexer (74ls154) was used, which provides up to 16 trigger or enable lines. This multiplexer was addressed by port A. Only one output is active-low at any time, the others being in the high state. Each of the outputs is strobed by the strobe pulse on the CTLA line of port A to ensure that the address on port A is stable. This is achieved by either ORing or NORing the trigger outputs with the strobe line depending on whether a positive or negative active output is required. If the signals are ORed this gives an active high output and NORing them gives an active low signal. The CTLA line is buffered with a single BC107 transistor to provide more drive current.

The data needed for a particular option is placed onto port B, and enabled by the appropriate trigger addressed from port A.

Describing each option of the interface separately:

1. ENABLE-HOLD option:

This is selected by the 0th output of the 74ls154 multiplexer, which is strobed through a NOR gate, and clocks a D-type flip-flop with the D input held high. The $\overline{Q}$ output feeds one input of another NOR gate, the other input of which comes from the $\overline{STORE}$ output of the 7226. The output clocks a second D-type f-f also with its D input held high. The Q output of this second f-f provides the HOLD input to the 7226. Thus, this circuitry provides a HOLD signal which only goes high once the rising edge of the $\overline{STORE}$ output occurs. The $\overline{STORE}$ output is buffered with a 74C901 CMOS to TTL buffer chip. Since the computer must wait until the HOLD output has gone high before continuing, further circuitry provides a computer-inhibit signal. This is taken from the $\overline{Q_1}$ and Q_2 outputs and fed to a NOR gate. Thus, a high inhibit-signal appears as soon as the first f-f is clocked which then goes low once the HOLD signal is set high. Further inhibit signals are required for operation of some of the other options and hence they are all ORed together.

2. Capture Data Option

A capture data pulse is needed, of sufficient width to give time for the BCD value of each digit to be captured in a separate latch. This is provided by the capture-data option on the 2nd output of the 74ls154 and triggers a monostable of 4mS duration. For safety, this is twice the time needed to multiplex the display once. The Q output of the monostable is ORed with the inhibit signal from the ENABLE-HOLD option, as described above, and inhibits the computer from output operations until the CAPTURE-PULSE has finished. The ORed output is again ORed with the inhibit signal from the Q-meter circuitry. The CAPTURE-DATA pulse is used to enable the data inputs of the 74ls173, 4bit, tristate latches. The data is latched by the digit driver outputs, inverted with 74C902 buffer chips to provide positive-going, leading edge, clocking pulses. The tristate outputs are connected to a common 4bit BCD bus, which in turn is connected to port B via a 74ls125 tristate buffer. The latter provides isolation for bi-directional data flow on this port.

3. RESET-HOLD option

Once the DATA-CAPTURE option has been utilised, the HOLD signal must be set low again. This is achieved by using the 1st trigger output, strobed through an OR gate, to reset both flip-flops of the ENABLE-HOLD option.

4. INCREMENT-COUNTER option

In order for the BCD values of each digit stored in the 74ls173 latches to be read into the computer, each latch must be taken out of the tristate and pulled onto the bus and read in turn. This is achieved by using a 74ls93 binary counter to address a 74ls138, 3 to 8 line multiplexer, each output of which enables a single latch onto the bus. The outputs of the 74ls138 are active low, of which only one output can be operational at a time. Thus, when the latches are to be read the counter is first reset to 0, setting the 0th output of the 74ls138 low, which enables the 0th latch on to the bus. Its value is read, after which the counter is incremented by one and the next latch read, etc until all eight digit values are inside the computer. The purpose of this option is to provide a pulse for incrementing the counter and is taken from the 4th trigger output, ORed with the strobe line.

5. RESET-COUNTER option

The counter which selects which latch is to be read by the computer must be reset to 0 at the start of a reading sequence. This is achieved by feeding the 3rd trigger output, NORed with the strobe line, to the reset inputs of the counter.

It is a simple matter to create the whole reading out of the individual BCD representations of each digit by multiplying by the appropriate factor of ten each time and then adding this to the total.

The following loop is repeated eight times:

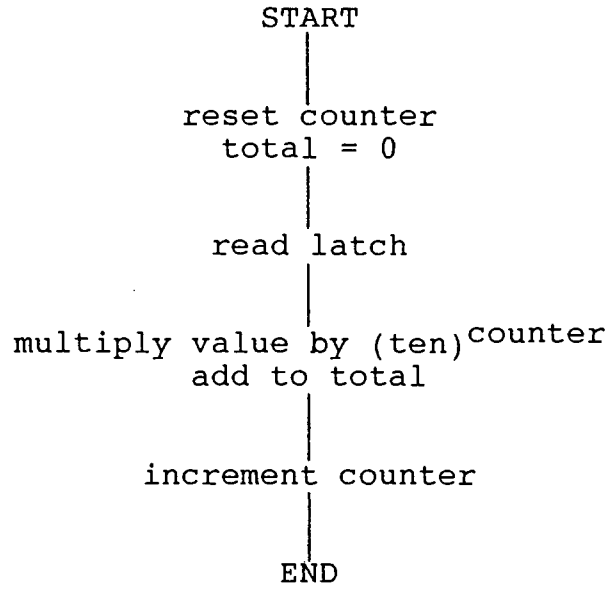

6. LATCH-RANGE option

The resolution or range of a particular measurement is selected by feeding the appropriate digit driver output to the RANGE input of the 7226. Since only four ranges are needed, the pre-designated digit driver outputs are fed to a 74ls153, 4 to 1 line data selector. In order to select a range by computer, an address must be sent to the 74ls153 to route the required digit driver signal to the RANGE input. This address must be latched so that its value remains fixed until a new range is required. The 74ls75 type latches are used. When a range is selected, the appropriate address is sent out on port B and latched into the 74ls75 by the LATCH-RANGE option, selected by port A. This latching option is provided by the 5th trigger output and NORed with the strobe line.

7. LATCH-FUNCTION option

This is similar to the LATCH-RANGE option as described above except the digit driver signals are routed to the FUNCTION input of the 7226. The address of the required function is output on port B and latched into the 74ls75 with the LATCH-FUNCTION pulse. This is provided by the 6th trigger output and NORed with the strobe line.

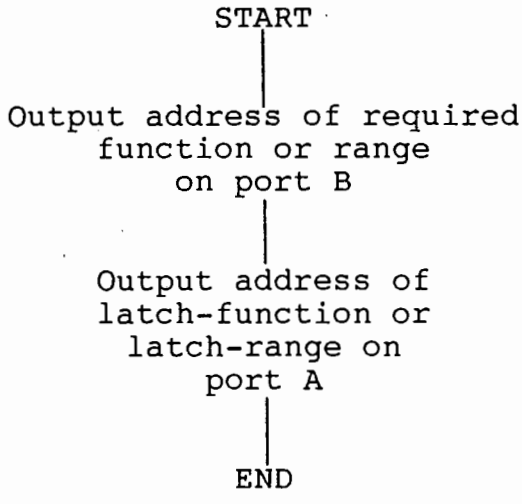

8. LATCH-INPUT-SELECT

Several different pulse trains are needed to be input to the 7226 for measurement. This routing is achieved using a 74ls151, 8 to 1 line data selector. The address of the required input is sent out on port B and held in 74ls75 latches. Each 74ls75 chip contains two latches and since a three bit address is to be stored, one and a half 74ls75's are used. The LATCH-INPUT-SELECT option provides the latching pulse. This is taken from the 7th trigger output and NORed with the strobe line.

Only three different inputs are required in this work leaving the other five spare:

1. Frequency of tuning-forks measured in period mode.
2. Measurement of Q in unit-counter mode
3. Measurement of temperature in frequency mode.

The output of the multiplexer drives the A input of the 7226, the B input of which is unused.

9. GP1-ON option

Several general purpose (GP) outputs are required to provide switching signals for some of the circuitry. The main requirement being a means of switching the drive signal to the tuning-fork on or off for Q measurements. Two GP control sections are provided using D-type flip-flops, with the D input held high. The Q and $\overline{Q}$ outputs plus the clocking pulse are available from each flip-flop for general use. The GP_1-ON option provides a clocking pulse to the first flip-flop which will set the Q output high. The 8th trigger output is used, and NORed with the strobe line.

10. GP_1-OFF option

The 9th trigger output is ORed with the strobe line and fed to the clear input of the first flip-flop as described above and sets the Q output low if operated. Thus the GP_1-ON and GP_1-OFF options allow the drive to the tuning fork to be switched on or off as required from the computer.

11. GP_2-ON and GP_2-OFF options

These are exactly the same as for the GP_1 case and provides a second switching output programmable from the computer. The 10th output NORed and the 11th output ORed with the strobe pulse are used respectively and feed the second flip-flop. This second switching output was found to be uneccessary and was not used in this work.

12. Unused trigger outputs

The 12,13,14,15 trigger outputs of the 74ls154 were unused and left unconnected, but provide an easy means of expanding the circuitry if required.

13. Bi-directional data flow

Data is both output and input to the computer via port B and hence some circuitry is required to prevent bus conflicts, i.e. the devices send data to the computer must be disconnected when data is being output from the computer. Therefore, input and

output operations on the port must be separated. This is simple in this case because the only data which is input to the computer is the BCD digit data stored in the 74ls173 latches. The separation is achieved by feeding the 4-bit, BCD bus to port B through a 74ls125 tristate buffer. If the enable input of this chip is high, then the data outputs will be in the high impedance state or tristate, which effectively disconnects them from port B. A further output line from the GPIO interface is used to direct data flow. This is the $\overline{\text{OUTB}}$ line which is high for input operations and low for output operations on port B. This line is inverted and sent to the enable line of the 74ls125 buffer which will then be tristate for output and enabled for input bus operations.

It will be noticed that only the first four bits of the B port are used, therefore the other four are pulled low with 100R resistors to ensure that definite voltage levels exist on these lines, preventing false byte values being read into the computer.

That completes the description of the program controlled interface to the 7226.

8.4. Description of the various measurements performed

8.4.1. Measurement of Q

The method used is that of the free-decay of oscillations technique (chapters 4 and 5), and is implemented electronically on the basis of a paper by Muaddi, Izzard, Dennis and Bell[41], and is a method used by Surtees[35]. The circuitry has been re-designed in this work, giving a considerable improvement in accuracy and scatter. This decrement technique is generally favoured for high Q systems like the tuning forks of this work, while the resonance bandwidth method is better for low Q values (less than 100, say).

The method requires two voltage set-points. When the decaying amplitude passes the upper set-point, a counter is incremented at the frequency of the decaying oscillations. The increment is stopped when the amplitude falls below the lower set-point and the value of the counter in conjunction with the ratio of the set-point voltages, gives the value of Q as described below.

The envelope of the decay of a linear oscillating system follows an exponential form according to equation (4.20) in chapter 4:

$$An = \exp(-\pi N/Q) \quad \ldots\ldots\ldots\ldots\ldots\ldots\ldots \quad (8.1)$$

This can be re-written as:

$$Q = \pi N/Ln(A_0/A_N) \quad \ldots\ldots\ldots\ldots\ldots\ldots\ldots \quad (8.2)$$

If the ratio:

$$\pi N/Ln(A_0/A_N) = 1 \quad \text{then } Q = N \text{ and } A_0/A_N = 23.14$$

If A_0 and A_N correspond to two voltage trigger levels of the electronic circuitry, then their ratio similarly has to be 23.14. This is too high for an accurate ratio to be achieved for a maximum of five volts: if A_0 is made 5v then A_n will have to be 5/23.14 = .22v. If this lower voltage drifts or has a noise voltage superimposed upon it, the error in taking Q = N may be considerable. A 1% error in the ratio A_0/A_n results in a 0.3% error in Q.

If instead, the ratio:

$$\pi N/Ln(A_0/A_N) = \tfrac{1}{2} \quad \text{then } Q = 2N \text{ and } A_0/A_N = 4.81$$

In this case, if A_0 is 5v then A_n = 1.04v which is susceptible to the same drift as the smaller voltage but is much less prone to noise problems: for a given noise voltage, the signal to noise ratio will be greater in the latter case. Furthermore, the smaller ratio is easier to obtain with accuracy, and this ratio was used in this work.

The object of the circuitry is to provide a line which remains high while the amplitude lies between the upper and lower set-points, which can be used to gate the pulse train to the counter (the 7226 in the unit-counter mode), (Diagram B.8).

The input signal to the Q measurement circuitry comes from the AGC unit (chapter 7) and is a direct measure of the vibration amplitude. The signal is low pass filtered to remove unwanted high frequency spikes and noise which would cause false operation of the circuit. The high voltage set-point was initially made adjustable and derived from a variable pot across the 5v supply for the TTL circuitry. This was done so that the Q could be measured at different vibration amplitudes, but was achieved instead by making the input signal from the AGC unit adjustable and so in the end the upper set point was made the 5v rail. The low-voltage set point is made a fixed ratio of this by two carefully chosen 1% resistors. The values used were 17k8 and 4k64 which gave actual measured values of 17k71 and 4k63 giving a ratio of 4.8251, and a Q scaling factor of 1.9961. This was taken to be 2.00 giving a systematic error of 0.19%, being much less than the more important random errors.

The signal from the AGC unit is input at an amplitude near the saturation point of the op-amps (15v). Hence, before the amplitude falls below the upper set-point (5v), considerable decay is required. This was done to allow the vibration amplitude to drop to small values before the Q measurement was taken, so that air-damping and non-linearity effects fall to low values and the decrement of the decay becomes exponential (chapter 5).

The main circuitry consists of three parts:

1. Detecting if input signal is below V_{high}.
2. Detecting if input signal is above V_{low}.
3. Combining (1) and (2) to gate the pulse train.

After the filter stage the signal is passed to three voltage comparators. The first is a zero-crossing detector which converts the analogue signal to an equal mark/space ratio, TTL compatible square wave. The other two form the basis of the upper and lower set-point detectors. Denoting the zero-crossing pulse train as z/c, the Vhigh crossing train as H and the Vlow train as L for clarity.

1. Detecting for signal below V_{high}

   The front end of this section is a voltage comparator which produces a pulse train if the analogue input signal is above the V_{high} set-point. This is followed by a schmitt-inverter producing an inverted version of the pulse train (H-train). The operation is as follows:

   1. The leading edge of the z/c train clocks a D type flip-flop no 1 ($f\text{-}f_1$) with the D input high. The Q_1 output is thus set high.

   2. The H-train is used to reset $f\text{-}f_1$ which will occur after a short time due to the delay between the rising and falling edges of the z/c train and H-train respectively. Hence, the Q_1 output will be set low again.

   3. The D input to $f\text{-}f_2$ is the Q_1 output and is clocked by the z/c-train. Therefore, if the Q1 output is low on the clocking edge, the Q_2 output remains low assuming it to be reset at the start.

   4. Once the analogue signal level has dropped below Vhigh the H-train will disappear but the z/c-train will still exist. Now, if step (1) is repeated, the Q_1 will not be reset after the setting pulse of the z/c-train. Hence, the D_2 input will be high and on the clocking pulse from the z/c-train, Q_2 will be set high remaining that way until the H-train re-appears once the drive to the tuning-fork is switched back on. This Q_2 signal is denoted by H-enable.

2. Detecting for signal above V_{low}

This is similar in operation to that for the V_{high} case except that it works in reverse. This time the D_2 input is the $\overline{Q_1}$ output of the first f-f. When the z/c-train clocks f-f_2, then while the signal is above Vlow and the L-train exists, then the Q_2 output will be set high on the first edge and remain that way for subsequent edges. Once the L-train disappears, then f-f_1 will no longer be reset, and the $\overline{Q_1}$ output will remain low. Hence, f-f_2 will have its D input low and the output will be clocked low at the next edge of the z/c-train. This is denoted by L-enable.

3. Gating the zero-crossing pulse train

The z/c-train is readily gated by feeding it, plus the L-enable and H-enable outputs to a three input AND gate. Thus a train of equal mark/space ratio pulses is produced which is fed to one input of the input multiplexer to the 7226.

The z/c-train is fed to another input of the input-multiplexer and is used for frequency measurement of the tuning-fork.

4. Q-measurement control signals

For an actual Q-measurement to be made on a tuning-fork during an experiment, several additional control signals are required:

1. A reset signal to the 7226 to ensure the counter is reset at the start of a measurement.

   This is taken from the $\overline{Q_2}$ output of f-f_2 of the Vhigh detector: this remains low resetting the counter until the signal drops below V_{high}. It is only required for Q-measurements and is hence disabled most of the time by ANDing this output with the GP_1 general purpose output. The GP_1 output is set high to enable the reset output and low to disable it.

2. A computer inhibit signal, so that the computer waits until the analoque signal has dropped below Vlow before taking the reading of the counter.

This is taken from the Q_2 output of f-f_2 since it only goes low once the signal has dropped below V_{low} and the unit-counter is no longer being incremented. It is only required for Q-measurements and is also enabled by ANDing with the GP_1 output. This gated inhibit line is in turn ORed with the inhibit line of the 7226 related circuitry.

3. The third control signal is used to switch the drive to the tuning-fork on and off .

This is also achieved with the first general purpose output by using the $\overline{GP_1}$ output (Diagram B.9). Switching is achieved using a single changeover contact reed-relay in the path of the input to the pre-amplifier/power-amplifier units. At switch-off, the input is earthed to prevent noise pick-up. The $\overline{GP_1}$ output is used because at power-up of the electronics a resistor/capacitor network resets all the flip-flops, and hence the drive is not switched on until instructed to do so by the computer.

8.4.2. Fixed number-of-cycle interrupts

Extra circuitry is required to provide an interrupt pulse to the GPIO at fixed number-of-cycle intervals during an experiment. This causes a sequence of measurements to be performed on the tuning-fork.

The frequency of the drive signal and the tuning-fork is the same, therefore the number of stressing cycles can be counted using the z/c-train of the Q meter. Hence, the z/c pulse train is fed to a series of decade counters which divide the frequency down by 10 each time. The 74ls390 is used, which contains two decade counters, giving a total division of 100 per chip. Initially, divisions of

1000, 10 000, 100 000, 1000 000 were provided for experimentation, but it was found that the best division is 10 000, giving an interrupt every 10 000 cycles. The interrupt pulse is provided by feeding the divided frequency to a monostable of 1mS pulse width. After the required number of pulses, the output of the last divider will go high and this positive edge triggers the mono, the output of which drives the FLGA handshake line of port A to provide interrupt pulses. The required interval is selected by hardwiring the appropriate output of the divider chain to the input of the monostable. In the design stage it was initially thought that the interval would have to be selectable from the computer, but was found to be uneccessary and the 10 000 division became a permanent feature.

8.4.3. Measurement of temperature

The temperature of the tuning forks is monitored throughout an experiment so that temperature changes can be observed during the fatigue process. It also enables the temperature coefficients of resonant frequency and Q to be found for experiments below the fatigue limit, so that a correction can be made for the fatigue data before the knee of the curve.

Two separate designs were tried out, in both cases the temperature is converted to a frequency for measurement by the 7226. This enables a high resolution to be achieved because the frequency change can be made large compared to the corresponding change in temperature. The drawback with this method is that the time required to take a measurement is long compared to using an A to D converter. If the frequency is measured to 1Hz this takes at least 1sec, whereas with an A/D of comparable resolution, the measurement takes a few uS. However, in this application speed is not important and this method provides a simple yet accurate measurement of temperature.

The sensor was mounted in a small piece of aluminium channel which was then fixed onto the tuning fork as close to the root as possible. This is where the stress is a maximum and hence where heat is generated in the specimen due to internal friction.

1. Temperature measurement circuit version 1

This was based upon an LM234 precision current source which has a temperature coefficient of 0.33%/°C. (Diagram B.10). The current output is fed directly to an LM331 precision voltage to frequency converter and this gives a conversion factor of 10Hz/°C. The frequency is measured to an accuracy of 1Hz by the 7226 and hence the temperature can be resolved to 0.1°C with this circuit. This was found to be insufficient because very small changes in temperature need to be accurately monitored and a second circuit was designed with 10 times the resolution.

2. Temperature measurement circuit version 2

An LM335 precision temperature sensor was used as the front end of this circuit. (Diagram B.11). These sensors have a voltage output of 10mV/°C and are pre-calibrated to ±1°C. In order to improve the resolution over the first circuit, the sensor output voltage was first buffered to provide a low impedance output and then followed by an amplifier of gain 10. However, this gives a voltage of about 2.93v at room temperature and 3.23v at 50°C, a factor of 0.1 (10%). Hence the dynamic range is restricted by the large common voltage. In order to re-gain the dynamic range an offset voltage is subtracted from it. This is done by powering the sensor between the -15v and 0v rails giving a negative output voltage and then adding a positive offset voltage to it. This is done using an inverting summing amplifier of gain 10 and avoids the need to use a differential amplifier which is more susceptible to drift in the op-amp. The positive offset voltage is derived from an LM723 voltage regulator giving a highly stable, low temperature coefficient voltage source. The offset voltage is set to be 2.63v which

corresponds to a temperature of -10°C enabling the sensor to be calibrated at 0°C in ice without the voltage going negative, i.e. the sensor voltage is always greater in magnitude than the offset voltage. Thus the output of the summing amplifier goes from 0.1v at 20°C to 3.33v at 50°C. This corresponds to a factor of 33 and hence the dynamic range has been considerably improved. The output of the summing amplifier is fed to an LM331 voltage to frequency converter and in this case the conversion is 100Hz/°C giving a resolution of 0.01°C and found to be adequate for this work. The output of the LM331 is fed to input-2 of the input-multiplexer to the 7226.

3. Calibration of temperature measurement

Calibration was achieved by drilling two holes in a large slab of aluminium, and then inserting the sensor into one and a thermometer into the other. The slab was heated up to about 80°C and placed in a well insulated box. The equivalent frequency values were measured by the interface in General-purpose mode at intervals of the cooling curve. The slow time constant ensures that the sensor and thermometer are isothermal. A final value was taken at 0°C by gently rubbing the sensor against a piece of melting ice. A plot of the values obtained, results in a very straight line. The regression line through the points gives the calibration equation which can be included in the computer program to enable direct conversion to degrees celsius. The equation obtained for the second circuit is shown in (Graph D.22.) in Appendix D:

Temperature = -16.77 + 0.00756 x Frequency

The correlation coefficient obtained for this equation was 0.9999, indicating a very linear response by the sensor over this range of temperature.

8.5. The start-up oscillator

Once a Q measurement has been made, the drive signal is switched back on by setting the GP_1 output low. However, by this time the amplitude of the oscillations will have almost reached zero and due to the high Q's of the tuning forks, a long time is needed for the oscillations to recover to the initial value. Furthermore, once a fork has fatigued to some extent, and the internal loss has increased, the oscillations do not always start-up spontaneously.

This problem was solved by incorporating a start-up oscillator in the system (Diagram B.9). The oscillator produces relatively high amplitude square waves which are fed to the pre-amplifier/power-amplifier for a fraction of a second at the falling edge of the GP_1 output.

The oscillator is a simple design based upon a 555 timer chip with adjustable frequency range between 140 to 160 Hz. The falling edge of the GP_1 output triggers a monostable with adjustable time constant, the output of which drives the coil of a second single pole change-over reed-relay in series with the first and switches in the oscillator signal for a fraction of a second. This enables a large amount of power to be transferred to the tuning-fork which ensures start-up under all conditions. Furthermore, thr time needed for the oscillations to build up to the working amplitude is greatly reduced.

The frequency of the oscillator is carefully pre-set to be nearly the same as that of the fork towards the end of a fatigue test where the most power is needed for reliable start-up. The length of the start-up pulse is also adjusted to ensure that no more energy than required is transferred, otherwise the amplitude could rise too high and cause over-stressing at the base of the tynes, ruining the experiment. The optimum time was found to be 35mS allowing about 5 cycles of the start-up oscillator through. The frequency of the start-up oscillator was found to be not that critical because the square waveform has such a large amplitude.

8.6. Testing the spread in Frequency and Q measurements

A large number of measurements were taken of a tuning fork oscillating at an amplitude well below the fatigue limit so that the only changes taking place were due to temperature. The readings were found to have a certain amount of spread even if a correction for temperature is made.
At each measurement, 1 reading of Q and F were taken, with 5 readings of temperature which ensured that the temperature measurement was the more accurate. This enables the temperature trends to be removed. The time between measurements was 15 seconds to allow the temperature within the fork to stabilise. It was found that taking them in quick succession caused a downward trend of the Q and F values due to the internal temperature changes of the sample.

The temperature rise is a function of amplitude x loss. For low amplitudes and loss, the heat flow to the bulk of the tuning fork is high enough to ensure that the temperature does not rise dramatically. This is not the case when the metal has fatigued, for which the amplitude and loss are high, producing local hot-spots near the fatigue point. Therefore, in this experiment, the temperature sensor gives an accurate measure of the temperature within the material and a reliable correction can be made.

1. Q measurements

The spread is due to several factors:

1. The hysteresis incorporated in the comparators causes an uncertainty as to the actual trigger point on successive measurements.

2. There is a quantisation error in the counter of ±1 count and since Q = 2N, the quantisation causes an error of ±2 in the Q measurement. This could be reduced to ±1 if a set-point voltage ratio of 23.14 is used. This was not felt to be necessary since the spread in readings was less than ½% with the original design.

3. There is a limit to the correction that can be made for temperature since this also affects the sensor and electronics, therefore there will always be some variation due to temperature.

A statistical analysis of 400 readings gave the following results:

The data was first de-trended to remove the temperature effects. This was done by graphing the Q values versus the averaged temperature readings and the slope of the best fit line through the points gives the temperature coefficient. This was found to be:

$$dQ/dT = -10.81 \quad [rad^{-1}/°C] \qquad \ldots\ldots\ldots\ldots\ldots\ldots \qquad (8.3)$$

The trend was removed from the points by referring them to 20 °C.

$$Qc = Q - (-10.81 \times (T - 20)) \qquad \ldots\ldots\ldots\ldots\ldots\ldots \qquad (8.4)$$

Where Qc = corrected Q value
Q = uncorrected Q value
T = temperature for that Q reading

Number of readings = 400
Mean = 987.0 [rad^{-1}]
Standard deviation = 0.55 [%]
Standard error of the mean = 0.028 [%]

The values were then normalised to the mean and converted to percent deviations from the mean. A histogram plot of these values is shown in appendix D (Graph D.2).

$$\text{Deviation} = (Q/Q_{mean} - 1) \times 100 \quad [\%] \quad \ldots\ldots\ldots\ldots \quad (8.5)$$

In conclusion, the Q instrumentation gives a resolution of better than 0.5%. The correction for temperature is an essential component in achieving this accuracy of measurement.

2. <u>The spread in frequency readings</u>

A similar analysis of the spread in frequency measurement can be done. The frequency data was again corrected for temperature by referring the values to 20°C. This was done using the following correction factor:

$$dF/dT = -.0188 \quad [Hz/°C] \quad \ldots\ldots\ldots\ldots\ldots\ldots\ldots\ldots \quad (8.6)$$

An analysis of 400 readings gives the following results:

Number of readings = 400
Mean = 151.56 [Hz]
Standard deviation = 2.1 [ppm]
Standard error of the mean = 0.11 [ppm]

The values were normalised to the mean and converted to parts per million (ppm) deviation from the mean.

$$\text{deviation} = (F/F_{mean} - 1) \times 1000\,000 \quad [ppm] \quad \ldots\ldots \quad (8.7)$$

A histogram plot of the deviation is shown in Graph D.1.

The frequency measurement has a resolution better than 2ppm. Again it is important to note that the temperature correction is essential for obtaining this result.

8.7. The HP-85 computer program

The program was written in basic, being the only language possible on the HP-85. This is not ideal since it does not have much structure and is not easily readable.

A full print-out of the program listing appears in appendix E at the back of this report.

In order to structure the program as much as possible, the program was broken down into small subroutines and two main sections giving two modes of operation:

1. A general purpose mode enabling the user to choose which parameter is to be measured and to change from one to another at will.
2. An experimental mode for performing fatigue experiments where the measurements are performed with a fixed sequence at regular intervals and the data printed out and/or stored on file if required.

1. The main program

The main program is a short section of basic code that calls up several sub-routines and decides the overall operation of the program. This allows the program to be extended or modified easily. The operation is as follows:

1. A subroutine is called up which sets up the GPIO interface and initialises several variables.

2. An introduction subroutine prompts the user as to which mode of operation is required, either general purpose or experimental and a flag is set accordingly.

The flow-chart of the over-all operation of the program is as follows:

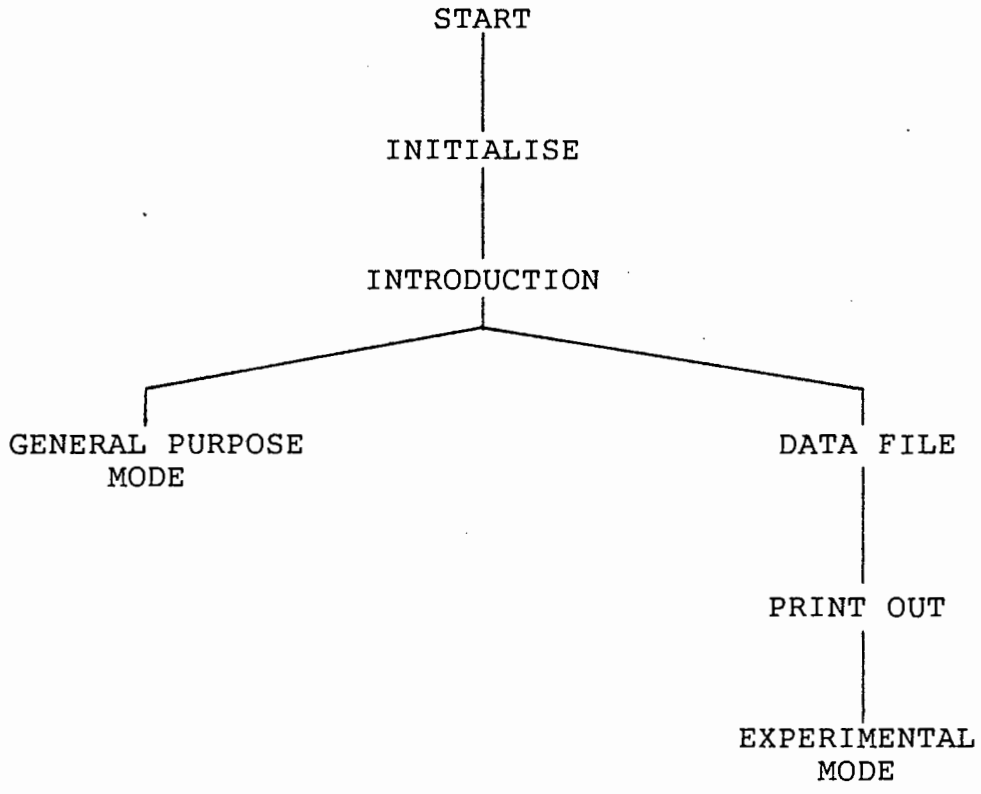

2. <u>The General-Purpose mode</u>

The HP-85 has eight user definable keys which can be incorporated into programs and operate as interrupts[42]. If one of the keys is pressed during a running program, a branch is taken to a specified line number or sub-routine. These keys are made use of here. Keys 1-4 are used to select the function, while keys 5-8 select the range or resolution of the measurement.

Key 1. Selects frequency measurement.
2. Selects Q measurement.
3. Selects period frequency measurement
4. Selects temperature measurement.

5. Measurement taken for 1 cycle of reference oscillator.
6. 10 cycles of reference oscillator
7. 100 cycles
8. 1000 cycles.

This allows all the parameters of the fork to be viewed as required for setting up procedures and general observation. If the Q option is chosen, the measurement is repeated every eight seconds until a new option is chosen. If the range is chosen so that a measurement is taken over 100 cycles of the reference oscillator, the resolution is 1Hz in the frequency measurement mode (temperature) and .001Hz in the period mode (fork frequency). From trial this was the resolution chosen for all the experimental mode measurements (except Q).

The operation of this section of the program is shown in the following flow-chart:

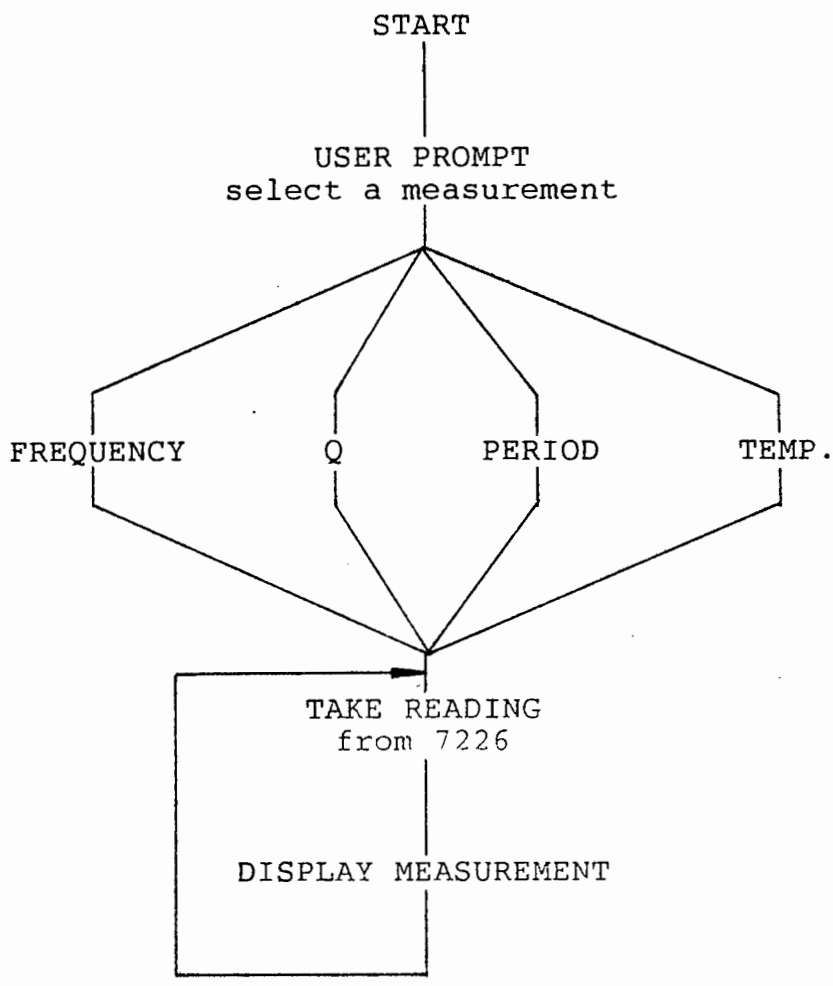

3. Experimental mode

For fatigue experiments it is important to take measurements at fixed number-of-cycle intervals. This is achieved by the use of interrupts. Circuitry in the hardware counts the number of cycles, and after the required number sends out an interrupt pulse to the GPIO interface which in turn interrupts the computer after the present line of the program has been executed. This causes the program to branch to a pre-defined line using the ON INTR statement of the I/O rom[43]

If the experimental mode is selected, then a sequence of measurements will be taken at regular intervals by the interruption of the computer from the interface circuitry. A complete series of measurements is denoted as a measurement block.

This section of the program operates as follows:

Once the formalities for data storage and printing have been completed, the program goes into a continuous loop displaying measurements of the fork frequency in period mode until an interrupt is received from the hardware. At this point, the program jumps out of the continuous loop and performs the following measurements:

1. The average of five resonant frequency measurements
2. The average of five temperature measurements.
3. The average of three Q measurements.

The averaged values are then printed out and/or stored onto file if required. The average of only three Q readings was taken otherwise too much time would be needed for one measurement block: measurements were required every 10 000 cycles and more Q readings

would have taken longer than the time for 10 000 cycles (about 1 minute at 150Hz).

The flow chart showing operation of the experimental mode is as follows:

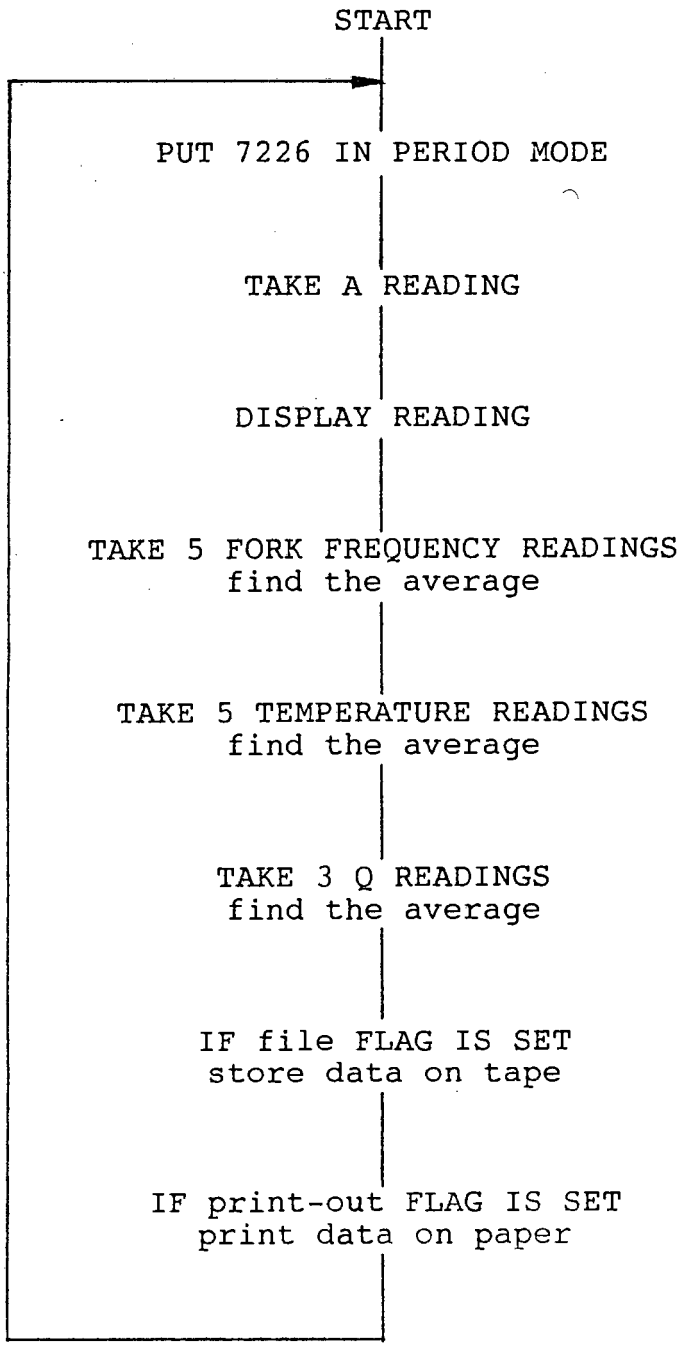

---X---

CHAPTER 9

THE IMPLEMENTATION OF THE 7226 INTERFACE ON THE IBM-PC COMPUTER

9.0. Introduction

Once the HP85 system was working and a number of fatigue experiments had been performed, it was decided to re-do the whole ICM 7226 interface using an IBM-PC compatible computer. The reasons for doing this were:

1. HP85 computers are being phased out by Hewlett-Packard and are now over 15 years old and somewhat outdated.
2. The basic language of the HP85 is very limited and a more powerful compiled language provides a much more acceptable arrangement and which is possible on the IBM.
3. A personal decision to obtain further experience in computer interfacing.

The circuit diagrams can be seen in appendix C. The overall system is shown in Figure 9.1, Diagram C.1 and Photographs G.8 and G.9.

The basis of the interface was the commercially available PC35 prototyping board[44]. This contains some address decoding and buffering circuitry providing the following:

1. 8 chip select outputs (CS0 to CS7).
2. 2 address lines (A0 and A1).
3. Address mapped I/O direction lines (IOR,IOW).
4. Memory mapped I/O direction lines (MEMR,MEMW).

The address map of the IBM-PC allows 32 addresses only for a prototyping card. These are from 300 hex to 31F hex (768 to 799 decimal). The PC35 decodes these 32 addresses to provide 8 chip-select outputs and two address lines giving each chip-select 4 addresses.

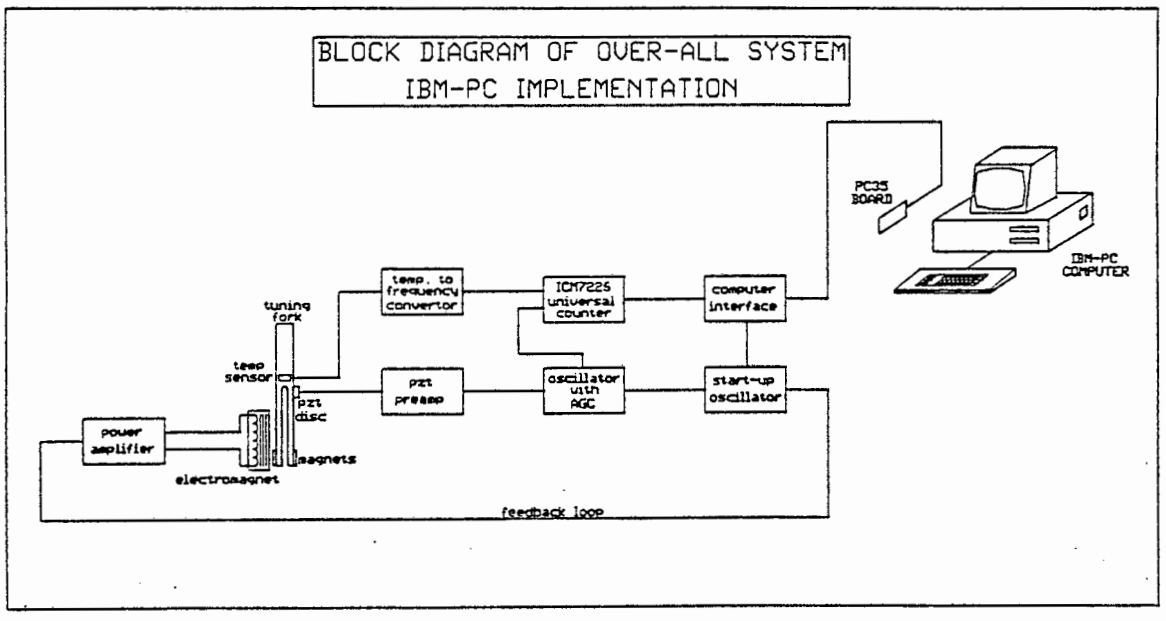

Fig.9.1. Overall system using the IBM-PC

The original PC35 board was modified because the section of the address decoding dealing with addresses 768 to 896 decimal, as supplied, enabled the chip-selects all the time. This caused a lot of audible noise to be produced by the wire-wrapped circuitry on the board due to the large amount of activity on the address bus during normal computer operation. This was prevented by allowing the decoding circuitry to only be active during the IOW or IOR pulses, i.e. during an I/O operation. This also reduces the possibility of glitching problems which may have occurred with the original design.

For the interface to the 7226, three address lines are required to give 8 possible states for some of the circuitry. Therefore, since more address lines are required than the 2 provided, the data bus was used for addressing purposes as well. The chip-selects of the PC35 are further decoded with the two address lines A0 and A1 to give extra chip select lines. In this way up to 32 chip select lines each with an 8 bit address bus can be produced giving 256 possible states. Only ten of the chip select lines are needed using up three of the original PC35 chip selects, leaving the remainder for interfacing with standard chips eg 8255 PPI's, A/D's, 8254 timers, etc. Refer to Diagrams C.2 and C.3.

The interface was designed on the same principle as the HP85 version by using many small sections that can be controlled from the computer. Thus a computer controlled interface rather than a hardware controlled interface was opted for, which gives greater flexibility since only the computer program has to be changed and makes the hardware more simple. The drawback is that the system will be a lot slower than the corresponding hardware design but in this case speed is not important.

9.1. The Interface Circuitry

The interface can be broken down into eight modules (Diagrams C.4, C.5, C.6A and C.6B):

1. READ-DATA (Diagram C.6A)

   This allows the data stored in the latches to be read into the computer. The 4 bit BCD bus from the 74ls173 latches is fed to the inputs of a 74ls373 octal latch having tristate outputs. The inputs 4,5,6,7 of the latter are grounded. To generate enable and latching signals, the CS0 and the A0,A1 lines from the PC35 decoding circuitry are fed to a 74ls27 three input NOR gate. The output of this is fed to an inverter and the original and inverted signals drive the CLOCK and ENABLE inputs respectively of the 74ls373. Thus when a digit is to be read, the computer

outputs an IOR pulse which clocks the data into the latches of the 74ls373 and at the same time enables the outputs onto the data bus which will be input to the computer a short time later.

2. SELECT-DIGIT (Diagram C.6A)

The digit which is to be read is enabled onto the bus by this module. A 74ls138 1 of 8 selector drives the tristate enable input of the 74ls173 latches. A three bit address decides which latch is pulled onto the bus. This address is output on the data bus and is latched by 74ls75's which in turn have a latching signal generated by decoding the CS0,A0,A1 signals for address 769. The A0 signal is inverted before sending it to the three input NOR gate.

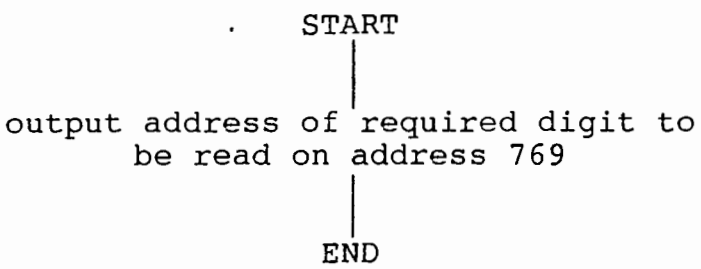

3. CAPTURE-DATA (Diagrams C.6A, C.7)

The CAPTURE-DATA module is activated by a CAPTURE-DATA pulse which is generated simply by decoding the CS2,A0,A1 signals with a 74ls27 NOR gate, the output of which is then inverted. The address of 779 is achieved by inverting the A0,A1 signals before they are sent to the 74ls27.

When the computer requires a measurement, a CAPTURE-DATA pulse is generated by outputting 0 on the data bus. In fact any data could be sent out because it is only the address which is used and not the data.

The CAPTURE-DATA module takes the CAPTURE-DATA pulse and uses it to clock a D type f/f (f/f1), having the D input tied high. Thus the Q1 output will be set high and this feeds the D input of a second D type f/f (f/f2). The clock input of f/f2 is the buffered STORE output from the 7226. Thus once the present measurement in progress is complete and the STORE output goes high, the Q2 output will be clocked high. This feeds the HOLD input of the 7226 which will then be frozen. This Q2 output also feeds the positive edge input (B) of a 74ls221 monostable having a pulse width of 5mS, the Qm output feeding the data enable inputs of the 74ls173 latches, allowing each digit BCD representation to be captured. The Qm output feeds the B input of a second monostable of time constant 1uS the Qm2 output driving the clear inputs of flip-flop 1 and 2. Thus the termination of the 5mS capture pulse triggers a 1uS reset pulse which sets the Q outputs of the f/f's low, removing the HOLD condition on the 7226.

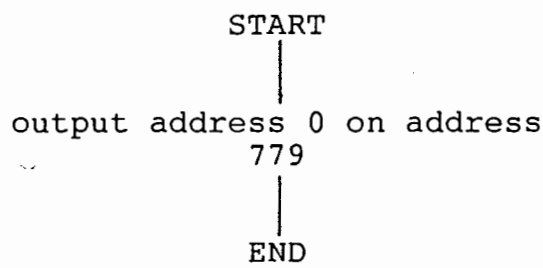

4. FUNCTION-SELECT (Diagram C.6B)

This selects which digit driver signal is to be routed to the FUNCTION input of the 7226. The buffered inverted digit driver outputs are fed to a 74ls153 4 to 1 data selector. The routing address is stored in 74ls75 latches which are enabled by decoded

CS0,A0,A1 signals on address 770. Since the digit driver signals are inverted, this is corrected by inverting the output of the 74ls153 before it is sent to the FUNCTION input of the 7226.

5. RANGE-SELECT (Diagram C.6B)

This is identical to the FUNCTION-SELECT module except that the digit driver signals are routed to the RANGE input instead.

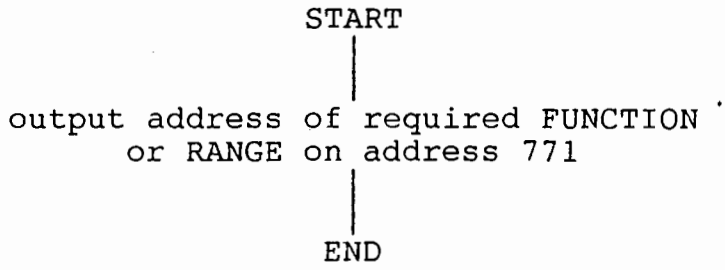

6. POLING-LINES (Diagram C.6B)

Unlike the HP85 there is no facility for inhibiting output operations on the buses and therefore poling lines are required to monitor the state of various sections of the interface. The state of these lines is monitored by the program until the required state occurs and thus the "inhibiting" is done by the program which merely wastes time until the operation can continue. Eight poling lines are provided which operate completely independently. The 8 inputs for poling are sent to a 74ls151 data selector whose address decides which input is routed to the output. The address is sent out on the data bus and latched in 74ls75's which are enabled on address 774. The output of the 74ls151 is sent to a 73ls373 tristate octal latch, the 7 remaining inputs being grounded. The outputs are connected to the data bus and clocking and tristate enabling is provided on address 775. The steps required in selecting and then reading a poling input are:

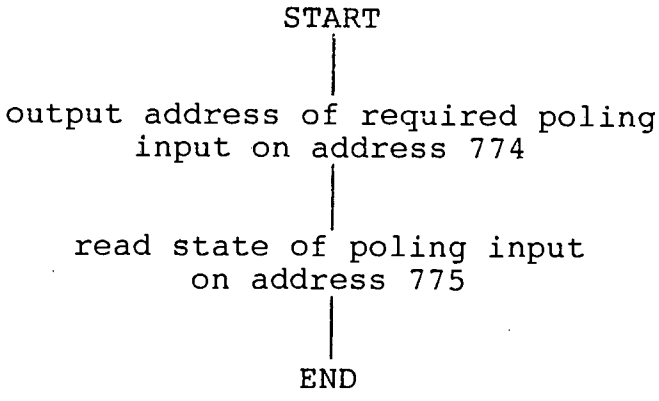

NB: Instead of selecting the input and then sending its 1 bit value over the eight bit data bus, each bit input of the 74ls373 could have been made a poling input. However, although this simplifies the circuitry, it is not as easy to use because when reading a particular input, the other bits have to be masked out.

7. INPUT-MULTIPLEXER (Diagram C.6B)

This allows up to eight different pulse trains to be input to the 7226 for measurement. This is similar to the poling-lines module. The eight inputs are fed to a 74ls151 the output of which feeds the A input of the 7226. The input select address is stored in 74ls75 latches which are enabled on address 777.

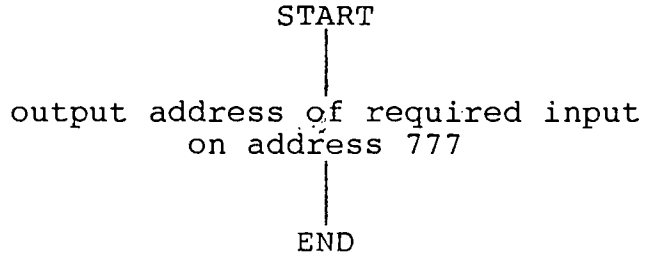

8. GENERAL-PURPOSE LINES (Diagram C.6A)

A much better arrangement was designed for providing control lines for the switching of external relays, etc. This design allows eight switching lines which can be individually set high or low. The general purpose outputs come from a 74ls259 8 bit addressable latch. This has an input bit which is routed to 1 of the 8 D type latches via a 3 bit address, which is then clocked to the corresponding output with a common clock input. The address comes straight from the data bus since no change will take place until the clocking pulse occurs. The input bit is latched by a 74ls75, enabled on address 772. The clocking signal is derived by decoding the CS1,A0,A1 signals for address 773.

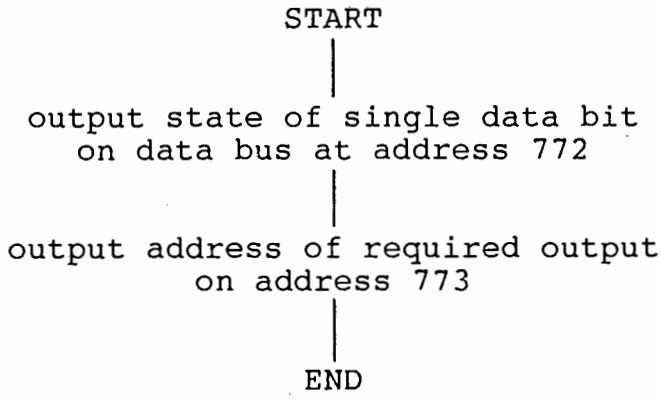

Only one of these general purpose outputs is needed for fatigue experiments. This is to switch the drive on and off and to enable the reset input to the 7226 for Q measurement.

These modules are connected to the PC35 circuitry as shown in block Diagram C.3. The wire-wrapping technique was used to build the circuit on the PC35 board which enables a high density of chips to be achieved. Enough space was left on the board for additional chips if required, e.g. an A/D would be useful.

9.1.1. The Q measurement module

The Q measurement circuit for the IBM pc is similar to that for the HP85 except for the computer inhibit feature (Diagram C.8). The reset output to the 7226 is enabled with the first general purpose output line which also turns the tuning-fork drive signal on and off. The circuit has to be poled to decide when a Q measurement is complete so that the value stored in the 7226 unit counter mode can be read. The L-enable line (Q2 output of section detecting if signal is above Vlow) is poled for this purpose ie when the signal is below Vlow the counter will have stopped incrementing and the L-enable signal will have gone low. This is sent to the second poling input.

9.2. The computer program

The program was written in TRUE BASIC[45,46]. This is a new version of the old BASIC language and is very similar to PASCAL. The language allows far more structure and eliminates the need for the GOTO statement. It is much more meaningful to read since whole words can be used for variable names instead of only single letters.

The program is again written in two sections, the first to convert the 7226 to a general purpose measurement instrument and the second to perform fatigue experiments.

This system worked very well. The main improvement being in the speed at which the computer operates, which is high enough to keep up with the 7226 in all ranges. With the HP85 system, at least 1sec was needed to read the data and hence in the 1sec range a reading was taken only on every 2nd or 3rd measurement. The other benefit is in the management of data. There is no restriction on file length and a more sophisticated data base type arrangement could be used, instead of creating a separate data file for each experiment.

---X---

CHAPTER 10

THE RESULTS OF THE EXPERIMENTAL WORK

10.0. Introduction

A fairly large number of tuning-fork specimens were machined from mild steel. Several of these were "wasted" during the design and setting up stage of the apparatus, and some were fatigued without recorded data to see in fact if fatigue was possible with this system. The remaining samples were used to perform various experiments.

10.1. The various experiments performed

10.1.1. Fatigue tests

A stepped type of testing was used in performing fatigue tests. Initially the amplitude is chosen to be below the suspected fatigue limit and a test run for at least 10 M-cycles to prove that no fatigue is taking place. The amplitude is then increased slightly and the test repeated until an amplitude is found where fatigue takes place in less than 10 M-cycles. The disadvantage of this method is that the sample will become progressively work-hardened with each step which raises the fatigue limit. This is also called coaxing of the specimen (chapter 3). This is especially true if the sample was in the annealed state at the start. However, in this work no serious tests were done to determine fatigue limits as the primary objective was to demonstrate the apparatus.

10.1.2. Temperature dependence tests

Temperature dependence was measured by vibrating the fork at an amplitude well below the fatigue limit so that the only changes occurring in the metal were due to temperature, with no permanent metallurgical alteration.

The whole rig assembly was slowly heated by including a 40W bulb underneath the main base channel section, with a small convection fan mounted at the back of the housing to make the apparatus as isothermal as possible. This combination enabled very slow rates of temperature climb to be achieved up to a steady-state value of about 40°C. Data was recorded for the heating and cooling curves.

The temperature effect shows some thermal hysteresis, being different for cooling and heating, because the temperature measured at the sensor depends on the heat flow through the sample which will be different according to the flow direction.

10.1.3. Relationship between temperature coefficients of frequency, length and elastic modulus.

From Rayleighs theory of similitude the parameters of a vibrating system which affect the frequency have a simple relation:

$$\frac{f\ F(x,y,z)}{\text{velocity}} = \text{constant} \quad \ldots\ldots\ldots\ldots\ldots\ldots\ldots \quad (10.1)$$

Where:

$F(x,y,z)$ = a function with the dimensions of length describing the three dimensional change in dimensions.

f = frequency.

For a vibrating reed (tuning-fork):

$$F(x,y,z) = l^2/w$$

Hence, 10.1 becomes:

$$f(l^2/w)/C = \text{constant} \quad \ldots\ldots\ldots\ldots\ldots\ldots\ldots \quad (10.2)$$

Where C = velocity of sound
l = length of reed
w = thickness of reed

For a solid material:

$$C = \sqrt{\frac{E}{p}} \quad \ldots\ldots\ldots\ldots\ldots\ldots\ldots\ldots\ldots\ldots \quad (10.3)$$

Where:
E = Youngs modulus
p = density

and substituting (10.3) into (10.2) gives:

$$f \frac{L^2}{w}\sqrt{\frac{p}{E}} = \text{constant} \quad \ldots\ldots\ldots\ldots\ldots\ldots \quad (10.4)$$

Taking the dimensions of equation (10.4):

$$f\ L^2\ L^{-1}\ M^{\frac{1}{2}}\ L^{-3/2}\ E^{-\frac{1}{2}} = \text{constant} \quad \ldots\ldots\ldots\ldots\ldots \quad (10.5)$$

Taking the logs of equation (10.5):

$$\ln(f) - \tfrac{1}{2}\ln(L) + \tfrac{1}{2}\ln(M) - \tfrac{1}{2}\ln(E) = \ln(\text{constant}) \quad \ldots \quad (10.6)$$

Differentiating (10.6) w.r.t temperature θ

$$\frac{1}{f}\frac{dF}{d\theta} - \tfrac{1}{2}\frac{1}{L}\frac{dL}{d\theta} - \tfrac{1}{2}\frac{1}{E}\frac{dE}{d\theta} = 0 \quad \ldots\ldots\ldots\ldots\ldots\ldots \quad (10.7)$$

Thus if we denote:
α_f = temperature coefficient of frequency
α_l = temperature coefficient of linear expansion
α_E = temperature coefficient of Youngs modulus
then substituting into (10.7) gives:

$$\alpha f = \tfrac{1}{2}(\alpha_l + \alpha_E) \quad \ldots\ldots\ldots\ldots\ldots\ldots\ldots\ldots \quad (10.8)$$

Hence the frequency coefficient is split equally between the coefficients of linear expansion and Youngs modulus. For steel the coefficient of Youngs modulus is ≈ 10 times that of linear expansion.

The change in Youngs modulus with temperature is significant in producing the change in frequency. Thus from the values found for the frequency coefficient, and by looking up the value of α_l in a handbook, the coefficient of the Youngs modulus can be found for the mild steel used in this work.

$$\alpha_E = 2\alpha_f - \alpha_l \quad \ldots\ldots\ldots\ldots\ldots\ldots\ldots\ldots\ldots\ldots \quad (10.9)$$

A typical value for α_l = 12.2 ppm [47]. ..... (10.10)

From this work, the average figure obtained for the frequency coefficient is:

$$df/d\theta = .01880 \text{ Hz/°C} \quad \ldots\ldots\ldots\ldots\ldots\ldots\ldots\ldots \quad (10.11)$$

A change of 1°C gives a change in frequency of 2%.

Converting (10.11), α_f = -126.0 ppm ..... (10.12)

Hence substituting (10.10) and (10.12) into (10.9):

$$\alpha_E = -2\text{x}126.0 - 12.2$$
$$= -264.2 \text{ ppm} \quad \ldots\ldots\ldots\ldots\ldots\ldots\ldots\ldots\ldots\ldots \quad (10.13)$$

Thus the rate of change of Youngs modulus with temperature is:

$$dE/d\theta = E \times \alpha_E = 20.0\text{x}10^{10} \times -264.2$$
$$= -47.2\text{x}10^{6} \text{ per°C} \quad \ldots\ldots\ldots\ldots\ldots\ldots\ldots\ldots \quad (10.14)$$

Thus a change of 1°C causes a change of 0.026% in Youngs modulus.

with good correlation coefficients (.99). The frequency is resolved to 1/100 Hz, by the measurement circuitry, which is greater than that of the temperature effect, so these curves show very little scatter and extremely high correlation coefficients for the regression line (.999). The resolution of the Q measurement is comparable to the temperature effect and so a high degree of scatter is observed, making the temperature effect on the Q less accurate to determine than that for the frequency, but high correlation coefficients are also obtained (.99).

The slope of the regression line gives the temperature coefficient. A typical set of results for a steel tuning-fork can be seen in Table 10.1 and Graphs D.3, D.4, D.5 and D.6.

	Heating		Cooling		Average
	Hz/°C	ppm	Hz/°C	ppm	ppm
Frequency	-0.0187	-125.3	-0.0189	-126.7	126.0
	1/rad/°C	ppk	1/rad/°C	ppk	ppk
Q	-11.2	-14.9	-10.4	-13.9	14.4

Table 10.1. Temperature coefficients

The temperature coefficients are used to correct for temperature changes in other experiments by referring values of frequency and loss to an arbitrary fixed temperature. This was chosen to be 20°C. The average of the cooling and heating values are used.

10.2.2. First fatigue run

The vibration amplitude is increased to about 3.0mm. A new run is started at room temperature with the circulation fan switched off. The computer is left to take readings which are stored on tape until 10 M-cycles has passed. At this point it is assumed that no fatigue is going to occur at that amplitude and the experiment is stopped.

10.2.3. Second fatigue run

The amplitude is increased to 3.5mm and a computer run is started. This particular fork fatigued at this amplitude after 5.5 M-cycles. The fatigue is viewed by plotting graphs of frequency and Q or loss (1/Q) versus the number of cycles (N). The overall experiment is shown in Graphs D.7, D.11 and D.12.

A feature of these graphs is that the loss effect seems to lead that of the frequency. An explanation of this is that the dislocations become tangled up and increasingly pinned, causing large increases in damping, but little change in material stiffness and hence frequency. The next stage is the formation of jogs when the dislocations break through the pinning points. It is from these jogs that cracks can develop (chapter 2). Thus it appears that the frequency only begins show large changes once a fatigue crack has been initiated, when the stiffness of the material begins to fall.

Further investigations can be performed on the frequency data. The portion of the curve from 0 to 400 cycles appears not to change on the overall graph. If this is plotted out on an expanded scale then the Graph D.10 is produced. The changes of frequency here are due mainly to temperature, shown in Graph D.9. Using the coefficient found in the temperature dependence experiment, a correction can be made by referring all the frequency values to 20°C. This reduces the scatter of the data which can then be plotted out using a much larger scale. Re-plotting the corrected values, (Graph D.8), shows that the previous scatter has disappeared giving a flat line until a sharp knee at about 3 M-cycles. This is interpreted as being the development of a micro-crack.

The Q data over the same region has considerably more scatter due to the lower resolution of the Q measurement (Graphs D.13 and D.15). If a similar temperature correction is made to the Q data, it will therefore, be less effective than for frequency. The Graphs D.14 and D.16 are produced. Again the knee can be observed to be forming at about 3.0 M-cycles. Therefore, the apparent lag of the frequency is

due to the stiffness of the material not changing very much in this region compared to the changes in internal friction. The important feature to note is the good sensitivity to material changes that can be achieved by correcting for the thermal changes.

Another interesting phenomenon occurs if the loss (1/Q values) are plotted against the frequency values. The Graph D.17 is produced. Initially all the points are concentrated over a small region where the flat portion of the f-N and Q-N graphs occur. Once the final knee portion is encountered, the values begin to change, producing a non-linearity in the Graph D.17. Once the final downward trend is reached, this produces a very linear curve and constitutes the majority of the Graph D.17. This is very interesting due to the extreme linearity (.998), and it means that the frequency and loss follow the same law, in this region.

The knee of the overall experiment, Graphs D.7, D.11 and D.12, is thought to be where the micro-crack transforms into a macro-crack which then propagates rapidly across the specimen, causing large changes in internal friction and stiffness of the material. Once the fracture is large enough, the tuning fork fails to oscillate. At this point the cracked tyne is almost completely severed. The fatigue crack usually only occurs in one tyne, the other remaining intact. This is due to the one being more favourable to crack initiation due to a surface defect, and once a crack is formed the effect is cumulative.

Thus, this system forms a very sensitive technique for monitoring internal material changes.

A selection of some fatigued forks can be seen in photograph G.10. Note that only some forks have their tynes completely fractured from the base. The experiment is usually stopped with most forks before the crack has propagated far enough to cause this severing.

10.3. The amplitude dependence of damping

The Q of the tuning-fork is referred to instead of the loss or internal friction because the measurements performed give the value for Q directly, and hence it is easier to explain the operation of the Q-meter in terms of the Q values obtained. As discussed in chapter 2, the Q and loss have a simple inverse relationship. (loss = 1/Q). The Q is an electrical circuit term whereas the loss, internal friction or damping are material or mechanical terms.

As already discussed in chapter 7, the amplitude at which the Q measurement is made, can easily be changed by altering the amplitude at which the analogue signal enters the Q meter. This amplitude is set by a pot on the front panel of the AGC unit, which adjusts the gain of the measurement amplifier.

The Q measurement can be taken at very small amplitudes by turning the gain of the amplifier up. Even if the signal is clipping while the fork is still being driven, then once it is switched off, the input signal from the pzt pre-amplifier will begin to drop and eventually fall to a value where the gain no longer causes clipping, and a decaying sine wave will be input to the Q meter. When this amplitude has fallen to the upper set-point the vibration amplitude will be extremely small.

To obtain some measure of the vibration amplitude at which the Q measurement is made on the decaying signal, it is no use measuring the input voltage before switch off since it becomes clipped for higher gains. Therefore, the resistance of the feedback pot of the measurement amplifier is measured instead, which directly relates to the amplitude the signal should have had in the absence of clipping. A Fluke multimeter being used for this purpose.

The amplitude dependence was demonstrated by running a fork at 2mm pk-pk amplitude which is below the fatigue limit, and taking a series of Q measurements at different settings of the measurement amplifier. Initially the maximum gain was used, giving an extremely

small amplitude at which the Q reading is taken, and at the end, the minimum gain possible was used where the amplitude at which the reading is taken is virtually the same as the initial vibration amplitude before switch-off. An average of 3 Q readings and the resistance of the pot being taken at each measurement. This produces data relating the damping to the vibration amplitude. The resistance values were inverted and normalised to a maximum value of 1. By multiplying these values by 100 and plotting them versus the Q readings, the change in Q as a percentage of the starting amplitude can be obtained. The results can be see in Graphs D.18 and D.20.

The damping is amplitude dependant because of two main factors (chapter 5).

1. Air-damping
2. The non-linearities of the material itself at higher amplitudes due to the change in elastic constants (anelasticity).

Thus, the graph includes both of these effects, which are difficult to separate. At low amplitudes (high Q), the non-linearities of the material should be disappearing, leaving only air-damping. This is shown by the graph where the loss has a steady value for low amplitudes, but which rises, with ever increasing rapidity, as the amplitude is increased.

10.3.1. Effect of extra air-loading

The air loading of the tynes, especially due to the magnets at the ends which have a larger surface area, was tested by inserting thin strips of plastic between the vibrating magnets and the poles of the electromagnet. This reduces the spacing, and causes extra compression and expansion of the air in this region. A considerable difference was observed even with strips of 1mm thickness. This demonstrates that the air damping plays an enormous role in the damping of the tuning-forks. In order to try and obtain some

quantitative data on the effect, the amplitude dependence of damping experiment as described above was repeated, but with the strips inserted. The results of the test with and without extra air loading can be seen in Graphs D.19 and D.21.

10.3.2. The efficiency of the drive system

An experiment was done to see how the efficiency of the drive system changed with vibration amplitude of the tuning-forks. This was done because the initial concept of the work was based on the realisation that the new samarium-cobalt magnets, together with a resonator specimen of high Q, had the potential of producing a highly efficient electro-mechanical coupling.

Consider the formula relating Q to the energy of a vibrating system:

$$Q = 2\pi \left(\frac{\text{energy stored}}{\text{energy lost/cycle}} \right) \quad \ldots\ldots\ldots\ldots\ldots\ldots\ldots \quad (10.15)$$

$$Q = 2\pi f \left(\frac{\text{energy stored}}{\text{average power loss}} \right) \quad \ldots\ldots\ldots\ldots\ldots\ldots\ldots \quad (10.16)$$

We can model the tuning fork as the classical viscously damped mass-spring resonance system (chapter 4). If the Q of the system is high then the fundamental frequency is given by:

$$f_0 = \frac{1}{2\pi}\sqrt{\frac{K}{M}} \quad \ldots\ldots\ldots\ldots\ldots\ldots\ldots\ldots\ldots\ldots\ldots \quad (10.17)$$

However, we need to find the equivalent mass M of the system. This can be done by adding small concentrated masses to the ends of the tynes and measuring the drop in frequency. In the experiment, two five cent pieces were glued to the end of each tyne.

$$f_1 = \frac{1}{2\pi}\sqrt{\frac{K}{M+m}} \quad \ldots\ldots\ldots\ldots\ldots\ldots\ldots\ldots\ldots\ldots\ldots \quad (10.18)$$

Thus combining equations (10.17) and (10.18) gives:

$$M = \frac{m f_1^2}{f_0^2 - f_1^2} \quad \ldots\ldots\ldots\ldots\ldots\ldots\ldots\ldots\ldots\ldots\ldots \quad (10.19)$$

The added mass was accurately determined by weighing 20 coins on a triple beam balance. This gives an average mass of

mass of 20 coins = 49.98g

mass of 1 coin = 2.499g

mass of 4 coins = 9.966g

Hence m = 9.966g ..... (10.20)

The energy of the equivalent system is given by

$$E = \tfrac{1}{2}Mw^2A^2$$
$$= \tfrac{1}{2}M(2\pi f)^2A^2$$
$$= 2M(\pi fA)^2 \quad \ldots\ldots (10.21)$$

Inserting (10.21) into equation (10.16) and re-arranging:

$$\text{average power loss} = 2\pi f\left(\frac{\text{energy stored}}{Q}\right) \quad \ldots\ldots (10.22)$$

$$\text{average power loss} = \frac{4M(\pi f)^3A^2}{Q} \quad \ldots\ldots (10.23)$$

Hence equation (10.23) gives the power lost from a vibrating system of equivalent mass M, amplitude A, frequency f and damping 1/Q.

The input power to the system is easily measured in this work by monitoring the electromagnet current, voltage and phase angle.

Thus the efficiency is calculated from:

$$\text{Efficiency} = \left(1 - \frac{P_{lost}}{P_{input}}\right) \times 100 \quad [\%] \quad \ldots\ldots (10.24)$$

$$= \left(1 - \frac{4M(\pi f)^3A^2}{QIrmsVrms\cos\phi}\right) \times 100 \quad [\%] \quad \ldots\ldots (10.25)$$

An experiment was carried out to determine the equivalent mass at four vibration amplitudes using equation 10.19 and the result 10.20. The results are shown in table (10.2) below.

amplitude		1.5mm	2.0mm	2.5mm	2.8mm
frequency	f_0	151.620	151.574	151.519	151.502
	f_1	144.505	144.485	144.389	144.428
equiv M		99.1g	99.4g	99.6	99.8g

Table 10.2. Equivalent mass values

The equivalent mass was found to not vary significantly with amplitude and therefore an average was taken giving a fixed value for M as 99.48g

The data necessary to calculate the efficiency over a wide range of vibration amplitudes was measured. The electromagnet coil current was used as the independent variable. At each value of I_{coil}, the coil voltage V_{coil} and phase shift was measured to determine the input power. Other measurements made were of the output voltage from the pzt pre-amplifier, the vibration amplitude, the frequency and the Q. All the results can be seen in Table 10.3.

From the results, the amplitude was plotted versus the output from the pzt pre-amplifier (Vpzt). This gives the expected straight line showing that the pzt transducer is linear, or that there is a linear relation between pk-pk amplitude and strain over this strain range (Graph D.26):

$$\text{Amplitude} = 0.00624\ \text{Vpzt} \quad [\text{mm}] \quad \ldots\ldots\ldots\ldots\ldots \quad (10.26)$$

From each set of readings the P_{lost} and P_{input} values were calculated. The variation of Pinput with vibration amplitude is shown in Graph D.23. A plot of Plost versus Pinput, gives a rather poor quadratic shaped curve. In order to smooth the data, a quadratic equation was fitted to the points (Graph D.24):

$$P_{lost} = .3682\ P_{input} - 0.001264\ P_{input}^2 \quad \ldots\ldots\ldots \quad (10.27)$$

From this regression equation the efficiency is easily found:

$$\text{Efficiency} = \left(\frac{P_{useful}}{P_{input}}\right) \times 100 \quad [\%] \quad \ldots\ldots\ldots\ldots\ldots \quad (10.28)$$

$$\text{Efficiency} = \left(\frac{P_{input} - P_{lost}}{P_{input}}\right) \times 100 \quad [\%] \quad \ldots\ldots\ldots \quad (10.29)$$

$$\text{Efficiency} = \left(1 - \frac{P_{lost}}{P_{input}}\right) \times 100 \quad [\%] \quad \ldots\ldots\ldots\ldots \quad (10.30)$$

$$= 63.18 - 0.1264\ P_{input} \quad [\%] \quad \ldots\ldots\ldots \quad (10.31)$$

With power in mW

This gives the expected result that the higher the amplitude, the more power is lost in air-damping and material non-linearities, lowering the efficiency. Obviously, the efficiency regressed to zero input power is meaningless.

By finding regression formulae relating Pinput to Vpzt and then to amplitude, an expression giving the efficiency as a function of amplitude can be produced:

$$\text{Efficiency} = 63.18 - 2.809 \cdot \text{Amplitude} \quad \ldots\ldots\ldots\ldots \quad (10.32)$$

With amplitude as pk-pk value in mm.

A plot of this equation is given by Graph D.25.

10.3.3. The amplitude dependence of frequency

From the above experiment, a plot of frequency versus amplitude gives a good approximation to a straight line (Graph D.27). The regression fit is:

$$f = 151.737 - 0.1136 \cdot \text{Amplitude} \quad [\text{Hz}] \quad \ldots\ldots\ldots\ldots \quad (10.33)$$

with a correlation coefficient = .9949

with amplitude as pk-pk in mm

The drop in frequency as the amplitude is increased is due to the elastic constants of the material changing: namely the Youngs modulus. This is due to several possibilities:

1. Anelasticity, where there is a stress-induced ordering process, allowing for example interstitial atoms to move to more favourable sites within the lattice which may lower the lattice energy, causing softening of the material.

2. It can, alternatively, be explained by the vibrating-string model of dislocation motion by Granato and Lucke[4,5,6] where the elastic modulus varies as the dislocation line breaks free from the pinning due to interstitial atoms (chapter 2). In the stress range experienced here, the change appears to be linear.

3. Temperature changes within the material. At higher amplitudes the amplitude x loss product will be increased, giving a greater rate of temperature rise. This is perhaps the most likely cause for the amplitude dependence of the frequency.

10.4. Microscopic investigations of fatigue surfaces

Several photographs of a typical fatigue surface from the tuning-forks were taken on the scanning electron microscopes (SEM). The purpose of this study was to obtain some idea of the nature of the fatigue being produced by this apparatus.

10.4.1. Scanning Electron Microscope photographs

Sample no 1

The sample tested had a very short fast fracture region, the majority of the surface being used for crack propagation.

1. Photograph SEM 1

   A general view of the fracture surface at 472mag. Crack growth is from top to bottom.

2. Photographs SEM 2, 3

   A closer view of the fracture surface showing fatigue striations. Crack growth is from top to bottom.

Sample No.2

This sample had a larger fast fracture region.

1. Photograph SEM 4

   A view of the crack initiation site which is in the centre. Close inspection reveals lines radiating from this point, which reach a steady state parallel condition

2. Photograph SEM 5

   A close up view of the fatigue striations on an individual grain.

2. Photograph SEM 6

   Another view of fatigue striations in a different region.

3. Photograph SEM 7

   This is a higher magnification view of SEM 6 above.

4. Photograph SEM 8

   The view of 8092 was rotated through 90° so that crack growth is from left to right. This enabled the cursor to be used to obtain the approximate striation spacing in this region and is 283nm.

5. Photograph SEM 9

This photograph shows the transition region between the smooth crack propagation area and the final fast fracture portion. The smooth region clearly becomes rougher and dimpled at the boundary.

6. Photograph SEM 10

A high magnification view of the final fracture zone showing its heavily dimpled nature. This is characteristic of ductile fracture due to plastic deformation.

7. Photograph SEM 11

A high magnification view of the final fracture region.

---X---

Reading	1	2	3	4	5	6	7	8	9	10	11	12	13
I_{coil} (mA)	25	50	75	100	125	150	200	225	250	300	350	400	450
V_{coil} (mV)	47	96	155	209	184	218	289	331	376	457	546	630	716
Phase (deg.)	5	7	12	14	20	25	36	42	44	45	47	48	50
V_{pzt} (mV)	34	66	99	127	156	177	216	263	253	285	318	354	387
Amplitude (mm)	0,30	0,55	0,80	0,90	1,16	1,35	1,60	1,65	1,80	1,90	2,15	2,35	2,55
Frequency - 151,00 (Hz)	0,698	0,672	0,648	0,630	0,611	0,592	0,564	0,551	0,536	0,511	0,488	0,467	0,448
Q	-	1068	1026	994	1114	1074	1026	1001	972	946	918	884	860

TABLE 10.3

CHAPTER 11

CONCLUSIONS

The first objective of this thesis was to design and build an apparatus for performing fatigue experiments on samples in the form of tuning forks at resonance. A computer controlled measurement system then monitors the performance of the resonance by taking measurements of frequency, Q and temperature of the specimen. Secondly, the apparatus was to be tested on a number of samples for temperature effects on the frequency and loss (Q), and for performing fatigue experiments.

The main motivation behind the technique, is the great sensitivity to changes in the internal structure of metals that is reflected in the resonance characteristics. Hence, the monitoring of the resonance parameters gives an ideal method of studying materials undergoing cyclic stressing.

The conclusions from the project are:

1. The construction of the apparatus in terms of mechanical and electronic components was achieved with great success with the result that a reliable system was produced.

2. The use of the powerful samarium cobalt magnets glued to the ends of the tynes allows a relatively easy means of driving the tuning forks electromagnetically, at vibration amplitudes high enough to cause fatiguing of the metal. The efficiency of the drive system was tested by modelling the tuning fork as a lumped mass-spring system, for which the equivalent mass was found (chapter 4) and (chapter 10). The efficiency is about 65% at

small amplitudes which decreases as the amplitude is increased, due to the increasing energy loss of the vibrating fork by air-damping and anelasticity effects.

3. The use of a small pzt disk glued to the side of the tuning fork, at the base of the tynes, provides an easy and effective means of developing a signal proportional to the strain. This signal can then be used to provide an electronic method of control of the flexural amplitude. The positive feedback oscillator arrangement, with AGC, gives good performance and due to the few electronic devices needed, it is therefore less susceptible to temperature effects. The use of an analogue multiplier as the variable gain element gives excellent performance.

5. The ICM 7226 universal counter device from Intersil is a good foundation for the measurement system that is required to keep a record of the the resonance performance of the tuning forks. At the low frequencies encountered (150Hz), the accuracy in the period mode is 1/100 Hz. The use of a voltage to frequency converter for measuring temperature allows an accuracy of 0.01°C. The combination of high resolution frequency and temperature measurements allows a good temperature correction to be made from which small changes in stiffness (frequency) of the material may be observed.

6. The free-decay technique for measuring the Q (loss) of the forks provides a means of eliminating air-damping and anelastic effects, by sampling the decay at low amplitudes. This allows the internal loss only of the material to be measured and gives a more accurate picture of any internal changes. The ICM 7226 in the unit counter mode, with some additional circuitry provides an easy solution to this measurement.

7. The use of the HP85 computer with the GPIO interface, enables a simple interface to be quickly constructed. The BASIC programming language, however, is very limited and makes the program difficult to follow, even for the programmer going back

to read it after some time. The IBM pc computer provides a more sensible arrangement, where the interface is also reasonably simple to implement, but the ability to use a number of high level compiled programming languages is a big advantage.

8. The temperature coefficients of frequency and Q (loss) can be found by vibrating at an amplitude below that necessary to produce fatigue, and then slowly heating the whole apparatus. The heating and cooling curves give slightly different results due to the difference in flow rate according to the flow direction. Plots of frequency and Q versus temperature give good straight lines with high correlation regression fits (0.99). From the slopes, the temperature coefficients can be found. The average frequency coefficient is -124ppm and that for the Q is -14.4ppk. By studying Rayleigh's Theory of similitude, the relation between the temperature coefficients of Young's modulus, linear expansivity and frequency can be found, from which the coefficient of Young's modulus can be calculated. The value obtained for the mild steel used here is -264.2 ppm.

9. A stepped type of fatigue testing was used. This is implemented by starting at an amplitude below the fatigue limit and running the experiment for at least 10 M-cycles, after which it is assumed that no fatigue is going to occur. The amplitude is increased slightly and the experiment repeated, until an amplitude is found that causes fatigue in less than 10 M-cycles. Plots of frequency and Q versus the number of cycles gives a graph that remains level for most of the time and then reaches a knee point, after which the frequency and Q take a downward trend, indicating that the stiffness of the material is dropping and the loss is increasing. Of course, the Q values can be inverted to give those of the loss, a plot of which gives the overall loss picture immediately.

10. If the points before the final knee are corrected for temperature and referred to 20°C, then the temperature changes can be removed, enabling the material changes to be isolated.

This method is especially significant for the frequency which has a resolution greater than the temperature changes. A re-plot shows the exact point of crack initiation, seen by a sudden downward trend. The corrected and referred Q values show a similar sharp bend, but there is far more scatter in the data due to the lower resolution of the Q measurement.

11. Another interesting phenomenon is obtained by plotting the loss versus the frequency. The values from the beginning which remain virtually constant, produce a stationary region on this graph. However, the points in the region past the final knee produce a remarkably straight line with regression coefficient of .998. This implies that the stiffness and internal friction follow a similar law over this region.

12. The dependence upon vibration amplitude of various factors was tested. The most significant was the effect of air-damping. Measurements of Q at a series of decay amplitudes were taken, for a fork initially vibrating below the fatigue point, by altering the signal input level to the Q meter. A plot of these values reveals that the damping changes rapidly for amplitudes just below the initial value, and reaches a steady state for very low amplitudes. There are two factors contributing to this. The air-loading effect on the ends of the tynes which have a large vibration amplitude and a large surface area due to the magnets. The non-linearity of the internal friction due to anelasticity effects within the material. The air loading was investigated further, by inserting thin strips of plastic in the space between the vibrating magnets and the inner faces of the poles of the electromagnet. A new series of Q measurements was taken, and the values plotted on the same axis as those obtained without the strips of plastic. This second graph shows that initially the damping is similar in magnitude, but reaches a lower steady state value. Therefore, the air-damping has a considerable effect on the damping of the tuning forks. It also demonstrates that the extraneous energy losses due to the clamp are very low indicating that the forks are

well isolated. Therefore, any effect which slightly alters the energy loss, causes a correspondingly large change in measured loss. Several researchers making damping measurements of materials at low amplitudes, have contained their apparatus in an evacuated chamber to eliminate air-loading effects. Experiments concerned with the fatigue effect, for which the changes in loss are large, this becomes uneccessary, because any extraneous energy loss effects are swamped by those of fatigue.

13. The amplitude dependence of the resonant frequency was studied during the measurements taken to calculate the efficiency. A plot of frequency versus pk-pk vibration amplitude gives a straight line graph of high regression fit (.99). The slope gives a change of -0.1136 Hz/mm. This is -750 ppm. The change in frequency is most likely to be due to changes in the temperature of the specimen in the region of maximum stress. Localised heating causes a change in the Young's modulus of the material, which is reflected in a change in frequency. A second explanation is the effect of anelasticity, where the Young's modulus changes with stress amplitude due to an internal ordering process. The interstitial atoms become re-arranged during the applied stress, and may occupy more favourable sites in the lattice, lowering the lattice energy.

14. To the naked eye, the smooth matt finish of the fatigue crack propagation region can be seen on the fractured surfaces of the specimens. The final catastrophic fracture region is also clearly visible.

15. The fatigue surfaces of some of the specimens were observed using an electron (SEM) microscope. The typical fatigue striations can clearly be seen.

Finally, the experiments performed using this apparatus indicate strongly that it would be a useful research tool in a materials laboratory. It would be unsuitable in an industrial environment because the form of the samples will only allow a few structures to be used. In place of a tuning fork, a double cantilever type sample could be used, in which case the stress concentration at the base is more easily calculable, it will however, have an inherently higher clamping loss, since it is not easily supported. The apparatus can easily be scaled up to take much larger specimens, which enables a greater volume of material to be contained in the region of interest and therefore give a more homogeneous sample.

------X------

APPENDIX A

DIAGRAMS OF THE ANALOGUE ELECTRONICS FOR DRIVING THE TUNING FORKS

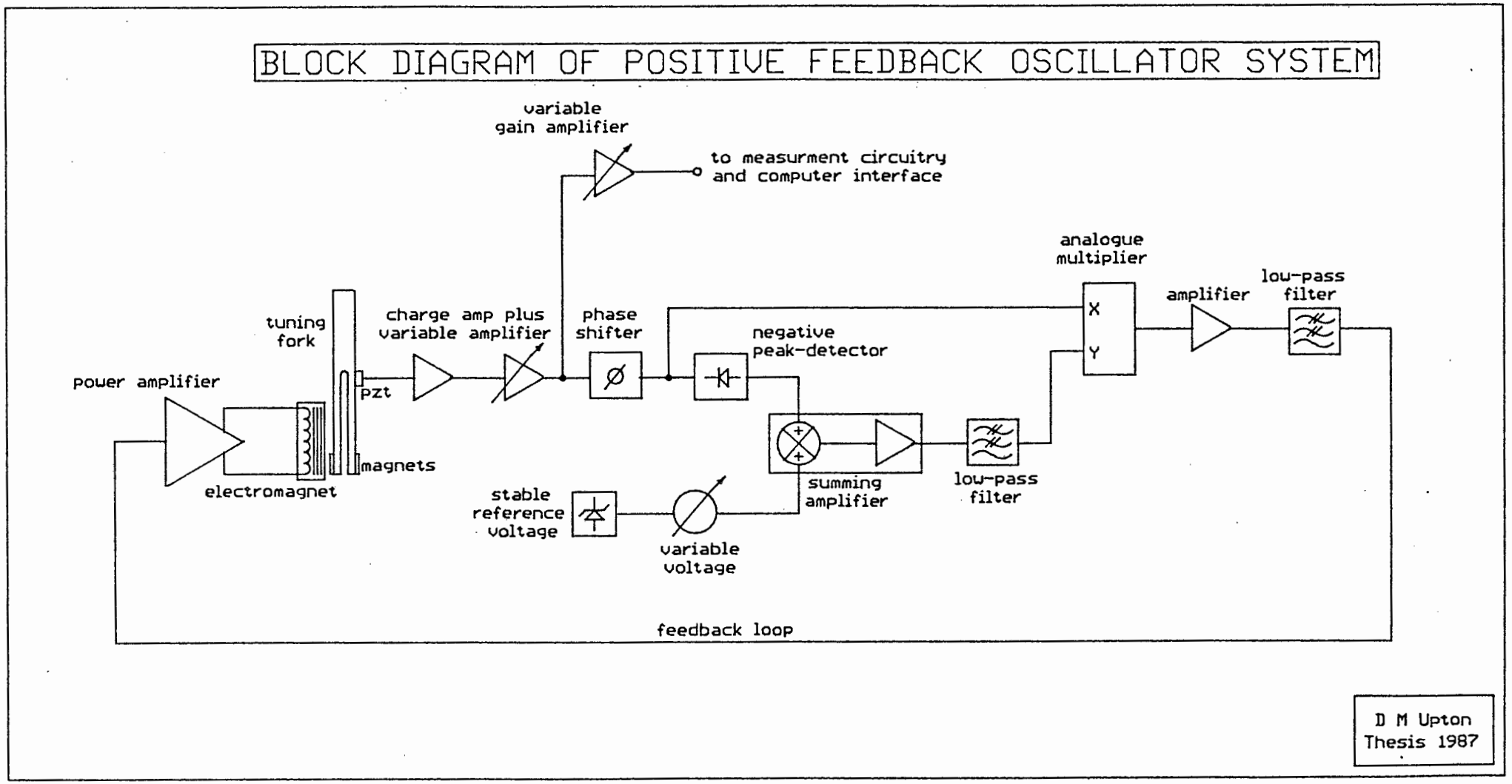
BLOCK DIAGRAM OF POSITIVE FEEDBACK OSCILLATOR SYSTEM
variable
gain amplifier
to measurment circuitry
and computer interface
analogue
multiplier
amplifier
low-pass
filter
tuning
fork
charge amp plus
variable amplifier
phase
shifter
negative
peak-detector
X
Y
power amplifier
pzt
magnets
electromagnet
stable
reference
voltage
variable
voltage
summing
amplifier
low-pass
filter
feedback loop
D M Upton
Thesis 1987

Diagram A.1.

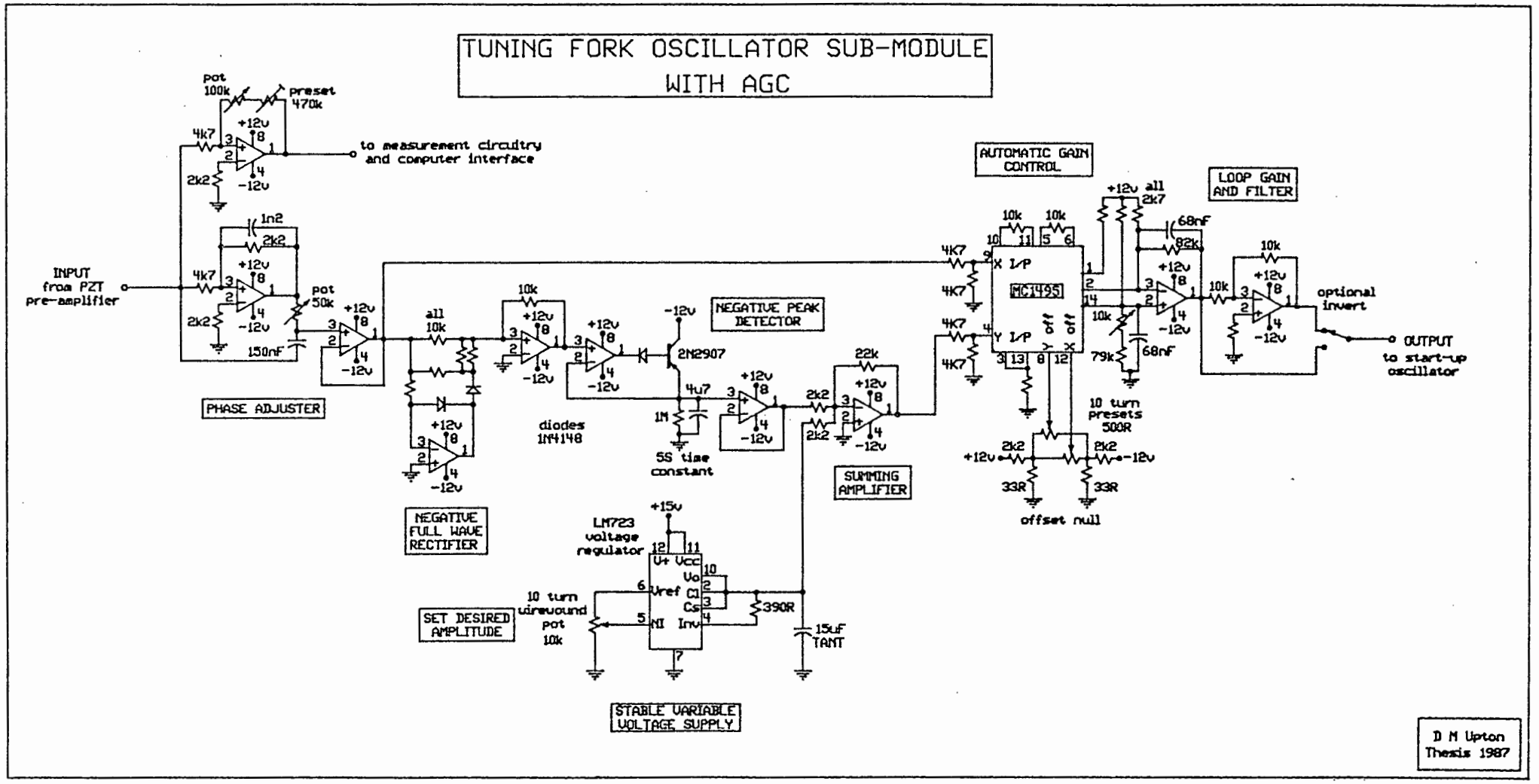
TUNING FORK OSCILLATOR SUB-MODULE
WITH AGC
pot 100k
preset 470k
to measurement circuitry and computer interface
INPUT from PZT pre-amplifier
PHASE ADJUSTER
pot 50k
150nF
all 10k
diodes 1N4148
NEGATIVE PEAK DETECTOR
2N2907
1M
4u7
55 time constant
NEGATIVE FULL WAVE RECTIFIER
SET DESIRED AMPLITUDE
10 turn wirewound pot 10k
LM723 voltage regulator
390R
15uF TANT
STABLE VARIABLE VOLTAGE SUPPLY
SUMMING AMPLIFIER
AUTOMATIC GAIN CONTROL
MC1495
10 turn presets 500R
offset null
LOOP GAIN AND FILTER
optional invert
OUTPUT to start-up oscillator
D M Upton Thesis 1987

Diagram A.2.

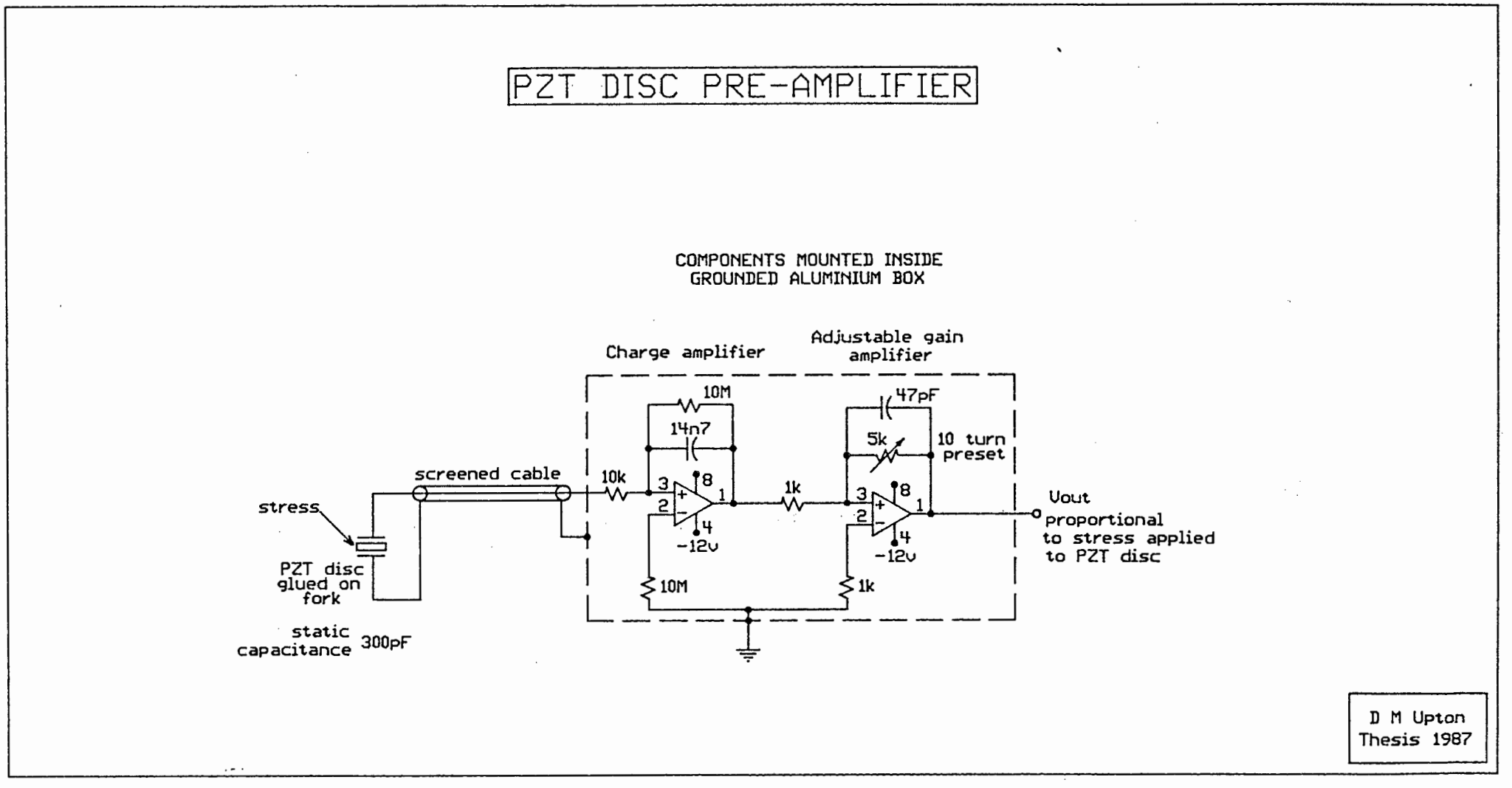
PZT DISC PRE-AMPLIFIER
COMPONENTS MOUNTED INSIDE
GROUNDED ALUMINIUM BOX
Charge amplifier
Adjustable gain
amplifier
10M
14n7
47pF
5k
10 turn
preset
screened cable
10k
1k
stress
PZT disc
glued on
fork
static
capacitance 300pF
-12v
-12v
10M
1k
Vout
proportional
to stress applied
to PZT disc
D M Upton
Thesis 1987

Diagram A.3.

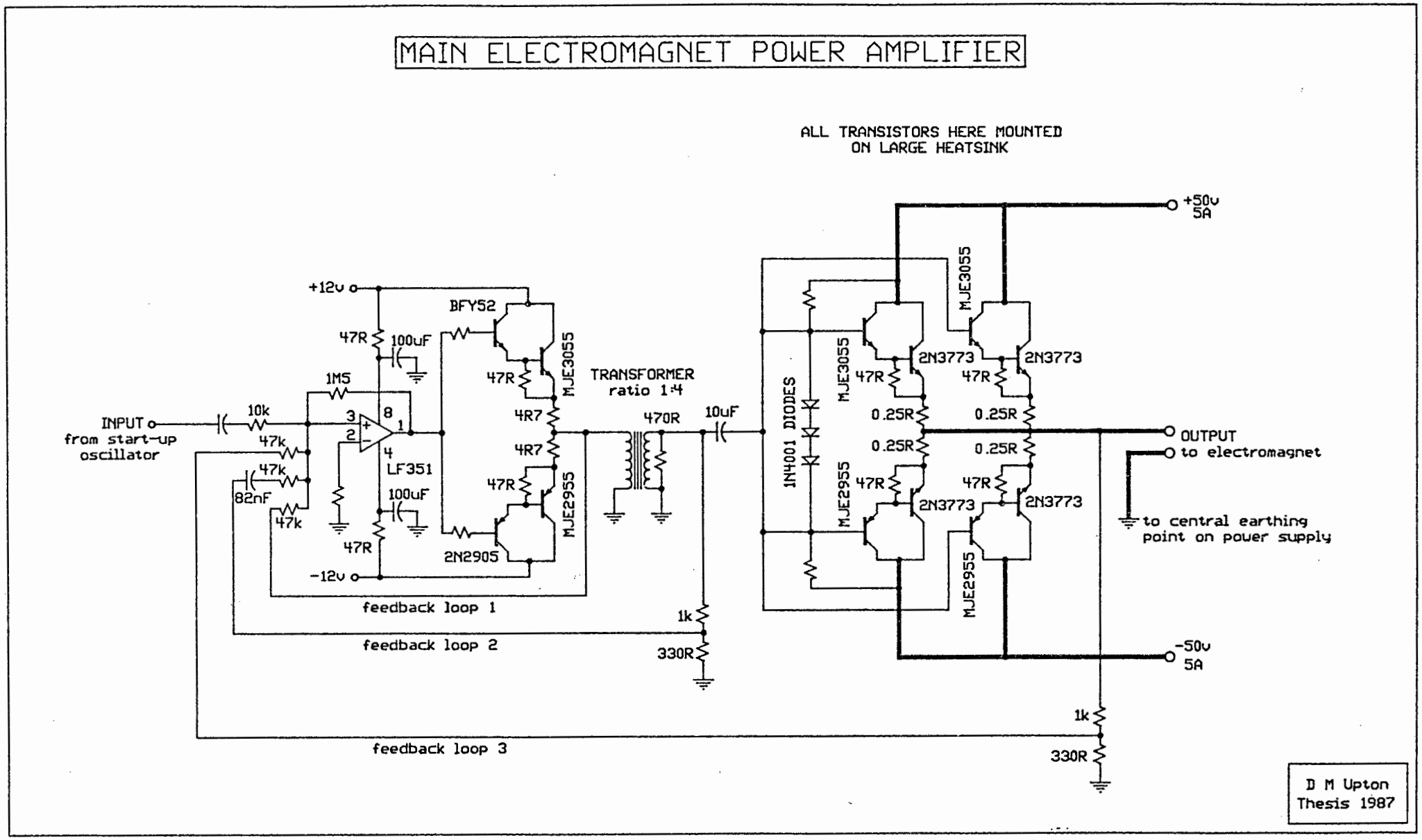
MAIN ELECTROMAGNET POWER AMPLIFIER
ALL TRANSISTORS HERE MOUNTED ON LARGE HEATSINK
+50v 5A
-50v 5A
+12v
-12v
INPUT from start-up oscillator
10k
47k
47k
82nF
47k
1M5
LF351
100uF
47R
100uF
47R
BFY52
MJE3055
47R
4R7
4R7
47R
MJE2955
2N2905
TRANSFORMER ratio 1:4
470R
10uF
1N4001 DIODES
MJE3055
MJE3055
2N3773
2N3773
47R
47R
0.25R
0.25R
0.25R
0.25R
47R
47R
MJE2955
2N3773
2N3773
MJE2955
OUTPUT to electromagnet
to central earthing point on power supply
1k
330R
1k
330R
feedback loop 1
feedback loop 2
feedback loop 3
D M Upton Thesis 1987

Diagram A.4.

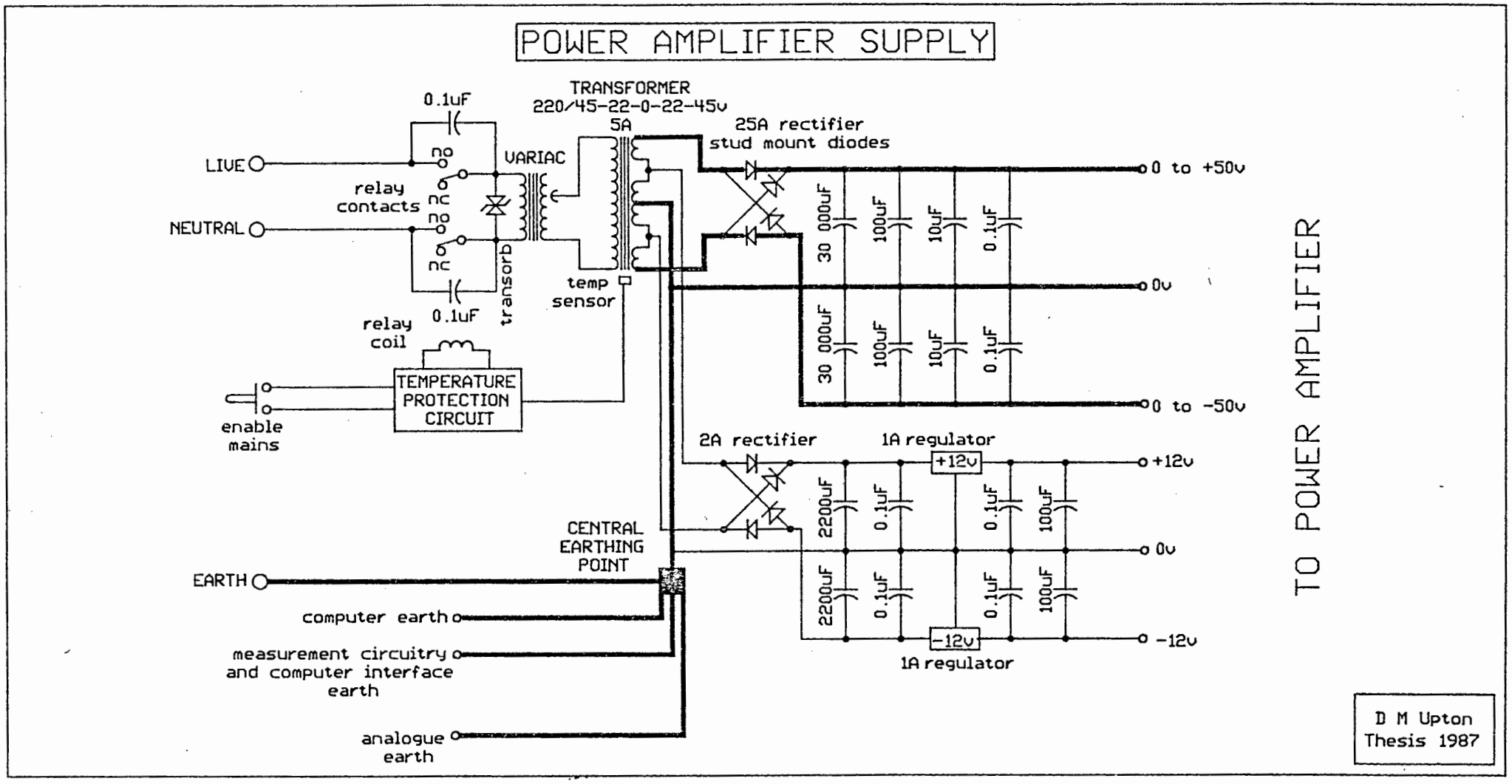
POWER AMPLIFIER SUPPLY
TRANSFORMER
220/45-22-0-22-45v
5A
0.1uF
LIVE
NEUTRAL
relay
contacts
no
nc
no
nc
VARIAC
transorb
0.1uF
relay
coil
TEMPERATURE
PROTECTION
CIRCUIT
enable
mains
temp
sensor
25A rectifier
stud mount diodes
30 000uF
100uF
10uF
0.1uF
0 to +50v
0v
0 to -50v
2A rectifier
1A regulator
+12v
2200uF
0.1uF
100uF
0v
-12v
1A regulator
CENTRAL
EARTHING
POINT
EARTH
computer earth
measurement circuitry
and computer interface
earth
analogue
earth
TO POWER AMPLIFIER
D M Upton
Thesis 1987

Diagram A.5.

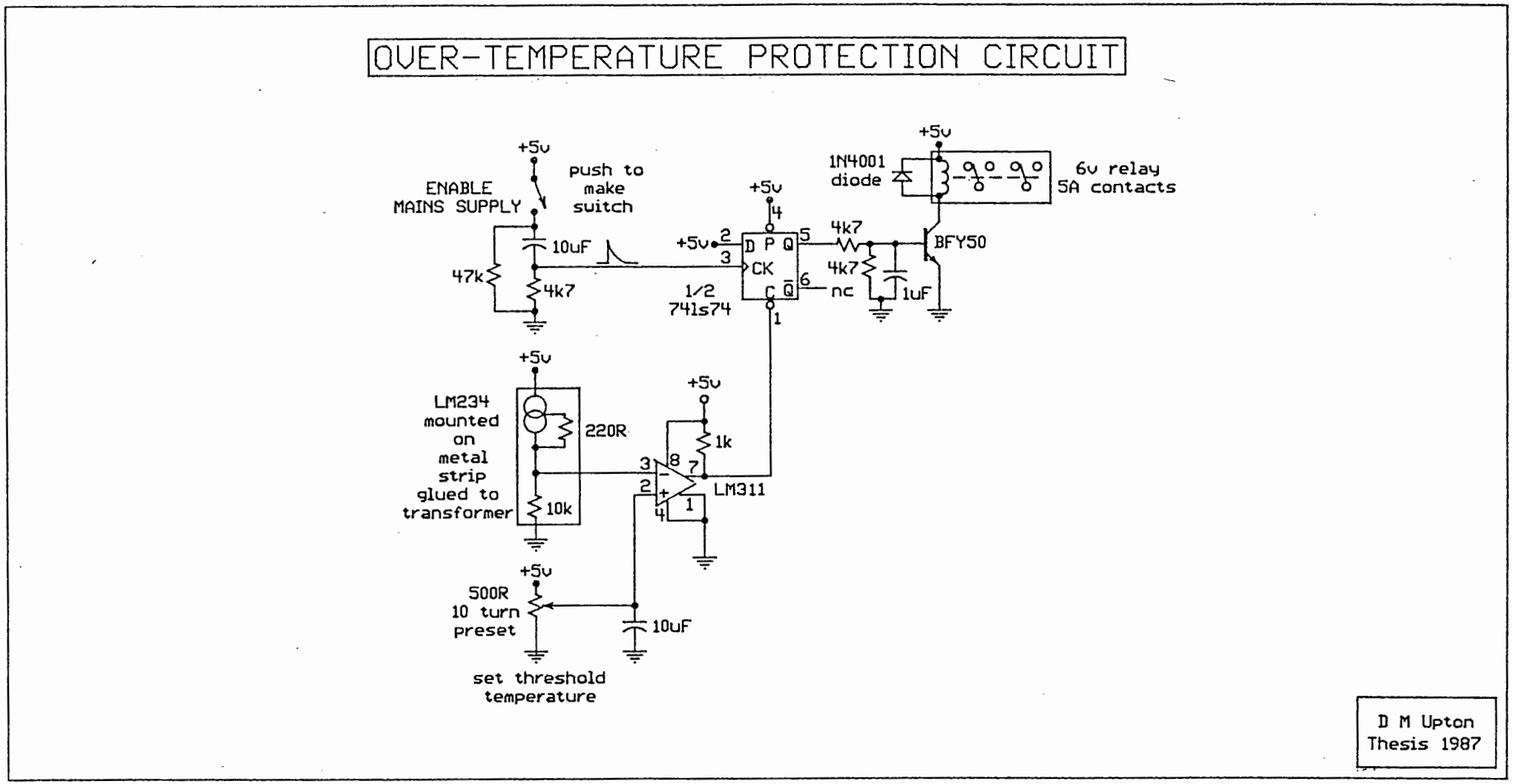
OVER-TEMPERATURE PROTECTION CIRCUIT
+5v
ENABLE
MAINS SUPPLY
push to
make
suitch
10uF
47k
4k7
+5v
2
3
D P Q
CK
C Q
1/2
74ls74
4
5
6
1
nc
+5v
1N4001
diode
6v relay
5A contacts
4k7
4k7
1uF
BFY50
+5v
LM234
mounted
on
metal
strip
glued to
transformer
220R
10k
+5v
1k
3
2
8
7
1
4
LM311
+5v
500R
10 turn
preset
10uF
set threshold
temperature
D M Upton
Thesis 1987

Diagram A.6.

APPENDIX B

DIAGRAMS OF THE INTERFACE ELECTRONICS TO THE HP85 COMPUTER

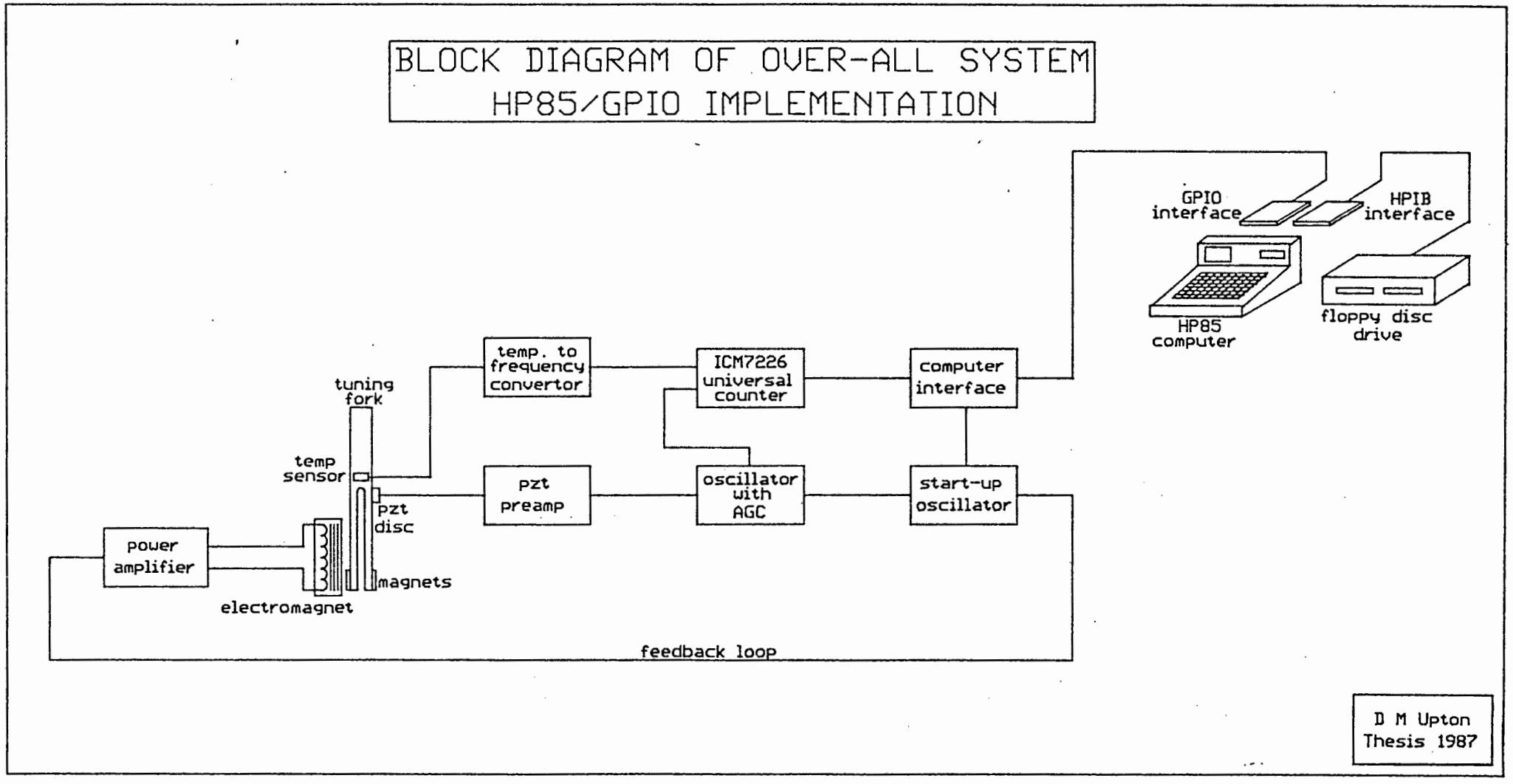
BLOCK DIAGRAM OF OVER-ALL SYSTEM
HP85/GPIO IMPLEMENTATION
GPIO interface
HPIB interface
HP85 computer
floppy disc drive
temp. to frequency convertor
ICM7226 universal counter
computer interface
tuning fork
temp sensor
pzt disc
pzt preamp
oscillator with AGC
start-up oscillator
power amplifier
magnets
electromagnet
feedback loop
D M Upton
Thesis 1987

Diagram B.1.

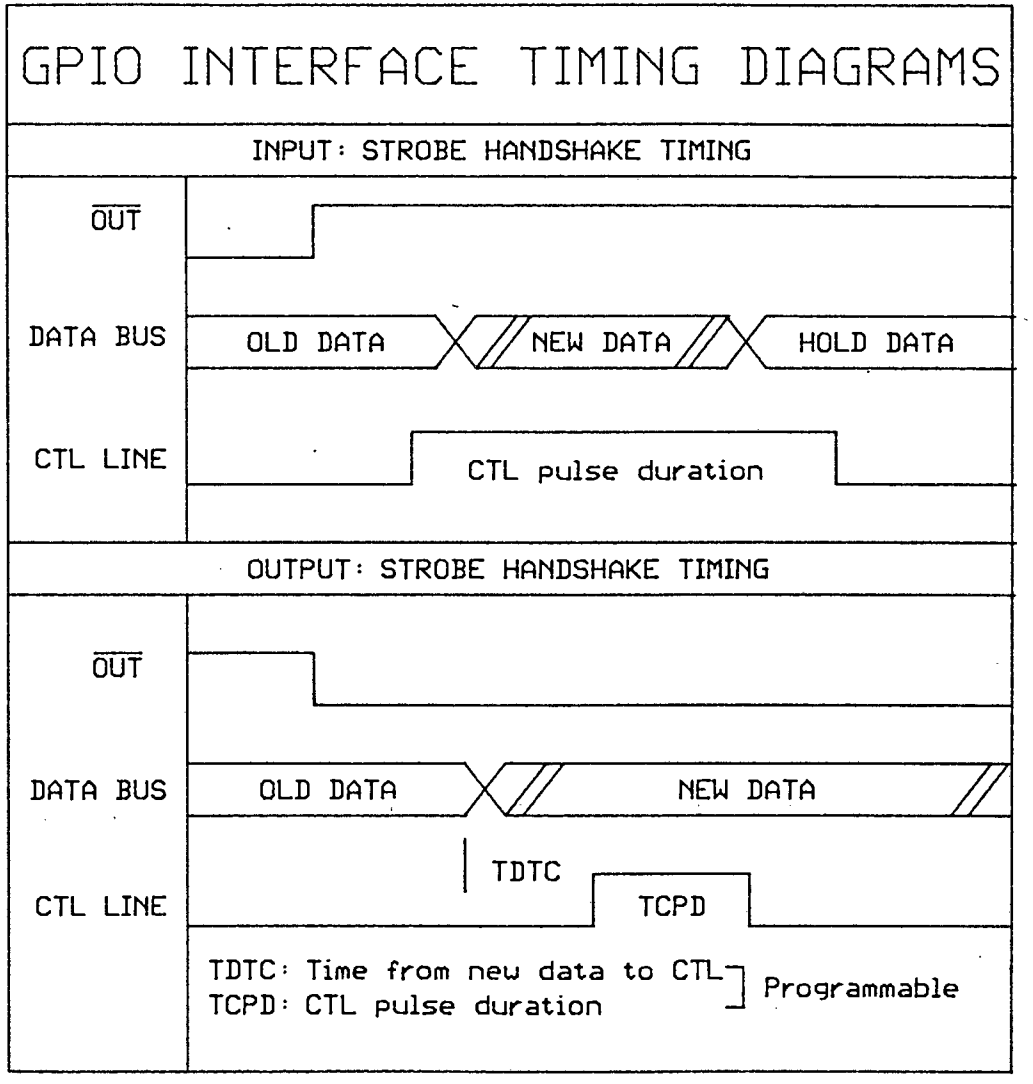
GPIO INTERFACE TIMING DIAGRAMS
INPUT: STROBE HANDSHAKE TIMING
OUT
DATA BUS
OLD DATA
NEW DATA
HOLD DATA
CTL LINE
CTL pulse duration
OUTPUT: STROBE HANDSHAKE TIMING
OUT
DATA BUS
OLD DATA
NEW DATA
TDTC
CTL LINE
TCPD
TDTC: Time from new data to CTL
TCPD: CTL pulse duration
Programmable
D M Upton
Thesis 1987

Diagram B.2.

PIN CONFIGURATION OF ICM 7226 BIPL

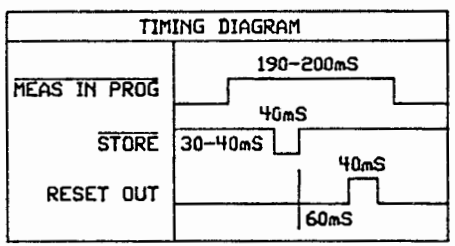

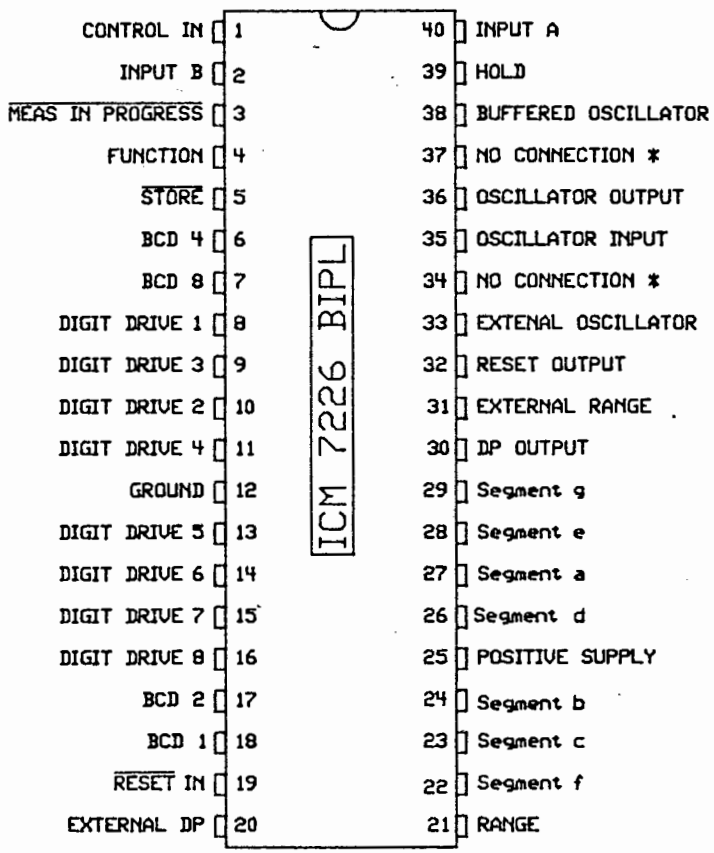

MULTIPLEXED CONTROL	
FUNCTION	DIGIT
Frequency	D1
Period	D8
Unit-count	D4
Osc freq	D3
RANGE	
0.01s/1 cycle	D1
0.1s/10 cycles	D2
1.0s/100 cycles	D3
10s/1k cycles	D4
CONTROL	
Blank display	D4 & Hold
Display test	D8
1MHz select	D2
Ext osc enable	D1
Ext dp enable	D3
Test	D5

* For maximum frequency stability connect to V+ or GROUND

D M Upton
Thesis 1987

Diagram B.3.

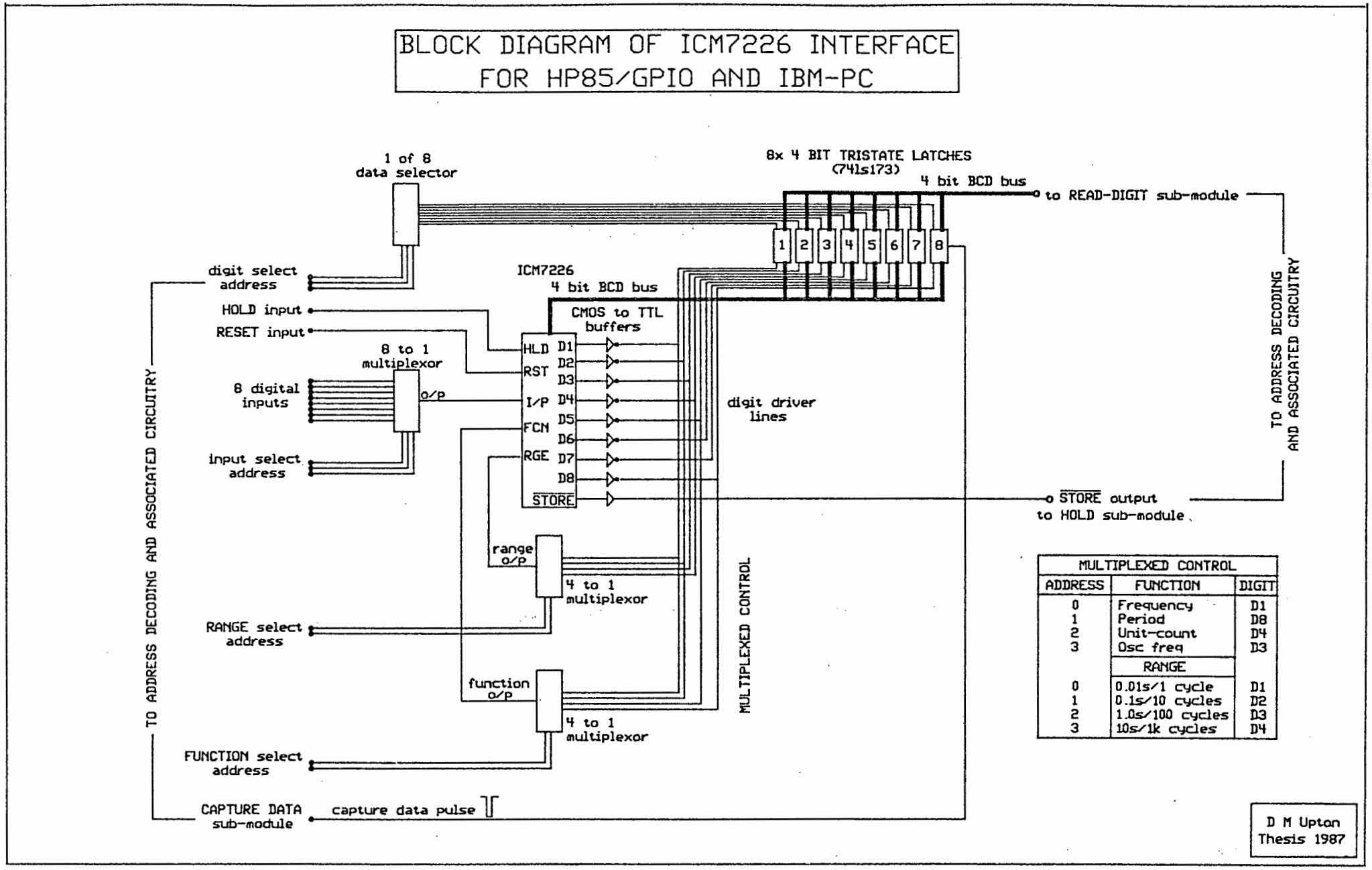
BLOCK DIAGRAM OF ICM7226 INTERFACE
FOR HP85/GPIO AND IBM-PC
1 of 8
data selector
8x 4 BIT TRISTATE LATCHES
(74ls173)
4 bit BCD bus
to READ-DIGIT sub-module
1
2
3
4
5
6
7
8
digit select
address
ICM7226
4 bit BCD bus
HOLD input
RESET input
CMOS to TTL
buffers
8 to 1
multiplexor
8 digital
inputs
o/p
HLD
RST
I/P
FCN
RGE
STORE
D1
D2
D3
D4
D5
D6
D7
D8
digit driver
lines
input select
address
TO ADDRESS DECODING
AND ASSOCIATED CIRCUITRY
STORE output
to HOLD sub-module
range
o/p
4 to 1
multiplexor
RANGE select
address
function
o/p
4 to 1
multiplexor
MULTIPLEXED CONTROL
FUNCTION select
address
CAPTURE DATA
sub-module
capture data pulse
TO ADDRESS DECODING AND ASSOCIATED CIRCUITRY
MULTIPLEXED CONTROL
ADDRESS
FUNCTION
DIGIT
0
Frequency
D1
1
Period
D8
2
Unit-count
D4
3
Osc freq
D3
RANGE
0
0.01s/1 cycle
D1
1
0.1s/10 cycles
D2
2
1.0s/100 cycles
D3
3
10s/1k cycles
D4
D M Upton
Thesis 1987

Diagram B.4.

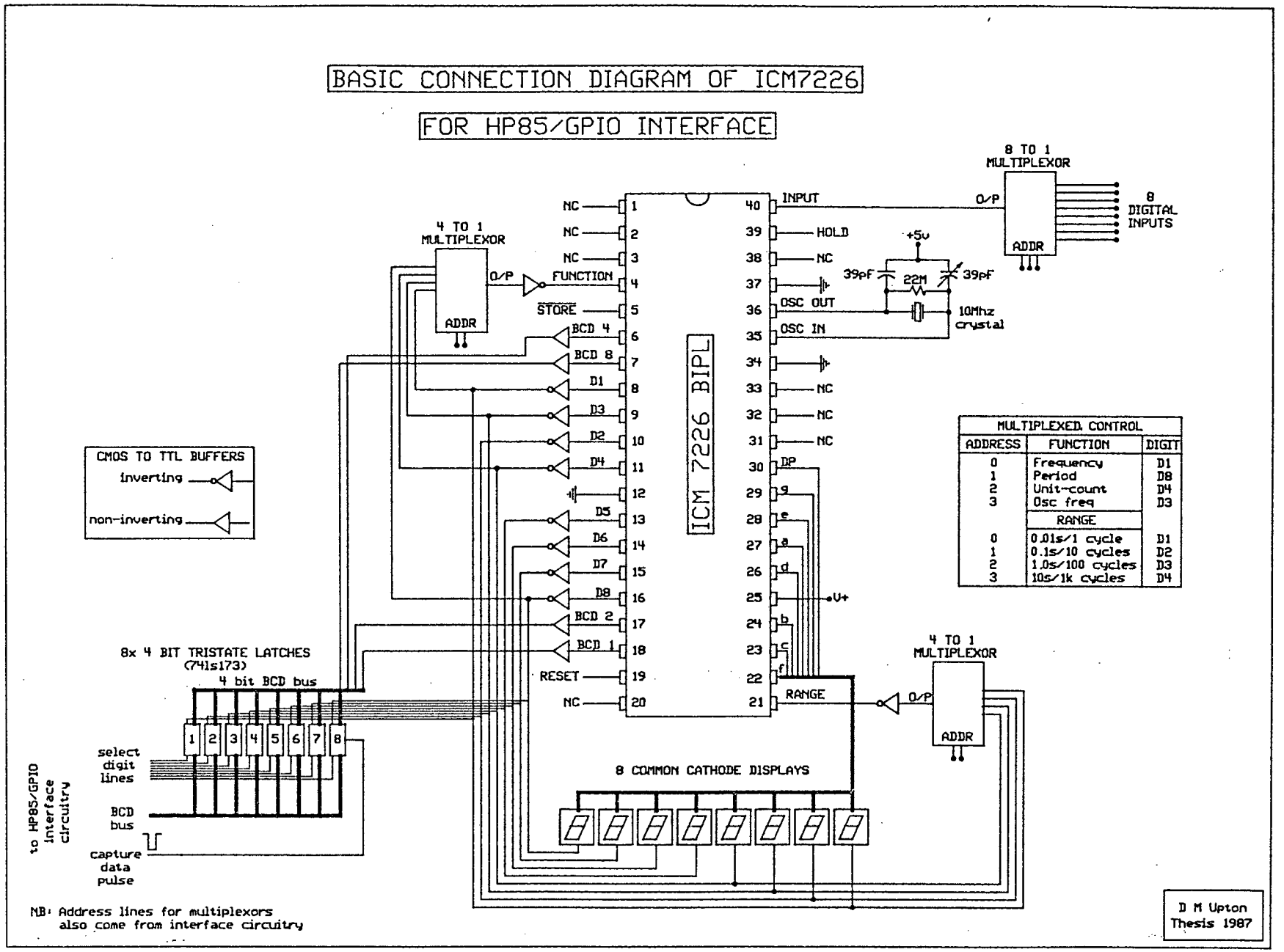
BASIC CONNECTION DIAGRAM OF ICM7226
FOR HP85/GPIO INTERFACE
8 TO 1 MULTIPLEXOR
O/P
ADDR
8 DIGITAL INPUTS
4 TO 1 MULTIPLEXOR
O/P
FUNCTION
STORE
ADDR
+5v
39pF
22M
39pF
10Mhz crystal
ICM 7226 BIPL
NC
NC
NC
NC
BCD 4
BCD 8
D1
D3
D2
D4
D5
D6
D7
D8
BCD 2
BCD 1
RESET
NC
INPUT
HOLD
NC
OSC OUT
OSC IN
NC
NC
NC
DP
g
e
a
d
V+
b
c
f
RANGE
CMOS TO TTL BUFFERS
inverting
non-inverting
MULTIPLEXED CONTROL
ADDRESS | FUNCTION | DIGIT
0 Frequency D1
1 Period D8
2 Unit-count D4
3 Osc freq D3
RANGE
0 0.01s/1 cycle D1
1 0.1s/10 cycles D2
2 1.0s/100 cycles D3
3 10s/1k cycles D4
8x 4 BIT TRISTATE LATCHES (74ls173)
4 bit BCD bus
1 2 3 4 5 6 7 8
select digit lines
BCD bus
capture data pulse
to HP85/GPIO interface circuitry
8 COMMON CATHODE DISPLAYS
4 TO 1 MULTIPLEXOR
O/P
ADDR
NB: Address lines for multiplexors also come from interface circuitry
D M Upton Thesis 1987

Diagram B.5.

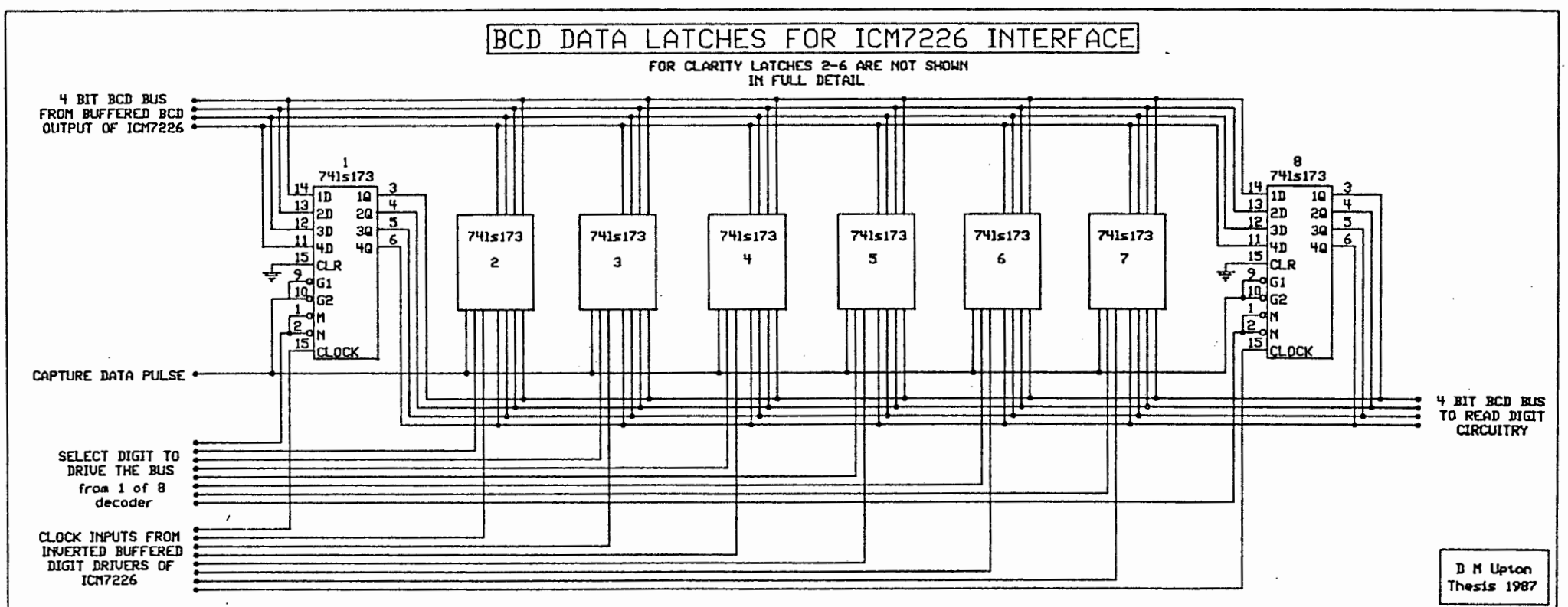
BCD DATA LATCHES FOR ICM7226 INTERFACE
FOR CLARITY LATCHES 2-6 ARE NOT SHOWN IN FULL DETAIL
4 BIT BCD BUS FROM BUFFERED BCD OUTPUT OF ICM7226
1
74ls173
8
74ls173
74ls173 2
74ls173 3
74ls173 4
74ls173 5
74ls173 6
74ls173 7
1D
2D
3D
4D
CLR
G1
G2
M
N
CLOCK
1Q
2Q
3Q
4Q
CAPTURE DATA PULSE
SELECT DIGIT TO DRIVE THE BUS from 1 of 8 decoder
CLOCK INPUTS FROM INVERTED BUFFERED DIGIT DRIVERS OF ICM7226
4 BIT BCD BUS TO READ DIGIT CIRCUITRY
D M Upton Thesis 1987

Diagram B.6.

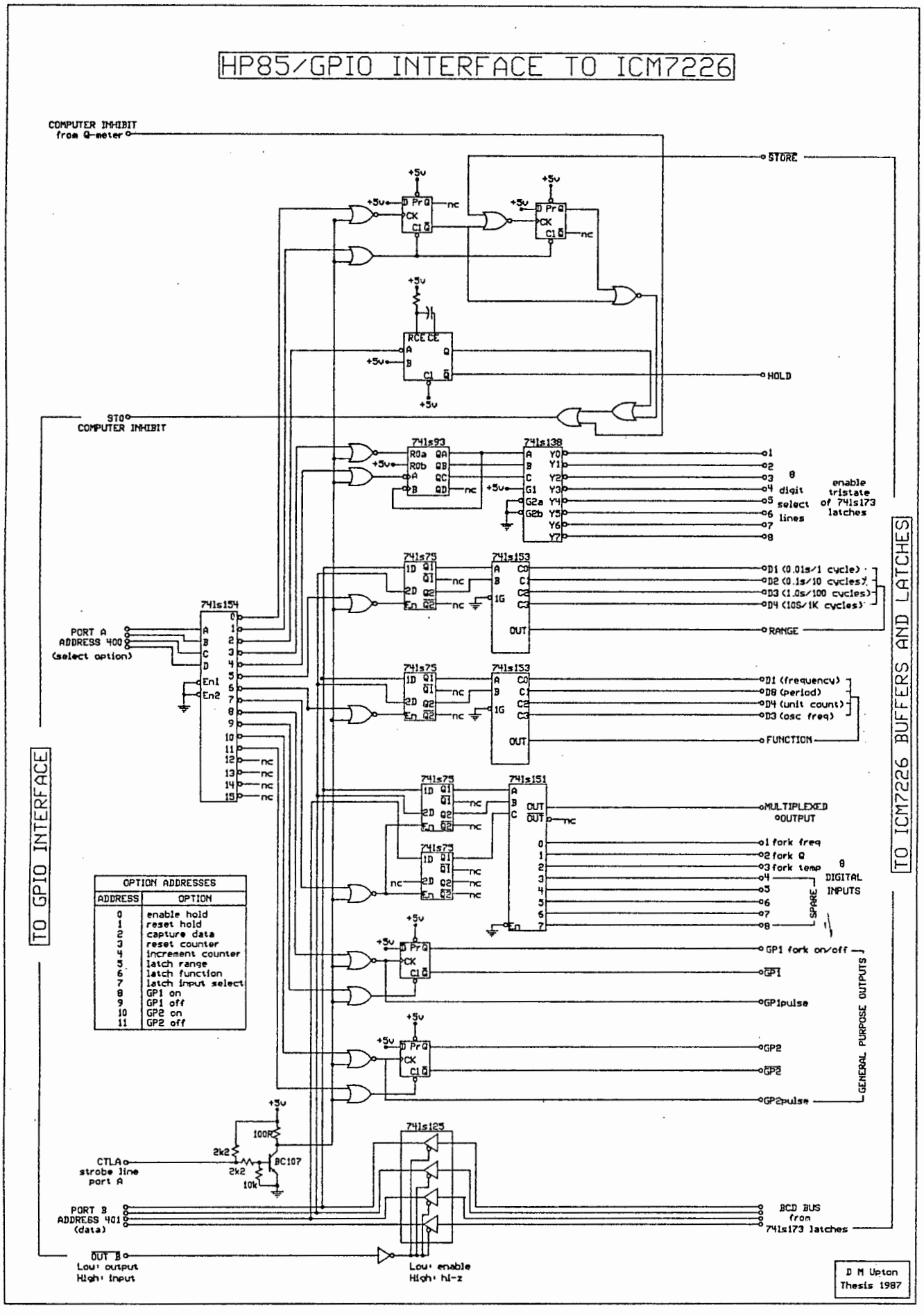
HP85/GPIO INTERFACE TO ICM7226
COMPUTER INHIBIT from Q-meter
STORE
HOLD
STO COMPUTER INHIBIT
741s93
741s138
8 digit select lines
enable tristate of 74ls173 latches
741s75
741s153
D1 (0.01s/1 cycle)
D2 (0.1s/10 cycles)
D3 (1.0s/100 cycles)
D4 (10S/1K cycles)
RANGE
741s154
PORT A ADDRESS 400 (select option)
D1 (frequency)
D8 (period)
D4 (unit count)
D3 (osc freq)
FUNCTION
741s151
MULTIPLEXED OUTPUT
1 fork freq
2 fork Q
3 fork temp
8 DIGITAL INPUTS
SPARE
GP1 fork on/off
GP1
GP1pulse
GP2
GP2
GP2pulse
GENERAL PURPOSE OUTPUTS
TO GPIO INTERFACE
TO ICM7226 BUFFERS AND LATCHES
OPTION ADDRESSES
ADDRESS | OPTION
0 enable hold
1 reset hold
2 capture data
3 reset counter
4 increment counter
5 latch range
6 latch function
7 latch input select
8 GP1 on
9 GP1 off
10 GP2 on
11 GP2 off
100R
2k2
2k2
10k
BC107
CTLA strobe line port A
741s125
PORT B ADDRESS 401 (data)
BCD BUS from 74ls173 latches
OUT B
Low: output
High: input
Low: enable
High: hi-z
D M Upton
Thesis 1987

DIAGRAM B.7

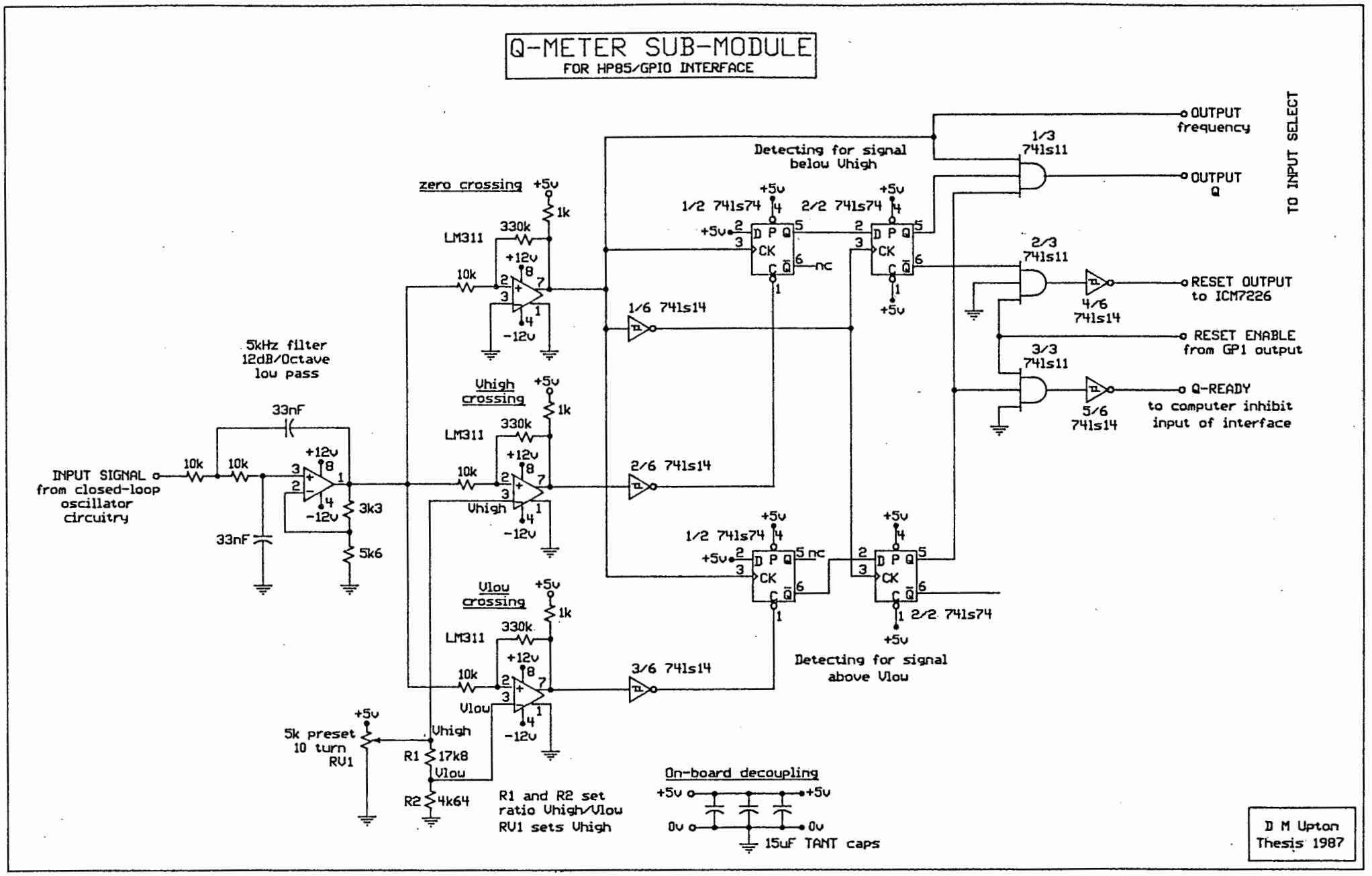
Q-METER SUB-MODULE
FOR HP85/GPIO INTERFACE
INPUT SIGNAL
from closed-loop
oscillator
circuitry
5kHz filter
12dB/Octave
low pass
33nF
10k
3k3
5k6
zero crossing
Vhigh
crossing
Vlow
crossing
LM311
330k
1k
+12v
-12v
+5v
0v
5k preset
10 turn
RV1
R1 17k8
R2 4k64
Vhigh
Vlow
R1 and R2 set
ratio Vhigh/Vlow
RV1 sets Vhigh
1/6 741s14
2/6 741s14
3/6 741s14
4/6
741s14
5/6
741s14
1/2 741s74
2/2 741s74
Detecting for signal
below Vhigh
Detecting for signal
above Vlow
1/3
741s11
2/3
741s11
3/3
741s11
OUTPUT
frequency
OUTPUT
Q
RESET OUTPUT
to ICM7226
RESET ENABLE
from GP1 output
Q-READY
to computer inhibit
input of interface
TO INPUT SELECT
On-board decoupling
15uF TANT caps
D M Upton
Thesis 1987

Diagram B.8.

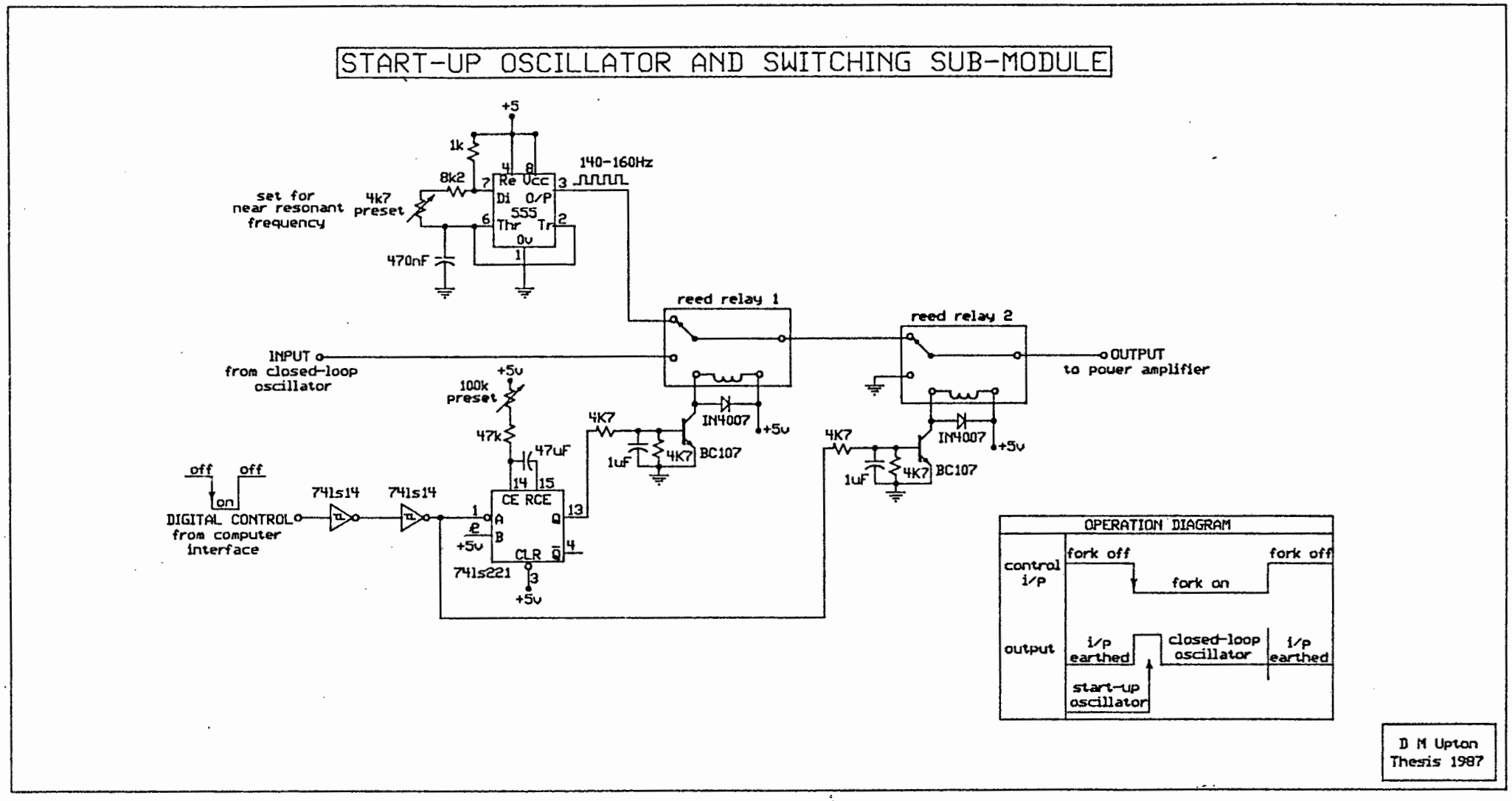
START-UP OSCILLATOR AND SWITCHING SUB-MODULE
+5
1k
8k2
4k7 preset
set for near resonant frequency
470nF
555
Re Vcc
Di O/P
Thr Tr
0v
140-160Hz
reed relay 1
reed relay 2
INPUT from closed-loop oscillator
OUTPUT to power amplifier
100k preset
47k
47uF
4K7
1uF
BC107
IN4007
+5v
off
on
DIGITAL CONTROL from computer interface
74ls14
74ls221
CE RCE
CLR
OPERATION DIAGRAM
control i/p
fork off
fork on
output
i/p earthed
closed-loop oscillator
start-up oscillator
D M Upton
Thesis 1987

Diagram B.9.

TEMPERATURE TO FREQUENCY CONVERTOR
Version 1

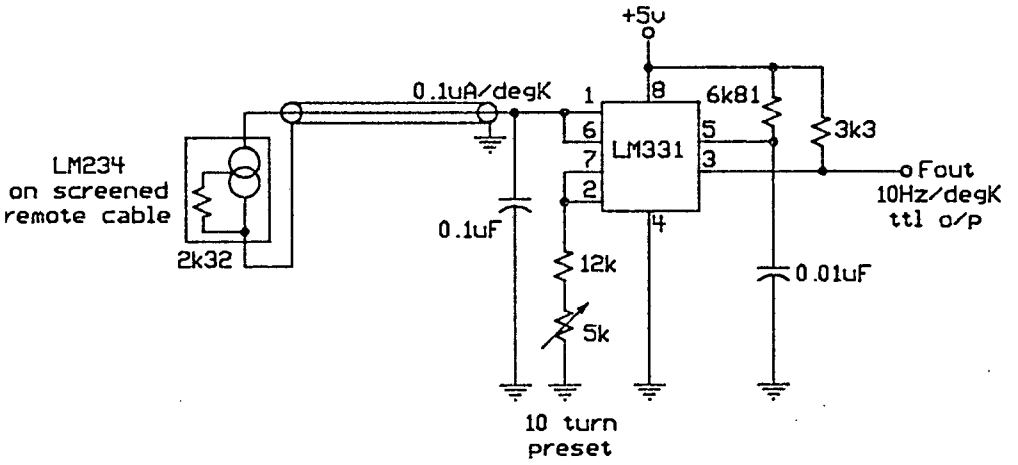

LM331: Precision voltage to frquency convertor

LM234: Current source type temperature sensor

D M Upton
Thesis 1987

Diagram B.10.

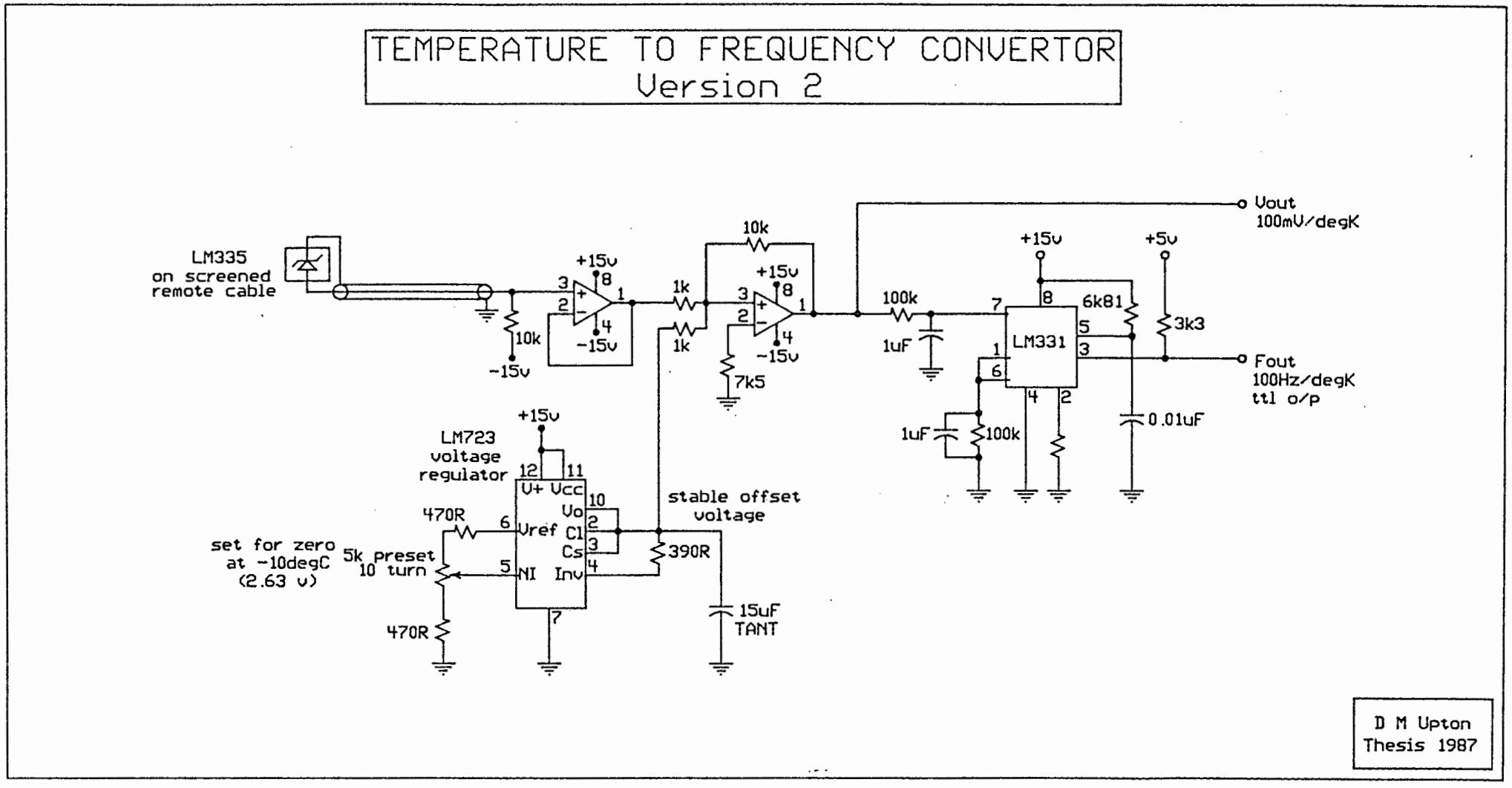
TEMPERATURE TO FREQUENCY CONVERTOR
Version 2
LM335
on screened
remote cable
10k
-15v
+15v
-15v
1k
1k
10k
+15v
-15v
7k5
100k
1uF
Vout
100mV/degK
+15v
+5v
6k81
3k3
LM331
Fout
100Hz/degK
ttl o/p
1uF
100k
0.01uF
LM723
voltage
regulator
+15v
U+ Vcc
Vo
Vref Cl
Cs
NI Inv
470R
set for zero
at -10degC
(2.63 v)
5k preset
10 turn
470R
stable offset
voltage
390R
15uF
TANT
D M Upton
Thesis 1987

Diagram B.11.

APPENDIX C

DIAGRAMS OF THE INTERFACE ELECTRONICS TO THE IBM-PC COMPUTER

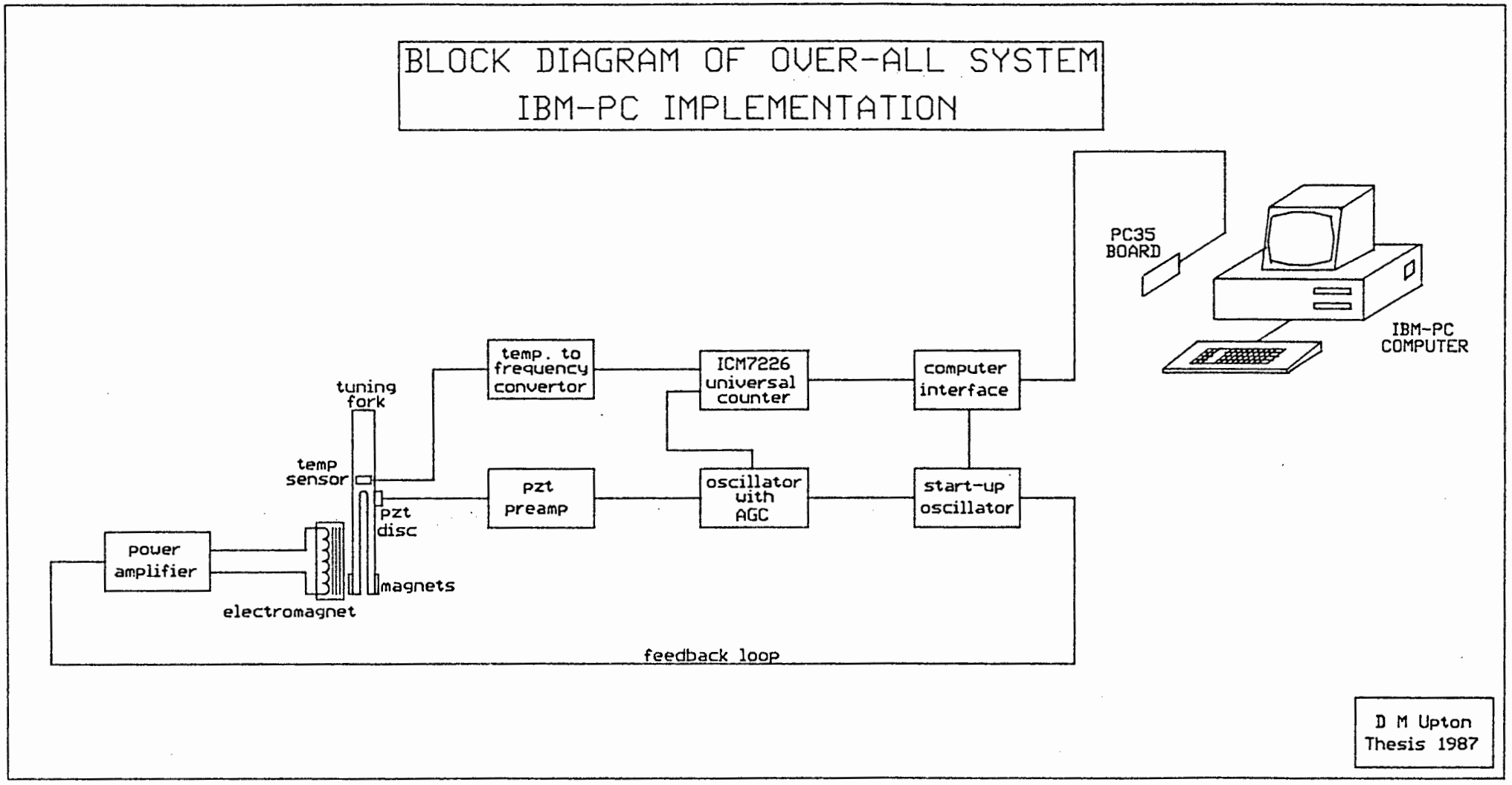
BLOCK DIAGRAM OF OVER-ALL SYSTEM
IBM-PC IMPLEMENTATION
PC35 BOARD
IBM-PC COMPUTER
temp. to frequency convertor
ICM7226 universal counter
computer interface
tuning fork
temp sensor
pzt preamp
oscillator with AGC
start-up oscillator
pzt disc
power amplifier
magnets
electromagnet
feedback loop
D M Upton
Thesis 1987

Diagram C.1.

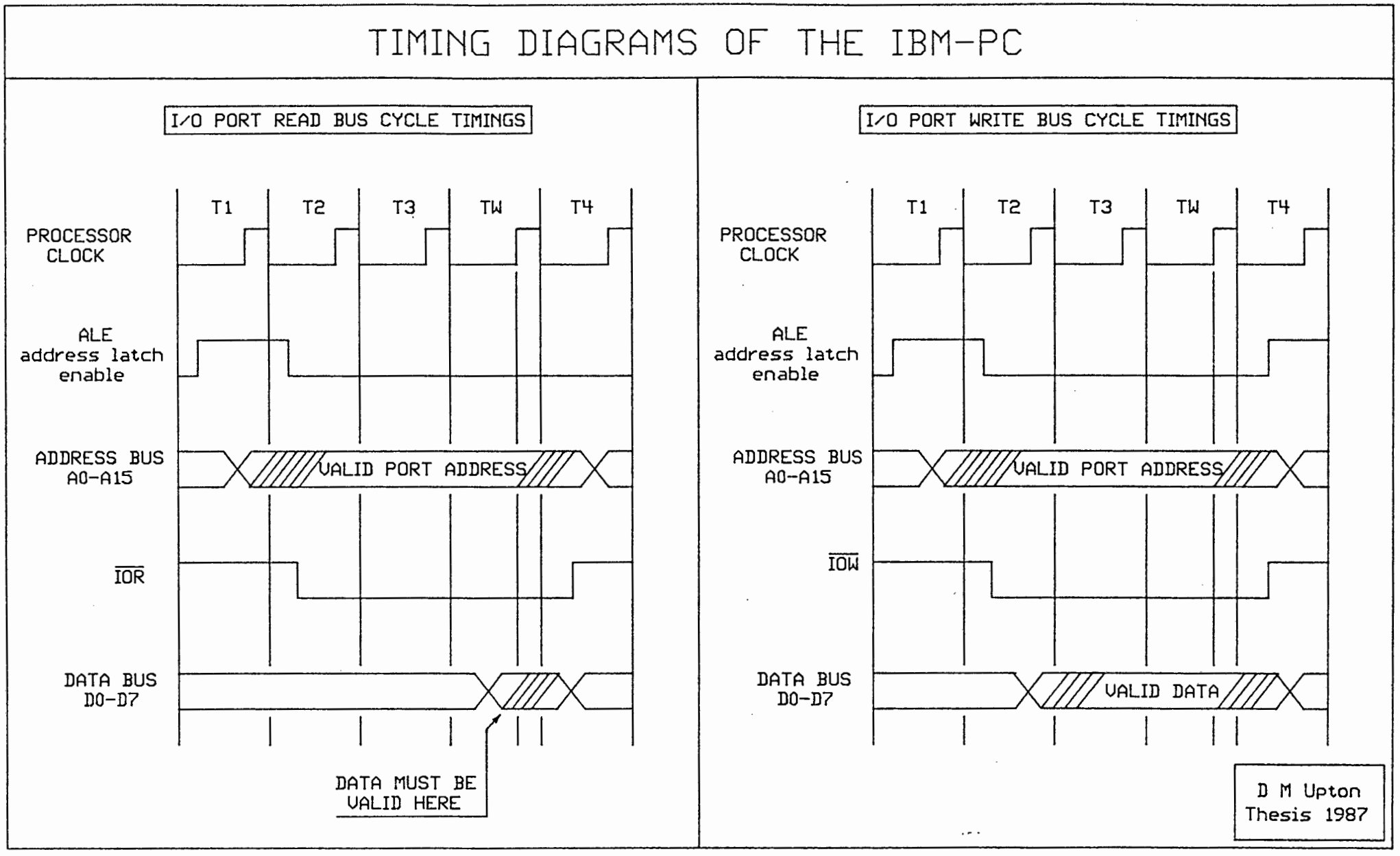
TIMING DIAGRAMS OF THE IBM-PC
I/O PORT READ BUS CYCLE TIMINGS
T1
T2
T3
TW
T4
PROCESSOR CLOCK
ALE address latch enable
ADDRESS BUS A0-A15
VALID PORT ADDRESS
IOR
DATA BUS D0-D7
DATA MUST BE VALID HERE
I/O PORT WRITE BUS CYCLE TIMINGS
T1
T2
T3
TW
T4
PROCESSOR CLOCK
ALE address latch enable
ADDRESS BUS A0-A15
VALID PORT ADDRESS
IOW
DATA BUS D0-D7
VALID DATA
D M Upton
Thesis 1987

Diagram C.2.

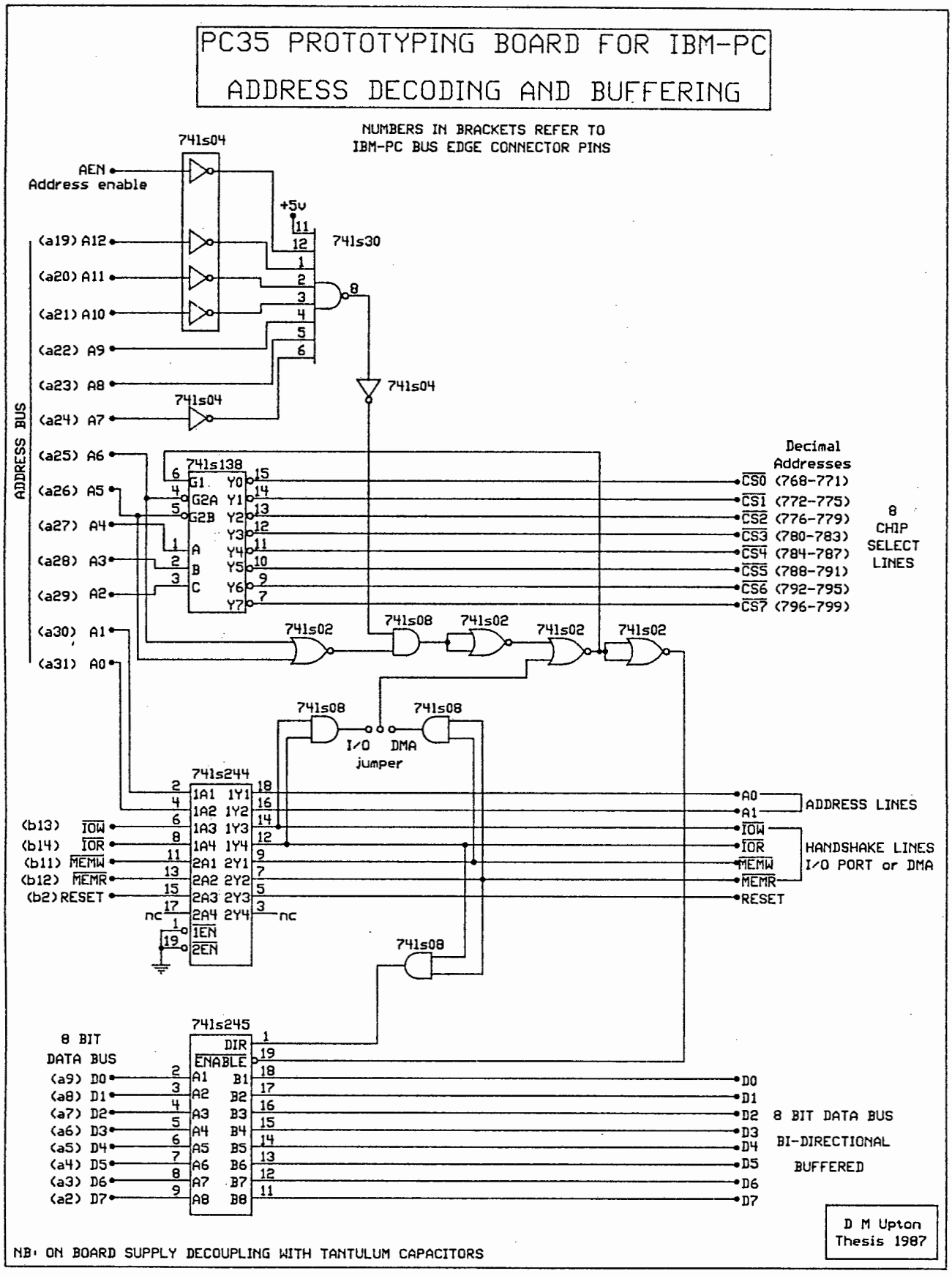
PC35 PROTOTYPING BOARD FOR IBM-PC
ADDRESS DECODING AND BUFFERING
NUMBERS IN BRACKETS REFER TO
IBM-PC BUS EDGE CONNECTOR PINS
ADDRESS BUS
AEN
Address enable
741s04
+5v
741s30
(a19) A12
(a20) A11
(a21) A10
(a22) A9
(a23) A8
(a24) A7
(a25) A6
(a26) A5
(a27) A4
(a28) A3
(a29) A2
(a30) A1
(a31) A0
741s138
G1
G2A
G2B
A
B
C
Y0
Y1
Y2
Y3
Y4
Y5
Y6
Y7
Decimal Addresses
CS0 (768-771)
CS1 (772-775)
CS2 (776-779)
CS3 (780-783)
CS4 (784-787)
CS5 (788-791)
CS6 (792-795)
CS7 (796-799)
8 CHIP SELECT LINES
741s02
741s08
I/O DMA jumper
741s244
1A1 1Y1
1A2 1Y2
1A3 1Y3
1A4 1Y4
2A1 2Y1
2A2 2Y2
2A3 2Y3
2A4 2Y4
1EN
2EN
(b13) IOW
(b14) IOR
(b11) MEMW
(b12) MEMR
(b2) RESET
nc
A0
A1
IOW
IOR
MEMW
MEMR
RESET
ADDRESS LINES
HANDSHAKE LINES I/O PORT or DMA
741s245
DIR
ENABLE
A1 B1
A2 B2
A3 B3
A4 B4
A5 B5
A6 B6
A7 B7
A8 B8
8 BIT DATA BUS
(a9) D0
(a8) D1
(a7) D2
(a6) D3
(a5) D4
(a4) D5
(a3) D6
(a2) D7
D0
D1
D2
D3
D4
D5
D6
D7
8 BIT DATA BUS BI-DIRECTIONAL BUFFERED
D M Upton
Thesis 1987
NB: ON BOARD SUPPLY DECOUPLING WITH TANTULUM CAPACITORS

Diagram C.3.

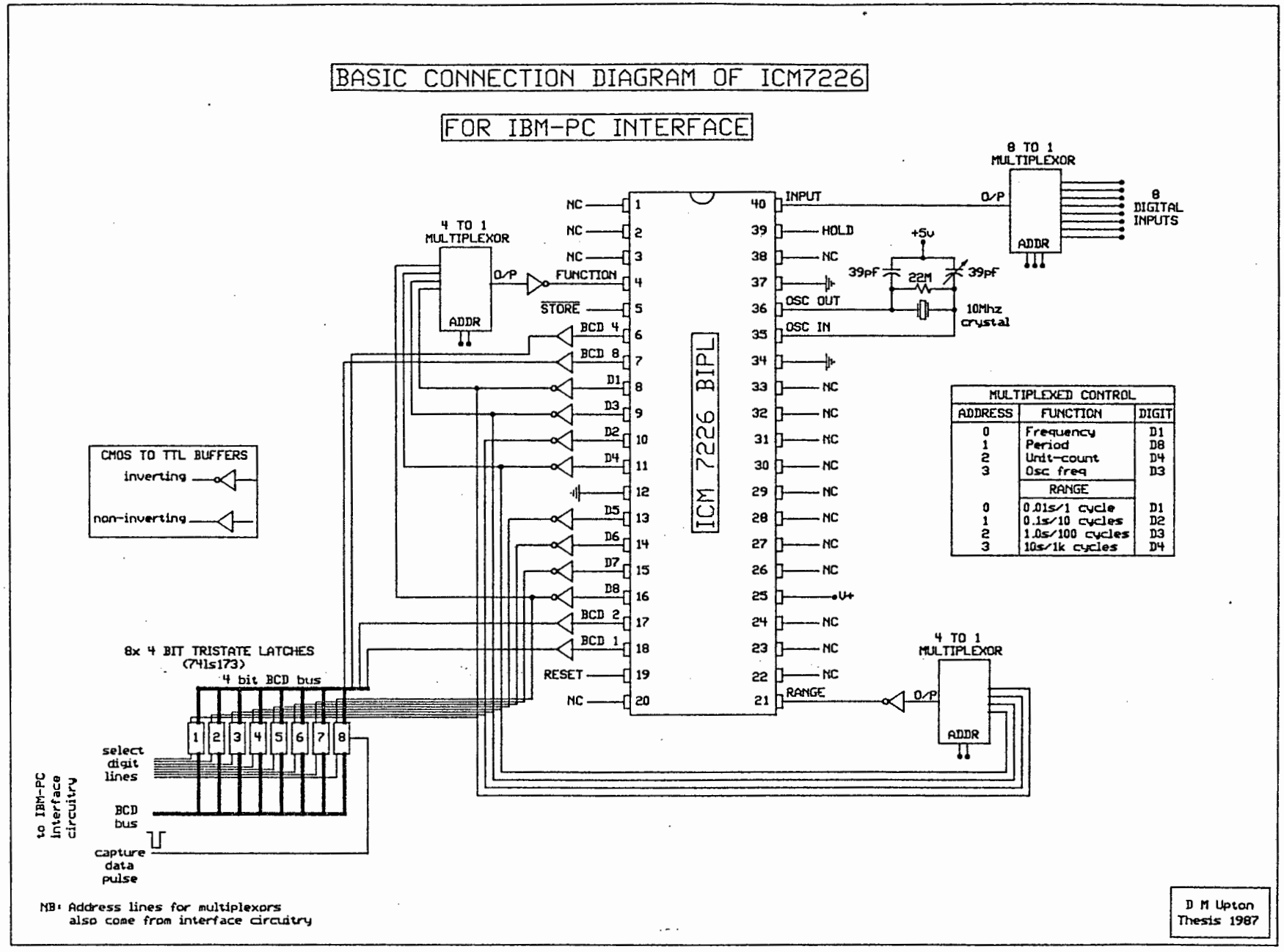
BASIC CONNECTION DIAGRAM OF ICM7226
FOR IBM-PC INTERFACE
ICM 7226 BIPL
NC 1
NC 2
NC 3
FUNCTION 4
STORE 5
BCD 4 6
BCD 8 7
D1 8
D3 9
D2 10
D4 11
12
D5 13
D6 14
D7 15
D8 16
BCD 2 17
BCD 1 18
RESET 19
NC 20
40 INPUT
39 HOLD
38 NC
37
36 OSC OUT
35 OSC IN
34
33 NC
32 NC
31 NC
30 NC
29 NC
28 NC
27 NC
26 NC
25 V+
24 NC
23 NC
22 NC
21 RANGE
4 TO 1 MULTIPLEXOR
O/P
ADDR
8 TO 1 MULTIPLEXOR
8 DIGITAL INPUTS
+5v
39pF
22M
39pF
10Mhz crystal
MULTIPLEXED CONTROL
ADDRESS | FUNCTION | DIGIT
0 Frequency D1
1 Period D8
2 Unit-count D4
3 Osc freq D3
RANGE
0 0.01s/1 cycle D1
1 0.1s/10 cycles D2
2 1.0s/100 cycles D3
3 10s/1k cycles D4
CMOS TO TTL BUFFERS
inverting
non-inverting
8x 4 BIT TRISTATE LATCHES (74ls173)
4 bit BCD bus
1 2 3 4 5 6 7 8
select digit lines
BCD bus
capture data pulse
to IBM-PC interface circuitry
NB: Address lines for multiplexors also come from interface circuitry
D M Upton Thesis 1987

Diagram C.4.

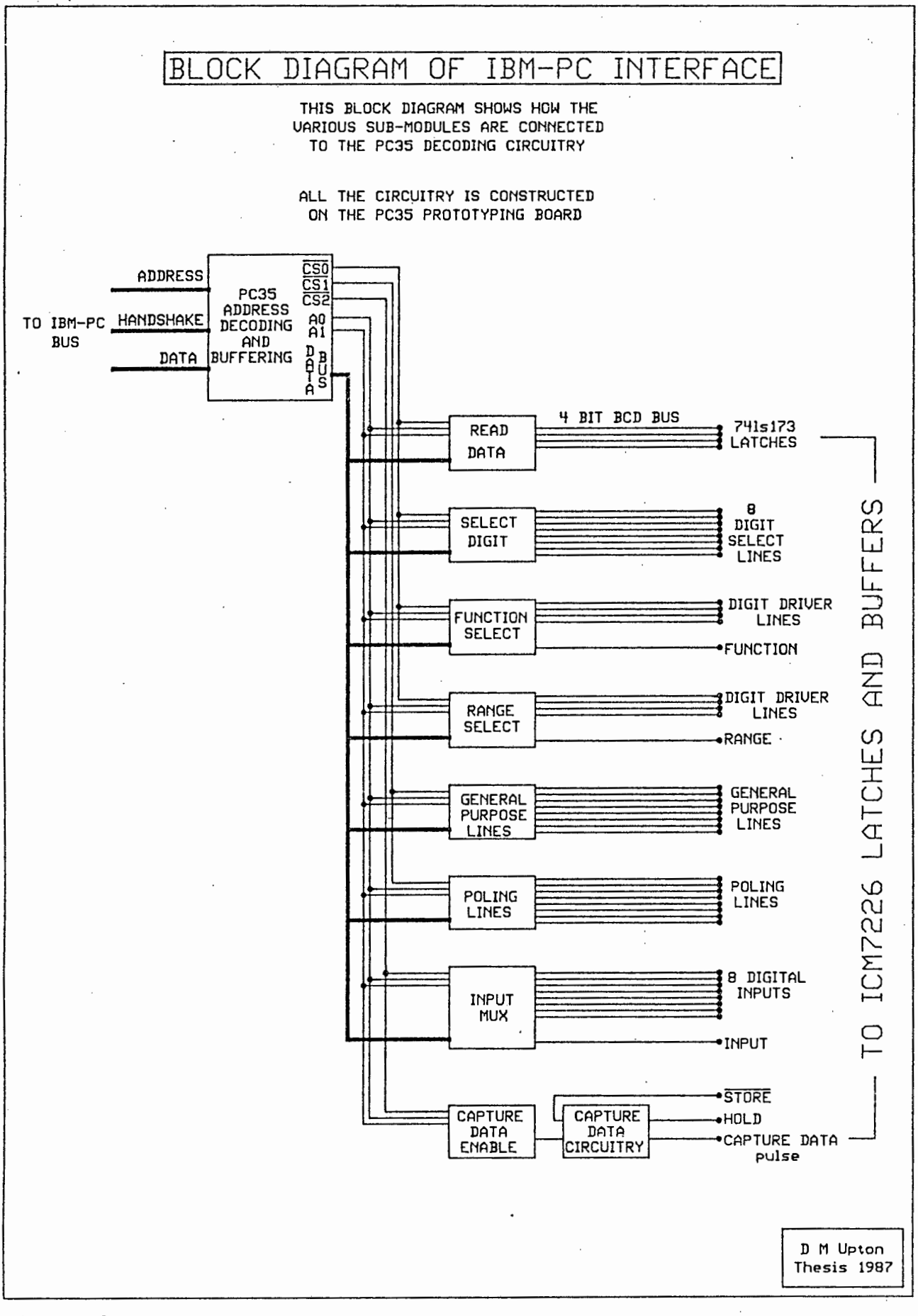
BLOCK DIAGRAM OF IBM-PC INTERFACE
THIS BLOCK DIAGRAM SHOWS HOW THE
VARIOUS SUB-MODULES ARE CONNECTED
TO THE PC35 DECODING CIRCUITRY
ALL THE CIRCUITRY IS CONSTRUCTED
ON THE PC35 PROTOTYPING BOARD
TO IBM-PC BUS
ADDRESS
HANDSHAKE
DATA
PC35 ADDRESS DECODING AND BUFFERING
CS0
CS1
CS2
A0
A1
DATA BUS
READ DATA
4 BIT BCD BUS
74ls173 LATCHES
SELECT DIGIT
8 DIGIT SELECT LINES
FUNCTION SELECT
DIGIT DRIVER LINES
FUNCTION
RANGE SELECT
DIGIT DRIVER LINES
RANGE
GENERAL PURPOSE LINES
GENERAL PURPOSE LINES
POLING LINES
POLING LINES
INPUT MUX
8 DIGITAL INPUTS
INPUT
CAPTURE DATA ENABLE
CAPTURE DATA CIRCUITRY
STORE
HOLD
CAPTURE DATA pulse
TO ICM7226 LATCHES AND BUFFERS
D M Upton
Thesis 1987

Diagram C.5.

ADDRESS DECODING FOR IBM-PC VERSION OF ICM7226 INTERFACE

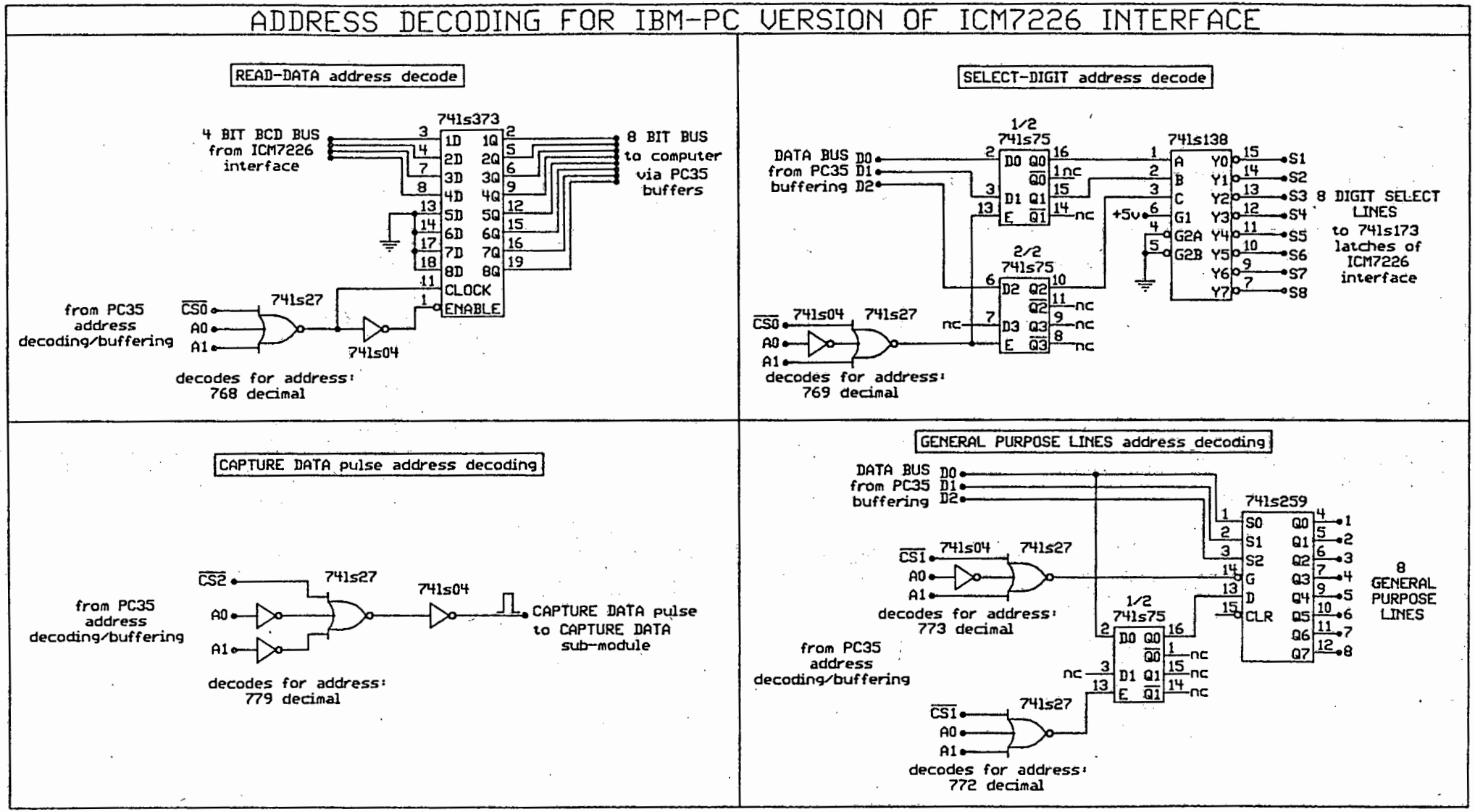

Diagram C.6A.

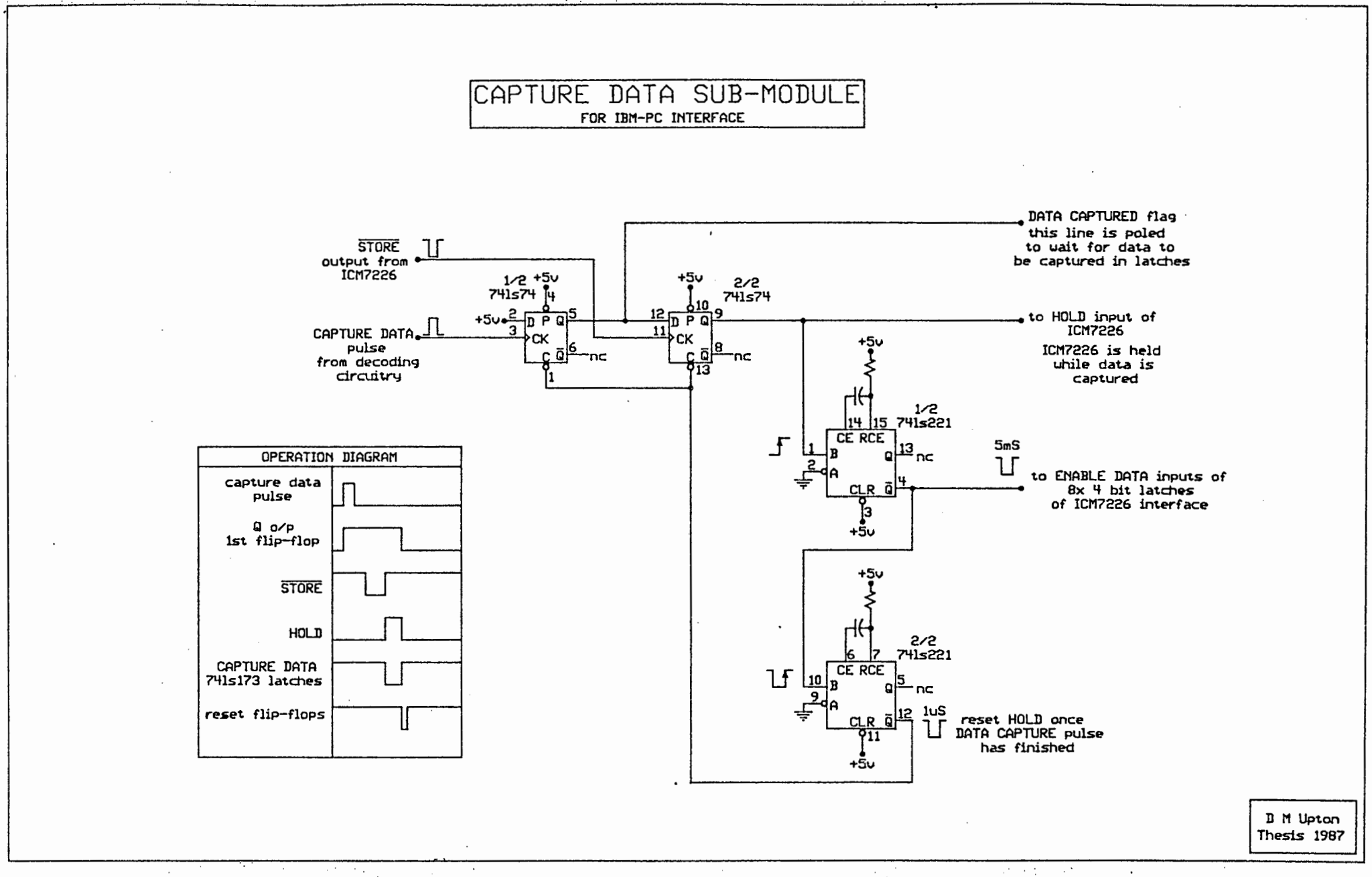
CAPTURE DATA SUB-MODULE
FOR IBM-PC INTERFACE
STORE
output from
ICM7226
CAPTURE DATA
pulse
from decoding
circuitry
1/2 +5v
74ls74
2/2
74ls74
+5v
DATA CAPTURED flag
this line is poled
to wait for data to
be captured in latches
to HOLD input of
ICM7226
ICM7226 is held
while data is
captured
1/2
74ls221
2/2
74ls221
5mS
to ENABLE DATA inputs of
8x 4 bit latches
of ICM7226 interface
1uS
reset HOLD once
DATA CAPTURE pulse
has finished
OPERATION DIAGRAM
capture data
pulse
Q o/p
1st flip-flop
STORE
HOLD
CAPTURE DATA
74ls173 latches
reset flip-flops
D M Upton
Thesis 1987

Diagram C.7.

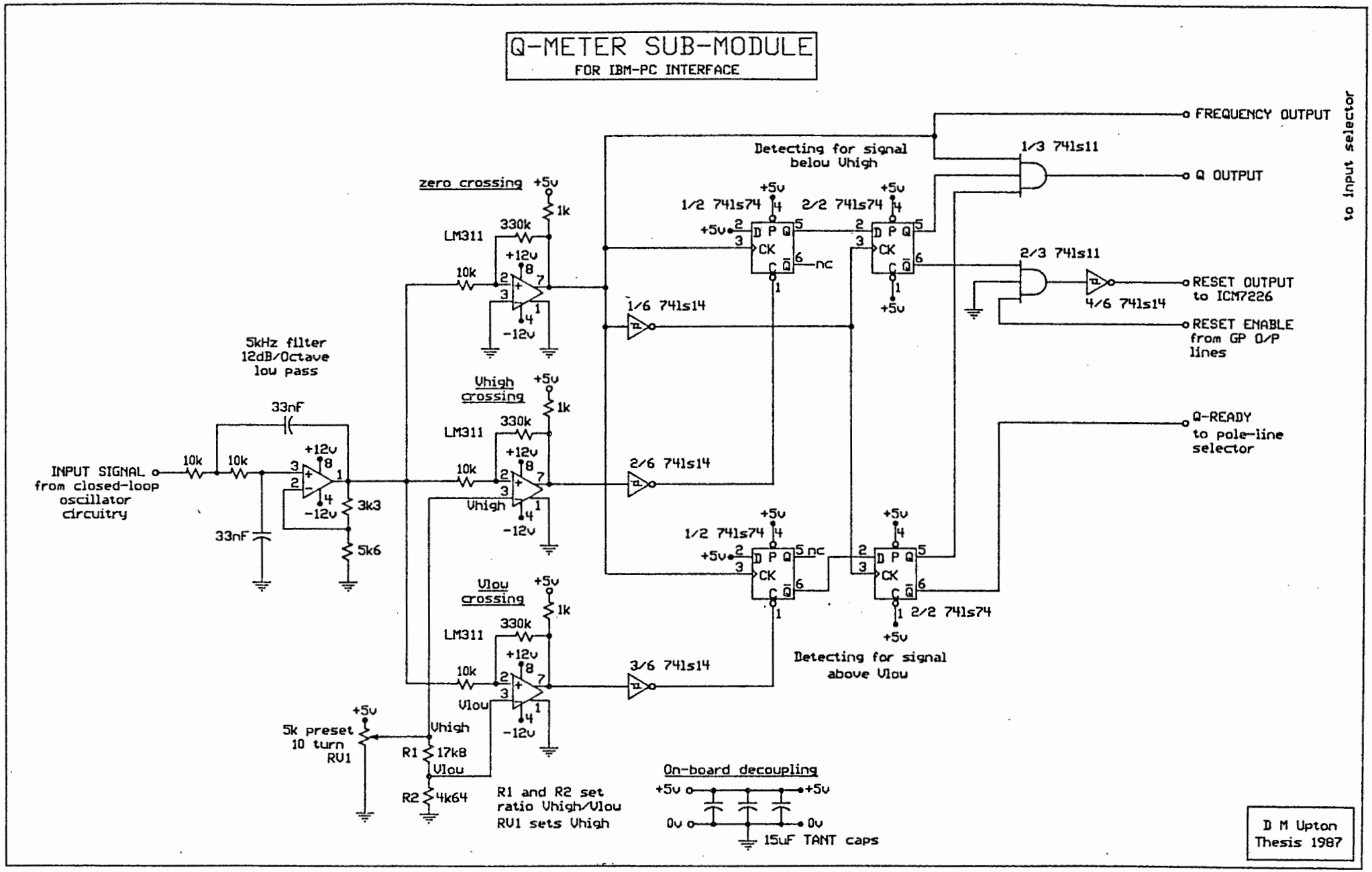
Q-METER SUB-MODULE
FOR IBM-PC INTERFACE
INPUT SIGNAL
from closed-loop
oscillator
circuitry
5kHz filter
12dB/Octave
low pass
33nF
10k
3k3
5k6
zero crossing
Vhigh
crossing
Vlou
crossing
LM311
330k
1k
+12v
-12v
+5v
5k preset
10 turn
RV1
R1 17k8
R2 4k64
Vhigh
Vlou
R1 and R2 set
ratio Vhigh/Vlou
RV1 sets Vhigh
1/6 741s14
2/6 741s14
3/6 741s14
4/6 741s14
1/2 741s74
2/2 741s74
D P Q
CK
nc
1/3 741s11
2/3 741s11
Detecting for signal
belou Vhigh
Detecting for signal
above Vlou
FREQUENCY OUTPUT
Q OUTPUT
RESET OUTPUT
to ICM7226
RESET ENABLE
from GP O/P
lines
Q-READY
to pole-line
selector
to input selector
On-board decoupling
0v
15uF TANT caps
D M Upton
Thesis 1987

Diagram C.8.

APPENDIX D

GRAPHS OF RESULTS FROM THE EXPERIMENTAL WORK

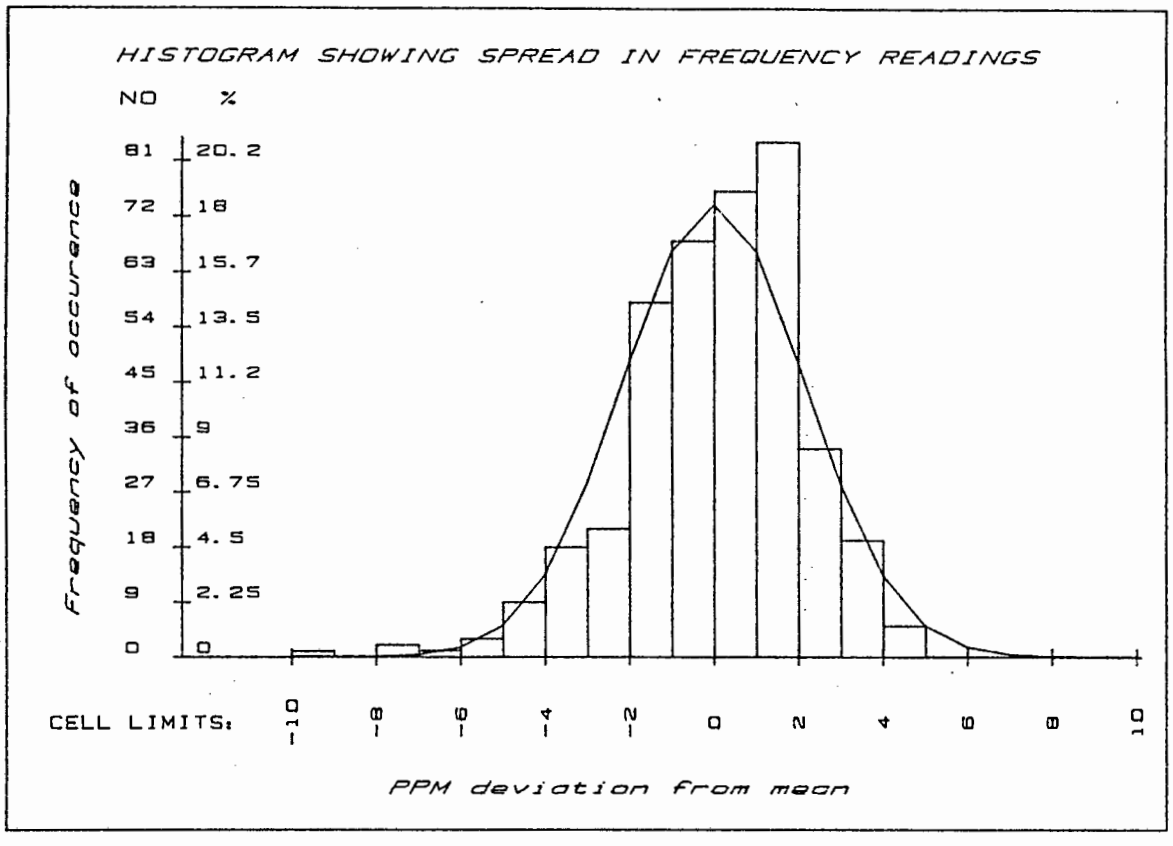

GRAPH D.1.

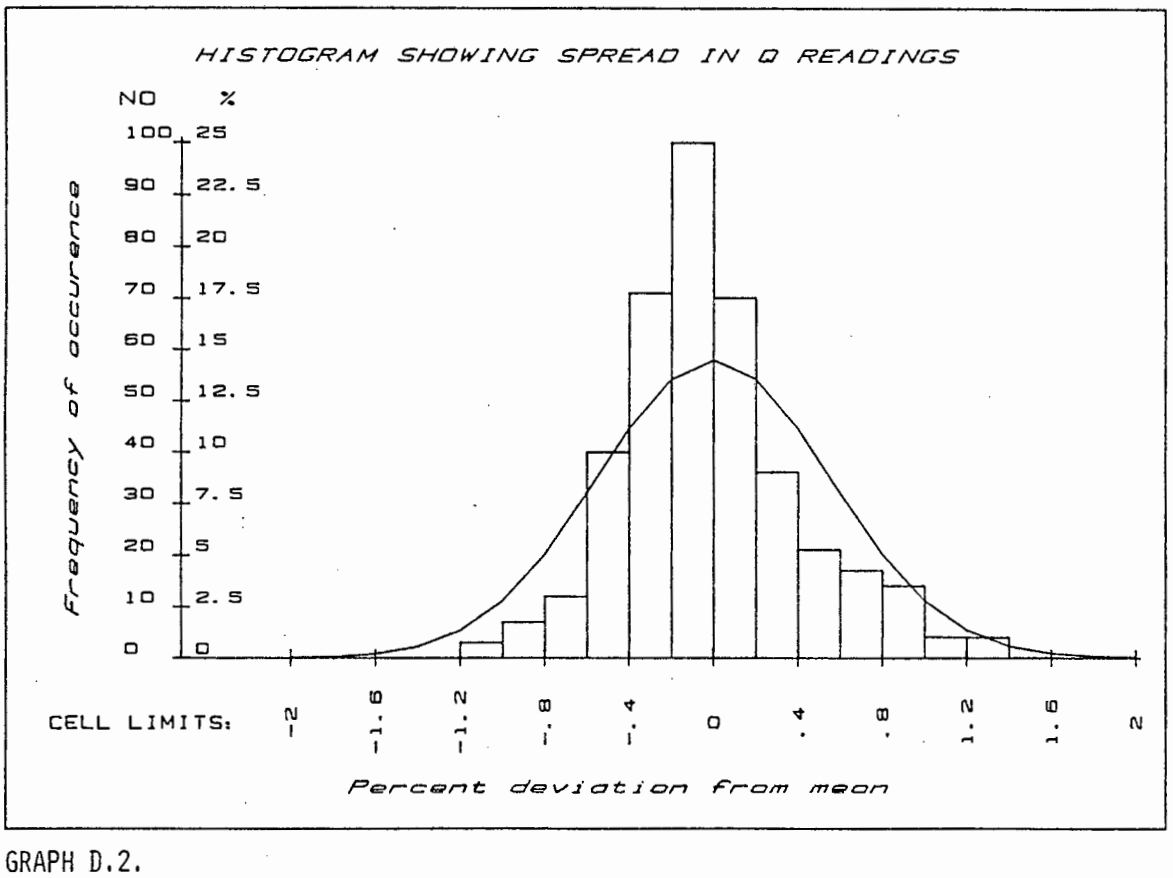

GRAPH D.2.

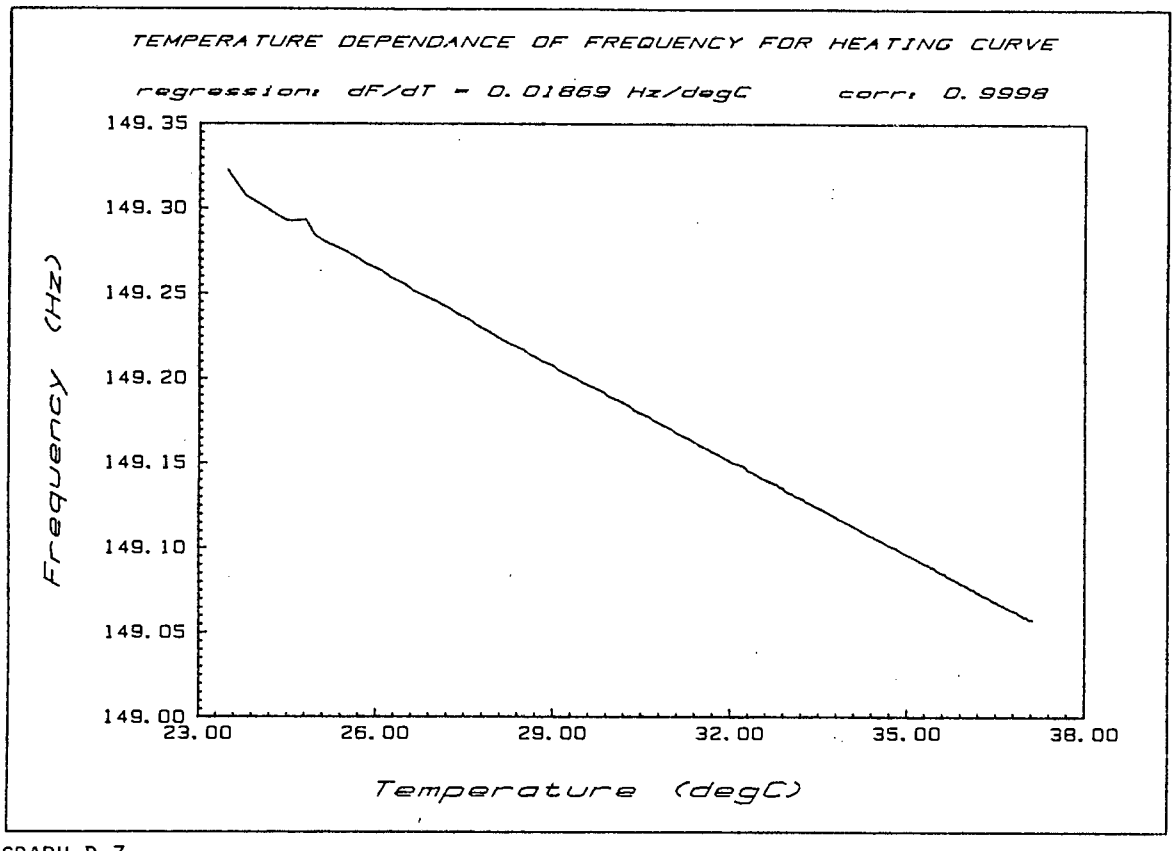

GRAPH D.3.

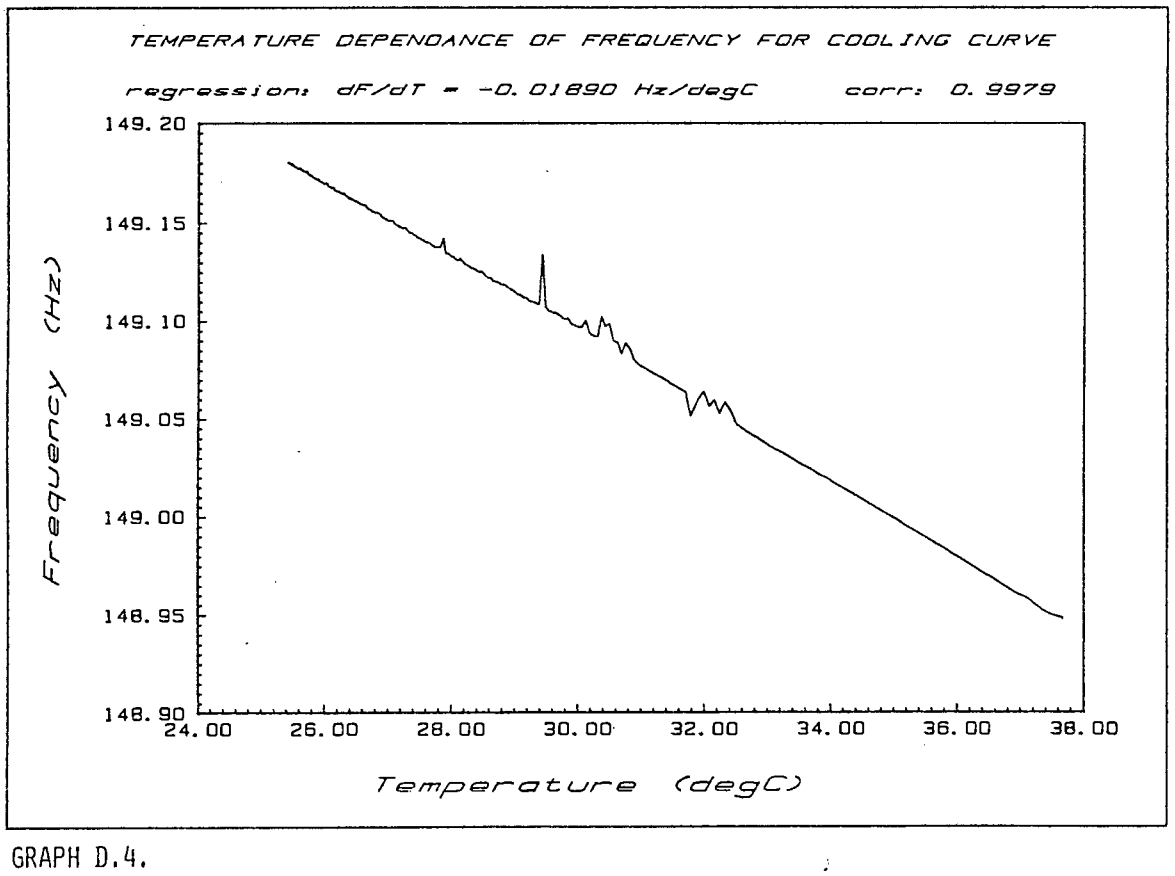

GRAPH D.4.

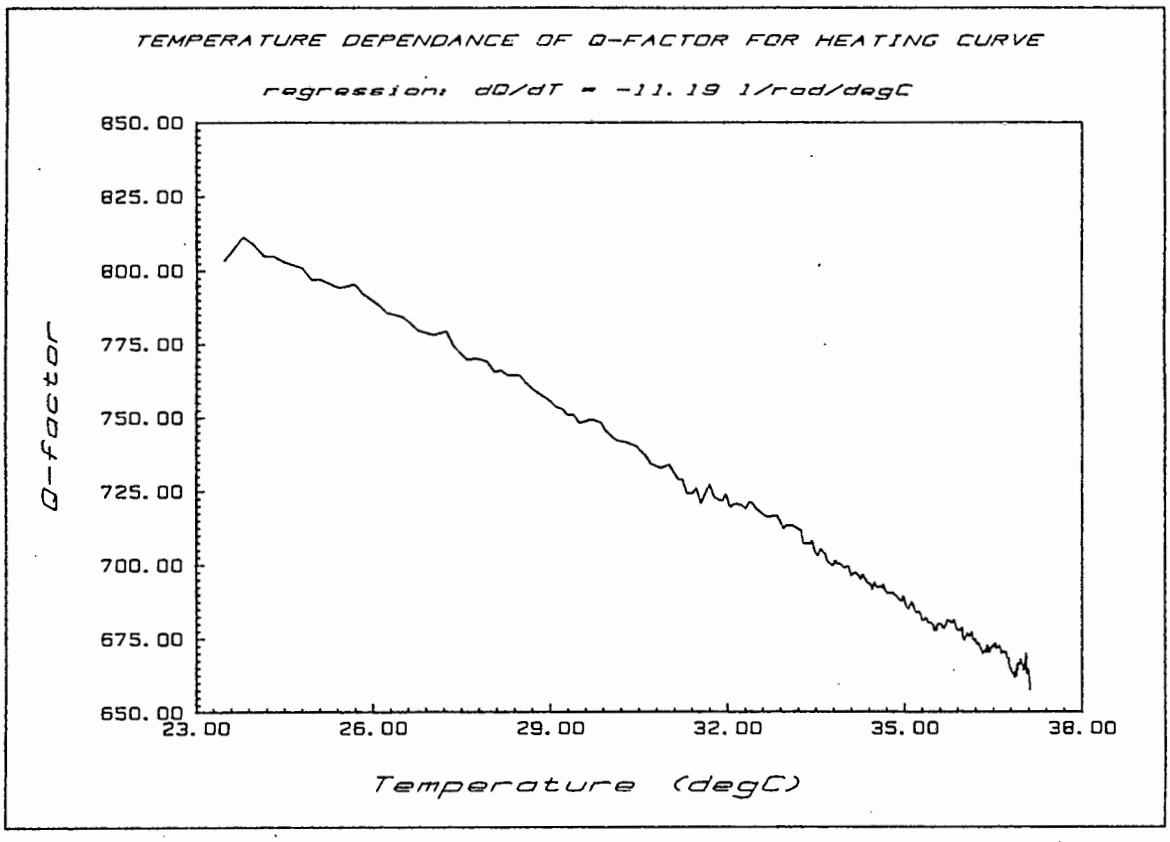

GRAPH D.5.

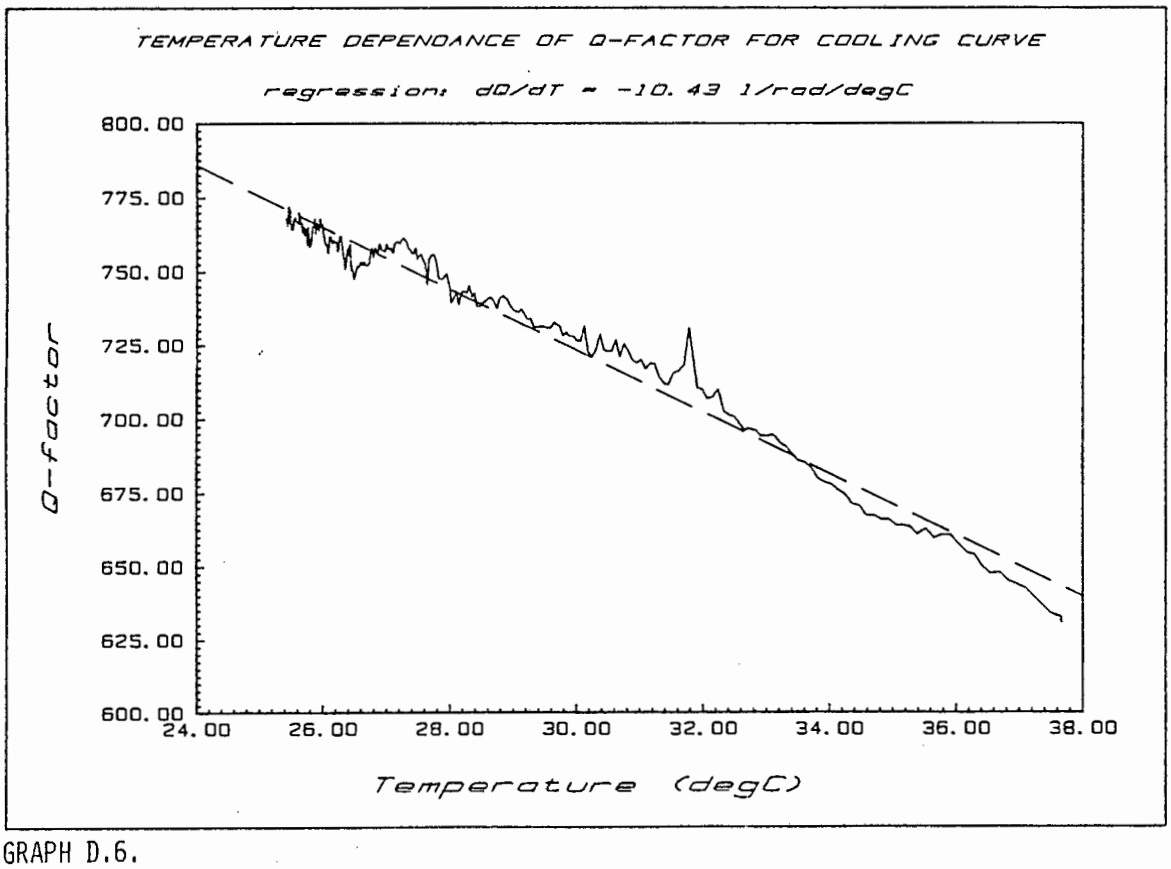

GRAPH D.6.

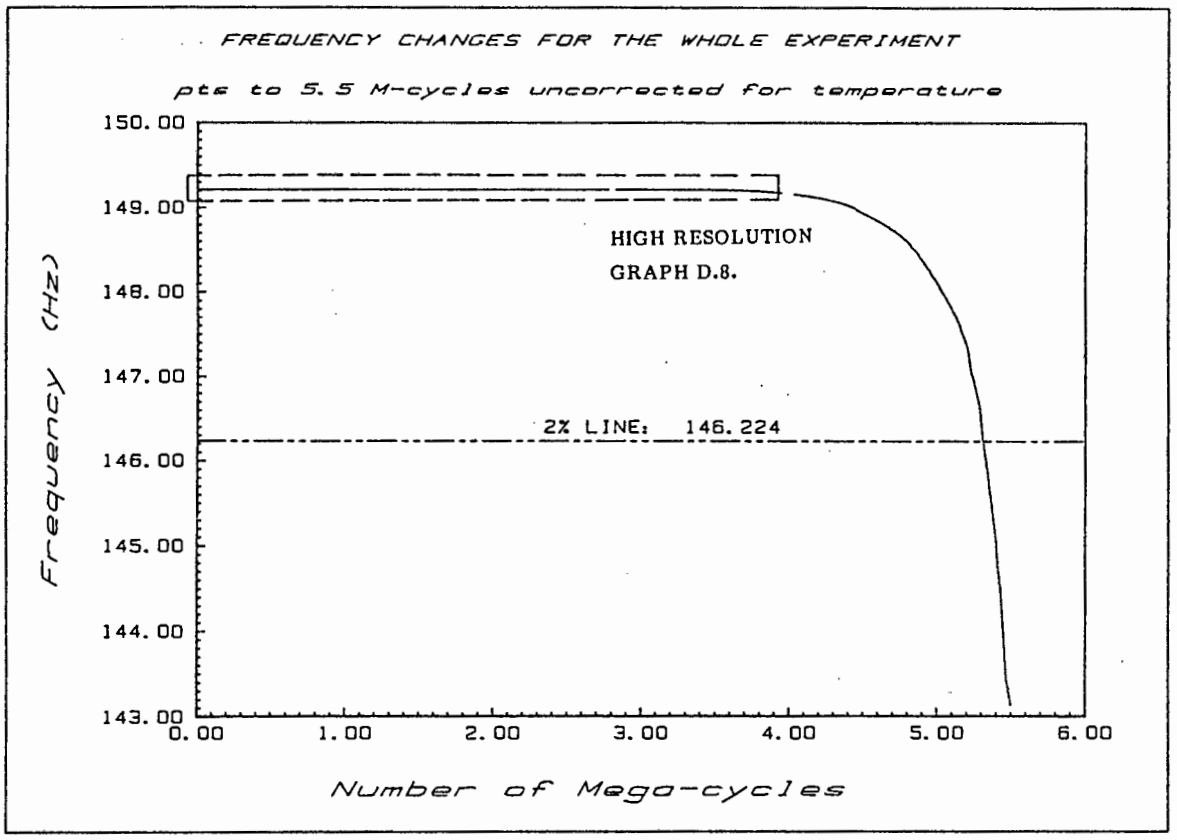

GRAPH D.7.

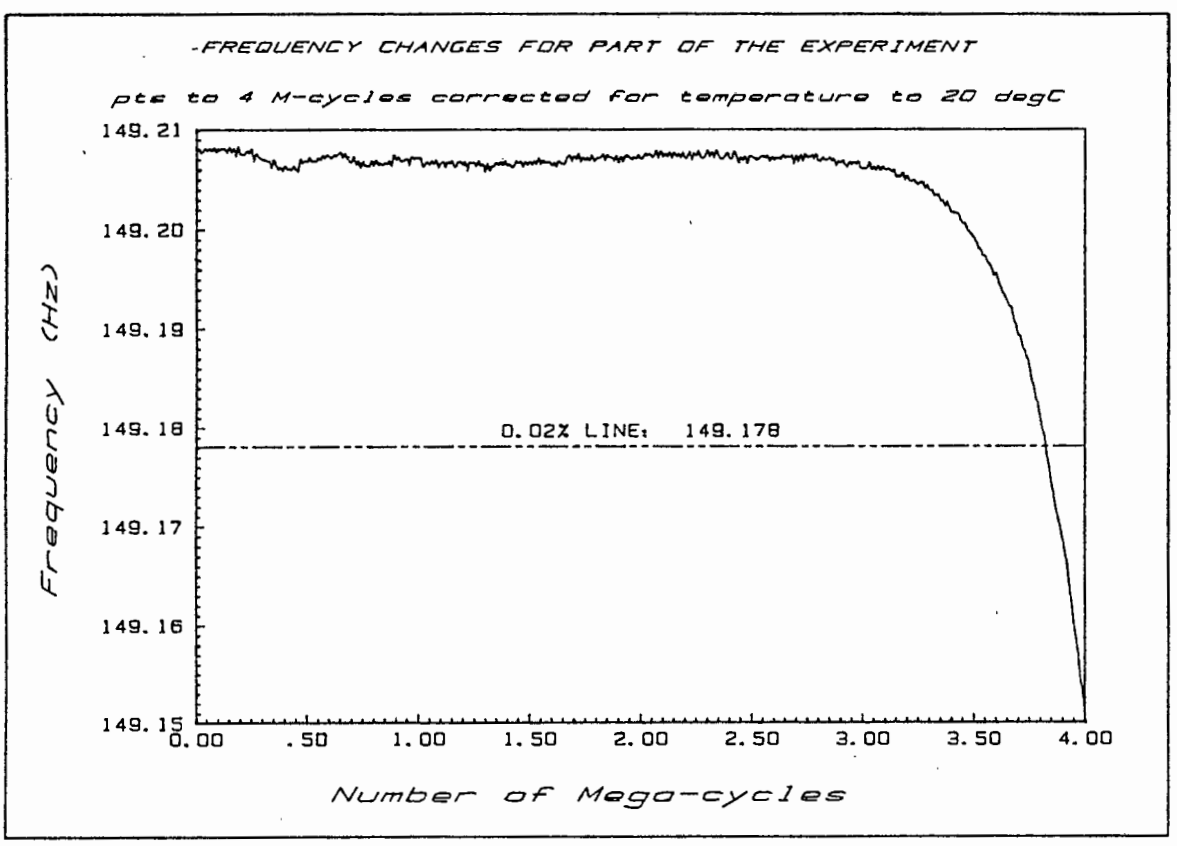

GRAPH D.8.

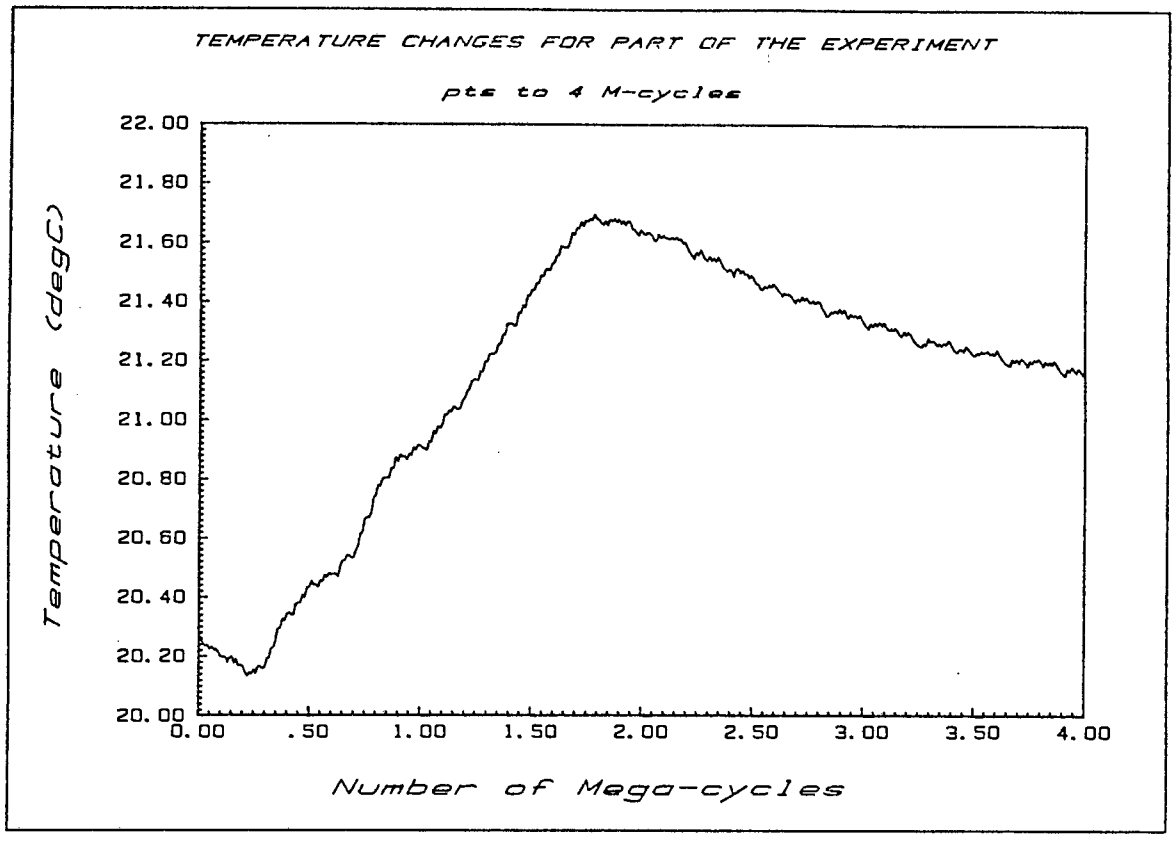

GRAPH D.9.

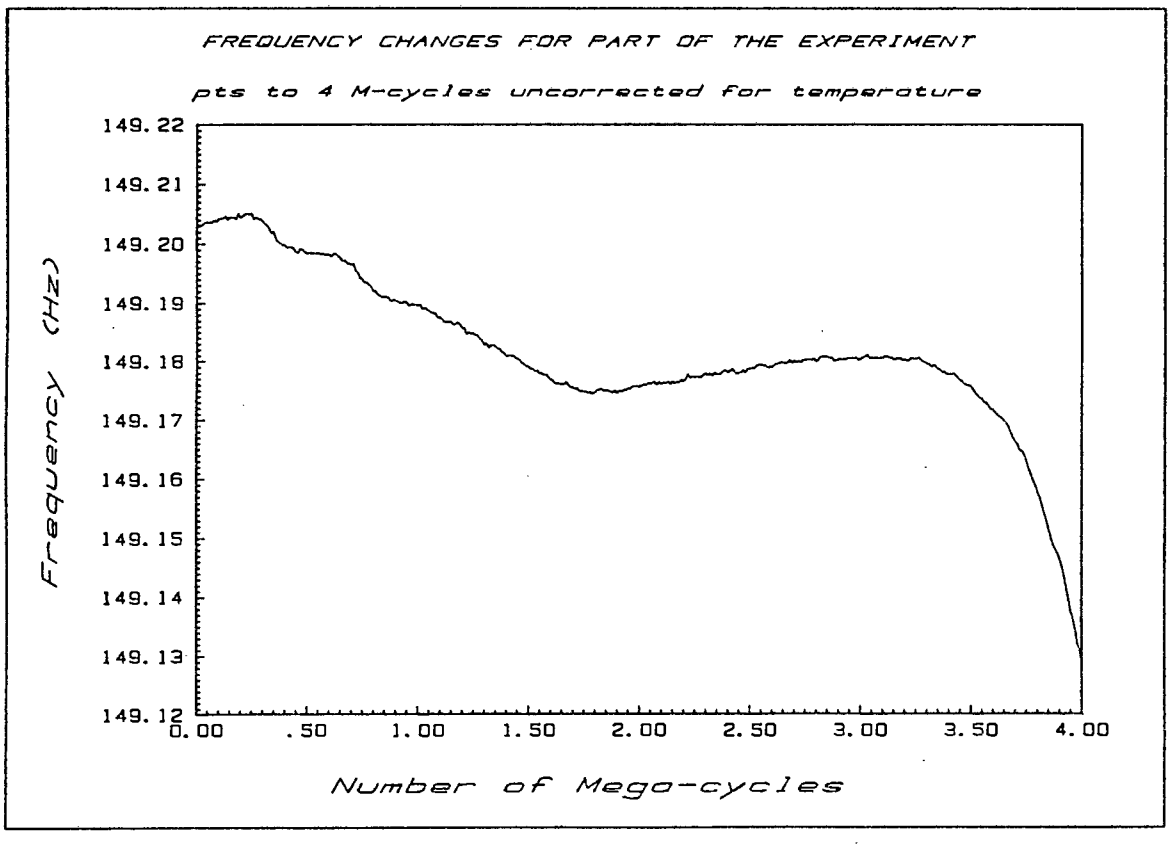

GRAPH D.10.

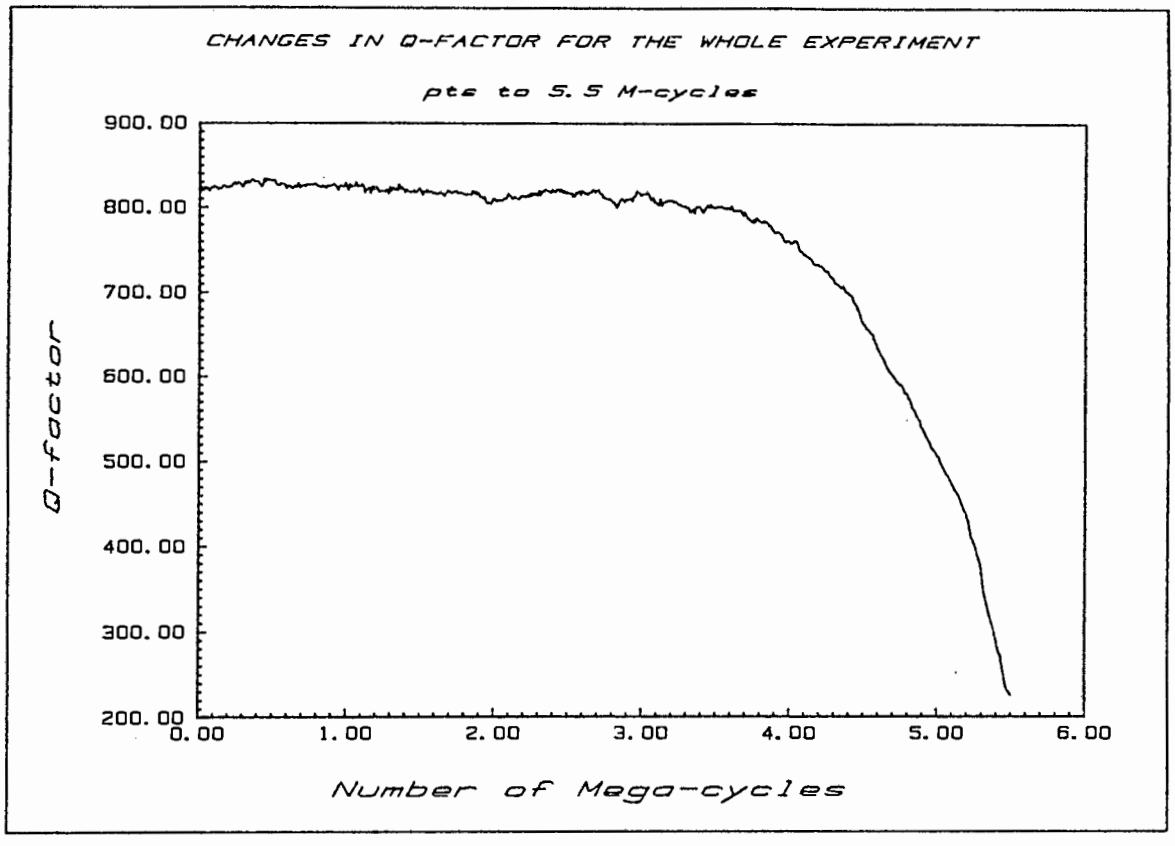

GRAPH D.11.

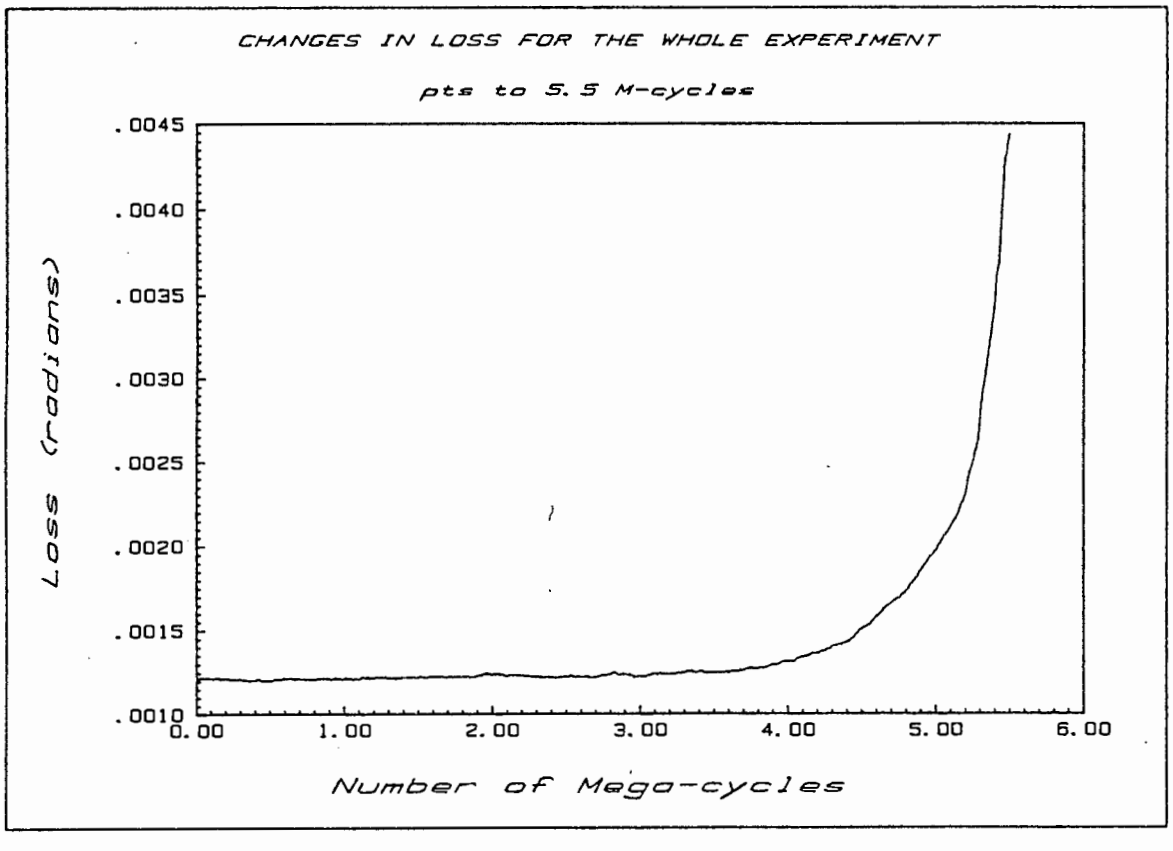

GRAPH D.12.

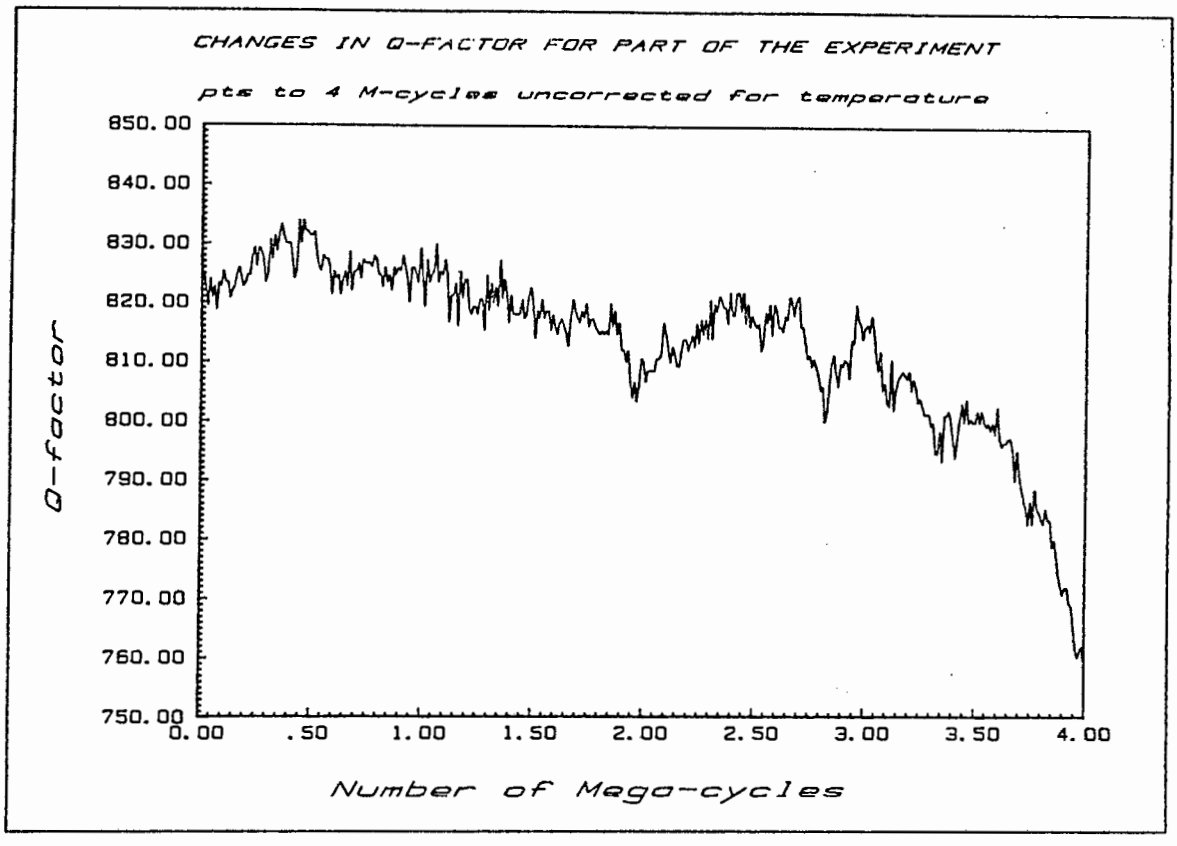

GRAPH D.13.

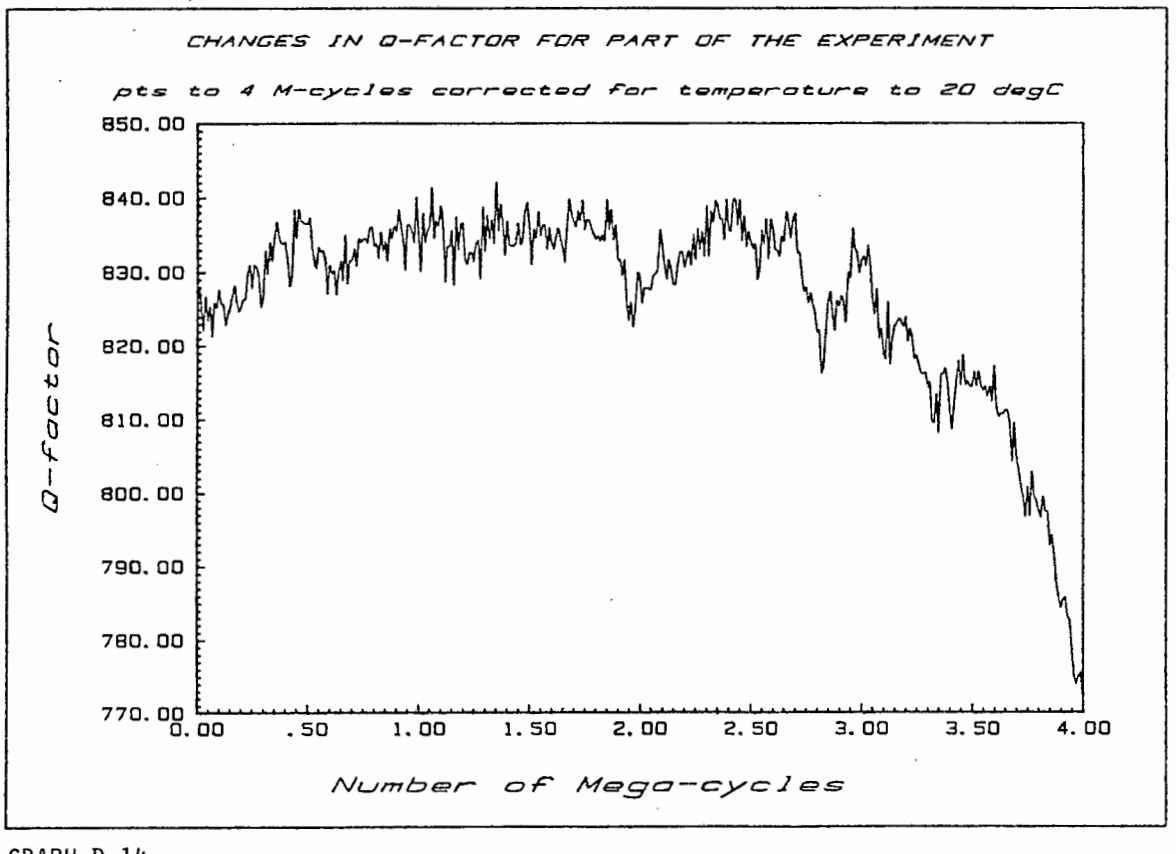

GRAPH D.14.

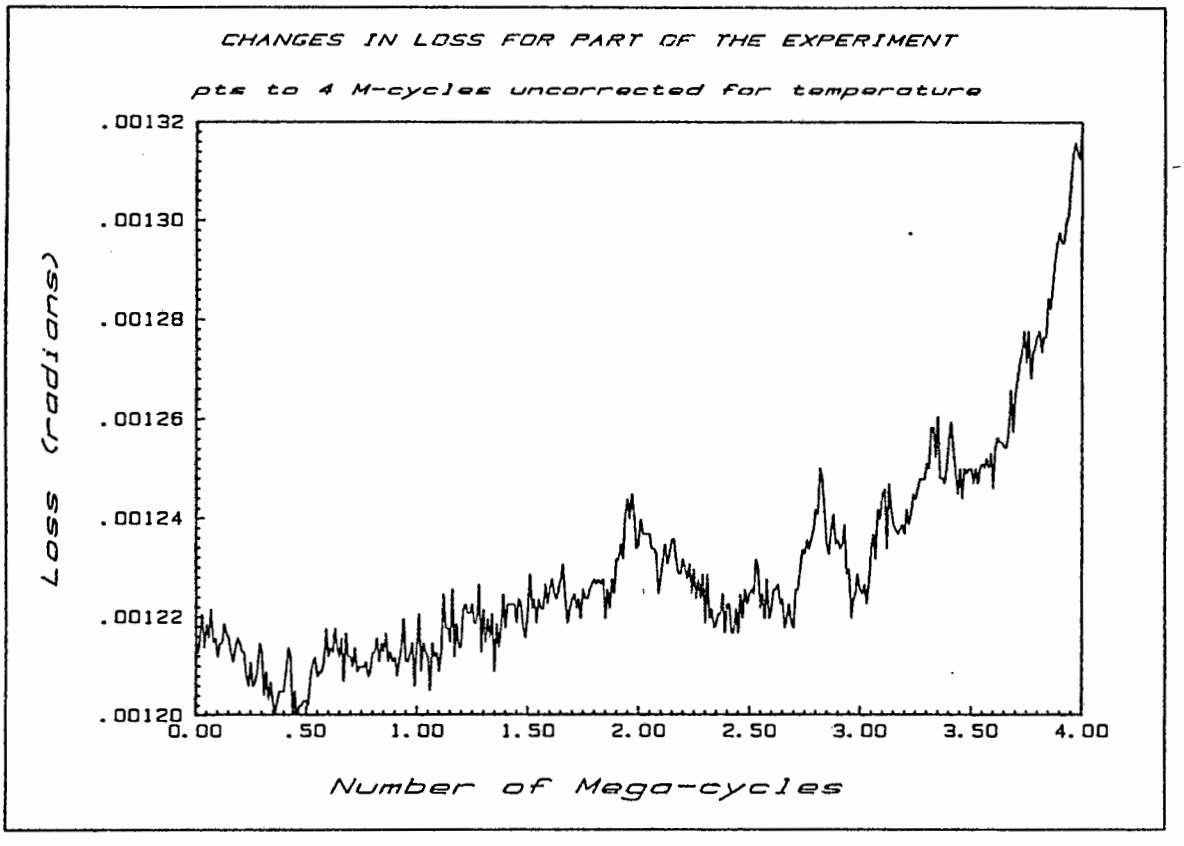

GRAPH D.15.

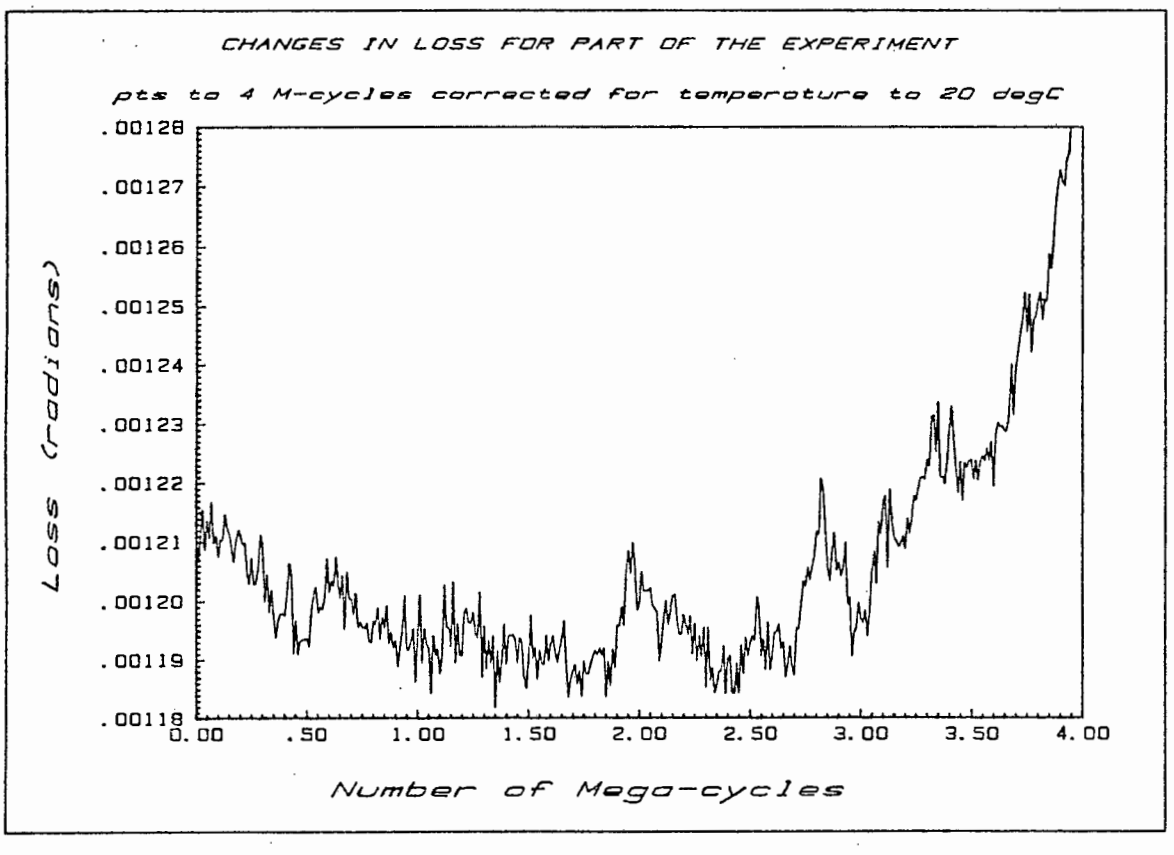

GRAPH D.16.

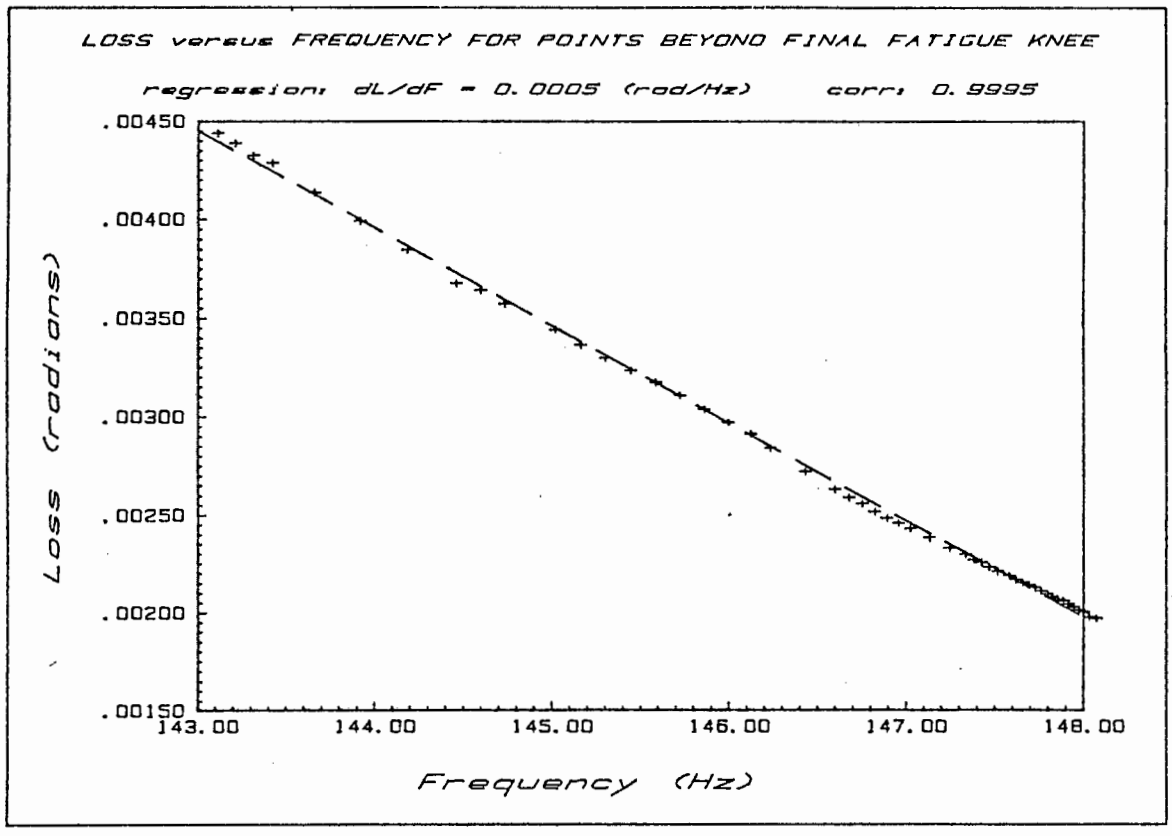
LOSS versus FREQUENCY FOR POINTS BEYOND FINAL FATIGUE KNEE
regression: dL/dF = 0.0005 (rad/Hz) corr: 0.9995
Loss (radians)
.00450
.00400
.00350
.00300
.00250
.00200
.00150
143.00
144.00
145.00
146.00
147.00
148.00
Frequency (Hz)

GRAPH D.17.

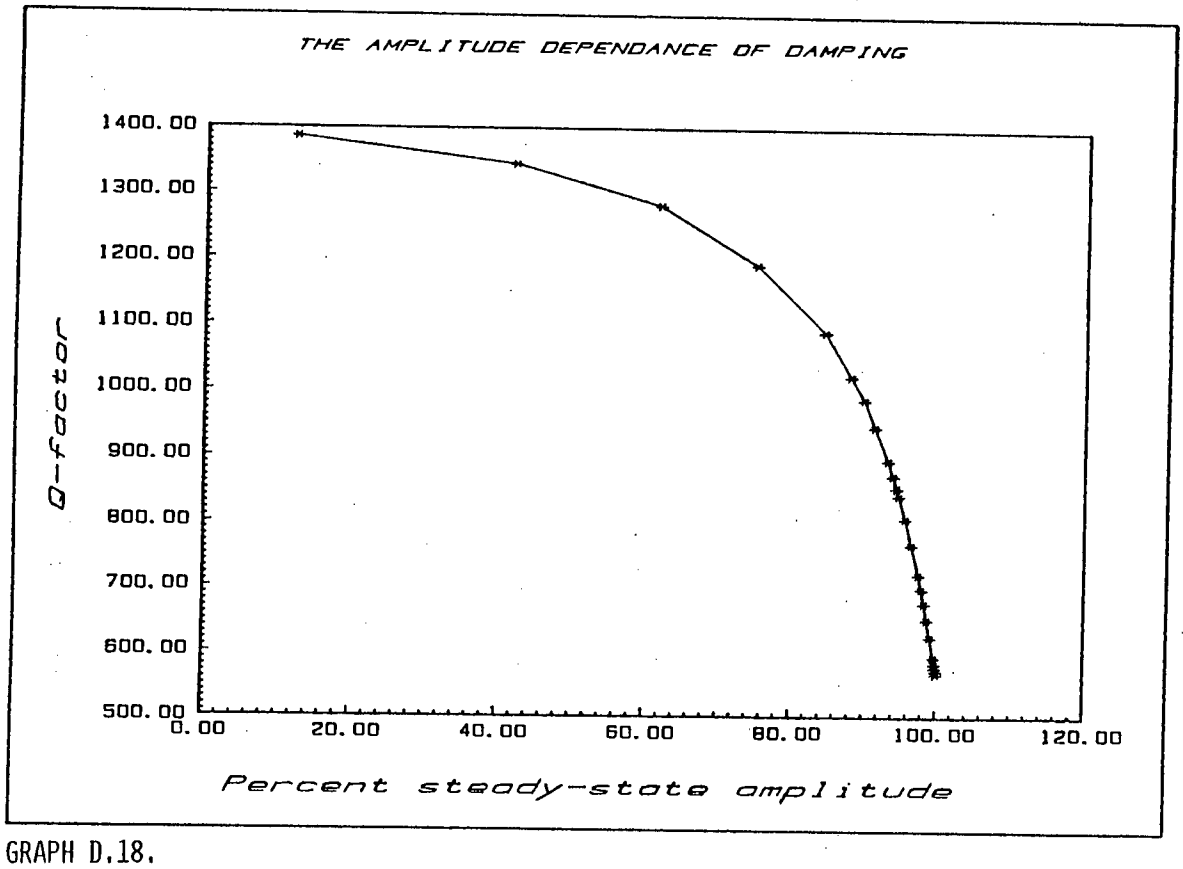

GRAPH D.18.

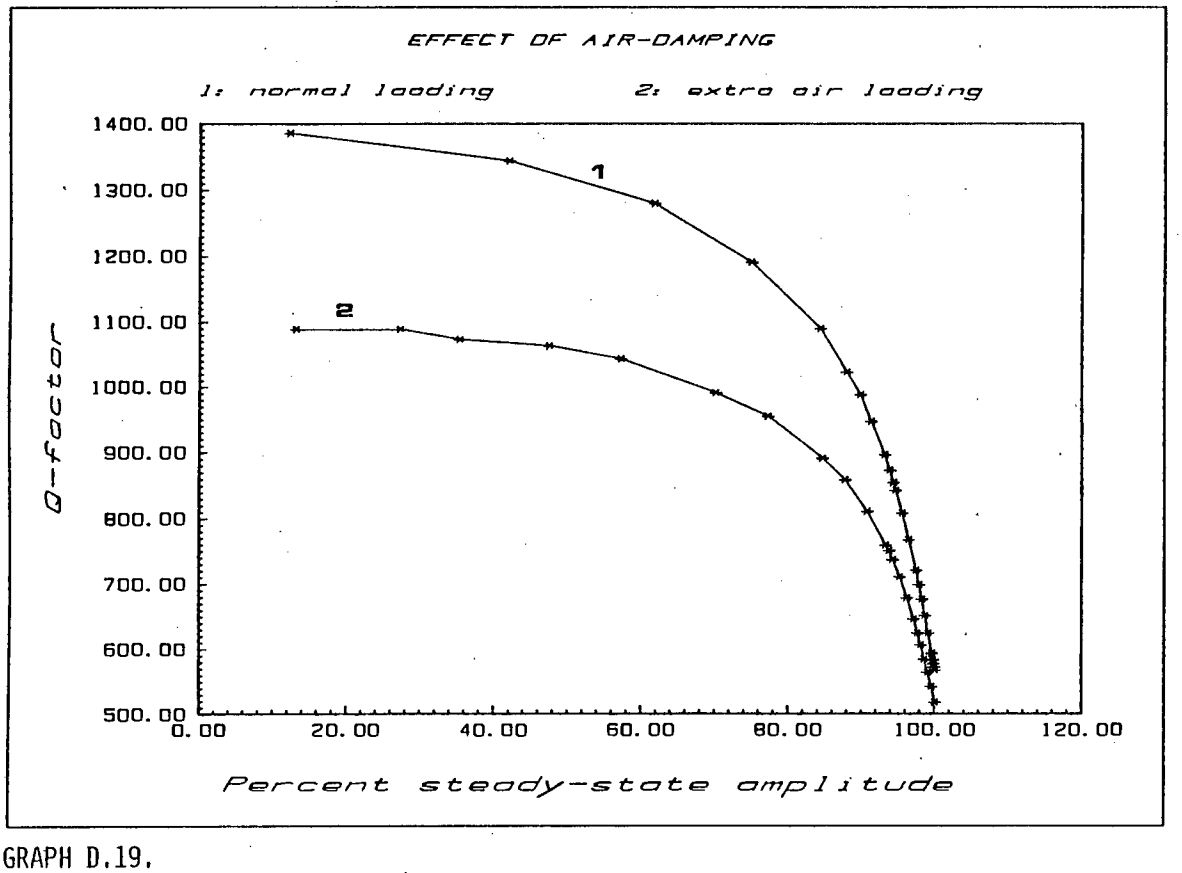

GRAPH D.19.

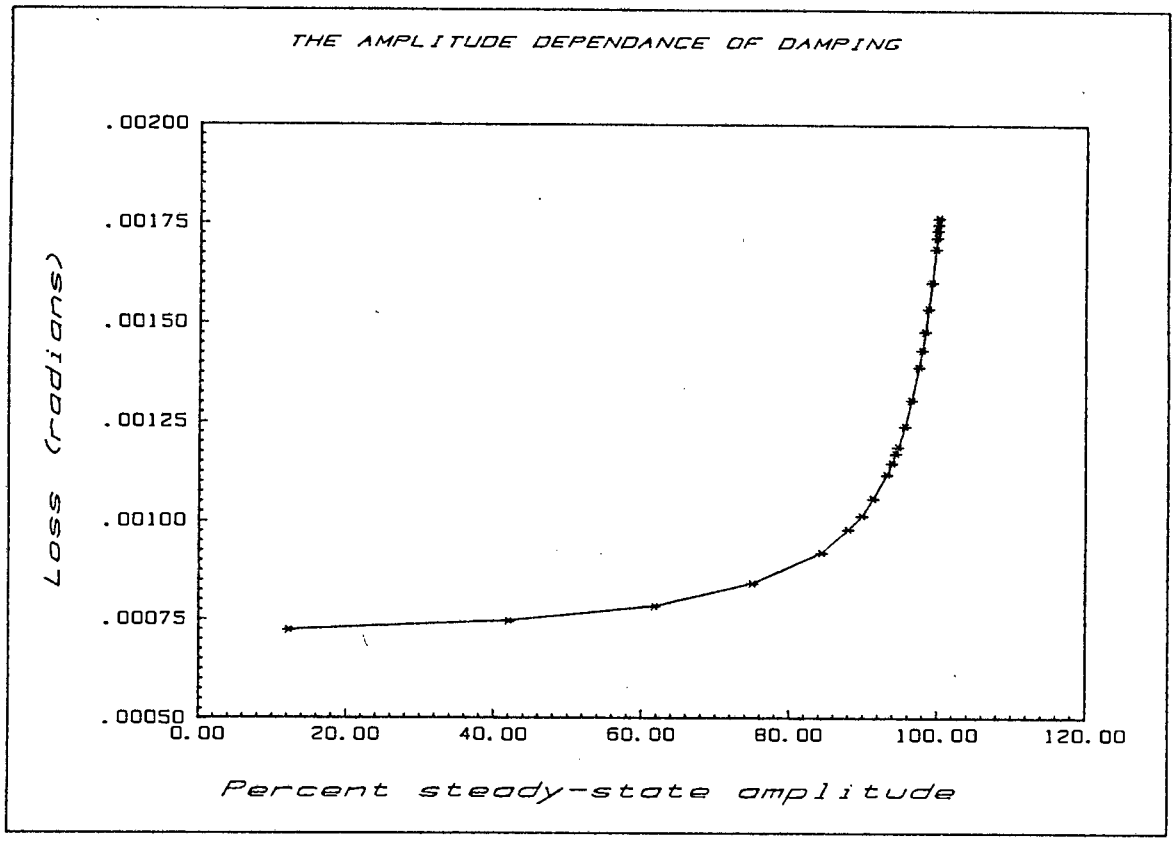

GRAPH D.20.

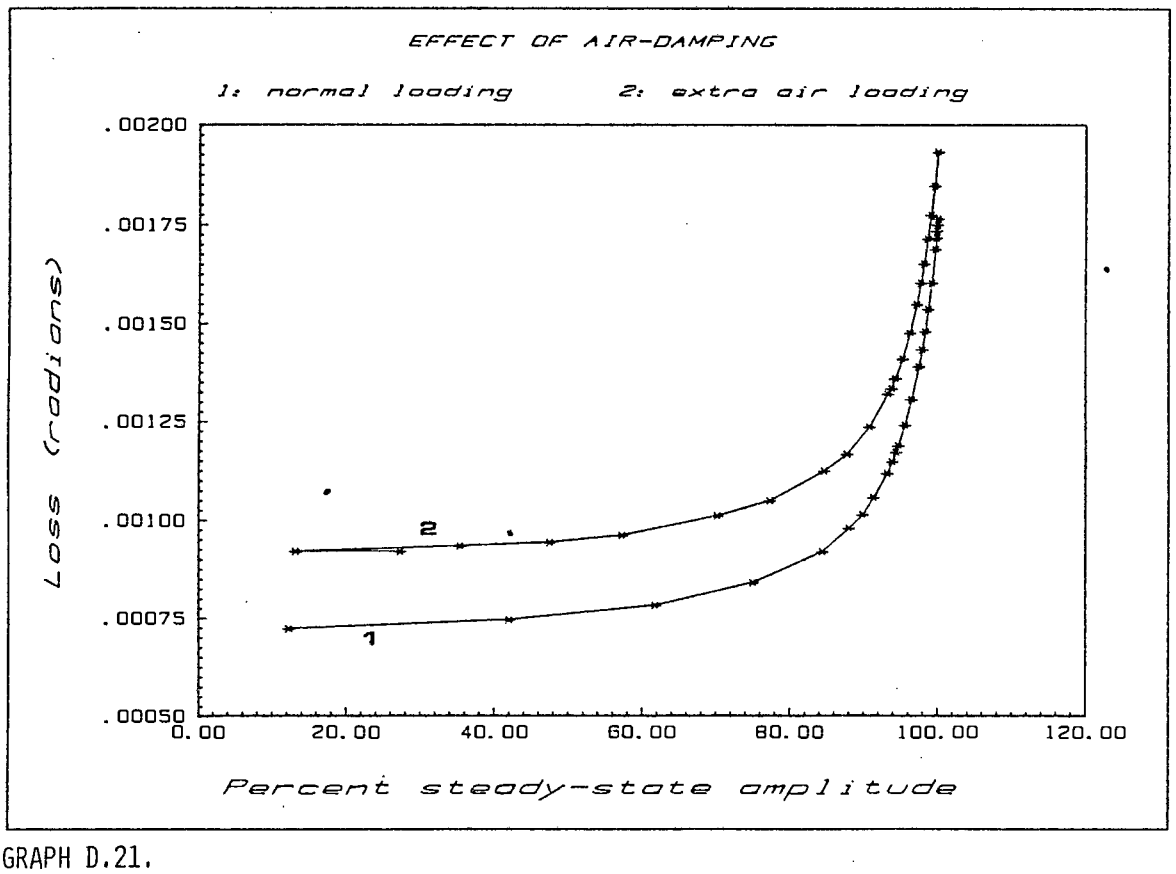

GRAPH D.21.

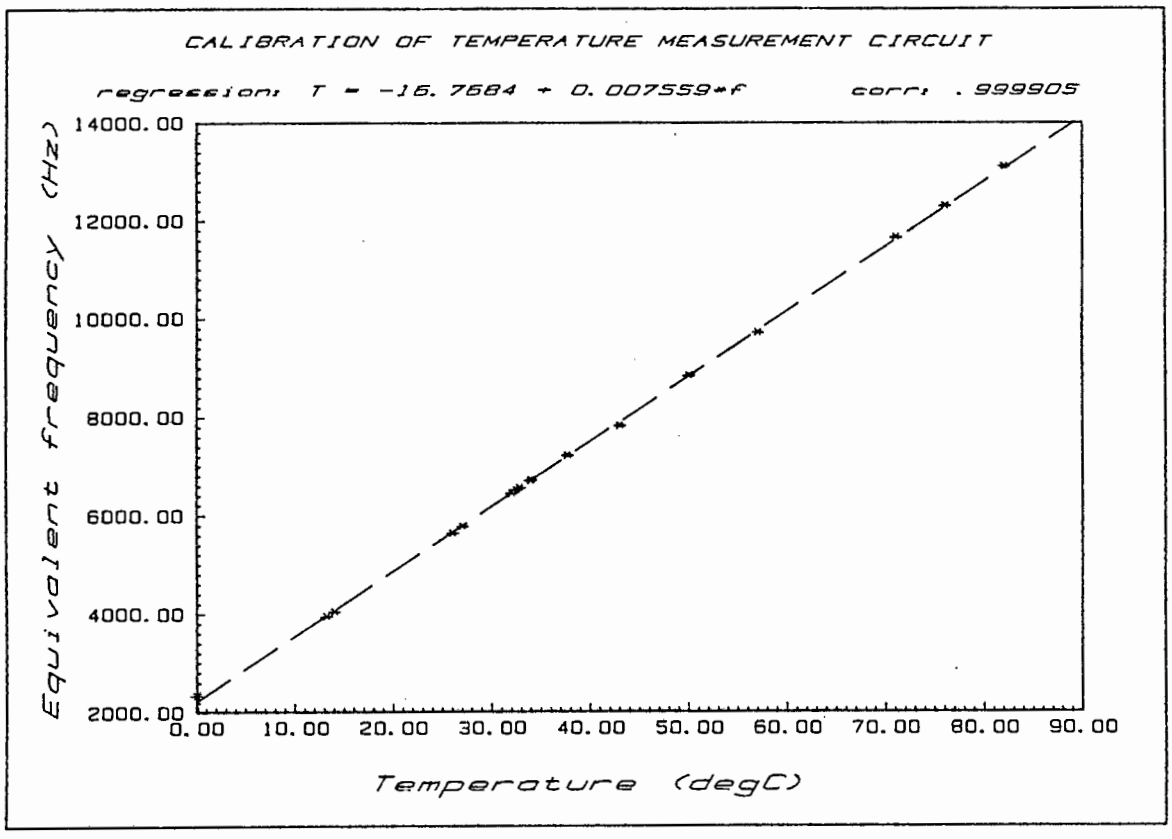

GRAPH D.22.

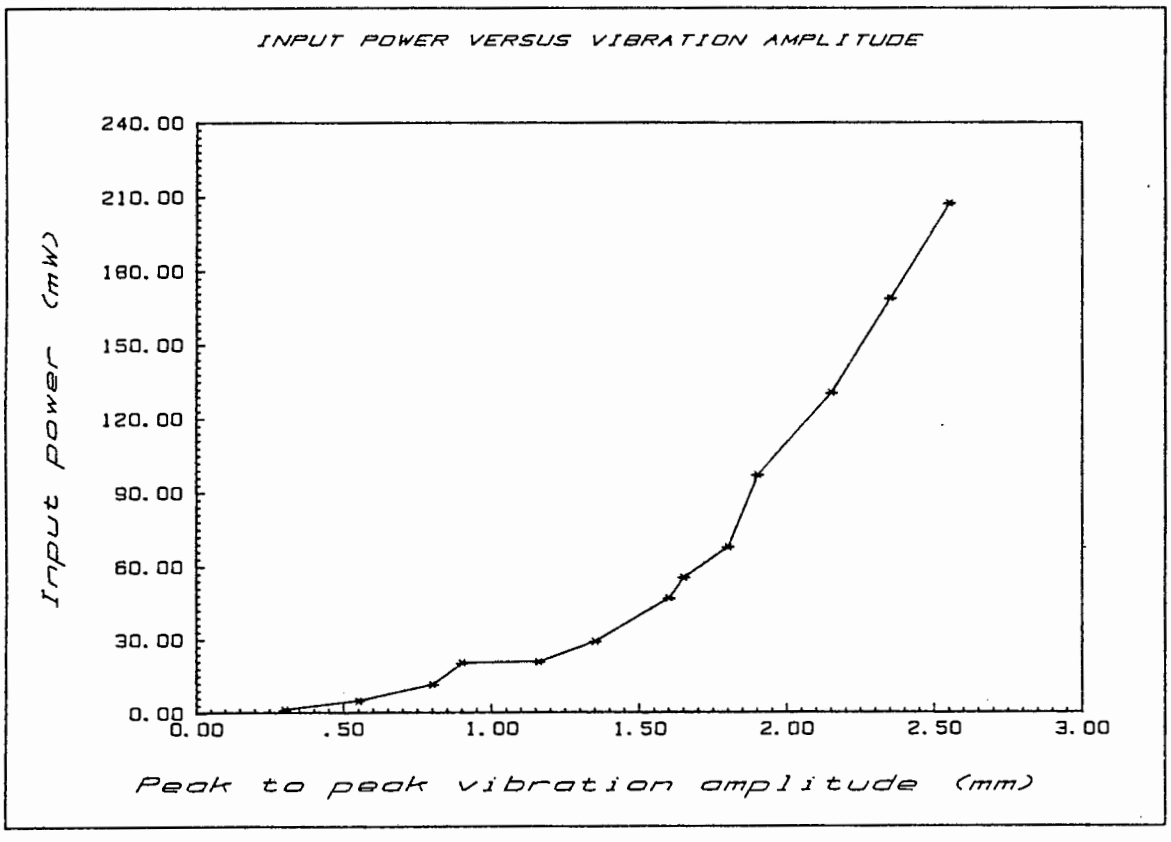

GRAPH D.23.

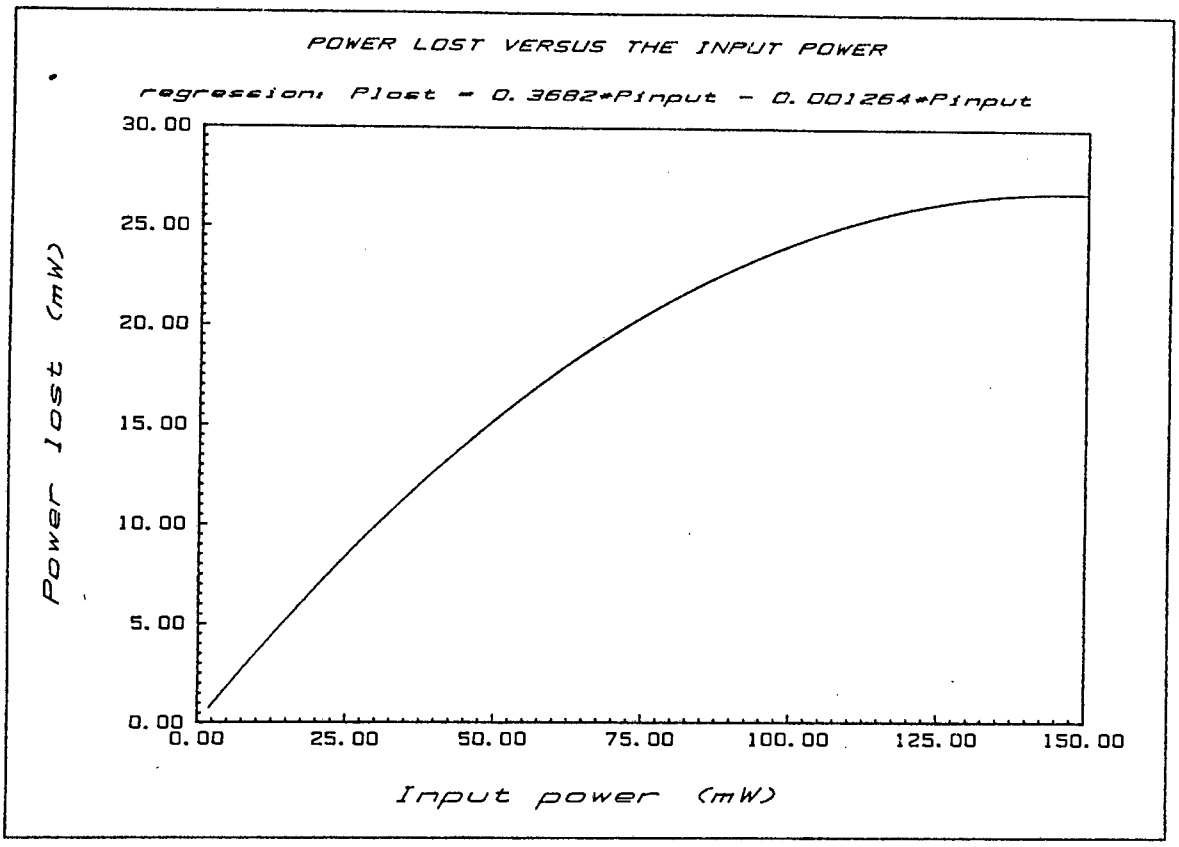

GRAPH D.24.

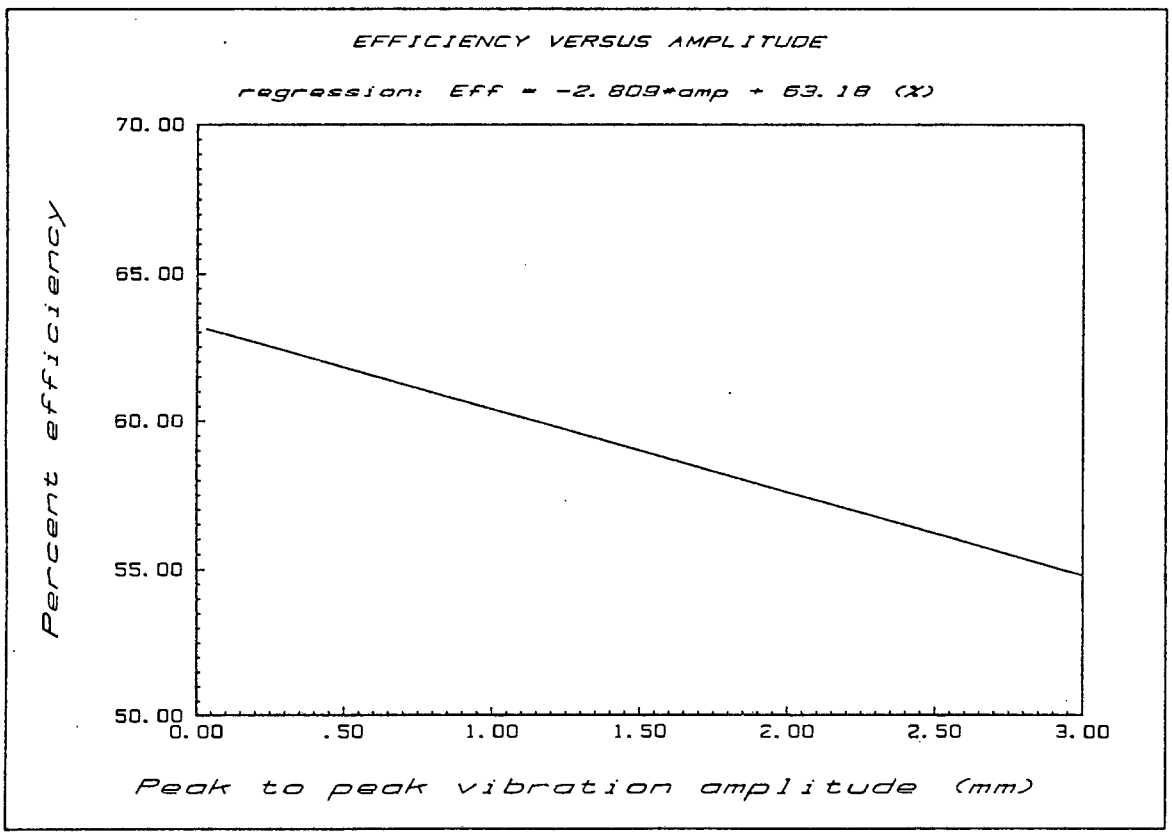

GRAPH D.25.

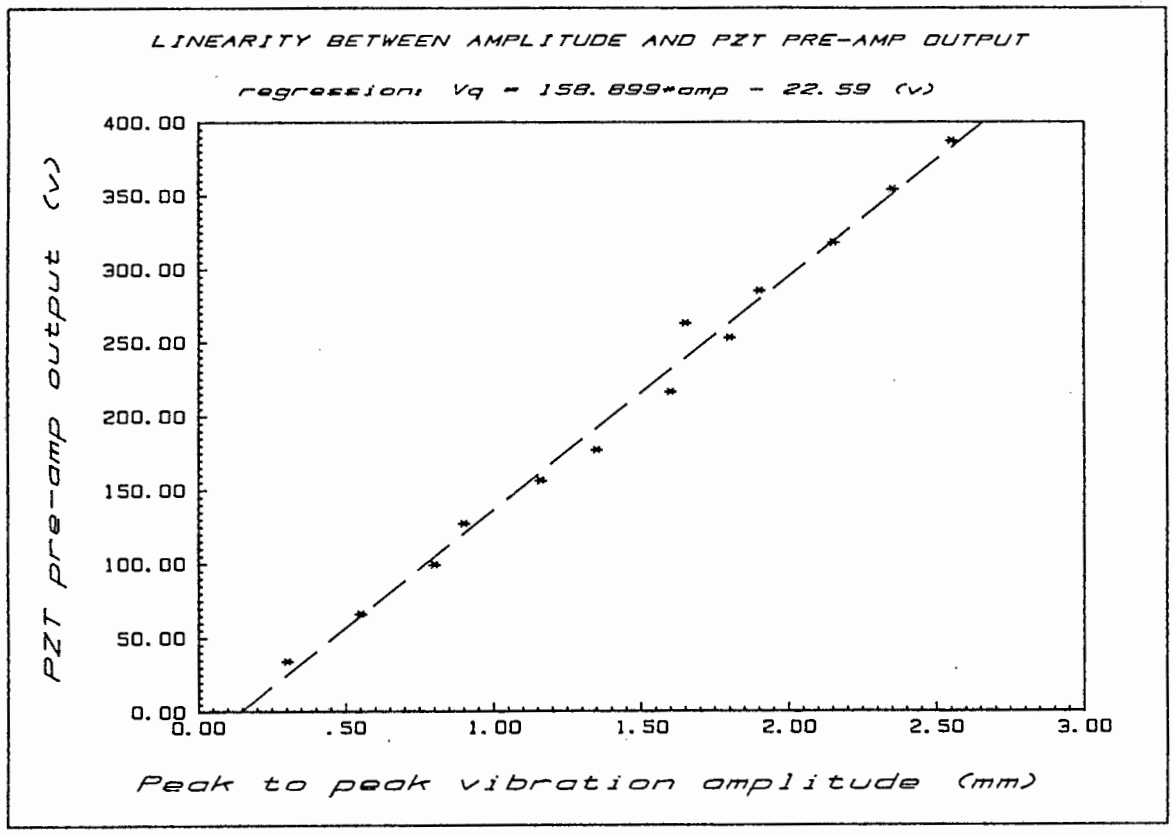

GRAPH D.26.

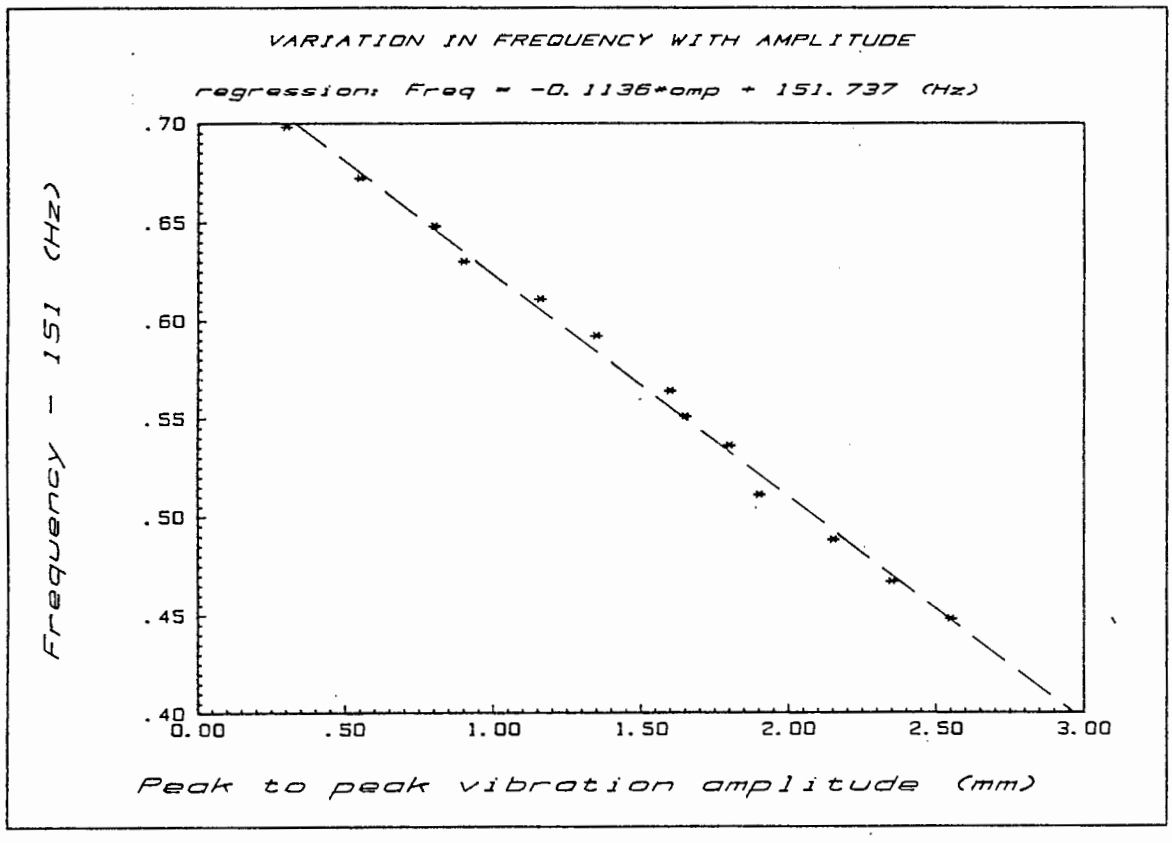

GRAPH D.27.

APPENDIX E

THE LISTING OF THE HP85 BASIC PROGRAM

DESCRIPTION OF THE VARIABLES USED IN THE HP85 COMPUTER PROGRAM

A$: general purpose character variable to store user input from the keyboard.

f$: the name of the data file

F1 : flag to indicate which mode of operation to use

F2 : flag to indicate if a data file is required

F3 : flag to indicate if a print-out of data is required

N : counter to store the total number of measurements taken

N1 : The number of readings to be taken before printing out

N2 : Counter to decide if data must be printed out in accordance with N1

S1 : scaling factor for measurements taken in the frequency mode

P1 : scaling factor for measurements taken in the period mode

C1 : flag to indicate which printing format is to be used in the general purpose mode

X : accumulated value of the digit values read from the 7226 interface

Y : temporary variable to store the current digit being read from the 7226 interface

I : loop counter used for reading the eight digit values

T : the scaled value of the total measurement reading from the 7226 interface to convert to temperature in °C.

F : the averaged frequency in the experimental mode

Q : the averaged Q readings taken in the experimental mode

T1 : the averaged unscaled temperature readings in the experimental mode

---X---

```
1000 ! ************************
1010 ! GENERAL PURPOSE PROGRAM
1020 !   TO INTERFACE THE HP85
1030 !     COMPUTER TO THE
1040 !  7226 UNIVERSAL COUNTER
1050 !  USING A GPIO INTERFACE.
1060 !
1070 !  THE PROGRAM ALLOWS TWO
1080 !    MODES OF OPERATION
1090 !
1100 !    G: GENERAL PURPOSE
1110 !       MEASUREMENT MODE
1120 !
1130 !    E: FATIGUE EXPERIMENT
1140 !       MODE.
1150 ! ************************
1160 !
1170 ! ----------------------
1180 ! MAIN PROGRAM
1190 ! ----------------------
1200 GOSUB 1370
1210 GOSUB 1600
1220 IF F1=0 THEN 3340
1230 IF F1<>1 THEN 1200
1240 GOSUB 1770
1250 GOSUB 1960
1260 ON INTR 4 GOTO 4010
1270 GOTO 3860
1280 ! ----------------------
1290 ! END OF MAIN PROGRAM
1300 ! ----------------------
1310 ! The sub-routines and two
1320 !      sections of the
1330 ! program are listed below
1340 ! ----------------------
1350 !
1360 !
1370 ! ----------------------
1380 ! INITIALISATION
1390 ! ----------------------
1400 CONTROL 4,3 ; 0
1410 CONTROL 4,4 ; 160
1420 CONTROL 4,6 ; 129
1430 CONTROL 4,8 ; 3
1440 CONTROL 4,9 ; 1
1450 OUTPUT 400 USING "#,B" ; 8
1460 OUTPUT 400 USING "#,B" ; 9
1470 CLEAR
1480 DISP
1490 DISP
1500 DISP "FORK SWITCHED ON"
1510 DISP "-----------------"
1520 WAIT 2000
1530 A$,F$=""
1540 F1,F2,F3,F4=0
1550 N,N1,N2=0
1560 S1=1
1570 P1=1000000000
1580 C1=0
1590 RETURN
1600 ! ----------------------
1610 ! INTRODUCTION
1620 ! ----------------------
1630 CLEAR
1640 DISP "HELLO !!! "
1650 DISP
1660 DISP "CHOOSE THE REQUIRED"
1670 DISP "MODE OF OPERATION"
1680 DISP
1690 DISP "EXPERIMENTAL (E) or"
1700 DISP "GENERAL PURPOSE (G)"
1710 INPUT A$
1720 IF A$="E" THEN F1=1
1730 GOTO 1760
1740 IF A$<>"G" THEN 1640
1750 F1=0
1760 RETURN
1770 ! ----------------------
1780 ! SETTING UP DATA FILE
1790 ! ----------------------
1800 CLEAR
1810 DISP "DATA FILE REQUIRED?"
1820 INPUT A$
1830 IF A$="N" THEN RETURN
1840 IF A$<>"Y" THEN 1810
1850 F2=1
1860 DISP "ENTER FILE NAME"
1870 INPUT F$
1880 F$=F$&";T"
1890 DISP "CREATE FILE?"
1900 INPUT A$
1910 IF A$="N" THEN 1940
1920 IF A$<>"Y" THEN 1890
1930 CREATE F$,1,32000
1940 ASSIGN# 1 TO F$
1950 RETURN
1960 ! ----------------------
1970 ! PRINT-OUT REQUIRED
1980 ! ----------------------
1990 CLEAR
2000 DISP "PRINT-OUT REQUIRED?"
2010 INPUT A$
2020 IF A$="N" THEN RETURN
2030 IF A$<>"Y" THEN 2000
2040 F3=1
2050 DISP "NUMBER READINGS PER"
2060 DISP "PRINTING?"
2070 INPUT N1
2080 RETURN
2090 ! ----------------------
2100 ! PRINTING DATA
2110 ! ----------------------
2120 PRINT USING 2130 ; N,F,Q,T
2130 IMAGE 5D,2X,4D.4D,2X,4D.2X,
2D.2D
2140 N2=0
2150 RETURN
2160 ! ----------------------
2170 ! STORING DATA
2180 ! ----------------------
2190 PRINT# 1 ; N,F,Q,T
2200 RETURN
2210 ! ----------------------
2220 ! TAKING A READING
2230 ! ----------------------
2240 X=0
```

```
2250 Y=0
2260 OUTPUT 400 USING "#,B" ; 0
2270 OUTPUT 400 USING "#,B" ; 2
2280 OUTPUT 400 USING "#,B" ; 1
2290 OUTPUT 400 USING "#,B" ; 3
2300 FOR I=0 TO 7
2310 ENTER 401 USING "#,B" ; Y
2320 X=X+Y*10^I
2330 OUTPUT 400 USING "#,B" ; 4
2340 NEXT I
2350 RETURN
2360 !
2370 !PROGRAM FOR Q MODE
2380 !
2390 OUTPUT 401 USING "#,B" ; 1
2400 OUTPUT 400 USING "#,B" ; 5
2410 OUTPUT 400 USING "#,B" ; 6
2420 OUTPUT 400 USING "#,B" ; 7
2430 CLEAR
2440 C1=2
2450 GOSUB 2210
2460 IF F1=1 THEN RETURN
2470 GOTO 3610
2480 !
2490 ! FREQUENCY MODE
2500 !
2510 OUTPUT 401 USING "#,B" ; 0
2520 OUTPUT 400 USING "#,B" ; 6
2530 OUTPUT 400 USING "#,B" ; 7
2540 OUTPUT 401 USING "#,B" ; 1
2550 OUTPUT 400 USING "#,B" ; 5
2560 OUTPUT 400 USING "#,B" ; 9
2570 CLEAR
2580 C1=1
2590 GOSUB 2210
2600 IF F1=1 THEN RETURN
2610 GOTO 3610
2620 !
2630 !PERIOD MODE
2640 !
2650 OUTPUT 401 USING "#,B" ; 2
2660 OUTPUT 400 USING "#,B" ; 6
2670 OUTPUT 401 USING "#,B" ; 1
2680 OUTPUT 400 USING "#,B" ; 5
2690 OUTPUT 400 USING "#,B" ; 7
2700 OUTPUT 401 USING "#,B" ; 0
2710 OUTPUT 400 USING "#,B" ; 7
2720 OUTPUT 400 USING "#,B" ; 9
2730 CLEAR
2740 C1=3
2750 GOSUB 2210
2760 IF F1=1 THEN RETURN
2770 GOTO 3610
2780 !
2790 !TEMPERATURE MODE
2800 !
2810 OUTPUT 401 USING "#,B" ; 0
2820 OUTPUT 400 USING "#,B" ; 6
2830 OUTPUT 401 USING "#,B" ; 1
2840 OUTPUT 400 USING "#,B" ; 5
2850 OUTPUT 401 USING "#,B" ; 2
2860 OUTPUT 400 USING "#,B" ; 7
2870 OUTPUT 400 USING "#,B" ; 9
2880 CLEAR
2890 C1=4
2900 GOSUB 2210
2910 IF F1=1 THEN RETURN
2920 GOTO 3610
2930 !
2940 !
2950 !
2960 OUTPUT 401 USING "#,B" ; 0
2970 OUTPUT 400 USING "#,B" ; 5
2980 S1=.01
2990 P1=10000000000
3000 GOSUB 2210
3010 CLEAR
3020 GOTO 3610
3030 !
3040 !
3050 !
3060 OUTPUT 401 USING "#,B" ; 1
3070 OUTPUT 400 USING "#,B" ; 5
3080 S1=.1
3090 P1=1000000000
3100 CLEAR
3110 GOSUB 2210
3120 GOTO 3610
3130 !
3140 !
3150 !
3160 OUTPUT 401 USING "#,B" ; 2
3170 OUTPUT 400 USING "#,B" ; 5
3180 S1=1
3190 P1=100000000
3200 CLEAR
3210 GOSUB 2210
3220 GOTO 3610
3230 !
3240 !
3250 !
3260 OUTPUT 401 USING "#,B" ; 3
3270 OUTPUT 400 USING "#,B" ; 5
3280 S1=10
3290 P1=10000000
3300 CLEAR
3310 GOSUB 2210
3320 GOTO 3610
3330 !
3340 !
3350 !GENERAL PURPOSE MODE
3360 !
3370 !
3380 ON ERROR GOTO 2620
3390 CLEAR
3400 ON KEY# 1,"FREQ" GOTO 2480
3410 ON KEY# 2,"Q" GOTO 2360
3420 ON KEY# 3,"PERIOD" GOTO 262
3430 WAIT 1000
3440 ON KEY# 4,"TEMP" GOTO 2780
3450 ON KEY# 5,"10 S" GOTO 3240
3460 ON KEY# 6,"1 S" GOTO 3140
3470 ON KEY# 7,".1 S" GOTO 3040
3480 ON KEY# 8,".01 S" GOTO 2940
3490 IF NOT (N=1 OR N=2 OR N=3) THEN
3500 CLEAR
3510 N=N-1
4040 IF F3=1 THEN GOSUB 3100
4050 N=N+1
4060 GOTO 3870
4070 END
```

APPENDIX F

THE DATA SHEET OF THE ICM 7226 BIPL
UNIVERSAL COUNTER CHIP FROM INTERSIL

INTERSIL

ICM7226A/B

10MHz Universal Counter System for LED Displays

FEATURES

- CMOS design for very low power
- Output drivers directly drive both digits and segments of large 8 digit LED displays. Both common anode and common cathode versions are available
- Measures frequencies from DC to 10MHz; periods from 0.5μs to 10s
- Stable high frequency oscillator uses either 1MHz or 10MHz crystal
- Control signals available for external systems operation
- Multiplexed BCD outputs

APPLICATIONS

- Frequency Counter
- Period Counter
- Unit Counter
- Frequency Ratio Counter
- Time Interval Counter

ORDERING INFORMATION

6

DISPLAY	DEVICE	PACKAGE	ORDER NUMBER
Common Anode	ICM7226A	CERDIP	ICM7226AIJL
		DICE	ICM7226A/D
Common Cathode	ICM7226B	Plastic	ICM7226BIPL
		DICE	ICM7226B/D

NOTE: An evaluation kit is available for these devices — order ICM7226AEV/KIT.

GENERAL DESCRIPTION

The ICM7226 is a fully integrated Universal Counter and LED display driver. It combines a high frequency oscillator, a decade timebase counter, an 8 decade data counter and latches, a 7 segment decoder, digit multiplexer, and segment and digit drivers which can directly drive large LED displays. The counter inputs accept a maximum frequency of 10MHz in **frequency** and **unit counter** modes and 2MHz in the other modes. Both inputs are digital inputs. In many applications, amplification and level shifting will be required to obtain proper digital signals for these inputs.

The ICM7226 can function as a frequency counter, period counter, frequency ratio (f_A/f_B) counter, time interval counter or a totalizing counter. The devices require either a 10MHz or 1MHz crystal timebase, or if desired an external timebase can also be used. For **period** and **time interval**, the 10MHz timebase gives a 0.1μsec resolution. In **period average** and **time interval average**, the resolution can be in the nanosecond range. In the **frequency** mode, the user can select accumulation time of 10ms, 100ms, 1s and 10s. With a 10s accumulation time, the frequency can be displayed to a resolution of 0.1Hz. There is a 0.2s interval between measurements in all ranges. Control signals are provided to enable gating and storing of prescaler data.

Leading zero blanking has been incorporated with frequency display in kHz and time in μs. The display is multiplexed at a 500Hz rate with a 12.2% duty cycle for each digit. The ICM7226A is designed for common anode display with typical peak segment currents of 25mA, and the ICM7226B is designed for common cathode displays with typical segment currents of 12mA. In the **display off** mode, both digit drivers & segment drivers are turned off, allowing the display to be used for other functions.

PIN CONFIGURATION (outline dwgs JL, PL)

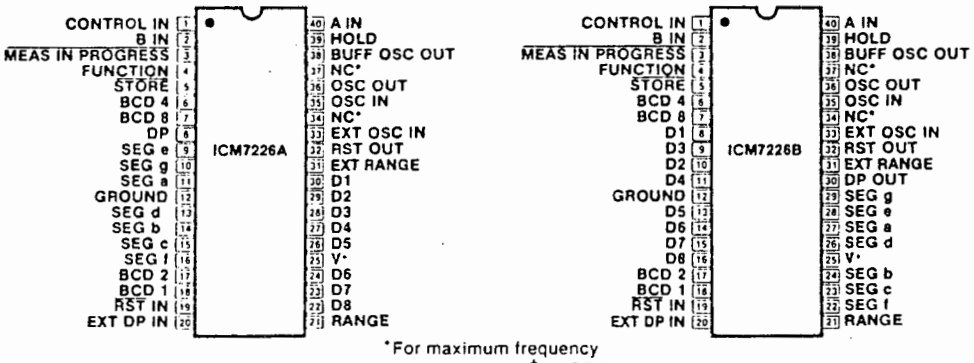

*For maximum frequency stability, connect to V^+ or GROUND

ABSOLUTE MAXIMUM RATINGS

Maximum Supply Voltage 6.5V
Maximum Digit Output Current 400mA
Maximum Segment Output Current 60mA
*Voltage on any Input or
Output Terminal (Note 1) ..... Not to exceed V^+ or GND by more than 0.3V
Maximum Power Dissipation at 70°C (Note 2)
ICM7226A 1.0W
ICM7226B 0.5W
Maximum Operating Temperature Range ..... −20°C to +85°C
Maximum Storage Temperature Range ..... −55°C to +125°C
Lead Temperature (soldering, 10 seconds) ..... 300°C

Stresses above those listed under Absolute Maximum Ratings may cause permanent damage to the device. These are stress ratings only, and functional operation of the device at these or any other conditions above those indicated in the operational sections of the specifications is not implied. Exposure to absolute maximum rating conditions for extended periods may affect device reliability.

*Note 1: Destructive latchup may occur if input signals are applied before the power supply is established or if inputs or outputs are forced to voltages exceeding V^+ or GROUND by 0.3V.

Note 2: Assumes all leads soldered or welded to PC board and free air flow.

ELECTRICAL CHARACTERISTICS

TEST CONDITIONS: $V^+ = 5.0V$, Test Circuit, $T_A = 25°C$, unless otherwise specified.

PARAMETER	SYMBOL	CONDITION	MIN	TYP	MAX	UNITS
Operating Supply Current	I^*_{OP}	Display Off Unused inputs to GROUND		2	5	mA
Supply Voltage Range	V_{SUPP}	-20°C < T_A < 85°C Input A, Input B Frequency at f_{MAX}	4.75		6.0	V
Maximum Guaranteed Frequency Input A, Pin 40	$f_{A(max)}$	-20°C < T_A < 85°C 4.75V < V^+ < 6.0V Figure 1 Function = Frequency, Ratio, Unit Counter Function = Period, Time Interval	10 2.5	14		MHz
Maximum Frequency Input B, Pin 2	$f_{B(max)}$	-20°C < T_A < 85°C 4.75V < V^+ < 6.0V Figure 2	2.5			
Minimum Separation Input A to Input B Time Interval Function		-20°C < T_A < 85°C 4.75V < V^+ < 6.0V Figure 3	250			ns
Maximum osc. freq. and ext. osc. freq. (minimum ext. osc. freq.)	f_{OSC}	-20°C < T_A < 85°C 4.75V < V^+ < 6.0V	(0.1)	10		MHz
Oscillator Transconductance	g_m	V^+ = 4.75V T_A = +85°C	2000			μs
Multiplex Frequency	f_{mux}	f_{osc} = 10 MHz		500		Hz
Time Between Measurements		f_{osc} = 10 MHz		200		ms
Minimum Input Rate of Charge	dV_{in}/dt	Inputs A, B	25	15		mV/μs

SEGMENT IDENTIFICATION AND DISPLAY FONT

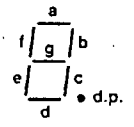

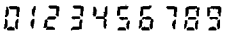

LED overflow indicator connections:
Overflow will be indicated on the decimal point output of digit 8.

	CATHODE	ANODE
ICM7226A	d.p.	D_8
ICM7226B	D_8	d.p.

ELECTRICAL CHARACTERISTICS (Continued)

TEST CONDITIONS: V^+ = 5.0V, test circuit, T_A = 25°C, unless otherwise specified.

PARAMETER	SYMBOL	CONDITION	MIN	TYP	MAX	UNITS
INPUT VOLTAGES PINS 2,19,33,39,40						
input low voltage	V_{IL}	−20°C < T_A < +70°C	1.0			V
input high voltage	V_{IH}				3.5	
PIN 2, 39, 40 INPUT LEAKAGE, A, B	I_{ILK}				20	µA
PIN 33						
input low voltage	V_{IL}	−20°C < T_A < 70°C	0.8			V
input high voltage	V_{IH}				2.0	
Input resistance to V^+ PINS 19,33	R_{IN}	V_{IN} = V^+ −1.0V.	100	400		kΩ
Input resistance to GROUND PIN 31	R_{IN}	V_{IN} = +1.0V	50	100		
Output Current PINS 3,5,6,7,17,18,32,38	I_{OL}	V_{OL} = +0.4V	400			µA
PINS 5,6,7,17,18,32	I_{OH}	V_{OH} = + 2.4V	100			µA
PINS 3,38	I_{OH}	V_{OH} = V^+ −0.8V	265			
ICM7226A PINS 22,23,24,26,27,28,29,30 DIGIT DRIVER						
high output current	I_{OH}	V_O = V^+ −2.0V	150	180		mA
low output current	I_{OL}	V_O = +1.0V		−0.3		
SEGMENT DRIVER PINS 8,9,10,11,13,14,15,16						
low output current	I_{OL}	V_O = +1.5V	25	35		mA
high output current	I_{OH}	V_O = V^+ −1.0V		100		µA
MULTIPLEX INPUTS PINS 1,4,20,21						
input low voltage	V_{IL}				0.8	V
input high voltage	V_{IH}		2.0			
input resistance to GROUND	R_{IN}	V_{IN} = +1.0V	50	100		kΩ
ICM7226B DIGIT DRIVER PINS 8,9,10,11,13,14,15,16						
low output current	I_{OL}	V_O = +1.0V	50	75		mA
high output current	I_{OH}	V_O = V^+ −2.5V		100		µA
SEGMENT DRIVER PINS 22,23,24,26,27,28,29,30						
high output current	I_{OH}	V_O = V^+ −2.0V	10	15		mA
leakage current	I_L	V_O = GROUND			10	µA
MULTIPLEX INPUTS PINS 1,4,20,21						
input low voltage	V_{IL}				V^+ −2.0	V
input high voltage	V_{IH}		V^+−0.8			
input resistance to V^+	R_{IN}	V_{IN} = V^+ −1.0V	200	360		kΩ

EVALUATION KIT

An evaluation kit is available for the ICM7226. It includes all the components necessary to assemble and evaluate a universal frequency/period counter based on the ICM7226. With the help of this kit, an engineer or technician can have the ICM7226 "up-and-running" in less than an hour. Specifically, the kit contains an ICM7226AIJL, a 10MHz quartz crystal, eight each 7-segment 0.3" LEDs, PC board, resistors, capacitors, diodes, switches and IC socket. Order Number ICM7226AEV/Kit.

INTERSIL

BLOCK DIAGRAM

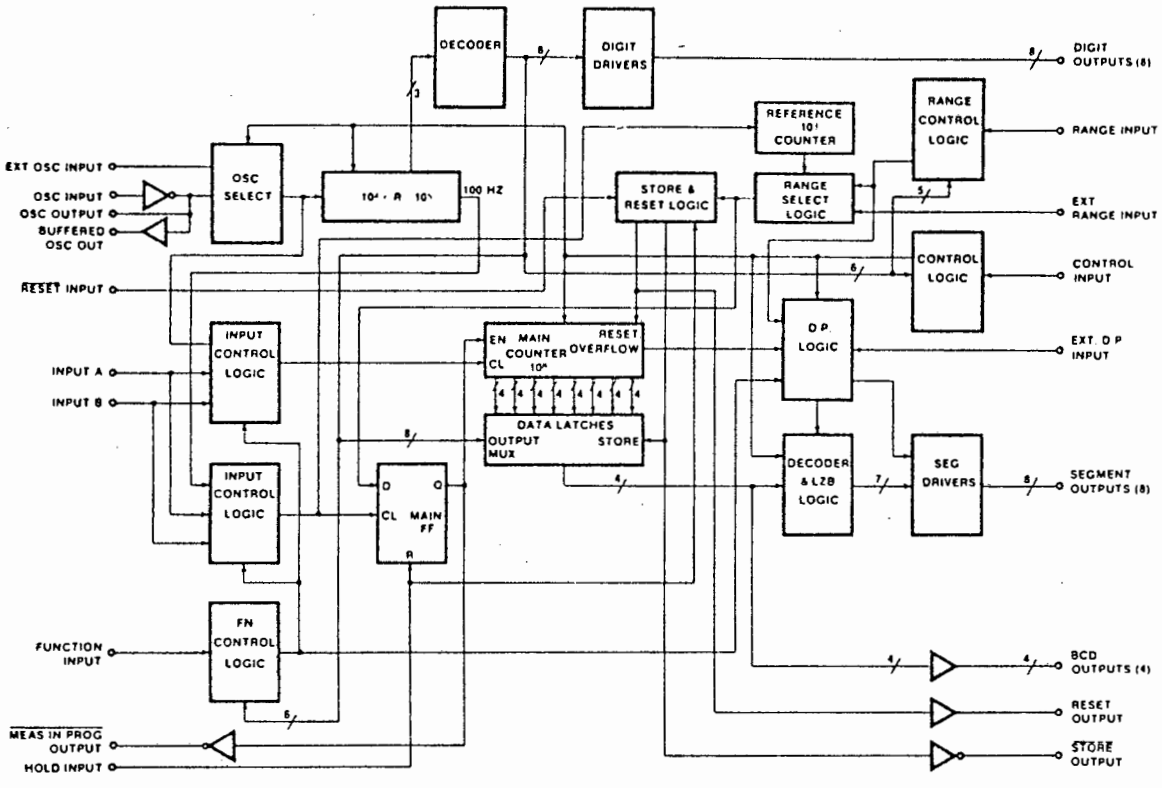

TEST CIRCUIT

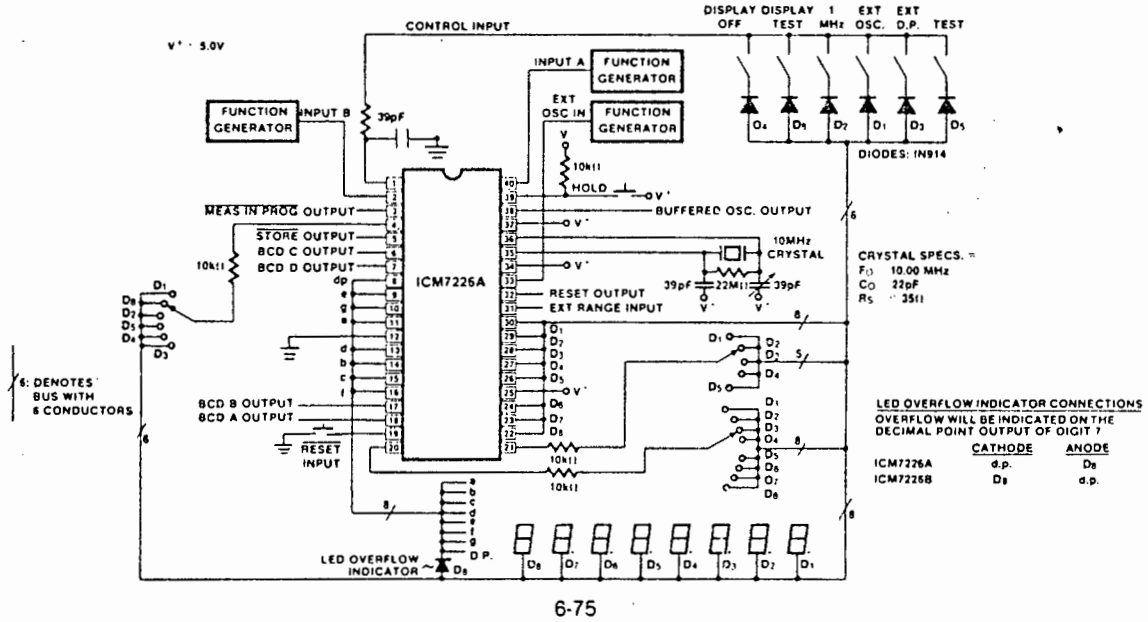

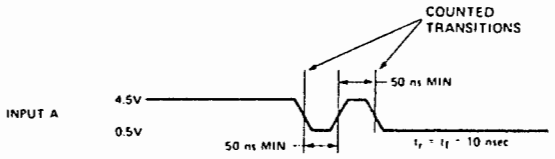

FIGURE 1. Waveform for Guaranteed Minimum $f_{A(max)}$ Function = Frequency, Frequency Ratio, Unit Counter.

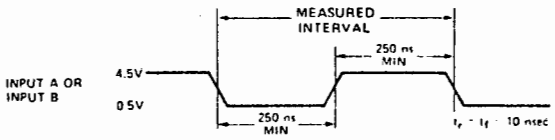

FIGURE 2. Waveform for Guaranteed Minimum $f_{B(max)}$ and $f_{A(max)}$ for Function = Period and Time Interval.

TIME INTERVAL MEASUREMENT

The ICM7226A/B can be used to accurately measure the time interval between two events. With a 10 MHz time-base crystal, the time between the two events can be as long as ten seconds. Accurate resolution in time interval measurement is 100ns.

The feature operates with Channel A going low at the start of the event to be measured, followed by Channel B going low at the end of the event.

When in the time interval mode and measuring a single event, the ICM7226A/B must first be "primed" prior to measuring the event of interest. This is done by first generating a negative going edge on Channel A followed by a negative going edge on Channel B to start the "measurement interval." The inputs are then primed ready for the measurement. Positive going edges on A and B, before or after the priming, will be needed to restore the original condition.

This can be easily accomplished with the following circuit: (Figure 3b).

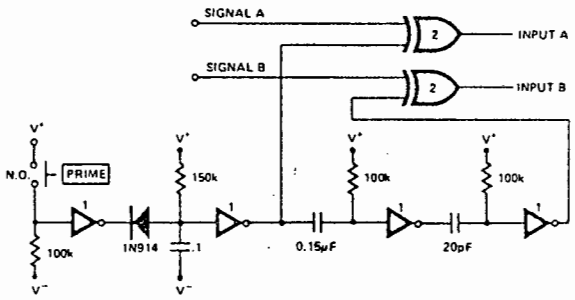

Device	Type
1	CD4049B Inverting Buffer
2	CD4070B Exclusive-OR

FIGURE 3b. Priming Circuit, Signal A&B High or Low.

Following the priming procedure (when in single event or 1 cycle range input) the device is ready to measure one (only) event.

When timing repetitive signals, it is not necessary to "prime" the ICM7226A/B as the first alternating signal states automatically prime the device. See Figure 3a.

During any time interval measurement cycle, the ICM7226A/B requires 200ms following B going low to update all internal logic. A new measurement cycle will not take place until completion of this internal update time.

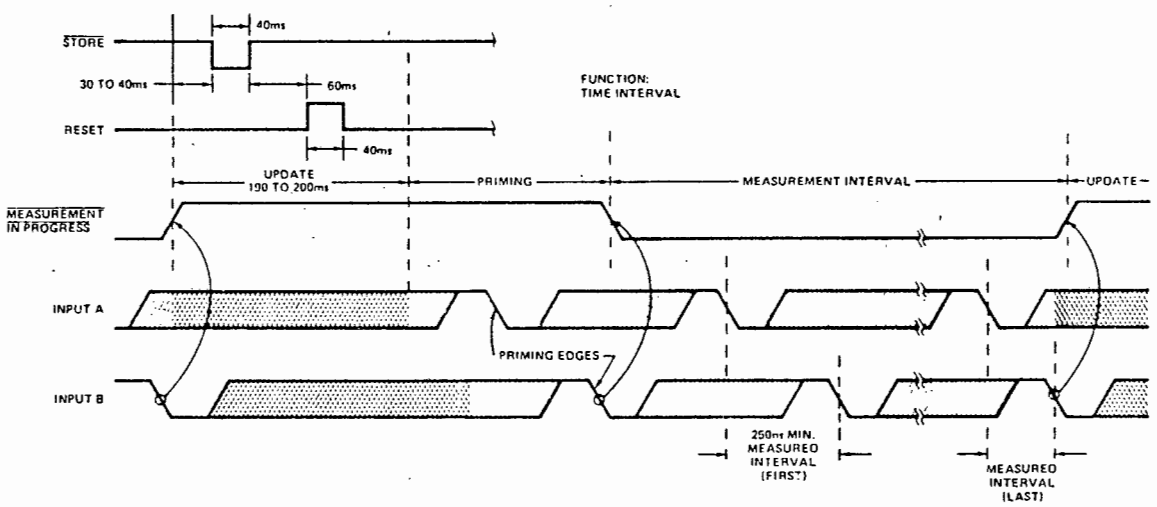

NOTE: IF RANGE IS SET TO 1 EVENT, FIRST AND LAST MEASURED INTERVAL WILL COINCIDE.

FIGURE 3a. Waveforms for Time Interval Measurement (Others are similar, without priming phase)

APPLICATION NOTES

GENERAL

INPUTS A & B

The signal to be measured is applied to INPUT A in **frequency period, unit counter, frequency ratio** and **time interval** modes. The other input signal to be measured is applied to INPUT B in **frequency ratio** and time interval. f_A should be higher than f_B during **frequency ratio.**

Both inputs are digital inputs with a typical switching threshold of 2.0V at $V^+ = 5.0V$ and input impedance of 250kΩ. For optimum performance, the peak to peak input signal should be at least 50% of the supply voltage and centered about the switching voltage. When these inputs are being driven from TTL logic, it is desirable to use a pullup resistor. The circuit counts high to low transitions at both inputs.

Note: The amplitude of the input should not exceed the supply by more than 0.3V otherwise, the circuit may be damaged.

MULTIPLEXED INPUTS

The FUNCTION, RANGE, CONTROL and EXTERNAL DECIMAL POINT inputs are time multiplexed to select the input function desired. This is achieved by connecting the appropriate digit driver output to the inputs. The input function, range and control inputs must be stable during the last half of each digit output, (typically 125μsec). The multiplex inputs are active high for the common anode ICM7226A, and active low for the common cathode ICM7226B.

Noise on the multiplex inputs can cause improper operation. This is particularly true when the **unit counter** mode of operation is selected, since changes in voltage on the digit drivers can be capacitively coupled through the LED diodes to the multiplex inputs. For maximum noise immunity, a 10kΩ resistor should be placed in series with the multiplex inputs as shown in the application notes.

Table 1 shows the functions selected by each digit for these inputs.

TABLE 1. Multiplexed Input Control

	FUNCTION	DIGIT
FUNCTION INPUT PIN 4	Frequency	D_1
	Period	D_8
	Frequency Ratio	D_2
	Time Interval	D_5
	Unit Counter	D_4
	Oscillator Frequency	D_3
RANGE INPUT PIN 21	0.01 Sec/1 Cycle	D_1
	0.1 Sec/10 Cycles	D_2
	1 Sec/100 Cycles	D_3
	10 Sec/1k Cycles	D_4
PIN 31	Enable External Range Input	D_5
CONTROL INPUT PIN 1	Blank Display	D_4&Hold
	Display Test	D_8
	1MHz Select	D_2
	External Oscillator Enable	D_1
	External Decimal Point Enable	D_3
	Test	D_5
EXTERNAL DECIMAL POINT INPUT, PIN 20	Decimal Point is Output for Same Digit That is Connected to This Input	

CONTROL INPUTS

Display Test - All segments are enabled continuously, giving a display of all 8's with decimal points. The display will be blanked if **display off** is selected at the same time.

Display Off - To enable the **display off** mode it is necessary to tie D_4 to the CONTROL input and have the HOLD input at V^+. The chip will remain in this mode until HOLD is switched low. While in the **display off** mode, the segment and digit driver outputs are open and the oscillator continues to run (with a typical supply current of 1.5mA with a 10MHz crystal) but no measurements are made. In addition, signals applied to the multiplexed inputs have no effect. A new measurement is initiated after the HOLD input goes low. (This mode does not operate when functioning as a unit counter.)

1MHz Select - The **1MHz select** mode allows use of a 1MHz crystal with the same digit multiplex rate and time between measurements as a 10MHz crystal. The internal decimal point is also shifted one digit to the right in **period** and **time interval**, since the least significant digit will be in 1μs increments rather than 0.1μs.

External Oscillator Enable - In this mode, the EXTernal OSCillator INput is used, rather than the on-chip oscillator, for the Timebase and Main Counter inputs in **period** and **time interval** modes. The on-chip oscillator will continue to function when the external oscillator is selected, but have no effect on circuit operation. The external oscillator input frequency must be greater than 100kHz or the chip will reset itself and enable the on-chip oscillator. Connect external oscillator to both OSC IN (pin 35) and EXT OSC IN (pin 33), or provide crystal for "default" oscillation, to avoid hang-up problems.

External Decimal Point Enable - When **external decimal point** is enabled, a decimal point will be displayed whenever the digit driver connected to the EXTERNAL DECIMAL POINT pin is active. Leading Zero Blanking will be disabled for all digits following the decimal point.

Test Mode - This is a special mode used only in high speed production testing, and serves no other purpose.

RANGE INPUT

The range input selects whether the measurement is made for 1, 10, 100 or 1000 counts of the reference counter, or if the EXTernal RANGE INput determines the measurement time. In all functional modes except **unit counter**, a change in the RANGE input will stop the measurement in progress, without updating the display, and initiate a new measurement. This prevents an erroneous first reading after the RANGE input is changed.

FUNCTION INPUT

Six functions can be selected. They are: **Frequency, Period, Time Interval, Unit Counter, Frequency Ratio and Oscillator Frequency.**

These functions select which signal is counted into the main counter and which signal is counted by the reference counter, as shown in Table 2. In **time interval**, a flip flop is set first by a 1→0 transition at INPUT A and then reset by a 1→0 transition at INPUT B. The oscillator is gated into the Main Counter during the time the flip flop is set. A change in the FUNCTION input will stop the measurement in progress without updating the display and then initiate a new measurement. This prevents an erroneous first reading after the FUNCTION input is changed. If the main counter overflows, an overflow indication is output on the Decimal Point Output during D_8.

TABLE 2. Input Routing

DESCRIPTION	MAIN COUNTER	REFERENCE COUNTER
Frequency (f_A)	Input A	100Hz (Oscillator ÷ 10^5 or 10^4)
Period (t_A)	Oscillator	Input A
Ratio (f_A/f_B)	Input A	Input B
Time Interval (A→B)	Osc ON Gate	Osc OFF Gate
Unit Counter(Count A)	Input A	Not Applicable
Osc. Freq. (f_{OSC})	Oscillator	100Hz (Osc ÷ 10^5 or 10^4)

EXTERNAL DECIMAL POINT INPUT

When the **external decimal point** is selected, this input is active. Any of the digits, except D_8, can be connected to this point. D_8 should not be used since it will override the overflow output and leading zeros will remain unblanked after the decimal point.

HOLD Input - Except in the **unit counter** mode, when the HOLD Input is at V^+, any measurement in progress (before $\overline{\text{STORE}}$ goes low) is stopped, the main counter is reset and the chip is held ready to initiate a new measurement as soon as HOLD goes low. The latches which hold the main counter data are not updated, so the last complete measurement is displayed. In **unit counter** mode when HOLD Input is at V^+, the counter is not stopped or reset, but the display is frozen at that instantaneous value. When HOLD goes low the count continues from the new value in the counter.

$\overline{\text{RESET}}$ Input - The $\overline{\text{RESET}}$ Input resets the main counter, stops any measurement in progress, and enables the main counter latches, resulting in an all zero output. A capacitor to ground will prevent any hang-ups on power-up.

EXTernal RANGE Input - The EXTernal RANGE Input is used to select other ranges than those provided on the chip. Figure 4 shows the relationship between MEASurement IN $\overline{\text{PROGRESS}}$ and EXTernal RANGE Input.

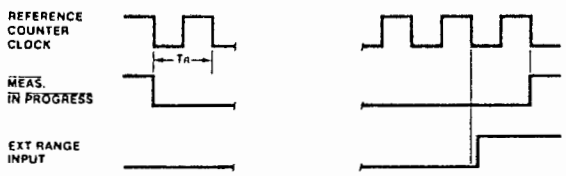

Figure 4: External Range Input to End of Measurement in Progress.

$\overline{\text{MEASUREMENT IN PROGRESS}}$, $\overline{\text{STORE}}$ AND RESET Outputs - These Outputs are provided to facilitate external interfacing. Figure 5 shows the relationship between these signals during the time between measurements. All three outputs can drive a low power Schottky TTL load. The $\overline{\text{MEASUREMENT IN PROGRESS}}$ output can directly drive one ECL load, if the ECL device is powered from the same power supply as the ICM7226.

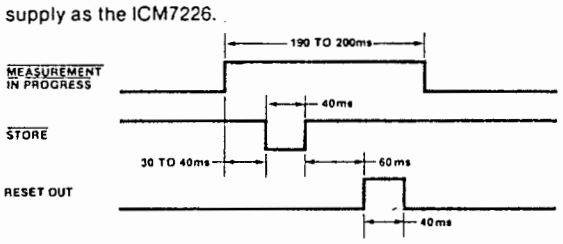

Figure 5: RESET OUT, $\overline{\text{STORE}}$, and $\overline{\text{MEASUREMENT IN PROGRESS}}$ Outputs Between Measurements.

BCD Outputs - The BCD representation of each digit output is available at the BCD outputs; see Table 3 for Truth Table. The positive going (ICM7226A - Common Anode) or negative going (ICM7226B - Common Cathode) digit drivers lag the BCD data by 2 to 6 microseconds; the leading edge of the digit drive signal should be used to externally latch the BCD data. Each BCD output will drive one low power Schottky TTL load and when interfacing low power Schottky TTL latches, it is necessary to use 1kΩ pull down resistors on the TTL inputs for optimum results. The display is multiplexed from MSD to LSD. Leading zero blanking has no effect on the BCD outputs.

TABLE 3 Truth Table BCD Outputs

NUMBER	BCD 8 PIN 7	BCD 4 PIN 6	BCD 2 PIN 17	BCD 1 PIN 18
0	0	0	0	0
1	0	0	0	1
2	0	0	1	0
3	0	0	1	1
4	0	1	0	0
5	0	1	0	1
6	0	1	1	0
7	0	1	1	1
8	1	0	0	0
9	1	0	0	1

BUFFered OSCillator OUTput - The BUFFered OSCillator OUTput has been provided to enable use of the on chip oscillator signal without loading the oscillator itself. This output will drive one low power Schottky TTL load. Care should be taken to minimize capacitive loading on this pin.

DISPLAY CONSIDERATIONS

The display is multiplexed at a 500Hz rate with a digit time of 244μs, and an interdigit blanking time of 6μs to prevent ghosting between digits. The decimal point and leading zero blanking have been implemented for right hand decimal point displays; zeros following the decimal point will not be blanked. Leading zero blanking will also be disabled if the Main Counter overflows. The internal decimal point control displays frequency in kHz and time in μs.

The ICM7226A is designed to drive common anode LED displays at a peak current of 25mA/segment, using displays with V_F = 1.8V at 25mA. The average DC current will be greater than 3mA under these conditions. The ICM7226B is designed to drive common cathode displays at a peak current of 15mA/segment, using displays with V_F = 1.8V at 15mA. Resistors can be added in series with the segment drivers to limit the display current, if required. Figures 6, 7, 8 and 9 show the digit and segment currents as a function of output voltage for common anode and common cathode drivers.

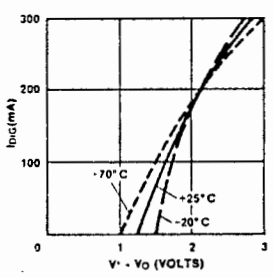

Figure 6: ICM7226A Typical I_{DIG} vs. V^+-V_O 4.5 ≤ V^+ ≤ 6.0V

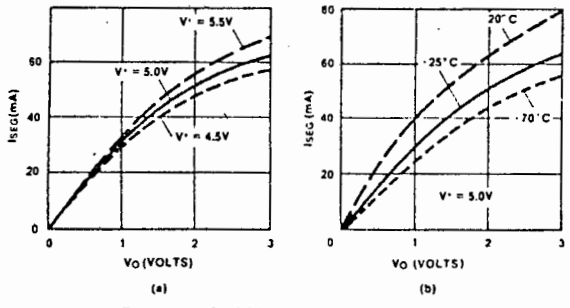

Figure 7: ICM7226A Typical I_{SEG} vs. V_O

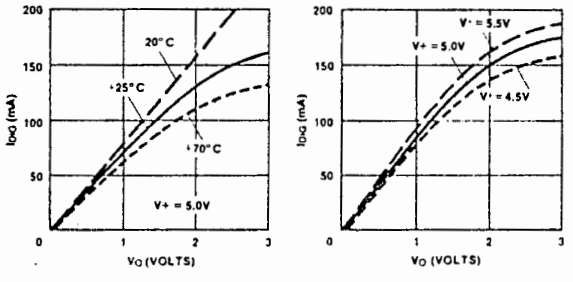

Figure 8: ICM7226B Typical I_{DIG} vs. V_O

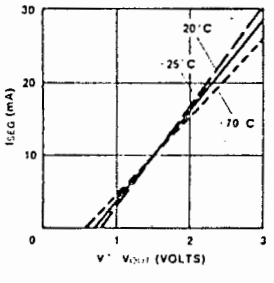

Figure 9: ICM7226B Typical I_{SEG} vs. (V^+-V_O) $4.5V \leq V^+ \leq 6.0V$

To increase the light output from the displays, V+ may be increased to 6.0V, however care should be taken to see that maximum power and current ratings are not exceeded.

The SEGment and Digit outputs in both the 7226A and B are not directly compatible with either TTL or CMOS logic. Therefore, level shifting with discrete transistors may be required to use these outputs as logic signals. External latching should be done on the leading edge of the digit signal.

ACCURACY

In a Universal Counter, crystal drift and quantization errors cause errors. In **frequency**, **period** and **time interval** modes, a signal derived from the oscillator is used either in the Reference Counter or Main Counter, and in these modes, an error in the oscillator frequency will cause an identical error in the measurement. For instance, an oscillator temperature coefficient of 20ppm/°C will cause a measurement error of 20ppm/°C.

In addition, there is a quantization error inherent in any digital measurement of ± 1 count. Clearly this error is reduced by displaying more digits. In the **frequency** mode, maximum accuracy is obtained with high frequency inputs, and in **period** mode maximum accuracy is obtained with low frequency inputs. As can be seen in Figure 10, the least accuracy will be obtained at 10kHz. In time **interval** measurements there is a maximum error of 1 count per interval. As a result there is the same inherent accuracy in all ranges, as shown in Figure 11. In **frequency ratio** measurement more accuracy can be obtained by averaging over more cycles of INPUT B as shown in Figure 12.

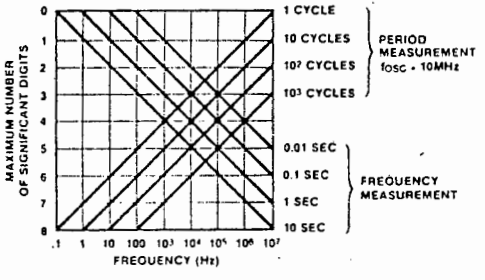

Figure 10: Maximum Accuracy of Frequency and Period Measurements Due to Limitations of Quantization Errors.

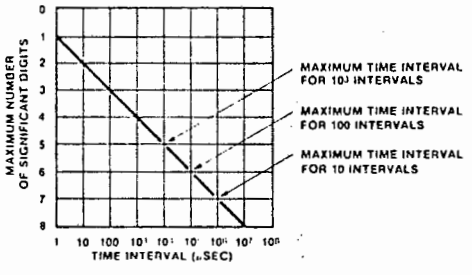

Figure 11: Maximum Accuracy of Time Interval Measurement Due to Limitations of Quantization Errors.

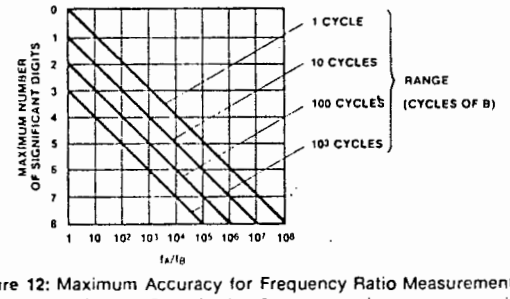

Figure 12: Maximum Accuracy for Frequency Ratio Measurement Due to Limitations of Quantization Errors.

CIRCUIT APPLICATIONS

The ICM7226 has been designed as a complete stand alone Universal Counter, or used with prescalers and other circuitry in a variety of applications. Since A IN and B IN are digital inputs, additional circuitry will be required in many applications, for input buffering, amplification, hysteresis, and level shifting to obtain the required digital voltages. For many applications an FET source follower can be used for input buffering, and an ECL 10116 line receiver can be used for amplification and

hysteresis to obtain high impedance input, sensitivity and bandwidth. However, cost and complexity of this circuitry can vary widely, depending upon the sensitivity and bandwidth required. When TTL prescalers or input buffers are used, pull up resistors to V+ should be used to obtain optimal voltage swing at A IN and B IN.

If prescalers aren't required, the ICM7226 can be used to implement a minimum component Universal counter as shown in figure 13.

For input frequencies up to 40MHz, the circuit shown in figure 14 can be used to implement a **frequency and period counter**. To obtain the correct value when measuring frequency and period, it is necessary to divide the 10MHz oscillator frequency down to 2.5MHz. In doing this the time between measurements is lengthened to 800ms and the display multiplex rate is decreased to 125Hz.

If the input frequency is prescaled by ten, the oscillator frequency can remain at either 10MHz or 1MHz, but the decimal point must be moved. Figure 15 shows use of a ÷10 prescaler in **frequency counter** mode. Additional logic has been added to enable the 7226 to count the input directly in **period** mode for maximum accuracy. Note that A IN comes from Q_C rather than Q_D, to obtain an input duty cycle of 40%. If an output with a duty cycle not near 50% must be used then it may be necessary to use a 74121 monostable multivibrator or similar circuit to stretch the input pulse to guarantee a 50ns minimum pulse width.

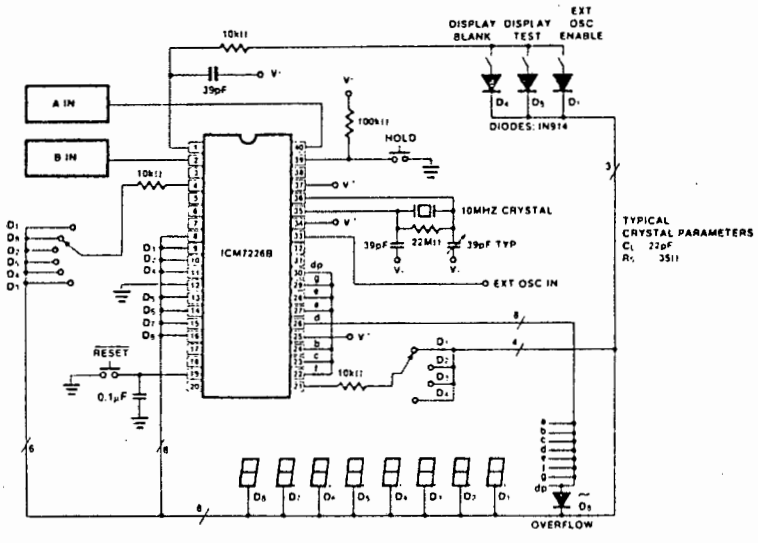

Figure 13: 10MHz Universal Counter

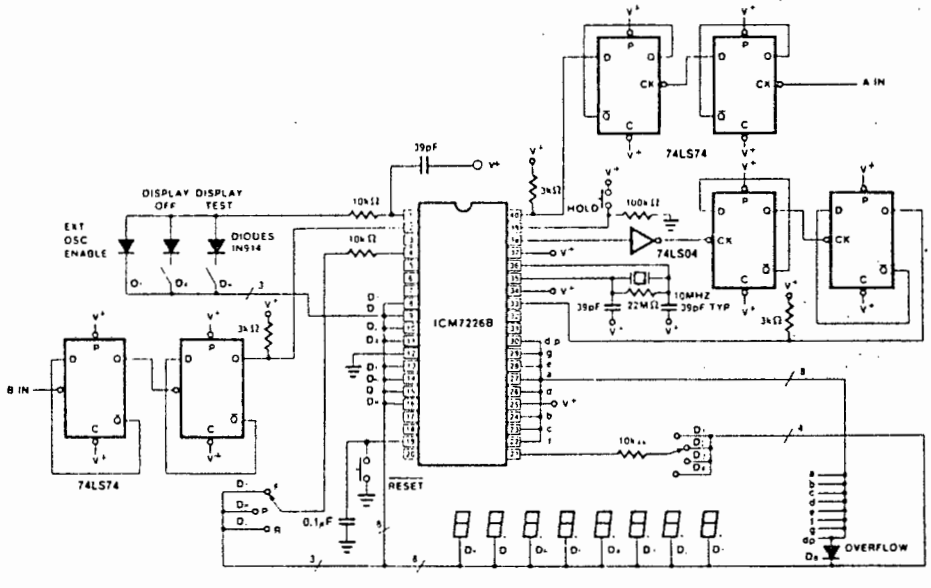

Notes: 1) If a 2.5MHz crystal is used, diode D1 and I.C.'s 1 and 2 can be eliminated.

Figure 14: 40MHz Frequency, Period Counter

Figure 16 shows the use of a CD4016 analog multiplexer to multiplex the digital outputs back to the FUNCTION Input. Since the CD4016 is a digitally controlled analog transmission gate, no level shifting of the digit output is required. CD4051's or CD4052's could also be used to select the proper inputs for the multiplexed input on the ICM7226 from 2 or 3 bit digital inputs. These analog multiplexers may also be used in systems in which the mode of operation is controlled by a microprocessor rather than directly from front panel switches. TTL multiplexers such as the 74153 or 74251 may also be used, but some additional circuitry will be required to convert the digit output to TTL compatible logic levels.

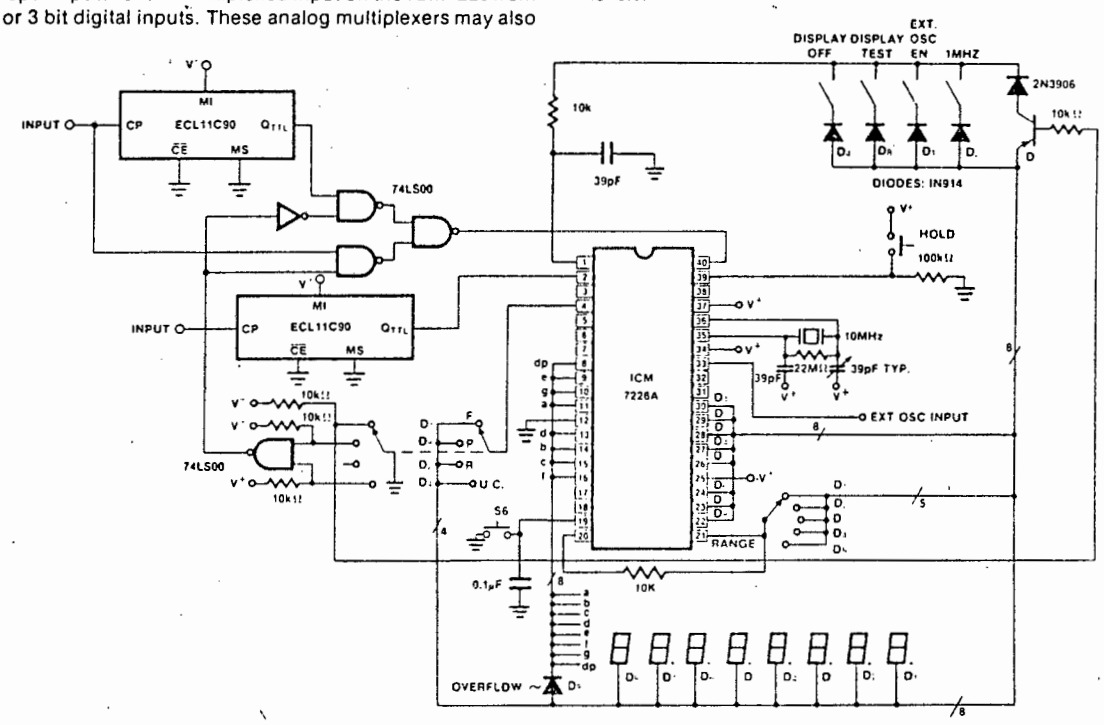

Figure 15: 100MHz Multi Function Counter

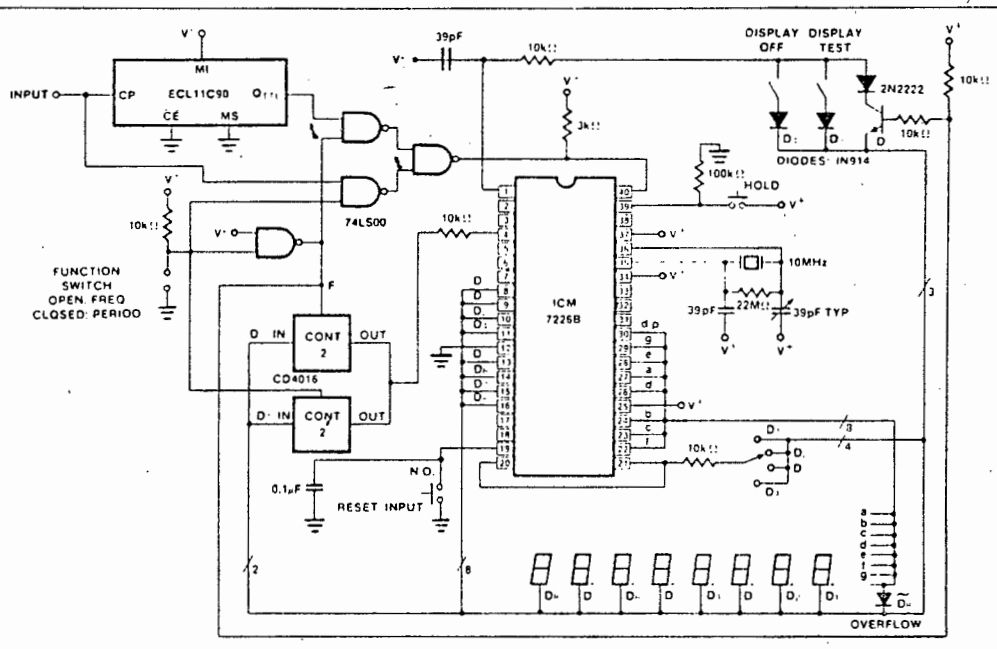

Figure 16: 100MHz Frequency Period Counter

The circuit shown in figure 17 can be used in any of the circuit applications shown to implement a single measurement mode of operation. This circuit uses the $\overline{\text{STORE}}$ output to put the ICM7226 into a hold mode. The HOLD input can also be used to reduce the time between measurements. The circuit shown in figure 18 puts a short pulse into the HOLD input a short time after STORE goes low. A new measurement will be initiated at the end of the pulse on the HOLD Input. This circuit reduces the time between measurements to less than 40ms from 200ms; use of the circuit shown in Figure 18 on the circuit shown in Figure 14 will reduce the time between measurements from 1600ms to 800ms.

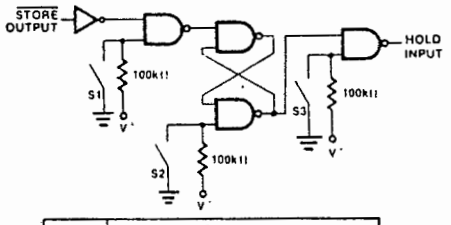

SWITCH	FUNCTION
S1	OPEN SINGLE MEAS MODE ENABLED
S2	CLOSED INITIATE NEW MEASUREMENT
S3	CLOSED HOLD INPUT

Figure 17: Single Measurement Circuit for Use With ICM7226

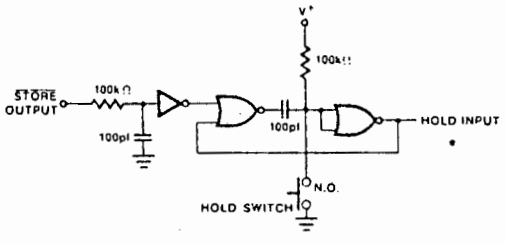

Figure 18: Circuit for Reducing Time Between Measurements

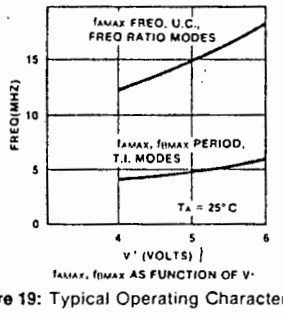

Figure 19: Typical Operating Characteristics

Figure 20 shows the ICM7226 being interfaced to LCD displays, by using its BCD outputs and 8 digit lines to drive 2 ICM7211 display drivers. The ICM7226 EV/Kit may easily be interfaced to 2 ICM7211 EV/Kits in this way. A similar arrangement can be used for driving vacuum fluorescent displays with the ICM7235.

OSCILLATOR CONSIDERATIONS

The oscillator is a high gain complementary FET inverter. An external resistor of 10MΩ or 22MΩ should be connected between the oscillator input and output to provide biasing. The oscillator is designed to work with a parallel resonant 10MHz quartz crystal with a static capacitance of 22pF and a series resistance of less than 35Ω. Among suitable crystals is the 10MHz CTS KNIGHTS ISI-002.

For a specific crystal and load capacitance, the required g_m can be calculated as follows:

$$g_m = \omega^2 C_{IN} C_{OUT} R_S \left(1+\frac{C_O}{C_L}\right)^2$$

where $C_L = \left(\frac{CinCout}{Cin+Cout}\right)$

C_O = Crystal static capacitance
R_S = Crystal Series Resistance
Cin = Input Capacitance
Cout = Output Capacitance
$\omega = 2\pi f$

The required g_m should exceed the g_m specified for the ICM7226 by at least 50% to insure reliable startup. The oscillator input and output pins each contribute about 4pF to C_{IN} and C_{OUT}. For maximum frequency stability, C_{IN} and C_{OUT} should be approximately twice the specified crystal static capacitance.

In cases where nondecade prescalers are used, it may be desirable to use a crystal which is neither 10MHz nor 1MHz. In this case both the multiplex rate and the time between measurements will be different. The multiplex rate is $f_{mux} = \frac{f_{osc}}{2 \times 10^4}$ for 10MHz mode and $f_{mux} = \frac{f_{osc}}{2 \times 10^3}$ for the 1MHz mode. The time between measurements is $\frac{2 \times 10^6}{f_{osc}}$ in the 10MHz mode and $\frac{2 \times 10^5}{f_{osc}}$ in the 1MHz mode. The buffered oscillator output should be used as an oscillator test point or to drive additional logic; this output will drive one low power Schottky TTL load. When the buffered oscillator output is used to drive CMOS or the external oscillator input, a 10kΩ resistor should be added from the buffered oscillator output to V^+.

The crystal and oscillator components should be located as close to the chip as practical to minimize pickup from other signals. In particular, coupling from the BUFfered OSCillator OUTput and EXTernal OSCillator INput to the OSCillator OUTput or OSCillator INput can cause undesirable shifts in oscillator frequency. To minimize this coupling, pins 34 and 37 should be connected to V^+ or GROUND and these two signals should be kept away from the oscillator circuit.

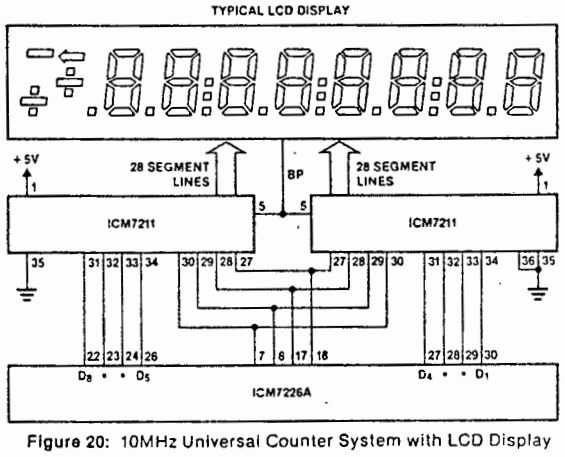

Figure 20: 10MHz Universal Counter System with LCD Display

APPENDIX G

SCANNING ELECTRON MICROSCOPE AND GENERAL PHOTOGRAPHS

APPENDIX G

SCANNING ELECTRON MICROSCOPE AND GENERAL PHOTOGRAPHS

Scanning Electron Microscope Photographs.

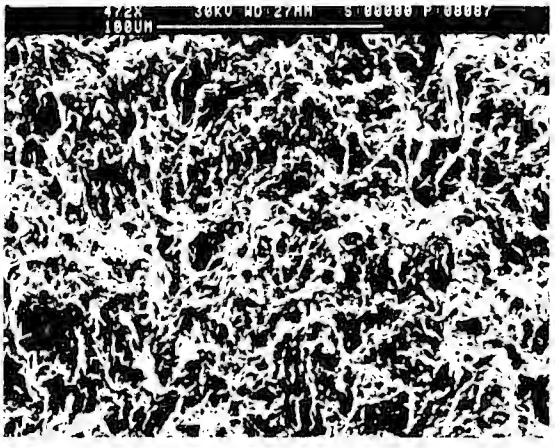

SEM 1.

SEM 2.

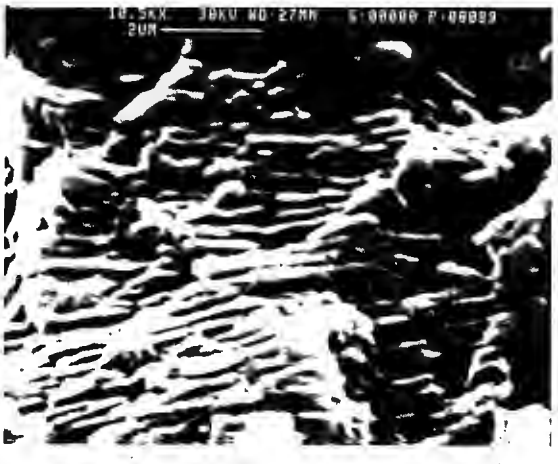

SEM 3.

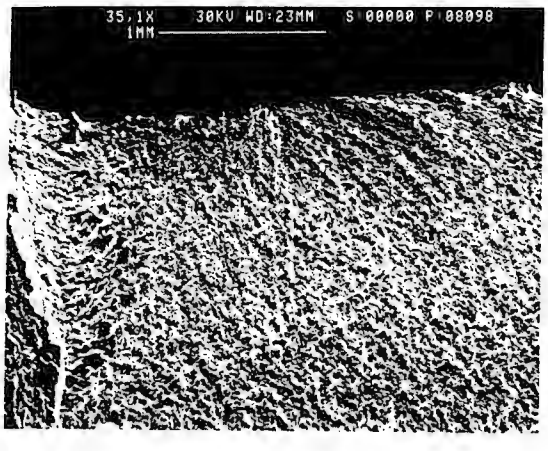

SEM 4.

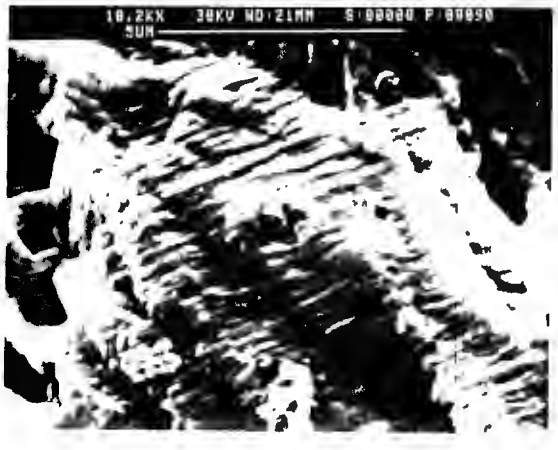

SEM 5.

Scanning Electron Microscope Photographs.

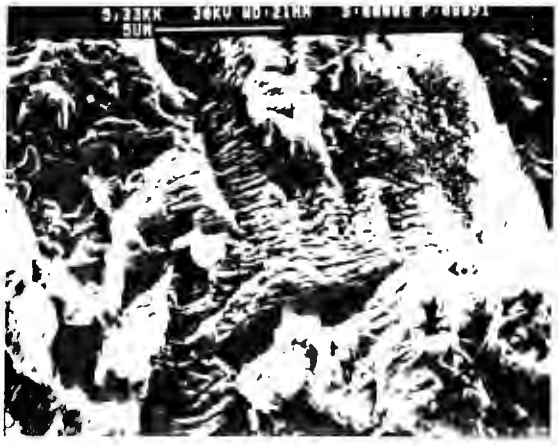

SEM 6.

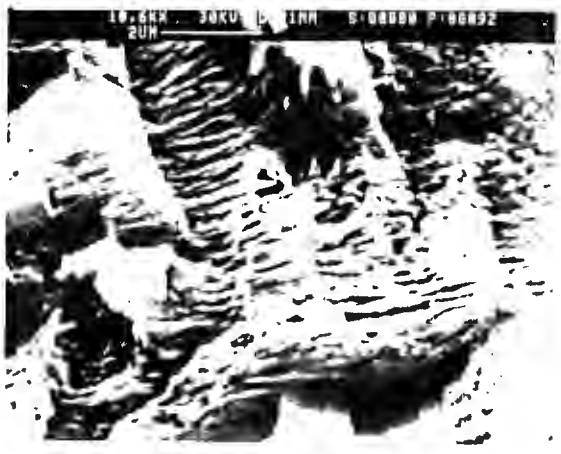

SEM 7.

SEM 8.

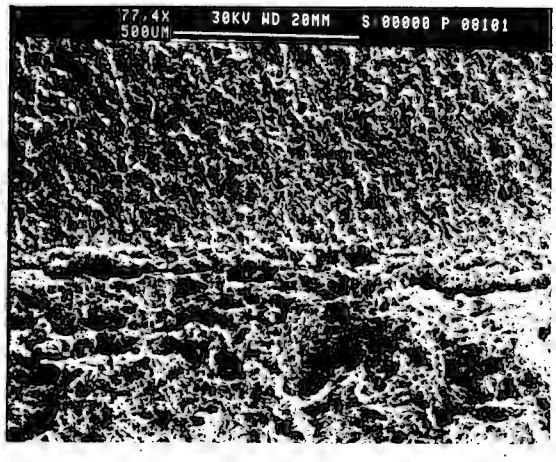

SEM 9.

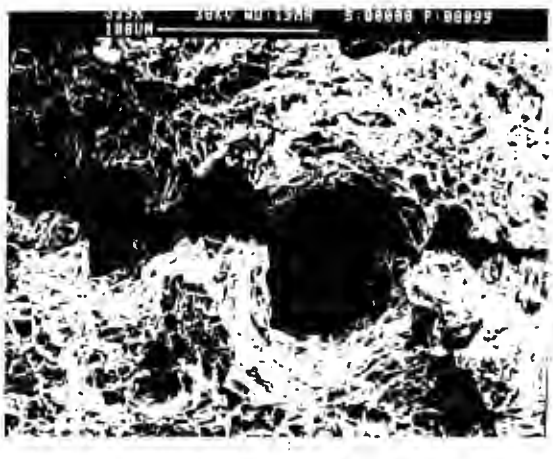

SEM 10.

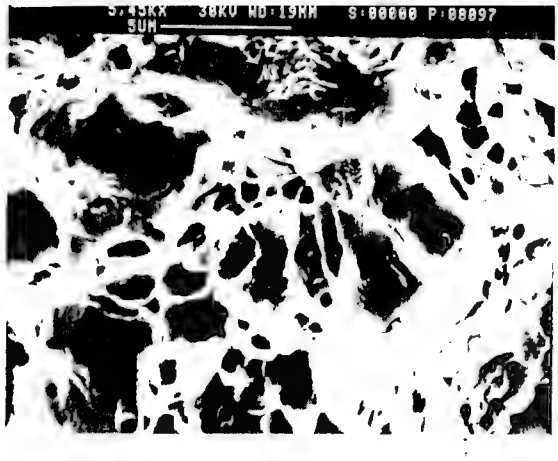

SEM 11.

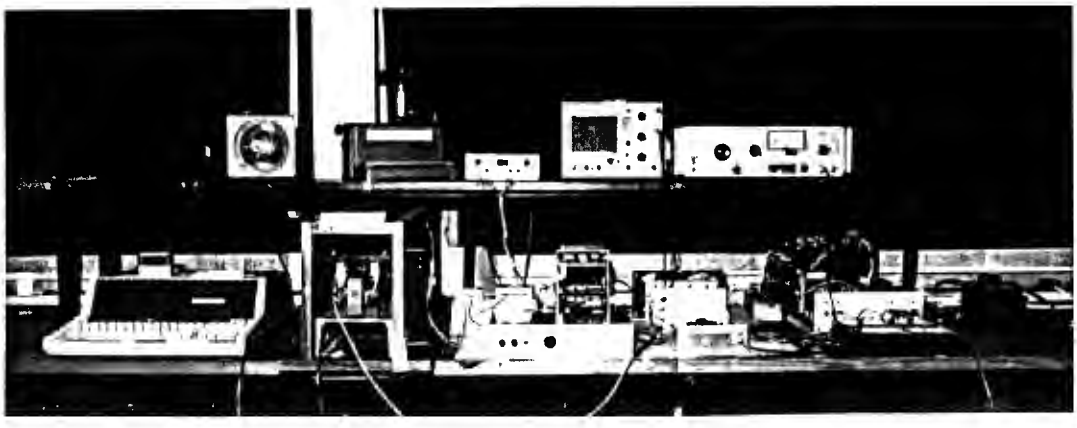

Photograph G.1.

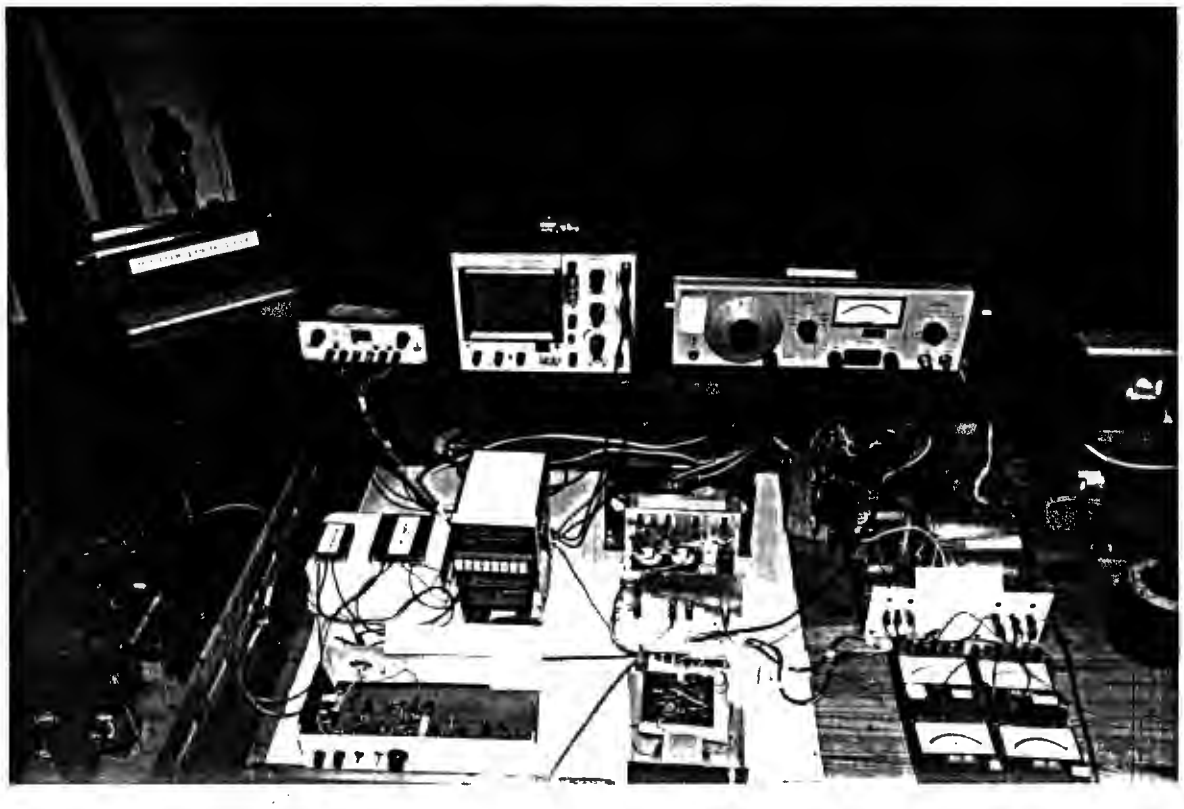

Photograph G.2.

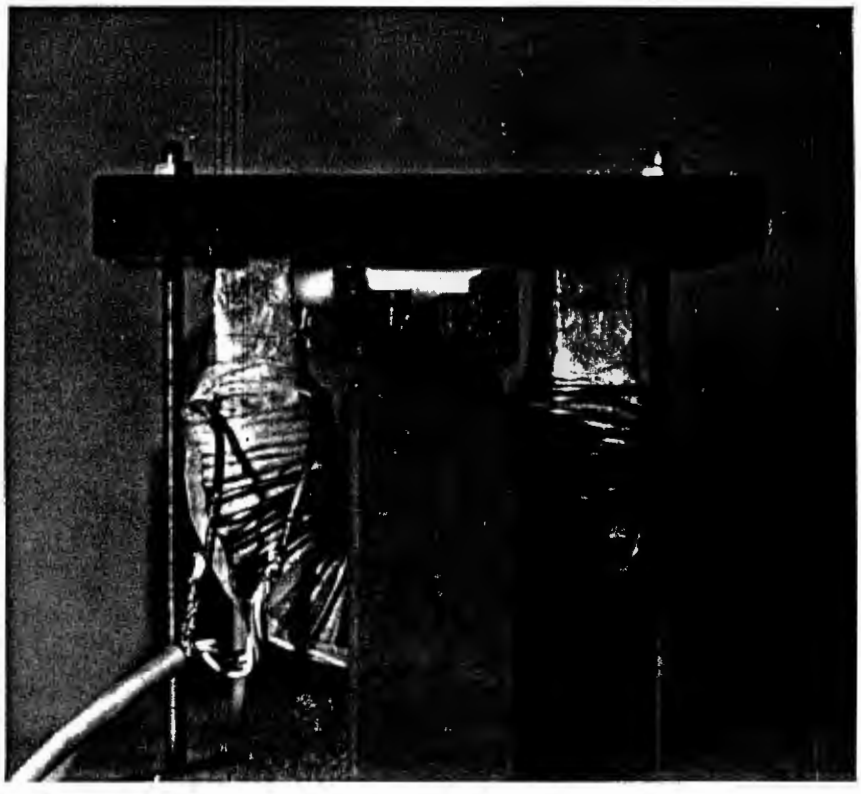

Photograph G.3.

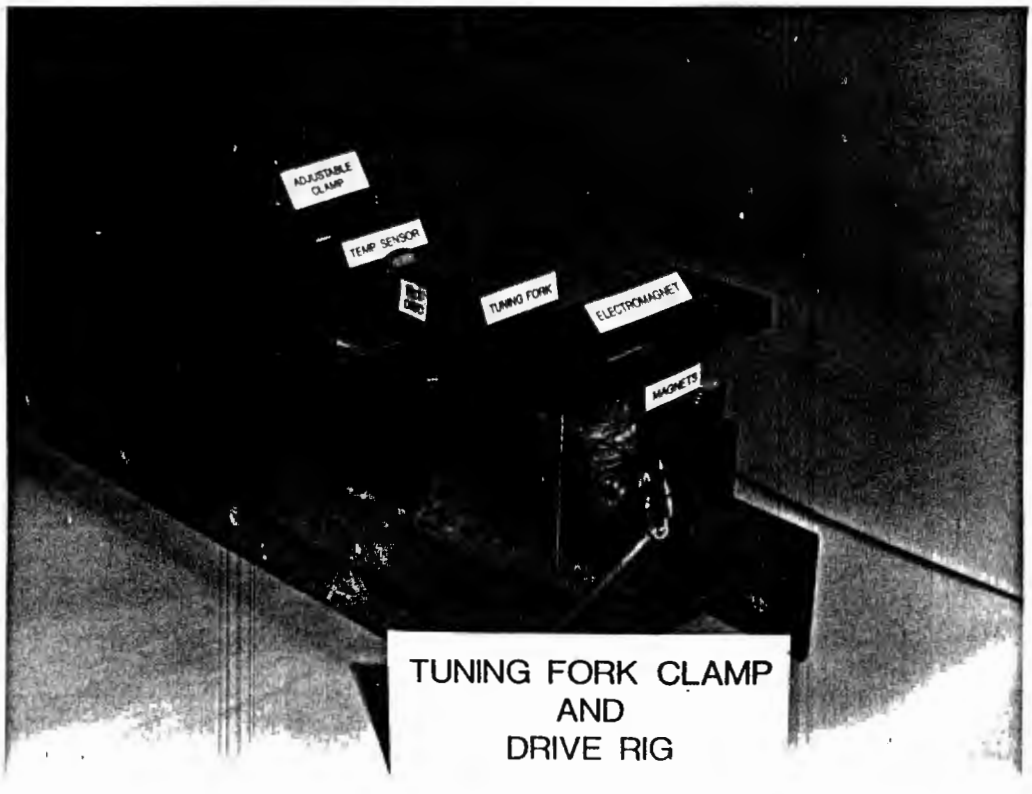

Photograph G.4.

Photograph G.5.

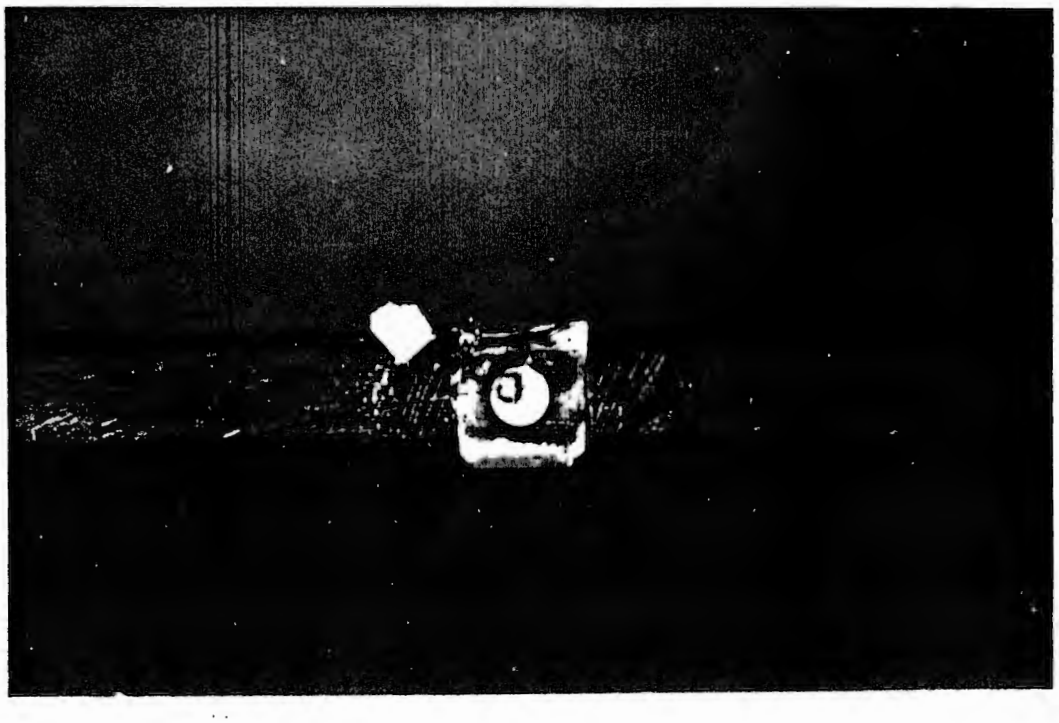

Photograph G.6.

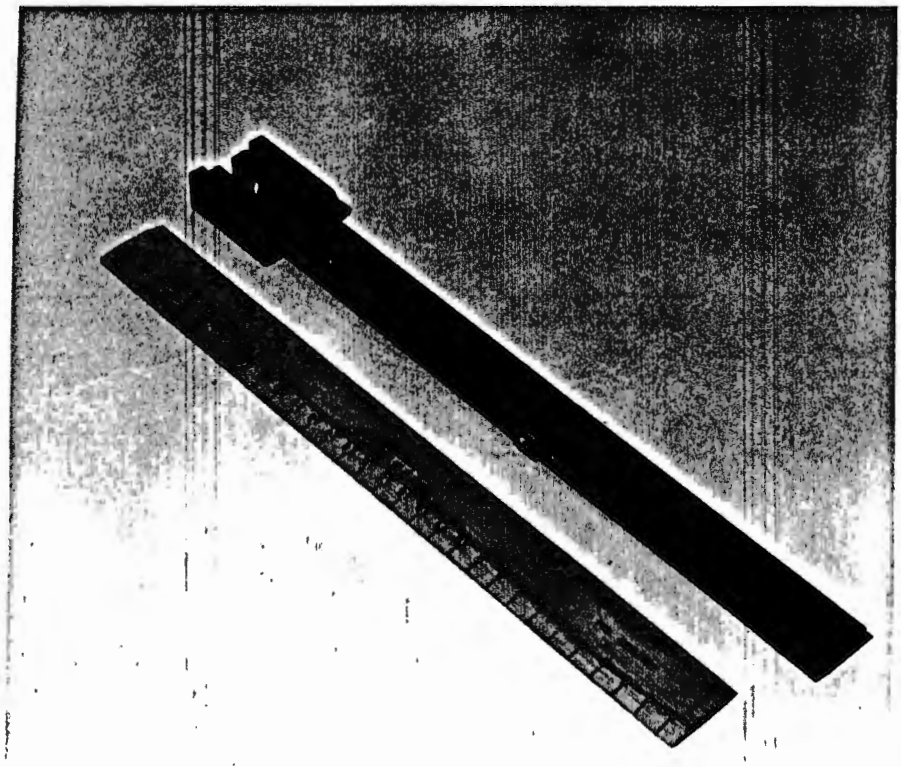

Photograph G.7.

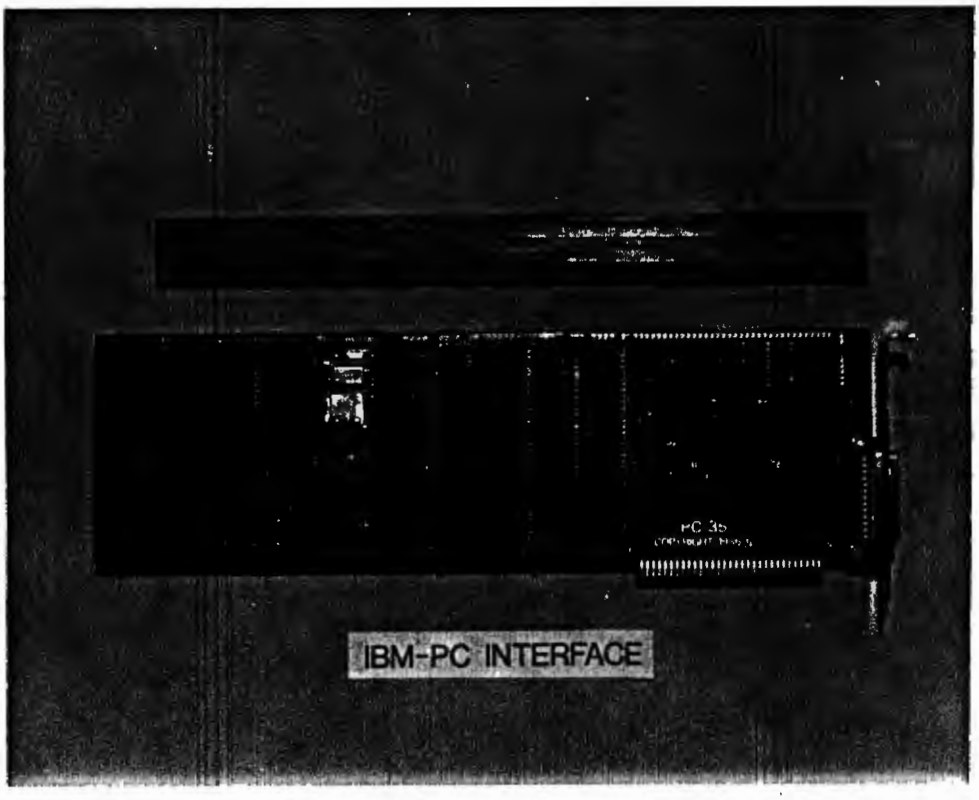

Photograph G.8.

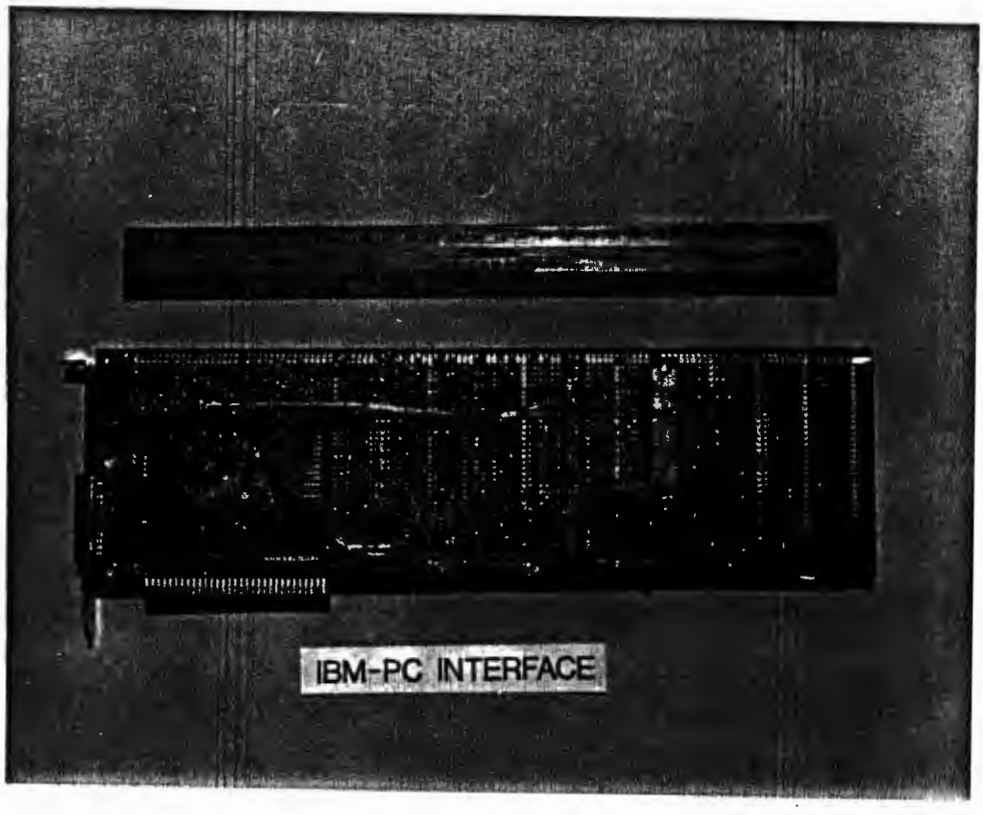

Photograph G.9.

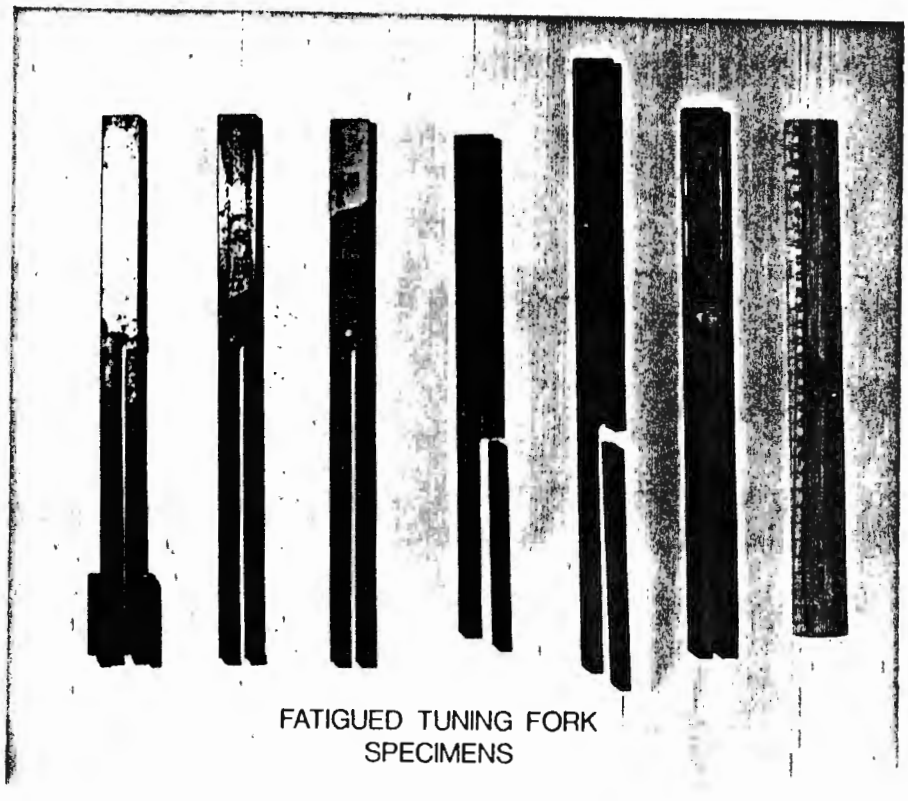

Photograph G.10.

LIST OF REFERENCES

1. Ashby M. F., "Engineering Materials. An introduction to their properties and applications", Pergamon Press Oxford England. Ch9, Ch10, v34, 1980.

2. Van Vlack L.H., "Materials Science for Engineers", Addison-Wesley Publishing Co. Ch6, Ch10, Ch11, 1970.

3. Honeycombe R.W.K., "The Plastic Deformation of Metals", Edward Arnold Publishers Ltd, Ch3, 1968.

4. Granato A.V. and Lücke K., "Theory of Mechanical Damping due to Dislocations", Journal of Applied Physics, v26, n6, pp583-593, 1956.

5. Bratina W.J., ""Internal Friction and Basic Fatigue Mechanisms", Physical Acoustics, Academic Press, Ch6, v3, part A "The Effect of Imperfections", 1966.

6. Granato A.V. and Lücke K., "The vibrating string model of dislocation damping", Physical Acoustics, Academic Press, Ch6, v4, part A: Applications to Quantum and solid state physics, p223, 1966.

7. Mason W.P., "Physical acoustics and the properties of solids", Journal of the Acoustical Society of America", v28, n6, pp1197-1206, November 1956.

8. Mason W.P., "Internal friction and fatigue in metals at large strain amplitudes", Journal of the Acoustical Society of America, v28, n6, pp1207-1218, November 1956.

9. Frost, Marsh and Pook L.P., "Metal Fatigue", Clarendon Press (London), 1974.

10. Pook L.P., "The role of crack growth in metal fatigue", The metals Society (London), 1983.

11. Colangelo N.J. and Heisser F.A., "Analysis of Metallurgical Failures", John Wiley and Sons, 1974

12. Klesnil M. and Lukas P., "Fatigue of metallic materials", Elsevier Scientific Publishing Company, 1980.

13. Steidel R.F., "An introduction to Mechanical Vibrations", John Wiley and Sons, 1971.

14. Harris C.M. and Crede C.E., "Shock and vibration handbook", McGraw-Hill Book Company (USA), 1976.

15. Dolan T.J., "Electrically excited resonant type fatigue testing equipment", Bulletin American Society for testing materials", pp60-68, July 1951.

16. Adams R.D. and Bacon D.G.C., "Measurement of the flexural damping capacity and dynamic Youngs modulus of metals and reinforced plastics", Journal of Physics D (applied physics), v6, pp27-41, 1973

17. Gibson R.F. and Plunkett R., "Experimental Mechanics", pp297-302, August 1977.

18. Lee J.M. and McConnell K.G., "Experimental Cross verification of Damping of three metals", Experimental Mechanics, pp347-353, September 1975.

19. Guberman H.D. and Beshers D.N., "Amplitude dependant internal friction and induced modulus defect in purified iron", Acta Metallurgica, v16, pp167-176, February 1968.

20. Adams R.D., "The damping Characteristics of certain steels, cast-irons and other metals", Journal of Sound and Vibration, v23, n2, pp199-216, 1972.

21. Adams R.D. and Fox M.A.O., "Measurement of the damping capacity and dynamic modulus of high damping metals under direct cyclic stress", Journal of Physics D (applied physics), v5, pp1274-1283, 1973.

22. Butera R.A. and Craig R.S., "Apparatus for direct determination and continuous recording of internal friction at constant amplitude", Review of Scientific Instruments, v37, n4, pp401-406, April 1966.

23. Miszenti G.S., "An automatic system for continuous measurement of internal friction and oscillation period at low frequency (1 c/s range)", Journal of Scientific Instruments, v43, pp820-824, 1966.

24. Schabtach C and Fehr R.O., "Measurement of the damping of engineering materials during flexural vibration at elevated temperatures", Journal of Applied Mechanics, v11, ppA86-A92, 1944.

25. Barker H.A. and Noble A.E., "Control of resonant vibration in a spring fatigue testing instrument", Proceedings IEE (England), v125, n9, pp1045-1050, October 1978.

26. Dorn L., "Correlation between the rate of damage and energy absorption of structural steel during fatigue testing", Material Science and Engineering, v53, pp251-256, 1982.

27. Schlät F., "Dynamic compliance measurement - a proposed new and efficient method to investigate crack nucleation and propagation phenomena", International Journal of Fracture, v19, ppR37-R40, 1982.

28. Hanstock R.F., "Damping capacity, strain hardening and fatigue", Proceedings Physical Society, v59, pp275-287, 1947.

29. Lazan B.J. and Wu T., "Damping, fatigue and dynamic stress-strain properties of mild steel", Proceedings American Society for testing materials, pp649-681, 1951.

30. Marloff R.H., "Resonant fatigue testing of riveted joints", Experimental Mechanics, pp37-43, February 1980.

31. Whaley P.W., Chen P.S. and Smith G.M., "Continuous measurement of material damping during fatigue tests", Experimental Mechanics, pp342-348, 1984.

32. Klimasara A., Fiore N.F. and Kuczynski G.C., "Automated resonance bar damping measurement system", Review of Scientific Instruments, v47, n9, pp1163-1166, September 1975.

33. Adams R.D. and Percival A.L., "Measurement of the strain dependant damping of metals in axial vibration", British Journal of Applied Physics (physics D), s2, v2, pp1693-1704,

1969.

34. Bell J.F.W. DSc, Project supervisor - personal interviews.

35. Surtees A.J., "Vibrating Transducers for Fluid Measurement", PhD Thesis, University of Cape Town, 1987.

36. Morse P.M., "Vibration and Sound", McGraw Hill Book Company, 1st edition, Ch4, 1936.

37. Alonso M. and Fin E.J., "University Physics", Addison-Wesley publishing company, v1 Mechanics, 1969.

38. Nelkon and Parker, "Advanced level physics", 3rd edition, 1970.

39. Horowitz P. and Hill W., "The Art of Electronics", Cambridge University Press, Ch3, 1983.

40. GPIO Interface Owners Manual, Hewlett packard Company, September 1982.

41. Muaddi J.A., Izzard M., Dennis J.k, and Bell J.F.W., "The design and application of a decrement Q meter as a non-destructive adhesion test for coatings", pp134-138.

42. HP85 Owners manual and programming guide, Hewlett Packard Company, Ch9, 1981.

43. IO Rom owners manual, Hewlett Packard Company, p111, January 1983.

44. PC35 prototyping board applications handbook.

45. Kemeny J.G. and Kurtz T.E., "True-Basic reference manual", Addison-Wesley publishing company", preface, 1985.

46. Hahn B.D., "Problem solving with true basic", Department of Applied Mathematics University of Cape Town, preface, 1987.

47. Smithells C.J., "Metals Reference Book", Butterworths London, 3rd edition, v2, p705, 1962.

BIBLIOGRAPHY

1. Electronics Today International magazine, September 1976, April 1981, June 1982.

2. Ryder G.H., "Strength of materials", 3rd edition in SI units, The Macmillan Press London, 1983.

3. National Semiconductors," Logic databook 1981", "CMOS databook 1978", "Linear databook 1982".

4. Maplin Electronic Supplies, "Catalogue 1986".

5. RS Electronic components suppliers, "Catalogue 1986"

6. Horowitz P. and Hill W., "The Art of Electronics", Cambridge University Press, 1983.

7. Philips Data Handbook, "Electronic components and materials", Part 19 Piezoelectric ceramics, 1984.

8. DeVoney C., "MS-DOS users guide", Que Corporation, 1984.

9. Kemeny J.G. and Kurtz T.E., "True-Basic Reference Manual", Addison-Wesley Publishing Company, 1985.

10. Motorola, "Linear databook", 1985.

11. Intersil, "Data acquisition handbook", 1982

12. Whiteman I.R., "A mathematical model depicting the stress-strain diagram and the hysteresis loop", Journal of Applied Mechanics, Transactions of the American Society of Mechanical Engineering, pp95-100, March 1959.

13. Feltner C.E. and Morrow J.D., "Microplastic strain hysteresis energy as a criterion for fatigue fracture", Journal of Basic Engineering, pp15-22, March 1961.

14. Adams R.D., "Damping of ferromagnetic materials at direct stress levels below the fatigue limit", Journal of applied physics, v5, pp1877-1889, 1972.

15. Smithells C.J., "Metals Reference Book", Butterworths London, 3rd edition, v1 and v2, 1962.

16. Kalmarczie P.J., "Energy trapped resonances in solid structures", PhD thesis, University of Aston in Burmingham, October 1976.

17. Muaddi J.A., "Vibrational methods applied to NDT testing and fluid density measurement", PhD thesis, University of Aston in Burmingham, 1982.

18. Fitzgerald A.E., Higginbotham D.E. and Grabel A., "Basic Electrical Engineering", McGraw Hill series in electrical engineering, 1984.

19. Healey M., "Principles of Automatic control", Hodder and Stoughton London, 1975.

20. Thomas G.B. and Finney R.L., "Calculus and analytical geometry", Addison-Wesley publishing company London, 1979.

21. The technology press of MIT, "Fatigue and fracture of metals, A symposium held at the Massachusetts Institute of Technology June 19-22 1950", John Wiley and Sons, inc (New York), 1952.

---X---